
SECONDARY STRUCTURES OF DNA AND PNA: FROM ORDERED SUPRAMOLECULAR G- QUADRUPLEXES TO PNA/DNA HETERODUPLEXES

Brunella Pinto

Dottorato in Biotecnologie – 30° ciclo

Università di Napoli Federico II



Dottorato in Biotecnologie – 30° ciclo

Università di Napoli Federico II



SECONDARY STRUCTURES OF DNA AND PNA: FROM ORDERED SUPRAMOLECULAR G- QUADRUPLEXES TO PNA/DNA HETERODUPLEXES

Brunella Pinto

Dottorando: Brunella Pinto

Relatore: Gennaro Piccialli

Coordinatore: Prof. Giovanni Sannia

Alla mia famiglia

INDICE

Preface	i
Short Abstract	iii
Long Abstract	iv
References	ix
Chapter 1 - “<i>DNA comes in many forms</i>”	1
1.1 Introduction	1
1.1.1 Therapeutic application of synthetic ODN	1
1.2 G-quadruplexes	2
1.2.1 Structural variability of G-Qs	4
1.2.2 The biological role of G-Qs	7
1.2.3 G-Qs and biotechnology	8
1.2.3.1 G-Qs self-assembly	8
1.2.3.2 Hydrogels	11
1.2.3.3 Biosensors	12
1.2.3.4 Conjugation to Gold-nanoparticles (AuNPs)	13
1.2.3.5 Nanomachines	14
1.3 Oligonucleotides analogues	15
1.4 G-quadruplexes from Synthetic ODN analogue	17
1.5 Aim of my research	18
1.6 References	20
Chapter 2 – “<i>Synthesis and characterization of new supramolecular structures from G-rich oligonucleotide sequences</i>”	23
2.1 Introduction	23
2.2 Results and discussion	25
2.2.1 Page	25
2.2.2 SEC analysis	26
2.2.3 Circular Dichroism	29

2.2.4 NMR	31
2.2.5 AFM analysis	32
2.3 Conclusions	34
2.4 Experimental Methods	35
2.4.1 DNA synthesis and Purification	35
2.4.2 Annealing Procedure	35
2.4.3 PAGE	35
2.4.4 HPLC-SEC analyses and isolation of Qn species	35
2.4.5 Circular Dichroism	36
2.4.6 NMR spectroscopy	36
2.4.7 AFM	36
2.5 References	37
 Chapter 3 – “<i>Target Protector PNA as a new tool in the treatment of Cystic Fibrosis</i>”	39
3.1 Introduction	39
3.2 Results and Discussion	41
3.2.1 CD and CD melting analyses	41
3.2.2 UV studies	42
3.2.3 Molecular Dynamics	43
3.2.4 Biological Assays	45
3.3 Conclusions	46
3.4 Materials and Methods	46
3.4.1. General Methods	46
3.4.2. DNA Synthesis and Analysis	47
3.4.3. PNA Synthesis and Analysis	47
3.4.4. Preparation of DNA/PNA Heteroduplexes (Annealing Procedure)	48
3.4.5. UV	48
3.4.6. CD and CD Melting Studies	48
3.4.7. Molecular Dynamics (MD) Simulations	48

3.4.8. Cell Line, Construct, and Transfections	49
3.5 Bibliography	51
 Chapter 4 – “Synthesis and Label Free Characterization of a Bimolecular PNA Homo Quadruplex for the construction of new K^+ sensing probes”	53
4.1 Introduction	53
4.2 Results and Discussion	55
4.2.1 Synthesis of the non-nucleotidic linker	55
4.2.2 Functionalization of the linker with PNA strands to form the bel-PNA	56
4.2.3 Evaluation of the ability of the bel-PNA to form a PNA-based quadruplex	57
4.3 Conclusions	61
4.4 Experimental section	61
4.4.1. Synthesis of Fmoc protected <i>bel</i> -linker 8	62
4.4.2 N,N'-(2-((tert-butyldimethylsilyl)oxy)propane-1.3-diyl)bis(2,2,2-trifluoroacetamide) (5)	62
4.4.3. 2-((tert-butyldimethylsilyl)oxy)propane-1.3-diamine (6)	62
4.4.4. bis((9H-fluoren-9-yl)methyl) (2-((tert-butyldimethylsilyl)oxy)propane- 1.3-diyl)dicarbamate (7)	62
4.4.5. bis((9H-fluoren-9-yl)methyl) (2-hydroxypropane-1.3-diyl) dicarbamate (2)	63
4.4.6. bis((9H-fluoren-9-yl)methyl)(2-(((2-cyanoethoxy)(diisopropylamino)phosphino)oxy)propane-1.3-diyl)dicarbamate (8)	63
4.4.7. Synthesis of <i>bel</i> -PNA 19	63
4.4.8. Obtainment of quadruplexes (annealing)	64
4.4.9. UV and CD studies	64
4.4.10 SERS studies	64
4.5 References	65
 Chapter 5 – “Concluding Remarks and Future Perspectives”	67
 APPENDIX	

PREFACE

My research activity has been focused to the use of oligonucleotides and oligonucleotide analogues in a broad range of fields. At first, I worked on the synthesis and structural characterization of a novel G-Quadruplex structure able to form higher order assemblies; secondly, I explored the properties of PNA as an efficient target protector agent to be used in the treatment of the Cystic Fibrosis; finally, but not less intriguing, in view of the simple and easy development of PNA-based biosensors, I synthesized a novel PNA quadruplex and characterized it by the means of SERS analysis; To achieve all these goals, I gained valuable experience in the synthesis of biologically relevant molecules, in the purification and in biophysical and biological characterization of such biomolecules.

The results of my contributions in my thesis research area will be discussed in the following chapters, and they have been published in the papers listed below:

- Chemistry Open, 2017, 6, 599 –605.

In this work, by using a combination of spectroscopic techniques and HPLC analysis, it has been proved that the sequence d(5'-CGG-3'-3'-TGGC-5') - containing a 3'-3' phosphodiester bond that reverse the polarity in the strand thus creating two 5'-ends - formed the quadruplex monomeric building block that was able to form long G-wires.

- Molecules 2017, 22(7), 1144.

I worked on the synthesis of new PNA sequences to be used for as target protector agent useful for the development of an innovative approach of the CF disease gene.

- Biochimica et Biophysica Acta (BBA), 2016, 1861, 5, 1222-1228.

In this work we exploited a new technique to demonstrate the ability to form G-Quadruplex structure of a CD-unfriendly complex.

Finally, during these years, I have been also involved in other works concerning the chemical synthesis and structural characterization of small organic molecules. The findings of these works are reported in:

- Mahal, A., D' Errico, S., Borbone, N., **Pinto, B.**, Costantino, V., Oliviero, G., Secondo, A., Tedeschi, V., Piccialli, V., Piccialli, G. Synthesis of cyclic N (1)-pentylinosine phosphate, a new structurally reduced cADPR analogue with calcium-mobilizing activity on PC12 cells, Beilstein Journal of Organic Chemistry, 2015, 11, 2689-95.
- D' Errico, S., Oliviero, G., Borbone, N., Nici, F., Piccialli, V., **Pinto, B.**, D'Alonzo, D., Mayol, L. and Piccialli, G. Synthesis of C6-Pyridylpurine Nucleosides by Reaction of Nebularine N1-Oxidewith Pyridinyl Grignard Reagents, Eur. J. Org. Chem. 2015, 2244–2249.

- D' Errico, S., Oliviero, G., Borbone, N., Piccialli, V., **Pinto, B.**, De Falco, F., Maiuri, M.C., Carnuccio, R., Costantino, V., Nici, F. and Piccialli, G. Synthesis and Pharmacological Evaluation of Modified Adenosines Joined to Mono-Functional Platinum Moieties, *Molecules* 2014, 19, 9339-9353.

SHORT ABSTRACT

Oligonucleotides and oligonucleotide analogues are extremely versatile molecules from a biotechnological point of view, since they could be used as scaffolds for the development of new drugs in therapeutics, but also for the development of new materials in nanotechnology.

The present thesis is included in this context and it is aimed at the discovery of all potential applications of these molecules.

In particular, my work is mainly focused on:

- ✓ The synthesis and characterization of a novel G-rich ODN sequence for the development of long G-wires;
- ✓ The synthesis and characterization of PNA sequences to be used in a novel approach for the treatment of Cystic Fibrosis;
- ✓ The synthesis and characterization of a short sequence of PNA conjugated to a novel bifunctional linker aimed at the obtainment of PNA-based quadruplex.

This has been possible exploiting my knowledge in solid phase and solution synthesis and by means of spectroscopic techniques.

LONG ABSTRACT

Gli oligonucleotidi sintetici (ON) sono corti filamenti di acidi nucleici di opportuna sequenza e lunghezza attualmente impiegati nel trattamento di importanti malattie dell'uomo, quali cancro e infezioni virali. Zamecnik e Stephenson furono i primi che proposero nel 1978 l'uso di oligonucleotidi sintetici per scopi terapeutici (1). Da quel momento, la comunità scientifica ha sempre di più riconosciuto l'importanza di tali molecole e proposto il loro uso nell'ambito della *medicinal chemistry* per la progettazione di nuovi farmaci. Gli oligonucleotidi, difatti, sono molecole capaci di interagire selettivamente ed in maniera stabile con sequenze di DNA o con l'RNA che possiedano una sequenza complementare, formando legami ad idrogeno tra le basi azotate, in accordo al modello di Watson-Crick.

Attualmente gli oligonucleotidi sintetici trovano applicazione come modelli di studi strutturali di strutture non canoniche di DNA, come molecole per la diagnosi e quindi nella progettazione di farmaci di nuova generazione. In questo contesto essi possono essere catalogati, in funzione del loro meccanismo di azione, come oligonucleotidi "antisense", "antigene" ed "aptameri". Tuttavia, anche in questo tipo di approccio è di estrema importanza valutare la risposta farmacocinetica, farmacodinamica e tossicologica di tali molecole. Infatti, è estremamente importante valutare, oltre l'attività biologica, anche la stabilità nei compartimenti intracellulari ed extracellulari, la capacità di tali molecole di attraversare le membrane biologiche e di giungere allo specifico bersaglio, in dosi efficaci e non tossiche. Gli ODN sintetici 'naturali' mostrano tuttavia una ridotta attività *in vivo*, dovuta sia a scarsa permeabilità delle membrane cellulari agli ODN naturali, che ad una rapida degradazione ad opera delle nucleasi cellulari. A questo proposito, l'attenzione della comunità scientifica si sta incentrando, in misura sempre maggiore negli ultimi anni, sulla ricerca e la sintesi di analoghi oligonucleotidici, chimicamente modificati o nel ponte zucchero-fosfato o nelle basi azotate o eventualmente coniugati con molecole, a basso o medio peso molecolare, capaci di conferire al composto ibrido una maggiore permeabilità alle barriere biologiche e una maggiore resistenza alle nucleasi cellulari. Diverse modifiche chimiche sono state quindi apportate con lo scopo di migliorare le proprietà farmacocinetiche degli oligonucleotidi (2, 3). Ed è in questo contesto che si collocano i PNA, ovvero gli Acidi Peptido-Nucleici. Essi sono dei mimici del DNA, in cui uno scheletro di tipo peptidico, dato dalla condensazione di unità monomeriche di 2-amminoetilglicina, sostituisce lo scheletro zucchero-fosfato degli acidi nucleici su cui sono innestate le normali basi adenina, timina, guanina e citosina (4). Tale struttura ha il vantaggio di essere non ionica e del tutto stabile alle nucleasi, alle proteasi e alle peptidasi. Ideati da Peter Nielsen nel 1991, i PNA sono capaci di formare con DNA e RNA composti dotati di elevata stabilità termica, e questo è reso possibile dalla mancanza di repulsione elettrostatica tra i filamenti che rende i duplex ibridi PNA/DNA e PNA/RNA molto più stabili degli omo ed etero-duplex (5).

La spiccata stabilità *in vivo*, la specifica ibridizzazione con gli acidi nucleici e l'assenza di tossicità, anche a concentrazioni relativamente elevate, hanno contribuito a rendere i PNA molecole promettenti per le applicazioni terapeutiche.

Sempre in questo contesto, negli ultimi decenni, numerosi studi sono stati rivolti anche verso un altro tipo di strutture: le strutture G-quadruplex. Le G-quadruplex sono strutture non canoniche di acido nucleico che si formano in sequenze ricche di guanine in presenza di cationi monovalenti come K^+ e Na^+ . Tali guanine hanno una naturale propensione ad auto associarsi in quartetti coplanari (o tetradi), stabilizzate

da legami a idrogeno di tipo Hoogsteen. Inoltre l'impilamento di diverse tetradi di guanine consente l'instaurarsi di interazioni di tipo π tra i diversi piani, e ciò contribuisce ulteriormente a stabilizzare tali strutture.

Nel 1910, Bang fu il primo a dimostrare che l'acido guanilidico era in grado di formare, in alte concentrazioni, una sostanza dalla consistenza gelatinosa, suggerendo quindi che sequenze ricche di guanine nel DNA avessero la capacità di formare strutture di ordine superiore (6). Tuttavia, la prima caratterizzazione di una struttura G-quadruplex risale solo al 1962 (7). Da quel momento, l'interesse scientifico verso le G-quadruplex non si è mai esaurito ma è anzi cresciuto in maniera esponenziale, arrivando al suo apice nel 2013, quando il gruppo di ricerca del prof. Balasubramanian ha pubblicato un articolo in *Nature Chemistry*, in cui ha descritto un metodo per la visualizzazione quantitativa in vivo delle G-quadruplex e fornito quindi prove sostanziali e dirette della loro naturale formazione all'interno del genoma umano (8).

Aldilà dell'interesse da un punto di vista biologico, tali strutture stanno riscuotendo ampi consensi anche nell'ambito delle nanotecnologie, per la loro capacità di formare strutture di ordine superiore tramite processi di autoassemblaggio (o *self-assembly*), idrogels, biosensori e nanomacchine. L'autoassemblaggio è il processo con il quale specifiche componenti si associano spontaneamente a dare un'architettura supramolecolare complessa e definita. Molte strutture biologiche si originano spontaneamente per autoassemblaggio di strutture chimiche più semplici ed il complesso biologico supramolecolare più celebre è sicuramente il DNA. Quello a cui generalmente ci si riferisce come la molecola del DNA è infatti un aggregato di due distinte macromolecole polinucleotidiche trattenute insieme da interazioni non covalenti. L'appaiamento tra le basi è il migliore esempio di come fattori geometrici e specificità elettronica delle interazioni determinino l'assunzione della struttura supramolecolare garantiscano la funzionalità della struttura stessa.

Le strutture G-quadruplex presentano anch'esse tale proprietà, difatti, grazie all'elevato grado di polimorfismo (9), possono dare origine ad un'ampia famiglia di strutture stabili, la cui plasticità conformazionale permette di sviluppare strutture molecolari superiori.

In quest'ambito le G-quadruplex sono state utilizzate per la costruzione di nanostrutture a base di DNA, quali G-wires. Tali sovrastrutture presentano diverse proprietà che le rendono estremamente interessanti da un punto di vista nanotecnologico. Studi teorici suggeriscono infatti che esse hanno buona capacità conduttiva, basso potenziale ossidativo e sono dotate inoltre di un'alta rigidità e buona stabilità termica e meccanica il che le rende eccellenti candidati nel campo delle nanotecnologie, nano elettronica e nello sviluppo di biosensori (10, 11).

I biosensori possono essere direttamente rappresentati come dispositivi che convertono un evento fisico o biologico in un segnale misurabile; essi sono composti dunque da un elemento di rilevamento biologico che fornisce selettività, e un trasduttore che converte le reazioni chimiche in segnali processabili. Le strutture G-quadruplex si stanno facendo molto spazio in questo contesto, in particolar modo per segnalare presenza di potassio in campioni biologici ed ambientali e sono particolarmente intriganti in quanto garantiscono bassi costi, selettività, efficienza e soprattutto semplicità (12). Risultati molto interessanti possono essere potenziati coniugando filamenti ricchi di guanine a nanoparticelle d'oro (13).

Una volta consolidata la possibilità delle G-quadruplex ad organizzarsi in sovrastrutture, numerosi ricercatori si sono interrogati sulla capacità degli analoghi oligonucleotidici -ricchi di guanine - di formare strutture di ordine superiore, in modo

tale da ottenere nuovi materiali nell'ambito delle nanotecnologie. Anche in questo caso, l'acido peptido-nucleico è il protagonista indiscusso in questo tipo di indagine. Oggigiorno però, esistono ancor pochi lavori che riportano la completa caratterizzazione di quadruplex a PNA (14, 15). Molti ricercatori infatti hanno soprattutto dimostrato la formazione di quadruplex di natura ibrida DNA-PNA, o addirittura di chimere PNA-DNA (16, 17). Lo studio della capacità del PNA ad arrangiarsi in strutture G-quadruplex dotate di elevato polimorfismo resta quindi una sfida aperta nell'ambito delle biotecnologie.

Il mio lavoro di tesi è dunque inserito in questo contesto ed è focalizzato principalmente sui seguenti punti:

- **Sintesi e caratterizzazione di nuove sequenze oligonucleotidiche capaci di formare strutture G-quadruplex di ordine superiore**

La caratterizzazione di strutture di ordine superiore a partire da strutture G-quadruplex rappresenta uno degli obiettivi principali dei ricercatori nell'ambito delle nanotecnologie. Le strutture G-quadruplex si sono rivelate strutture molto versatili per la costruzione di sovrastrutture e biosensori, e ciò è dovuto principalmente alla facilità con cui esse possono essere ottenute, e all'elevato grado di polimorfismo a cui possono dare origine.

Recentemente, nel gruppo di ricerca del prof. Piccialli è stata identificata una nuova modalità di dimerizzazione di strutture G-quadruplex attraverso uno *stacking* testa-testa di due blocchi di quadruplex derivanti dal filamento $5'$ -CGGTGGT- $3'$: attraverso diversi studi spettroscopici è stato dimostrato che le citosine all'estremità $5'$ agivano da colla idrofobica tra i due blocchi di quadruplex (18). Tale lavoro è stato successivamente ampliato, andando a sintetizzare una piccola libreria di oligonucleotidi a sequenza diversa, e dimostrando anche in questo caso, la possibilità di formare dimeri di quadruplex stabili (19).

In questo contesto si inserisce il mio lavoro di dottorato: l'idea è quella di sintetizzare un nuovo filamento oligonucleotidico contenente un'inversione di polarità in modo tale da poter ottenere due estremità $5'$ nello stesso filamento. La capacità di questo filamento di formare blocchi G-quadruplex, in grado poi a loro volta, di polimerizzare formando strutture G-wire di ordine superiore sfruttando le estremità "adesive" in $5'$, è stata poi ampiamente indagata attraverso l'utilizzo di tecniche quali PAGE, SEC-HPLC e studi spettroscopici.

In particolar modo, una volta annilato il nostro campione in presenza di potassio, è stato possibile visualizzare, in base alla loro diversa mobilità elettroforetica, una distribuzione di oggetti quadruplex, a partire dalla specie monomerica (specie più veloce) fino ad arrivare ad una miscela indistinguibile di oggetti di ordine superiore (specie più lente). Particolarmente interessante è stata poi l'analisi SEC-HPLC; i cromatogrammi ottenuti ci hanno permesso di identificare, analizzando i tempi di ritenzione, tutti i multimeri formati dalla specie in esame e di isolare tali oggetti. Variando inoltre le condizioni sperimentali, è stato possibile dimostrare che il *pattern* dei picchi è concentrazione-temperatura dipendente. Ancora, le spettroscopie di dicroismo circolare e di NMR hanno contribuito a caratterizzare ulteriormente tali strutture di ordine superiore, mentre, infine, l'analisi AFM ha permesso di visualizzare tali strutture e di definirne le dimensioni.

- **Sintesi e caratterizzazione di nuove sequenze di PNA da utilizzare in una nuova strategia diretta al trattamento della Fibrosi Cistica**

La fibrosi cistica (FC) è la malattia genetica rara più diffusa che solo in Italia colpisce circa 1 neonato su 3.000. La malattia si verifica quando un bambino eredita due copie alterate del gene CFTR (Cystic Fibrosis Transmembrane Regulator), una da ciascun genitore (20).

Il gene CFTR codifica la sintesi della proteina CFTR che se ben funzionante regola il movimento del cloro, al quale segue il movimento dell'acqua, dall'interno verso l'esterno delle cellule epiteliali delle ghiandole mucose. Il malfunzionamento o assenza della proteina CFTR interessa tutte le ghiandole a secrezione mucosa determinando una carenza di cloro e acqua nelle secrezioni. Le secrezioni mucose povere di acqua e vischiose tendono a ristagnare provocando così l'ostruzione degli organi interessati, e continue infiammazioni-infezioni degli stessi. La terapia di questa malattia ha avuto negli ultimi anni notevole sviluppo. Infatti, accanto ad una terapia dei sintomi oggi si stanno facendo spazio sempre più le terapie geniche che mirano ad una correzione del difetto di base in alcune forme geniche di FC. Una delle terapie che ha riscosso più successo è quella che prevede il bersagliamento dei miRNA, ovvero delle brevi sequenze di RNA non codificante coinvolte nella patogenesi della malattia. Infatti questi, essendo complementari al 3'UTR (UnTranslated Region) del trascritto del gene CFTR, sono responsabili della riduzione dell'espressione della proteina, causando la malattia o l'aggravarsi del suo fenotipo. I microRNA, inoltre, sembrano essere responsabili del mantenimento di bassi livelli di CFTR negli adulti (21). Il bersagliamento dei miRNA può essere effettuato usando molecole quali il PNA. Nel gruppo di ricerca del professor Piccialli sono state precedentemente esplorate le potenzialità del PNA come agente anti-miRNA (22–24). Studi spettroscopici hanno dimostrato che tali PNA sono capaci di formare ibridi stabili con il target, mentre studi *in vitro* hanno dimostrato che i PNA riconoscono i target nelle cellule. Nonostante i promettenti risultati ottenuti, il sequestro dei miRNA potrebbe portare, a lungo andare, a tutta una serie di effetti collaterali in quanto responsabili anche di altri ruoli biologici. In questo contesto si è inserito il mio lavoro di dottorato, ovvero nel mettere a punto una nuova strategia che non mirasse più ai miRNA, ma avesse come target la regione 3'UTR del gene (strategia *target protector*). In questo modo, mascherando la regione di legame del miRNA, quest'ultimo è libero di svolgere le sue funzioni, e contemporaneamente, l'effetto dovrebbe essere quello di incrementare la produzione della proteina CFTR. A questo proposito dunque, sono state sintetizzate e caratterizzate 2 sequenze di PNA, di 13 e 7 basi (e relative sequenze *scramble* usate come controllo negativo) e attraverso studi spettroscopici, quali dicroismo circolare e UV, è stata valutata la loro abilità di formare strutture ibride con il target: da tali esperimenti è emerso che entrambe le sequenze PNA sono in grado di formare eteroduplex di tipo antiparallelo con il bersaglio, la cui stabilità termica è stata valutata attraverso CD *melting*. Tali risultati sono stati supportati da studi di dinamica molecolare. Infine, preliminari saggi biologici eseguiti sul costrutto della luciferasi, hanno messo in evidenza che l'azione del PNA è in grado di ripristinare significativamente l'attività luciferasica.

Sintesi e caratterizzazione di un breve segmento di PNA coniugato ad un linker bifunzionale con lo scopo di ottenere nuove quadruplex a PNA bimolecolari

In questo contesto, l'obiettivo del mio lavoro di dottorato è stato quello di continuare ad indagare sulle infinite potenzialità del PNA, questa volta non da un punto di vista biologico, ma valutando la sua capacità di formare nuove strutture del tipo G-quadruplex, utili per la costruzione di nuovi nanomateriali. Sfruttando come punto di partenza l'expertise del gruppo di ricerca del prof. Piccialli nella sintesi di linker ramificati (25–28), l'approccio ha previsto la preliminare sintesi di un nuovo tipo di linker bidentato, funzionalizzato poi da sequenze di PNA ricche in guanine. La molecola così ottenuta, chiamata bel-PNA, è stata poi sospesa in potassio e la capacità di assemblarsi in quadruplex è stata valutata attraverso studi spettroscopici. In particolare, attraverso la preliminare analisi di dicroismo circolare è stato possibile dimostrare che il bel-PNA è in grado di strutturarsi in quadruplex di tipo antiparallelo; tuttavia, essendo il PNA una molecola achirale, l'analisi CD richiede il supporto di un altro tipo di tecnica. In questo contesto si inserisce la spettroscopia SERS, che si è dimostrata uno strumento indispensabile per la caratterizzazione strutturale di tale tipo di molecola.

Riferimenti

1. Zamecnik, P.C. and Stephenson, M.L. (1978) Inhibition of Rous sarcoma virus replication and cell transformation by a specific oligodeoxynucleotide. *Biochemistry*, 75, 280–284.
2. Verma, S. and Eckstein, F. (1998) MODIFIED OLIGONUCLEOTIDES: Synthesis and Strategy for Users. *Annu. Rev. Biochem.*, 67, 99–134.
3. Eckstein, F. (1966) Nucleoside Phosphorothioates. *J. Am. Chem. Soc.*, 10.1021/ja00970a054.
4. Nielsen, P.E. and Egholm, M. (1999) An Introduction to Peptide Nucleic Acid. *Curr. Issues Molec. Biol.*, 1, 89–104.
5. Giesen, U., Kleider, W., Berding, C., Geiger, A., Ørum, H. and Nielsen, P.E. (1998) A formula for thermal stability (T_m) prediction of PNA / DNA duplexes. *Current*, 26, 5004–5006.
6. Bryan, T.M. and Baumann, P. (2011) G-Quadruplexes: From Guanine Gels to Chemotherapeutics. *Mol. Biotechnol.*, 49, 198–208.
7. Gellert, I., Lipsett, M.N. and Davies, D.R. (1962) HELIX FORMATION BY GUANYLIC ACID. *Proc Natl Acad Sci U S A*, 48, 2013–2018.
8. Biffi, G., Tannahill, D., McCafferty, J. and Balasubramanian, S. (2013) Quantitative visualization of DNA G-quadruplex structures in human cells. *Nat. Chem.*, 5, 182–6.
9. Burge, S., Parkinson, G.N., Hazel, P., Todd, A.K. and Neidle, S. (2006) Quadruplex DNA: sequence, topology and structure. *Nucleic Acids Res.*, 34, 5402–5415.
10. Hessari, N.M. a ani, Spindler, L., Troha, T., Lam, W.C., Drevenšek-Olenik, I. and da Silva, M.W. ebba (2014) Programmed self-assembly of a quadruplex DNA nanowire. *Chemistry*, 20, 3626–3630.
11. Livshits, G.I., Stern, A., Rotem, D., Borovok, N., Eidelstein, G., Migliore, A., Penzo, E., Wind, S.J., Di Felice, R., Skourtis, S.S., et al. (2014) Long-range charge transport in single G-quadruplex DNA molecules. *Nat. Nanotechnol.*, 9, 1040–1046.
12. Ruttkay-Nedecky, B., Kudr, J., Nejdli, L., Maskova, D., Kizek, R. and Adam, V. (2013) G-quadruplexes as sensing probes. *Molecules*, 18, 14760–14779.
13. Chen, Z.B., Guo, J.X., Ma, H., Zhou, T. and Li, X.X. (2014) A simple colorimetric

- sensor for potassium ion based on DNA G-quadruplex conformation and salt-induced gold nanoparticles aggregation. *Anal. Methods*, 6, 8018–8021.
14. Datta,B., Bier,M.E., Roy,S. and Armitage,B.A. (2005) Quadruplex formation by a guanine-rich PNA oligomer. *J. Am. Chem. Soc.*, 127, 4199–4207.
 15. Krishnan-Ghosh,Y., Stephens,E. and Balasubramanian,S. (2004) A PNA 4 Quadruplex. *J. AM. CHEM. SOC.*, 126, 5944–5945.
 16. Petraccone,L., Pagano,B., Esposito,V., Randazzo,A., Piccialli,G., Barone,G., Mattia,C.A. and Giancola,C. (2005) Thermodynamics and Kinetics of PNA-DNA Quadruplex-Forming Chimeras. *JACS*, 127, 16215–16223.
 17. Datta,B., Schmitt,C. and Armitage,B.A. (2003) Formation of a PNA 2 -DNA 2 Hybrid Quadruplex. *JACS*, 125, 4111–4118.
 18. Borbone,N., Amato,J., Oliviero,G., D'Atri,V., Gabelica,V., De Pauw,E., Piccialli,G. and Mayol,L. (2011) D(CGGTGGT) forms an octameric parallel G-quadruplex via stacking of unusual G(:C):G(:C):G(:C):G(:C) octads. *Nucleic Acids Res.*, 39, 7848–7857.
 19. D'Atri,V., Borbone,N., Amato,J., Gabelica,V., D'Errico,S., Piccialli,G., Mayol,L. and Oliviero,G. (2014) DNA-based nanostructures: The effect of the base sequence on octamer formation from d(XGGYGGT) tetramolecular G-quadruplexes. *Biochimie*, 99, 119–128.
 20. Elborn,J.S. (2016) Cystic fibrosis. *Lancet*, 388, 2519–2531.
 21. McKiernan,P.J. and Greene,C.M. (2015) MicroRNA Dysregulation in Cystic Fibrosis. *Mediators Inflamm.*, 2015, 529642.
 22. Amato,F., Seia,M., Giordano,S., Elce,A., Zarrilli,F., Castaldo,G. and Tomaiuolo,R. (2013) Gene Mutation in MicroRNA Target Sites of CFTR Gene: A Novel Pathogenetic Mechanism in Cystic Fibrosis? *PLoS One*, 8, 1–6.
 23. Amato,F., Tomaiuolo,R., Nici,F., Borbone,N., Elce,A., Catalanotti,B., D'Errico,S., Morgillo,C.M., De Rosa,G., Mayol,L., *et al.* (2014) Exploitation of a very small peptide nucleic acid as a new inhibitor of miR-509-3p involved in the regulation of cystic fibrosis disease-gene expression. *Biomed Res. Int.*, 2014, 68–71.
 24. Amato,F., Tomaiuolo,R., Borbone,N., Elce,A., Amato,J., D'errico,S., De Rosa,G., Mayol,L., Piccialli,G., Oliviero,G., *et al.* Design, synthesis and biochemical investigation, by in vitro luciferase reporter system, of peptide nucleic acids as new inhibitors of miR-509-3p involved in the regulation of cystic fibrosis disease-gene expression. 10.1039/c3md00257h.
 25. Oliviero,G., Amato,J., Borbone,N., Galeone,A., Varra,M., Piccialli,G. and Mayol,L. (2006) Synthesis and Characterization of DNA Quadruplexes Containing T-Tetrads Formed by Bunch-Oligonucleotides. *Biophys. Chem.*, 81, 194–201.
 26. Borbone,N., Oliviero,G., Amato,J., D'Errico,S., Galeone,A., Piccialli,G. and Mayol,L. (2007) Synthesis and characterization of tetra-end linked oligonucleotides capable of forming monomolecular G-quadruplexes. *Nucleosides. Nucleotides Nucleic Acids*, 26, 1231–6.
 27. Oliviero,G., Amato,J., Borbone,N., Galeone,A., Petraccone,L., Varra,M., Piccialli,G. and Mayol,L. (2006) Synthesis and characterization of monomolecular DNA G-quadruplexes formed by tetra-end-linked oligonucleotides. *Bioconjug. Chem.*, 17, 889–898.
 28. Oliviero,G., Borbone,N., Amato,J., D'Errico,S., Galeone,A., Piccialli,G., Varra,M. and Mayol,L. (2009) Synthesis of quadruplex-forming tetra-end-linked oligonucleotides: Effects of the linker size on quadruplex topology and stability. *Biopolymers*, 91, 466–477.

Chapter 1

“DNA comes in many forms” (1)

1.1 Introduction

Nucleic acid structures are fundamental to cellular function and the regulation of several biological events (2). Oligonucleotides (ODNs) are short sequences of nucleic acids, 15-100 nucleotides in length, usually obtained by chemical synthesis and they represent the simplest form of nucleic acid endowed with therapeutic function. The term oligonucleotide is derived from the Greek “oligo,” which means few or small. The length of the oligonucleotide is usually denoted by the term “mer,” which is Greek for “part.”

In the last few years, the scientific community has recognized the importance of synthetic oligonucleotides as new therapeutic agents to be used in the field of medicinal chemistry, as they are molecules capable to selectively and firmly interact with DNA and RNA. This ability is based on the single-strand DNA property to recognize a DNA or RNA strand that possesses a complementary sequence through the constitution of hydrogen bonds between the bases based on the Watson-Crick model. Despite the non-covalent nature of the bonds, the whole number of joints makes the affinity between two complementary strands extremely high ($k_d = 1 \times 10^{-15}$ Mol/L); moreover, the hybridization events between the bases allows a highly specific target recognition.

In 1978, Zamecnik and Stephenson were the first to demonstrate the potential of a synthetic ODN to attenuate the expression of selected genes (3). As from their pioneeristic work, the era of oligonucleotide (ON) therapeutics began.

1.1.1 Therapeutic application of synthetic ODN

Synthetic oligonucleotides possess a wide range of applications, including structural studies of non-canonical DNA secondary structures, studies in diagnostic field, and development of new drugs.

In recent years, a new pharmacological approach has developed and this involves the use of ODN as highly selective molecules in regulating gene expression and in which they act much more upstream than traditional drugs that typically target proteins. For instance, they can be catalogued considering their target and mechanism of action, as “antisense” or “antigene” agents, when they target a specific mRNA or a tract of duplex DNA, respectively, or as “aptamers”, when selectively recognize a specific protein.

In the antisense therapy, short sequences of ODN bind the cytosolic messenger RNA (mRNA) produced by the gene by duplex formation, with the effect of inactivating and turning off the gene (4). This synthesized nucleic acid is termed an “anti-sense” oligonucleotide (ASO) because its base sequence is complementary to the gene's messenger RNA (mRNA), which is called the “sense” sequence.

Antisense oligonucleotides have been researched as potential drugs for diseases such as cancers, diabetes, amyotrophic lateral sclerosis (ALS), Duchenne muscular dystrophy, spinal muscular atrophy and more. In 1998, the US FDA approved an antisense oligonucleotide (ASO), Vitravene, for the treatment of AIDS-related cytomegalovirus retinitis

(5). The recent approval of Kynamro (6) confirms the clinical potential of the antisense approach.

In the antigene approach, oligonucleotides can bind with a high specificity of recognition to the major groove of double helical DNA by forming Hoogsteen type bonds with purine bases of the Watson-Crick base pairs, resulting in triple helix formation. Consequently, triplex-forming oligonucleotides (TFOs) can selectively inhibit gene expression at the transcriptional level or repair genetic defect by direct genome modification in human cells (7). Targeting oligonucleotides to the gene itself (the antigene or triple helix strategy) presents several advantages as compared to antisense oligonucleotides or ribozymes which are heading to messenger RNAs, since there are only two copies (two alleles) of the targeted gene whereas there may be thousands of copies of a messenger RNA. This means that by blocking mRNA translation even by inducing sequence-targeted cleavage of the RNA chain does not prevent the corresponding gene from being transcribed, thereby repopulating the RNA pool (8).

Nucleic acid aptamers are short, single-stranded DNA or RNA molecules (20–100 nucleotides in length) with defined structures that can specifically bind to a molecular target via three-dimensional structures. These three-dimensional interactions, including hydrophobic and electrostatic interactions, hydrogen bonding, van der Waals forces, shape complementarity and base stacking, are essential for aptamer binding affinity and specificity and drive the formation of aptamer–target complexes (9). An example of aptamer is embodied by pegaptanib, an aptamer-derived anti-VEGF compound shown to be effective in treating age-related macular degeneration (10). It received FDA approval in 2004.

1.2 G-quadruplexes

It is well known that ODN sequences can fold into a huge number of structural motifs, in order to assemble the functional structural conformation for their precise biological roles in the cellular environments. These motifs include duplexes, hairpins, triplexes, and G-quadruplexes (2) (Fig.5).

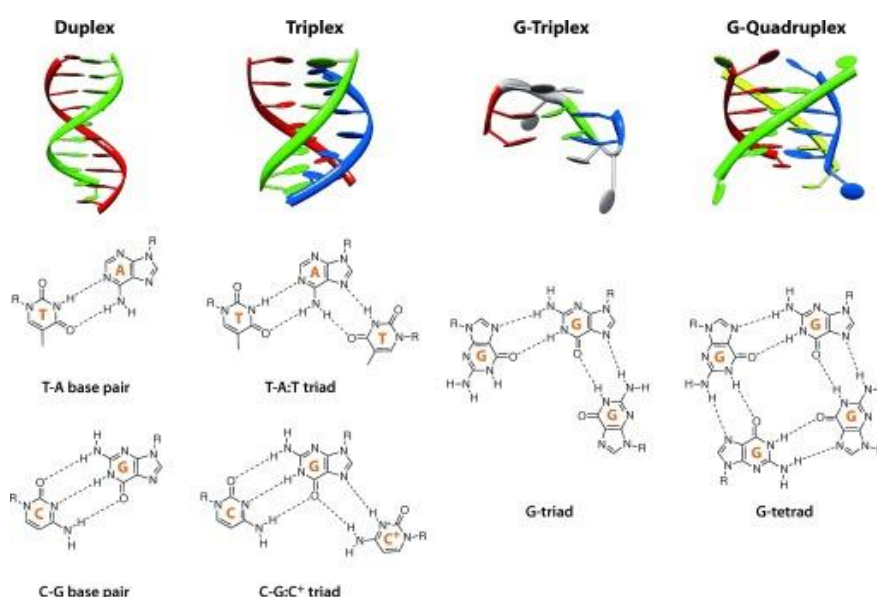


Figure 5: Top: Schematic illustration of the duplex, triplex, G-triplex, and G-quadruplex structures. Bottom: Examples of base pairing.

In particular, Guanine (G)-rich sequences can self-associate into stacks of G-quartets to form G-quadruplexes. In 1910, Bang demonstrated that guanylic acid formed gels at high concentration, providing the first evidence that guanine (G)-rich sequences might form higher-order structures (11); however, the first characterization of a G-tetrad structure was obtained in 1962 by Gellert and co-workers who demonstrated that guanylic acid owned the ability to form tetrameric structures by self-association (12). Considered just an oddity for a long time, their effective biological relevance has been recognized only three decades later, being discovered once in eukaryotic chromosomal telomeric DNA and later in gene promoter regions (13), in a number of human genes involved in growth and proliferation (14), in immunoglobulin switch regions (15), as well as in ribosomal DNA (16) and RNA (17, 18). The evidence for the formation of G-quadruplex structures in the genome of human cells was eventually demonstrated in 2013 by the research group of Prof. Balasubramanian, with a work published on Nature (19).

The "bricks" at the base of the construction of these structures are the G-quartets (Fig.6); the four guanine bases form a square co-planar array where each base is both a hydrogen bond donor and hydrogen bond acceptor. Involvement of both the N1 and N2 of one face with the O6 and N7 of the second face on guanosine yields eight hydrogen bonds per planar G-quartet.

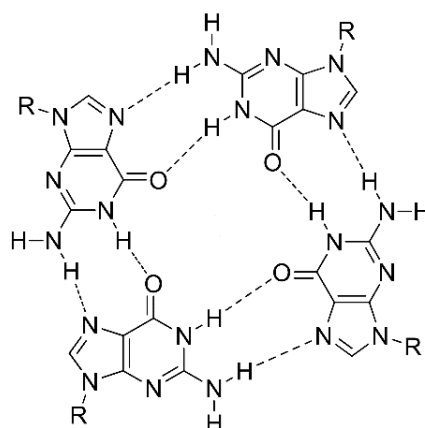


Figure 6: The planar arrangement of four guanine bases bonded by eight Hoogsteen hydrogen bonds.

The square planar layout creates a central cavity delimited by the carbonylic oxygen of the guanine bases; This cavity constitutes a specific binding site for metal ions, essential for the formation and stabilization of these macromolecular complexes. The most effective cations in the stabilization of G-quadruplex structures are K^+ and Na^+ ; Each ion has a precise coordinate geometry, particularly in the case of K^+ , an anti-prismatic bipyramid coordinate geometry is observed with the involvement of two G planes, for a total of eight carbonyl oxygen equally coordinating the central cation (Fig.7).

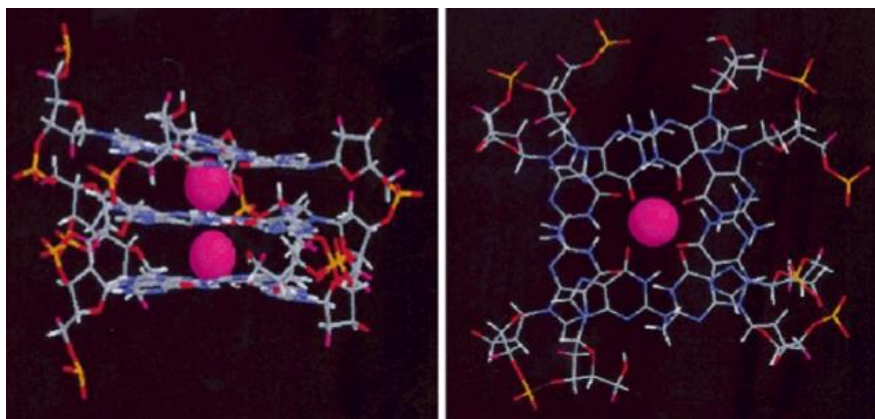


Figure 7: The position of potassium in the central cavity and between two quartets.

The overlapping of guanine planes, positioned at a distance of 3 Angstrom from each other, contributes to further stabilizing the quadruplex structure by π - π stacking interactions (20). From the association of four G-rich oligonucleotide strands, a right-handed helicoidal structure is obtained (Fig.8).

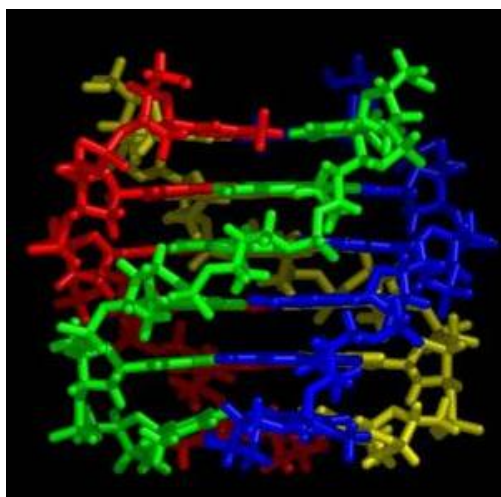


Figure 8: The right-handed helicoidal structure obtained from the association of four G-rich oligonucleotides.

1.2.1 Structural variability of G-Qs

Structural studies of G-quadruplexes have demonstrated that the G-rich sequences can form highly polymorphic G-quadruplexes (21), and the variation in these structures depends on the sequences and the experimental conditions (e.g. coexisting metal ions, metal ion concentration, and degree of molecular crowding) (22); in particular, the G-quadruplexes can differ by the stoichiometry of strands, their orientation and glycoside conformation of the guanines involved in each tetrad (Fig.9).

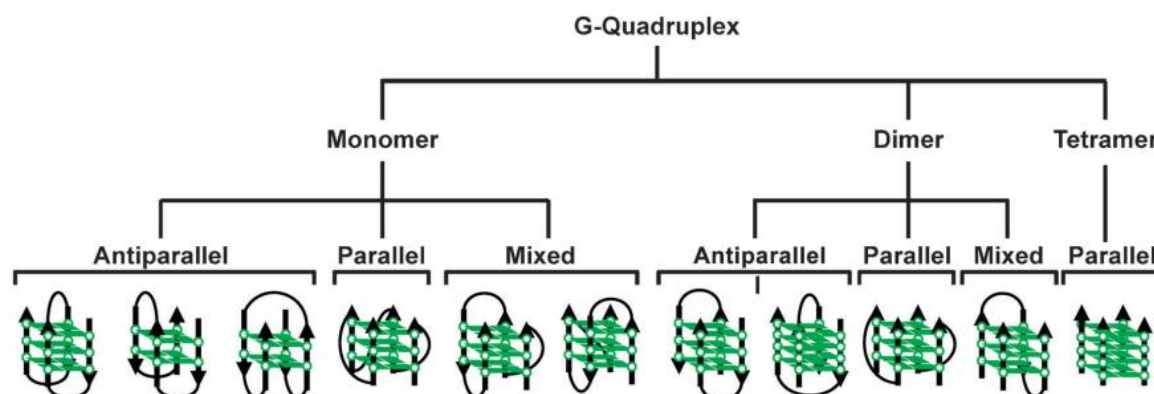


Figure 9: Polymorphism of G-quadruplexes.

First of all, G-Quadruplex structures may form from the folding of a single oligonucleotide chain (giving rise to a monomolecular G-quadruplex) (23) or from the interaction between two (Bimolecular G-quadruplex) (24) or four (tetramolecular G Quadruplex) (25) different oligonucleotide strands.

NMR spectroscopic analysis showed that oligonucleotides containing short guanine runs, for example $X_n G_p X_n$ (with X_n any nucleotide of length n and G_p any number of guanines involved in tetrad formation of length p) are able to form highly symmetrical G-quadruplexes having four parallel strands. Structures containing these short guanine runs, such as $d(TGGGGT)_4$ have been determined by crystallographic and NMR methods to reveal a parallel stranded arrangement, where the phosphate backbone runs in the same direction and all the bases are in an *anti* glycosidic orientation (25, 26).

More complex structures and topologies can form from strands containing two guanine repeats separated by non-guanine nucleotides, for example $X_n G_o X_p G_o X_n$, where X_n is any non-guanine nucleotide of length n , G_o is any number of guanines involved in tetrad formation of length o , and X_p is any nucleotide of length p involved in loop formation. An oligonucleotide with these Guanine-rich regions can fold into a hairpin by the formation of Hoogsteen-type bonds between guanines belonging to different regions. The dimerization of a hairpin leads to the formation of a bimolecular G-quadruplex. The topology of these quadruplexes depends on which of the strands are connected together. The element linking the strands together can be diagonal, lateral (edgewise), or external (propeller, strand exchange, double-chain-reversal) to the quadruplex. These linking nucleotides are critical in determining quadruplex stability in term of length and sequence. An example of this type of G-quadruplex is provided by the fragment of the telomeric sequence of *Oxytricha*, $d(G_4T_4G_4)$ (Fig.8), which, from NMR studies in solution with Na^+ ions, revealed the ability to organize in a bimolecular G-quadruplex with diagonal loops (27).

A single G-rich oligonucleotide strand with the general sequence $X_n G_o X_p G_o X_p G_o X_p G_o X_n$, with X_n is any non-guanine nucleotide of length n , G_o is any number of guanines involved in tetrad formation of length o , and X_p is any nucleotide of length p involved in loop formation, may fold to form a monomolecular G-quadruplex structure with three loops. The folding topologies available to monomolecular quadruplex are more varied and complex than those available to the tetramolecular or bimolecular quadruplex due to the additional linking nucleotides. Loops generally force the strands of the structure to fit in antiparallel; An indicative example of this type of structure is given from the Thrombin-Binding Aptamer (TBA), $d(GGTTGGTGTGGTTGG)$ (Fig.9) (28). By NMR studies, it has been seen that in

solution this oligonucleotide forms a monomolecular quadruplex that is shaped like a chair, with two stacked G-quartets connected by two TT loops and a central 3-base TGT loop.

G-Qs can be also classified because of orientation of the strands and the connecting loops. G-Q structures possessing all the strands in the same orientation are parallel quadruplexes, while opposite orientation of the strands give rise to antiparallel or hybrid quadruplexes. In general, parallel quadruplexes have all the guanosine glycosidic angles in the *anti*-conformation, while antiparallel quadruplexes show both *anti* and *syn* glycosidic angles (Fig.10).

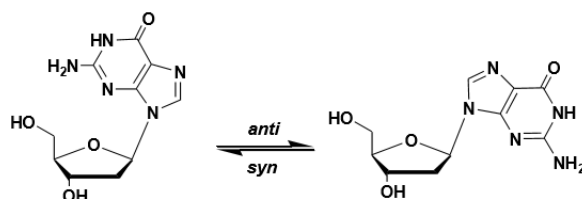


Figure 10: glycosidic bond conformations.

Regarding the connecting loops, propeller type loops are those which connect the bottom G-quartet to the top G-quartet of adjacent strands with the same orientation; lateral loops, also known as edge-wise loops, link adjacent strands, while diagonal loops join opposite strands (Fig.11).

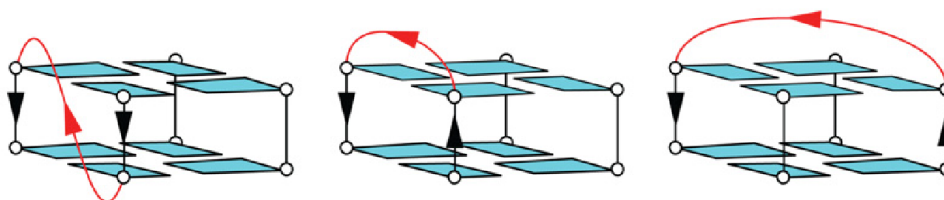


Figure 11: Propeller loops (left), lateral loops (center) and diagonal loops (right).

Finally, a fundamental role is played by the cations on the folding and thermodynamics of G-Qs (29) (Fig.12).



Figure 12: G-tetrad with the Metal Ion in the central cavity.

The cation and quadruplex interaction is based primarily on the kind of ion located at the central channel formed by the quartet arrangement. The positions of the ions can be in the quartet plane or between the planes of the quartet depending on the ion and the structure of the GQ. The ions contribute to charge screening, by reducing the strong negative electrostatic potential generated by the guanine O6 oxygen atoms. Molecular dynamics simulation studies suggest that lack of cations at the centre of the quartet destabilizes the GQ structure as it is electronically unfavourable.

For their physiological relevance, the most extensively studied ions are K^+ and Na^+ . Their different behaviour about their location within the cavity result from their dimension: the smaller sodium cations can reside in plane with the G-quartet, whereas potassium can coordinate between two tetrads. However, several other monovalent and divalent ions have also been shown to influence the structure and stability of GQs. Some of the very early studies on role of cations on the stability of GQ structures suggested the order as $\text{K}^+ > \text{Ca}^{2+} > \text{Na}^+ > \text{Mg}^{2+} > \text{Li}^+$ and $\text{K}^+ > \text{Rb}^+ > \text{Cs}^+$.

1.2.2 The biological role of G-Qs

G-quadruplex structures have attracted considerable interests because of their importance in regulating biological functions, such as gene expression, gene regulation, and in being pharmaceutical targets (30). The presence of thousands of sequences capable of forming G-Quadruplex structures in important regions of many genes, including the telomeric ends of eukaryotic chromosomes and promoter regions of genes and oncogenes, has been demonstrated, thus suggesting a possible role of the G-quadruplexes in the regulation of transcriptional and replicative processes. For instance, in human cells, the telomeric ends of chromosomes consist of a double-stranded repeat of G-rich sequence TTAGGG, and of a ~200-nt single-stranded G-rich overhang beyond the double-stranded region, which is able to assemble into G-quadruplex structures. During each round of chromosome replication, telomeres shorten by 50-200 base pair, until they reach a critical length below which the programmed death of the cell (or apoptosis) occurs. The ribonucleoprotein telomerase provides such a compensatory mechanism. Since somatic cells progressively undergo to a decrease of the telomerase expression, it follows that the shortening of

telomeres is at the base of the cell aging process. On the other hand, the telomerase enzyme is overexpressed in more than 85% tumours, so tumour cells have unlimited proliferative potential. Subsequently, small molecules able to induce or stabilise telomeric G-quadruplex structures have been studied for their ability to inhibit telomerase activity and act as anticancer agents (31). Therefore, the G-quadruplexes could be considered promising targets for the development of novel anti-tumour drugs.

Further interest in quadruple helix structures is due to the fact that they constitute the scaffold of many aptamers. Aptamers are small DNA or RNA molecules able to assume specific three dimensional structuring in order to achieve a very high binding affinity towards specific proteins, such as thrombin or some HIV proteins, thus demonstrating promising biological properties and possible pharmacological applications (32). Particularly, one of the most studied G-quadruplex-based aptamer class is that of thrombin-binding aptamers (TBAs), which bind to α -thrombin, a key protein involved in the clotting process, preventing the pathological process of thrombosis. It was also demonstrated that in this case the structuring in the G-quadruplex and its consequent stability, are essential requirements for the explication of biophysical and biological effects of TBA (33).

1.2.3 G-Qs and biotechnology.

1.2.3.1 G-Qs self-assembly.

In recent years, G-quadruplexes have become the focus of attention because they can be used as building blocks to create supramolecular structures. In fact, G-rich oligonucleotides are able to self-assemble into high-ordered structures by multimerization between G-quadruplex units (34).

Self-assembly of biological important small molecules into nanostructure has evolved as an attractive strategy for fabricating materials with a broad range of potential applications in catalysis, sensing, electronics, medical diagnostics and drug delivery.

In literature examples of polymeric species arising from quadruplex structures have already been reported. Several studies have shown that the G-quadruplex can give rise to supramolecular structures such as G-wires, in which each quadruplex building block is stacked one upon the other; the resulting superstructure grows along the axis orthogonal to G-tetrad planes and reaches the length of thousand nanometers (Fig.13).

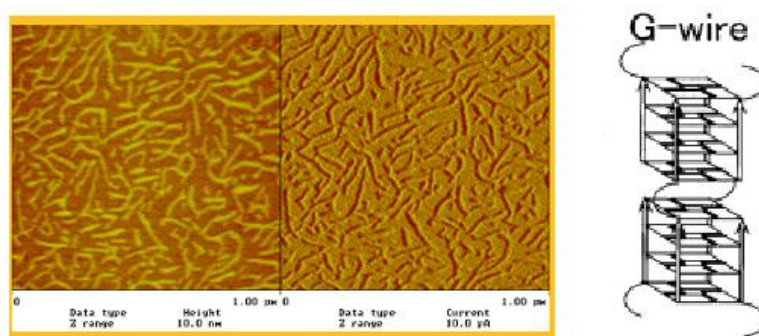


Figure 13: AFM images of G-wire and model of a typical G-wire.

Marsh and al., in 1994, showed that sequence $5'\text{GGGGTTGGGG}3'$, corresponding to telomeric repetition of *Tetrahymena Thermophila*, can assume different conformations (34, 35). The G-rich strand can fold and dimerize giving rise to the formation of a bimolecular G-Quadruplex with parallel, lateral opposite or diagonal loops. On the other hand, the oligomer may also associate with other three G-rich strands resulting in tetrameric structure. In this condition, the oligonucleotide can spontaneously self-assemble in high-ordered structures by interaction between deoxyguanosine quartets located at terminals 5' and 3' (Fig.14). Atomic force microscopy (AFM) and layer scanning microscopy (HLSTM) are among the most commonly used technique to investigate the formation of such polymers.

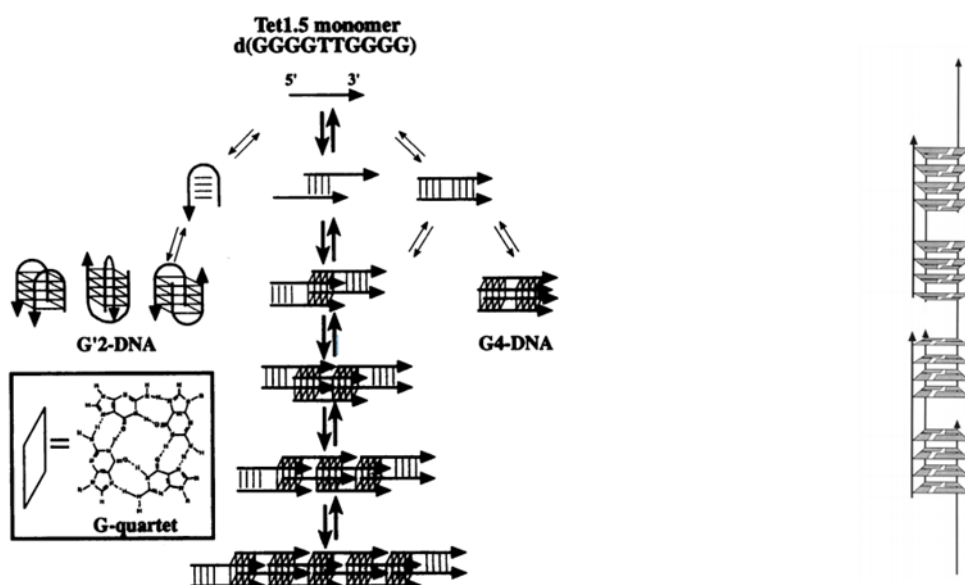


Figure 14: On the left, comparison of G-DNA conformations that Tet 1.5 may adopt and G-wire model on the right. Tet 1.5 adopts an out of register (slipped) tetrameric association forming G4-DNA domains stabilized by monovalent cations. The overlapping slipped G4-DNA structures are responsible for the formation of the G-wire.

More recently, the research group of Prof. Wu studied the geometrical size of $\text{Na}_2(5'\text{-GMP})$ supramolecular structures at pH 8 by a combination of diffusion NMR and DLS methods (36); In general, two distinct types of aggregate species are present in an aqueous solution of $\text{Na}_2(5'\text{-GMP})$. One type consists of stacking $5'\text{-GMP}$ monomers, and the other contains stacking G-quartets. Both types of aggregates can be modeled as rod-like cylinders. The cylinder diameter is 10 and 26 Å for monomer aggregates and quartet aggregates, respectively. For $\text{Na}_2(5'\text{-GMP})$ concentrations between 18 and 34 wt %, the cylinders formed by stacking G-quartets have an average length between 8 and 30 nm, corresponding to a stack of ~24-87 G-quartets (Fig.15).

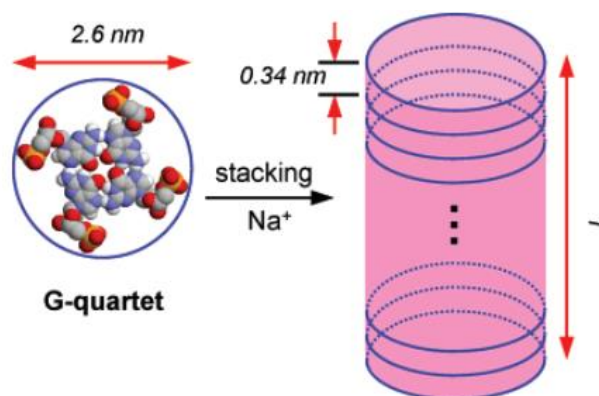


Figure 15: Schematic illustration of the molecular cylinder formed by Na₂-(5'-GMP) self-assembly.

Another possible way of forming higher aggregates is through an interlock mode as observed by Krishnan-Ghosh et al. (37): they demonstrated, by means of spectroscopic techniques, that a tetranucleotide sequence d(GGGT) has been shown to self-assemble into an interlocking quadruplex dimer; in particular the novel structure arose from the dimerization of a parallel, “slipped” tetramolecular quadruplex that has its diagonal strands staggered by one base. This “slippage” results in two guanine bases at the 5' end of the quadruplex being presented diagonally that are not involved in tetrads. Two such “slipped” quadruplexes dimerize via these free G-bases at the 5' ends by forming an extra G-tetrad (Fig.16).

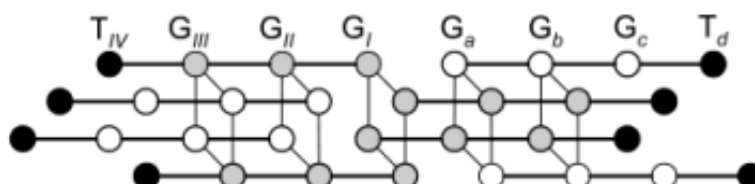


Figure 16: interlocked quadruplex formed by the dimerization of two staggered or “slipped” quadruplexes.

Nishigaki and Biyani proposed another model, tentatively called “G-Lego” for higher-molecular weight aggregates formed by the sequence d(G₁₁T) (38). In this model, the single strand loop back on itself to form a transient structure; Then, two of such folded monomers form a parallel or antiparallel/later or diagonal bimolecular G-quadruplex structure by sharing the hydrogen bonds between each pair of strands, thus constituting a starting unit of G-Lego (c). Next, the access of two of such unitary G-quartets may fall into a stable binding due to the unique contribution of terminal thymine-thymine interactions and thus may lead to rearrange their hydrogen bonding and thus associate to recombine and formed a tetramolecular parallel G-quadruplex (d). By continuing the same process, higher order aggregates can propagate linearly towards nano-structures like a modular toy “Lego” (Fig.17).

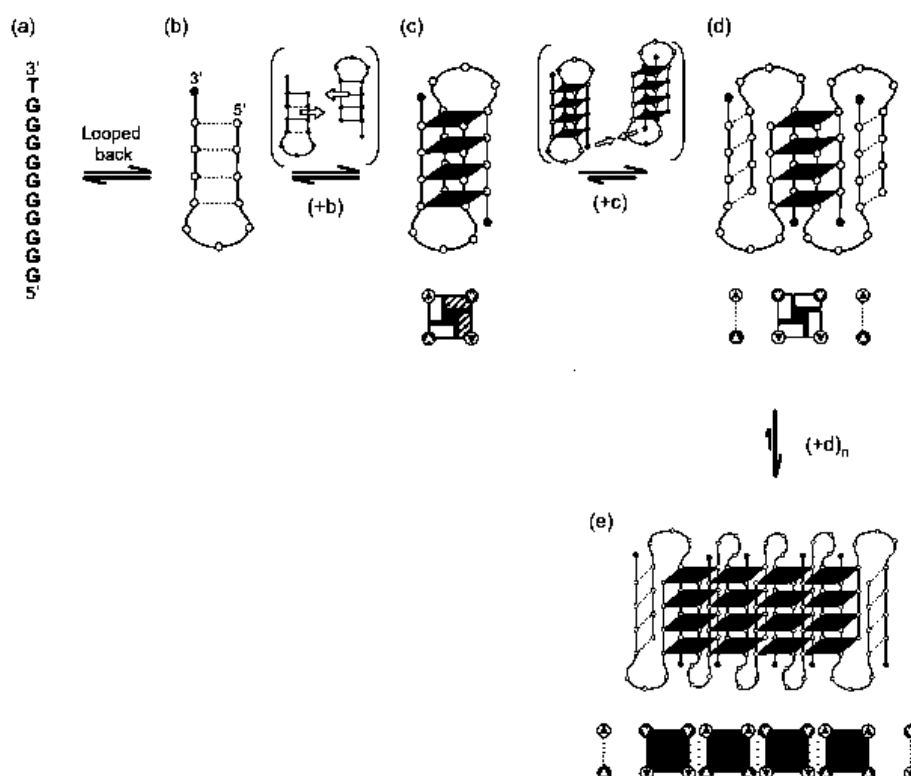


Figure 17: model for the g-Lego.

It has been demonstrated that such supramolecular structures are also extraordinarily stable; heating at 80 °C or dissolving in 8 M urea did not denature them (39). This one and other properties make the G-wires extremely interesting from a nanotechnological point of view. Theoretical studies suggest that they have good conductivity, low oxidative potential and are also equipped with a high rigidity and optimal thermal and mechanical stability that make them good candidates in the field nanotechnologies, nano-electronics and the development of biosensors.

1.2.3.2 Hydrogels

G-quadruplex multimerization could be extended to a fibrous network to form supramolecular hydrogels (40). In recent years, hydrogels have been applied extensively in the development of platforms for biomedical and bioengineering purposes. With a three-dimensional network, hydrogels can encapsulate a large amount of cargos, protect the cargos from environmental variations, and/or control cargo release by designing the gel structure in response to microenvironment variations. Stimuli-sensitive hydrogels are ideal candidates for developing self-regulated drug-delivery and -release systems. For many years, hydrogels have been generally developed by using long and complex procedures, and once produced, the release of the cargo didn't exhibit a constant rate, but a two-step release profiles. In a very recent work, Shi and co-workers suggested the construction of a new G-quadruplex based hydrogel (Fig.18).

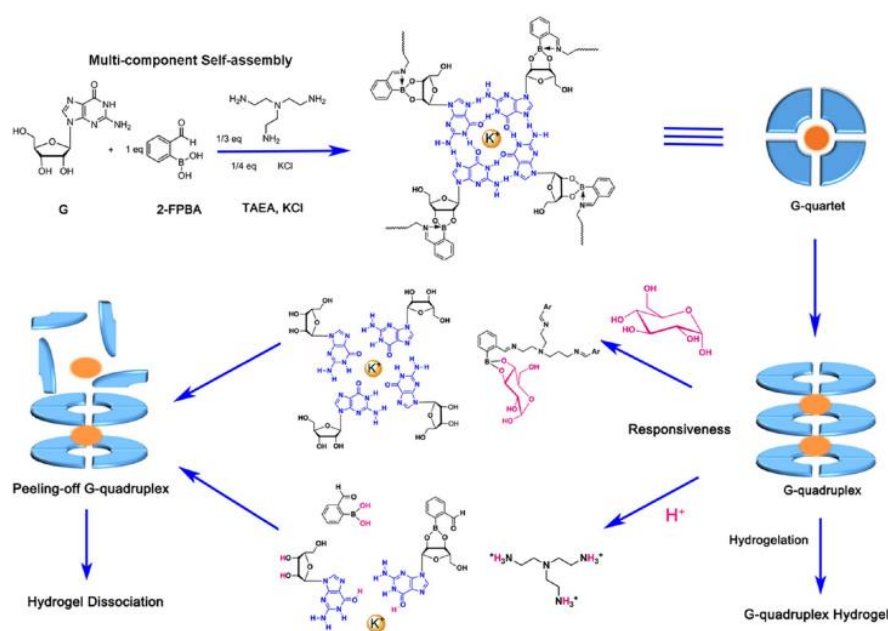


Figure 18: Schematic Representation of the multicomponent Self-Assembly of Guanosine, 2-FPBA, TAEA, and KCl and the Dissociation of the G-Quadruplex Hydrogels.

In particular, in this work, they developed supramolecular G-quadruplex hydrogels by multicomponent self-assembly of guanosine, TAEA, and 2-FPBA. On the basis of the formation of a G-quartet via Hoogsteen-type hydrogen bonding among four guanosines mediated by potassium cations, the stacking of G-quartets and the iminoboronate bonds spontaneously and synergistically formed among guanosine, Tris(2-aminoethyl)amine (TAEA), and 2-formylphenylboronic acid (2-FPBA). The iminoboronate bonds contribute to facilitate the formation of the hydrogel and also endowed it with glucose and acid responsiveness. This kind of supramolecular G-quadruplex hydrogel formed by multicomponent self-assembly of small molecules with features of versatility and commercial availability of building blocks, pH and glucose-responsiveness, and zero-order drug-release behaviour may be a promising candidate for application in biological fields.

1.2.3.3 Biosensors

Not less important in the field of nanotechnology is the use of G-quadruplexes for the development of biosensor. Biosensors are analytical tools that combine biological materials, such as proteins, DNA/RNA and other selective chemicals to physicochemical signal transducer.

An example of the use of G-quadruplex-based sensor was furnished by Takenaka's group (41) (Fig.19). They used a modified TBA as a fluorescent indicator for detecting K^+ in water, by anchoring pyrene groups to the 5' and 3' ends to the TBA sequence; the probe that they obtained was coined "Potassium Sensing Oligonucleotides (PSO)-py". The mechanism that makes the biosensor work is very simple: in the absence of K^+ , the PSO-py is in the unfolded state, so it provides only a little excimer emission, while in the presence of K^+ , the 5' and 3' ends of the folded DNA stacks pyrenes in a face-to-face geometry to give a new excimer band. This system represents a promising sensor for the real-time detection of K^+ in biological and environmental samples, due to its simplicity, high-responsiveness, and

selectivity. In fact, the presence of other cations gives only little interferences, since K^+ binds with high affinity to the TBA G-quadruplex.

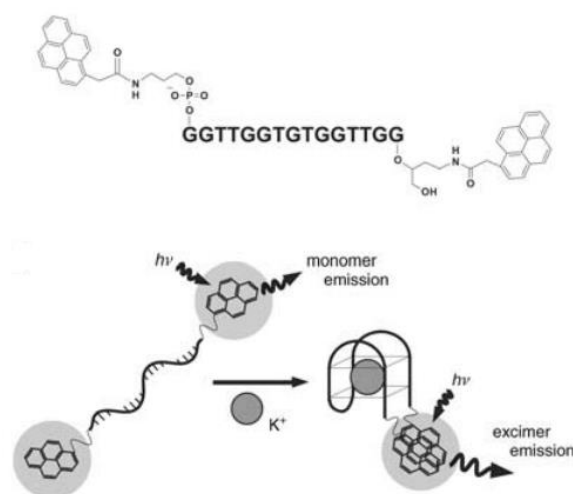


Figure 19: Chemical structure of the PSO-py and the expected G-quadruplex induced by potassium binding. Pyrene excimer emission occurs in the presence of potassium.

1.2.3.4 Conjugation to Gold-nanoparticles (AuNPs).

G-quadruplexes have also been conjugated with metallic nanoparticles producing more sensitive biosensors. In this frame, the gold nanoparticles (GNPs) have resulted very attractive as a colorimetric indicator. In fact, they have a high extinction coefficients and distance-dependent optical properties. The colour of the GNP suspension is greatly affected by the particle stability and inter-particle distance. For example, the dispersed GNPs give wine-red suspensions, while their aggregation produces a blue-purple colour. For example, as reported in literature, by connecting AuNPs (as probes) and suitable G-rich fragments (as the recognition element) is possible to obtain a rapid, simple, high sensitive and excellent selective sensor for the determination of K^+ , exploiting the conformation change from the "random coil" to a compact rigid G-quadruplex formed by the aggregation of the nanoparticles in solution. In the work of Chen et al. potassium ions (K^+) were detected by gold nanoparticles (AuNPs) (Fig.20). To assay for K^+ ions, the thiolated aptamers were conjugated to AuNPs separately via the strong Au-S bond. In the absence of K^+ , the aptamer-modified AuNPs dispersed well in the solution, and the G-rich nucleic acid was in the random coil state. However, once a solution containing K^+ was introduced, K^+ could specifically bind to the aptamer and induced the aptamer-AuNPs switching from a well dispersed state to an aggregated one, resulting in a change in the UV-vis absorption spectra of the solution. The linear range of the colorimetric aptasensor covered a large variation of K^+ concentration from 5 nM to 1 μ M and the detection limit of 5 nM was obtained. Moreover, this assay was able to detect K^+ with high selectivity and had great potential applications (42).

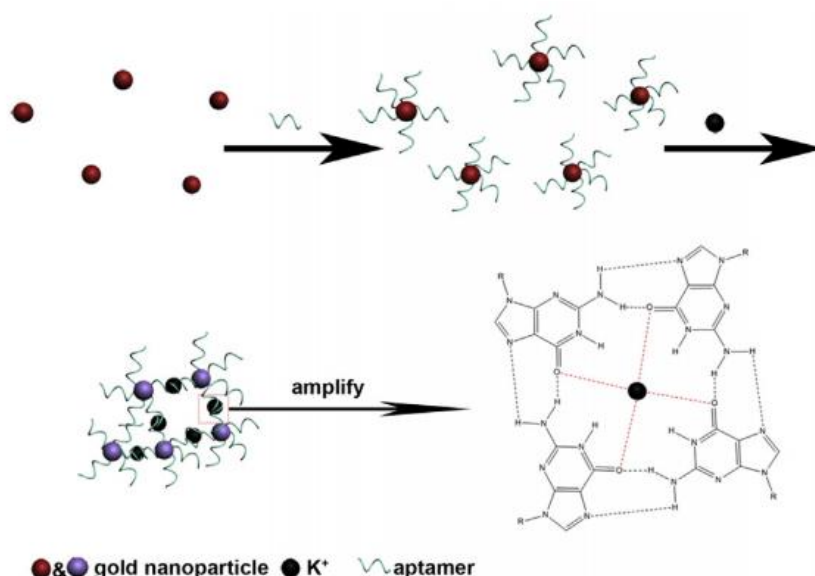


Figure 20: Schematic diagram showing the principle of colorimetric detection of potassium ions using aptamer-functionalized gold nanoparticles. The gold particles are represented in two colours to demonstrate the colour change observed after addition of K^+ .

1.2.3.5 Nanomachines

Another intriguing application of G-quadruplex in biotechnology is the development of “DNA nanomachines”: DNA nanomachines are nanorobots made entirely or partially of DNA. DNA nanomachines can switch among defined molecular conformations and can be used as sensing, computing, actuating or therapeutic nanodevices. For instance, Quadruplex structures comprise a wide class of well-defined conformational states. Their conformation and stability can be tuned by varying the sequence and/or the length sequences, by modifying different solution conditions, such as salt composition or pH, or by using small molecules that specifically bind to them (43). Furthermore, the G-quadruplex based machine exhibits a rapid response in comparison to using highly expensive instruments and complicated sample preparation (44). For example, Alberti and Mergny, by using the FRET techniques, demonstrated the conformational equilibrium between the duplex DNA and the G-quadruplex DNA. They defined a nanomachine. This nanomachine could be cycled between the folded G-quadruplex state and the duplex by sequential addition of DNA strands, the so-called “C-fuel” and “G-fuel”: the C-fuel extends the F21T quadruplex to generate a duplex conformation, while by adding the G-fuel, the C-fuel is removed from F21T that can refold in a quadruplex form (Fig.21).



Figure 21: Principle of the device and sequence of the oligomers with The Tm of the two duplexes.

1.3 Oligonucleotide analogues.

Nucleic acids are subjected to several chemical base modifications *in vivo*, such as methylation or phosphorylation, in order to obtain derivatives endowed of precise cellular functions. Inspired by nature, and moved by the aim to develop molecules with improved features, very soon, synthetic chemists realized the necessity of including chemical modifications to ODNs. In fact, ODNs are susceptible to nucleases, and so unstable in biological fluids; for these reasons their use for therapeutic applications has been limited. Furthermore, the effective delivery of oligonucleotides *in vivo* represents the major challenge for the scientific community.

The introduction of the phosphorothioate modification by Fritz Eckstein in 1966 is arguably one of the most important contributions to the field of therapeutic ODN (45). Nowadays, various chemically modified oligonucleotides have been synthesized (46); they incorporate modifications not only to the phosphodiester backbone (first generation of analogues), but also to the sugar (second generation of analogues) or nucleobases portions. Not less important is the third generation of analogues, that includes Locked Nucleic Acids (LNAs), morpholinos and Peptide Nucleic Acids (PNAs). In particular, PNAs have revealed themselves as the most powerful and intriguing ODN analogues having a variety of biotechnological application. They were developed by the biochemist Peter Nielsen in 1991 (47). PNAs are DNA/RNA mimic in which the phosphate deoxyribose backbone is replaced by uncharged N-(2-aminoethyl)-glycine linkages (Fig.2).

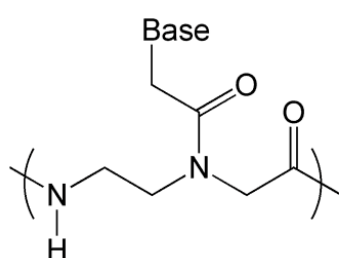


Figure 2: structure of PNA

Nucleobases, attached through methylene carbonyl linkages to the glycine amino group, recognize complementary sequences by standard Watson-Crick pairing. Because PNAs have a neutral backbone, hybridization doesn't suffer the intra-strand repulsion and, on the contrary, it occurs with enhanced affinity and rates of association. Moreover, PNA doesn't seem to be substrates for nucleases or proteases and absence of a repetitive charged backbone also prevents PNA from binding to proteins that normally recognize polyanions, avoiding a major source of nonspecific interactions (48, 49). They have been synthesized through the selective alkylation at the N9 position of the purine or the N1 position of the pyrimidines, as showed in Figure 3.

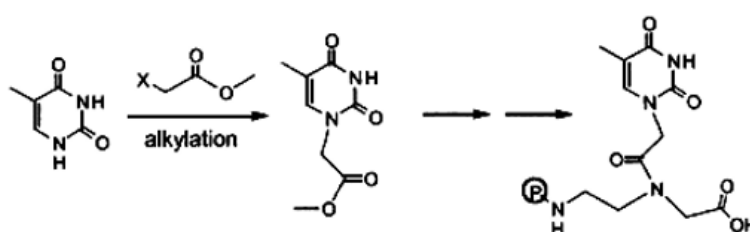


Figure 3: key steps in the chemical synthesis of PNA monomer.

Due to the peptide nature of its backbone, the PNA subunits are generally assembled through the well-established Solid Phase Peptide Synthesis (SPPS) protocols and can be easily performed on automated synthesizers.

PNAs hybridize with complementary DNA and RNA strands to form right-handed, double-helical complexes based on the Watson–Crick rules. Because the PNA backbones do not bear negatively charged phosphate groups, they are not affected to charge repulsion and the formed complexes own higher thermal stabilities than DNA counterparts (50). It is also known that the PNAs recognize and bind complementary strands in both directions, parallel and antiparallel. In the antiparallel-type hybridization, PNA amino termini face the 3'-end of the DNA strand, whereas PNA amino termini face the 5'-end of the purine DNA strand in the parallel-type hybrids (51). From a thermodynamic point of view, the antiparallel binding mode is preferred.

Furthermore, homopyrimidine PNA oligomers form triplex complexes. These complexes are extremely stable and contain an internal PNA–DNA–PNA triplex involving combined Hoogsteen (parallel orientation) and Watson–Crick (anti-parallel orientation) base pairing and an unbound DNA strand displaced in a D-loop structure (52).

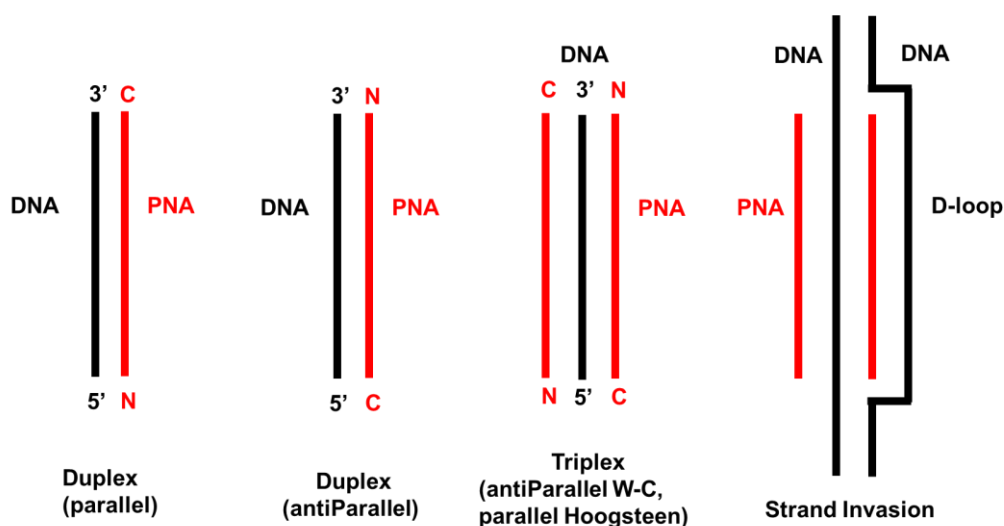


Figure 4: PNA-DNA binding mode.

Due to their notable properties, such as high chemical and thermal stability, resistance to enzymatic degradation as well as the very favourable RNA and DNA hybridization properties, they have been exploited in a variety of contexts, including the antigene and antisense strategy, diagnostic applications and, more recently, as aptamers.

1.4 G-quadruplexes from Synthetic ODN analogue

G-quadruplexes can also form from oligonucleotide analogues.

Among all the ODN analogues, Peptide Nucleic Acid (PNA) represent the most fascinating derivative; in PNA the anionic phosphate backbone is replaced by neutral N-(2-aminoethyl) glycine linkages. For its hybrid nature, PNA have widespread application in many areas of molecular biology.

To date, in literature only few papers report the characterization of complex PNA-based quadruplex and the study of the ability of PNA to form G-quadruplexes represents a challenging field for many researchers. For example, Armitage and colleagues demonstrated that PNA strands can invade DNA G-quadruplex to form hybrid PNA₂-DNA₂ G-quadruplexes (53). For instance, FRET measurements using labelled polymers indicated that strands were organized such that the two DNA strands are parallel with each other and the 5'-ends of the DNA point in the same direction as the N-Termini of the PNA strands. Furthermore, they also observed, from the CD melting profile, that the hybrid G-quadruplex had a faster association kinetics compared to the natural counterpart, and it was probably due to the lack of negative charges along the PNA backbone and to the electrostatic attraction of the positively charged PNA and the anionic DNA (Fig.22).

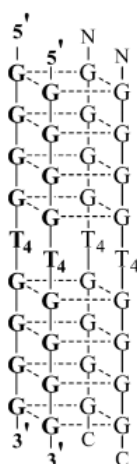


Figure 22: Possible structure of a PNA₂-DNA₂ hybrid quadruplex.

After Armitage's paper, Balasubramanian and co-workers reported the formation of intermolecular G-quadruplex composed only of four short PNA strands that aligned in an anti-parallel fashion (54). Later Armitage showed that also longer sequences were able to form either a four-stranded G-q or a two stranded hairpin dimer (55).

Most recently Giancola and colleagues described the formation of a G-q formed by chimeras sequences that contain a single PNA residue at the end of a ODN strand (Fig.23). They also demonstrated that the chimeras were more stable of the natural counterparts (56).

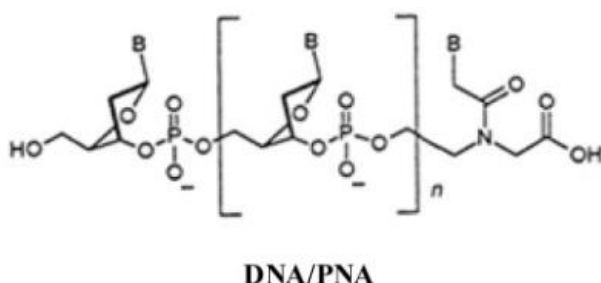


Figure 23: Structure of DNA/PNA Chimera

Altering the polymer backbone, it is possible new G-quadruplexes with a variety of potential applications in supramolecular chemistry, biotechnology and nanotechnology. In addition, studies on ODN analogues may lead to a deeper knowledge amount G-quadruplex potential and may clarify the structural factors that control issues about the thermodynamics and kinetics of the G-quadruplex motif in the parent DNA.

1.5 Aim of my research

My project is included in this wide context and it is aimed at exploiting the several features and applications of oligonucleotides and analogues. In particular, my research activity is devoted to unravel the use of oligonucleotides and oligonucleotide analogues in a broad

range of fields, which includes the development of new approaches for the simple construction of biosensors and the development of novel drug candidates to gene regulation. Specifically, my research activity is focused on the synthesis and characterization of suitable G-rich oligonucleotides able to form supramolecular structures, the synthesis and characterization of new PNA sequences for the development of an innovative approach to the treatment of Cystic Fibrosis, and, finally, the synthesis and characterization of a PNA Quadruplex for the construction of new K^+ sensing probes.

Objective 1. Supramolecular structures from G- Quadruplex

This part of the PhD research program was focused on the synthesis of suitable G-rich oligonucleotides and on of their ability to form supramolecular structures. The formation of high-ordered aggregates should depend by the cation species, temperature, pH, concentration, sequence, length and polarity of the G-rich ON employed. In this frame, the study of all the necessary conditions for the structuring of polymeric species arising from G-quadruplexes remain a big challenge in the field of self-assembly.

Recently, in the research group of Professor Piccialli, it was proved that the sequence CGGXGGT (where X = T, A, C or G) can form a nanostructure of about 4 nm in length, consisting of eight well organized strands. This octamer formation takes place through a dimerization process, which is allowed by the 5'-5' stacking of two tetramolecular G-quadruplex subunits, and assisted by the formation of an unusual G(:C):G(:C):G(:C):G(:C) octad arrangement, involving C1 and G2 bases of each CGGXGGT strand. In this context, my PhD work has been focused on the synthesis of a novel G-rich sequence and on the study of its ability to form supramolecular structures, with the aim to obtain long G-wires poly-(Q)_n like.

Objective 2. Peptide Nucleic Acid (PNA) as fascinating tool in gene regulation.

Encouraged by the positive results given by PNAs, we decided to explore the several properties of this molecules in a biological context, by synthesizing new PNA sequences, 13 and 7 bases long, complementary to a sequence within the promoter of the CFTR gene. The aim of our work is to clarify the role of PNAs as new therapeutic agents for all the Cystic Fibrosis (CF) cases characterized by mutations that do not completely abolish the protein function, with the final goal to improve or resolve a severe CF phenotype by virtue of the increased expression of the protein and the increased chloride flow.

Objective 3. Peptide Nucleic Acid (PNA) for the construction of new PNA-based Quadruplex scaffold.

In this context, the aim of my work was to carry on the investigation the infinite potential of PNAs, this time not only from a biological point of view, but considering its ability to form new PNA-based quadruplex, useful for the construction of new nanomaterials. The approach envisaged the preliminary synthesis of a new type of ambident linker, then functionalized by short sequences of G-rich sequences of PNA. Through the use of spectroscopic techniques, the ability of that molecule to form quadruplex structures was then evaluated. This work is aimed at obtaining new types of sensors.

1.6 References

1. Rich, A. (1993) DNA comes in many forms. *Gene*, 135, 99–109.
2. Kwok, C.K. and Merrick, C.J. (2017) G-Quadruplexes : Prediction , Characterization , and Biological Application. *Trends Biotechnol.*, xx, 1–17.
3. Zamecnik, P.C. and Stephenson, M.L. (1978) Inhibition of Rous sarcoma virus replication and cell transformation by a specific oligodeoxynucleotide. *Biochemistry*, 75, 280–284.
4. Gewirtz, A.M., Sokol, D.L. and Ratajczak, M.Z. (2013) Nucleic Acid Therapeutics: State of the Art and Future Prospects. *Blood*, 92, 712–736.
5. Roehr, B. (1998) Fomivirsen approved for CMV retinitis. *J. Int. Assoc. Physicians AIDS Care*, 4, 14–6.
6. Hair, P., Cameron, F. and McKeage, K. (2013) Mipomersen sodium: First global approval. *Drugs*, 73, 487–493.
7. CROOKE, S.T. (1998) Vitravene™—Another Piece in the Mosaic. *Antisense Nucleic Acid Drug Dev.*, 8, vii–viii.
8. D.Praseuth, A.L.Guieysse and C.Hélène (1999) Triple helix formation and the antigene strategy for sequence-specific control of gene expression. *Biochim. Biophys. Acta - Gene Struct. Expr.*, 1489, 181–206.
9. Jiehua Zhou and John Rossi (2017) Aptamers as targeted therapeutics: current potential and challenges. *Nat. Rev.*, 16, 181–203.
10. Ng, Eugene W. M.; Shima, David T.; Calias, Perry; Cunningham, Emmett T. Jr.; Guyer, David R. ; Adamis, A.P. (2006) Pegaptanib, a targeted anti-VEGF aptamer for ocular vascular disease. *Nat. Rev.*, 5, 123–132.
11. Bryan, T.M. and Baumann, P. (2011) G-Quadruplexes: From Guanine Gels to Chemotherapeutics. *Mol. Biotechnol.*, 49, 198–208.
12. Gellert, I., Lipsett, M.N. and Davies, D.R. (1962) HELIX FORMATION BY GUANYLIC ACID. *Proc Natl Acad Sci U S A*, 48, 2013–2018.
13. Siddiqui-Jain, A., Grand, C.L., Bearss, D.J. and Hurley, L.H. (2002) Direct evidence for a G-quadruplex in a promoter region and its targeting with a small molecule to repress c-MYC transcription. *PNAS*, 99, 11593–11598.
14. Bochman, Matthew L.; Paeschke, Katrin; Zakian, V.A. (2012) DNA secondary structures: stability and function of G- quadruplex structures. *Nat Rev Genet*, 13, 770–780.
15. Maizels, N. (2006) Dynamic roles for G4 DNA in the biology of eukaryotic cells. *Nat. Struct. Mol. Biol.*, 13, 1055–1059.
16. Drygin, D., Siddiqui-Jain, A., O'Brien, S., Schwaebe, M., Lin, A., Bliesath, J., Ho, C.B., Proffitt, C., Trent, K., Whitten, J.P., *et al.* (2009) Anticancer Activity of CX-3543: A Direct Inhibitor of rRNA Biogenesis. *Cancer Res.*, 69, 7653–7661.
17. Kumari, S., Bugaut, A., Huppert, J.L. and Balasubramanian, S. (2007) An RNA G-quadruplex in the 5' UTR of the NRAS proto- oncogene modulates translation. *Nat Chem Biol*, 3, 218–221.
18. Wieland, M. and Hartig, J.S. (2007) RNA Quadruplex-Based Modulation of Gene Expression. *Chem. Biol.*, 14, 757–763.
19. Biffi, G., Tannahill, D., McCafferty, J. and Balasubramanian, S. (2013) Quantitative visualization of DNA G-quadruplex structures in human cells. *Nat. Chem.*, 5, 182–6.
20. Zimmerman, S.B. (1975) An 'Acid' Structure for Polyriboguanilyc Acid Observed by X-Kuy Diffraction. *Biopolymers*, 14, 3–4.
21. Burge, S., Parkinson, G.N., Hazel, P., Todd, A.K. and Neidle, S. (2006) Quadruplex DNA: Sequence, topology and structure. *Nucleic Acids Res.*, 34, 5402–5415.
22. Yaku, Hidenobu; Fujimoto, Takeshi; Murashima, Takashi; Miyoshi, Daisuke; Sugimoto, N. (2012) Phthalocyanines: a new class of G-quadruplex-ligands with many potential applications. *Chem. Commun.*, 48, 6203–6216.

23. Wang,Y. and Patel,D.J. (1994) Solution structure of the Tetrahymena telomeric repeat d(T2G4)4 G-tetraplex. *J. Mol. Biol.*, 2, 1141–1156.
24. Keniry,M.A., Strahan,G.D., Owen,E.A. and Shafer,R.H. (1995) Solution Structure of the Na⁺ form of the Dimeric Guanine Quadruplex [d(G3T4G3)]₂. *Eur. J. Biochem.*, 233, 631–643.
25. Laughlan,G., Murchie,A., Norman,D., Moore,M., Moody,P., Lilley,D. and Luisi,B. (1994) The high-resolution crystal structure of a parallel-stranded guanine tetraplex. *Science* (80-.), 265, 520–524.
26. Phillips,K., Dauter,Z., Murchie,A.I.H., Lilley,D.M.J. and Luisi,B. (1997) The crystal structure of a parallel-stranded guanine tetraplex at 0.95Å resolution. *J. Mol. Biol.*, 273, 171–182.
27. Risitano,A. and Fox,K.R. (2003) Stability of Intramolecular DNA Quadruplexes: Comparison with DNA Duplexes. *Biochemistry*, 42, 6507–6513.
28. Qin,Y. and Hurley,L.H. (2008) Structures, folding patterns, and functions of intramolecular DNA G-quadruplexes found in eukaryotic promoter regions. *Biochimie*, 90, 1149–1171.
29. Bhattacharyya,D., Arachchilage,G.M. and Basu,S. (2016) Metal Cations in G-Quadruplex Folding and Stability. *Front. Chem.*, 4, 1–14.
30. Rhodes,D. and Lipps,H.J. (2015) G-quadruplexes and their regulatory roles in biology. *Nucleic Acids Res.*, 43, 8627–8637.
31. Kim,N., Piatyszek,M., Prowse,K., Harley,C., West,M., Ho,P., Coviello,G., Wright,W., Weinrich,S. and Shay,J. (1994) Specific association of human telomerase activity with immortal cells and cancer. *Science* (80-.), 266, 2011–2015.
32. O. Tucker,W., T. Shum,K. and A. Tanner,J. (2012) G-quadruplex DNA Aptamers and their Ligands: Structure, Function and Application. *Curr. Pharm. Des.*, 18, 2014–2026.
33. Avino,A., Fabrega,C., Tintore,M. and Eritja,R. (2012) Thrombin Binding Aptamer, More than a Simple Aptamer: Chemically Modified Derivatives and Biomedical Applications. *Curr. Pharm. Des.*, 18, 2036–2047.
34. Marsh,T.C., Vesenska,J. and Henderson,E. (1995) A new DNA nanostructure, the G-wire, imaged by scanning probe microscopy. *Nucleic Acids Res.*, 23, 696–700.
35. Marsh,T.G., Henderson,E., Marsh,T.C. and Henderson,E. (1994) G-Wires: Self-Assembly of a Telomeric Oligonucleotide, d(GGGTTGGGG), into Large Superstructures. *Biochemistry*, 33, 10718–10724.
36. Wong,A., Ida,R., Spindler,L., Wu,G., Kl,C., Engineering,M., Jamo,V., Ljubljana,S.- and Slo,V. (2005) Disodium Guanosine 5' -Monophosphate Self-Associates into Nanoscale Cylinders at pH 8: A Combined Diffusion NMR Spectroscopy and Dynamic Light Scattering Study. *J. CHEM. SOC., CHEM. COMMUN*, 10.1021/ja042794d.
37. Krishnan-Ghosh,Y., Liu,D. and Balasubramanian,S. (2004) Formation of an Interlocked Quadruplex Dimer by d(GGGT). *JACS*, 126, 11009–11016.
38. Biyani,M. and Nishigaki,K. (2005) Structural characterization of ultra-stable higher-ordered aggregates generated by novel guanine-rich DNA sequences. *Gene*, 364, 130–138.
39. Sun,H., Xiang,J., Zhou,Q., Yang,Q., Xu,G. and Tang,Y. (2010) Temperature-sensitive supramolecules self-assembled by G-quadruplex DNA. *Int. J. Biol. Macromol.*, 46, 123–125.
40. Li,Y., Liu,Y., Ma,R., Xu,Y., Zhang,Y., Li,B., An,Y. and Shi,L. (2017) A G - Quadruplex Hydrogel via Multicomponent Self-Assembly: Formation and Zero-Order Controlled Release. *ACS Appl. Mater. Interfaces*, 9, 13056–13067.
41. Nagatoishi,S. and Nojima, Takahiko; Juskowiak, Bernard; Takenaka,S. (2005) A Pyrene-Labeled G-Quadruplex Oligonucleotide as a Fluorescent Probe for Potassium Ion Detection in Biological Applications. *Angew. Chemie - Int. Ed.*, 44, 5067–5070.

42. Chen,Z., Huang,Y., Li,X., Zhou,T. and Ma,H. (2013) Colorimetric detection of potassium ions using aptamer-functionalized gold nanoparticles. *Anal. Chim. Acta*, 787, 189–192.
43. Alberti,P., Bourdoncle,A., Saccà,B., Lacroix,L. and Mergny,J. (2006) DNA nanomachines and nanostructures involving quadruplexes. *Org. Chem.*, 4, 3383–3391.
44. Bagheryan,Z., Raoof,J.B. and Ojani; Reza,O. (2016) A switchable Gquadruplex device with the potential of a nanomachine for anticancer drug detection. *Int. J. Biol. Macromol.*, 83, 97–102.
45. Eckstein,F. (1966) Nucleoside Phosphorothioates. *J. Am. Chem. Soc.*, 10.1021/ja00970a054.
46. Verma,S. and Eckstein,F. (1998) MODIFIED OLIGONUCLEOTIDES: Synthesis and Strategy for Users. *Annu. Rev. Biochem*, 67, 99–134.
47. Nielsen,P.E. and Egholm,M. (1999) An Introduction to Peptide Nucleic Acid. *Curr. Issues Molec. Biol.*, 1, 89–104.
48. Corey,D.R. (1997) Peptide nucleic acids: Expanding the scope of nucleic acid recognition. *Trends Biotechnol.*, 15, 224–229.
49. Nielsen,P.E. (1999) Peptide nucleic acid. A molecule with two identities. *Acc. Chem. Res.*, 32, 624–630.
50. Giesen,U., Kleider,W., Berding,C., Geiger,A., Ørum,H. and Nielsen,P.E. (1998) A formula for thermal stability (T_m) prediction of PNA / DNA duplexes. *Current*, 26, 5004–5006.
51. Pfeffer,N.J., Hanvey,J.C., Bisi,J.E., Thomson,S.A., Hassman,C.F., Noble,S.A. and Babiss,L.E. (1993) Strand-invasion of duplex DNA by peptide nucleic acid oligomers. *Biochemistry*, 90, 10648–10652.
52. Hansen,M.E., Bentin,T. and Nielsen,P.E. (2009) High-affinity triplex targeting of double stranded DNA using chemically modified peptide nucleic acid oligomers. *Nucleic Acids Res.*, 37, 4498–4507.
53. Datta,B., Schmitt,C. and Armitage,B.A. (2003) Formation of a PNA 2 -DNA 2 Hybrid Quadruplex. *JACS*, 125, 4111–4118.
54. Krishnan-Ghosh,Y., Stephens,E. and Balasubramanian,S. (2004) A PNA 4 Quadruplex. *J. AM. CHEM. SOC*, 126, 5944–5945.
55. Datta,B., Bier,M.E., Roy,S. and Armitage,B.A. (2005) Quadruplex formation by a guanine-rich PNA oligomer. *J. Am. Chem. Soc.*, 127, 4199–4207.
56. Petraccone,L., Pagano,B., Esposito,V., Randazzo,A., Piccialli,G., Barone,G., Mattia,C.A. and Giancola,C. (2005) Thermodynamics and Kinetics of PNA-DNA Quadruplex-Forming Chimeras. *JACS*, 127, 16215–16223.

Chapter 2

Synthesis and characterization of new supramolecular structures from G-rich oligonucleotide sequences.

2.1 Introduction

In recent years, DNA and DNA-based polymers have attracted the researchers' attention for their versatile and programmable structure. In particular, in the field of nanotechnology and molecular electronics, double strand DNA (dsDNA) has been considered, for a long time, a promising building block for the construction of electronic devices, such as conductive wires, due to its self-assembling and molecular recognition properties and for its structure that allows the charge transport along the molecule (1, 2); on the other hand, recent studies on DNA-based systems failed, showing contradictory or irreproducible results (3). The possibility to develop advanced systems for the construction of DNA-based wires and devices remains a considerable challenge for all the scientific community.

Among all the possible systems, the most attracting candidate was embodied by G-quadruplexes for their ability to form higher-order assemblies by multimerization between several G-quadruplex units (4–7), confirming their use in the fields of nano-biomaterials and nano-biodevices (8–10). Several studies have shown that G-quadruplexes can give rise to supramolecular structures such as the most studied “interlocked slipped strands”, characterized by intercalation of g-rich strand oligonucleotides (11), and the “g-wires”, in which the quadruplex are piled one upon the other by end-to-end stacking (5); the resulting superstructure grows along the axis orthogonal to G-tetrad planes and reaches the length of thousand nanometers. These structures were extraordinarily stable; heating at 80 °C or dissolving in 8 M urea did not denature them (12). One of the identified structural moieties required for supramolecular assembly of G-quadruplexes is the presence of a stretch of guanines at the 5' or 3' termini of parallel G-quadruplex-forming GROs. The presence of even a single base other than G at 5' or 3' termini seems to prevent the dimerization (11).

Starting from these data, with a paper published on NAR (Nucleic Acid Research) on 2011, the research group of Professor Piccialli identified a novel dimerization pathway (13). In particular, they observed that the sequence 5'-CGGTGGT-3' is able to fold in a dimeric structure (2Q), that is a highly symmetrical octamer in which the 5'-end cytosine does not prevent the adhesive 5'-5' stacking and acts like an “hydrophobic glue” between the two G-quadruplex tetramers. The dimerization is allowed by head-to-head stacking between two unusual octads (Fig.1).

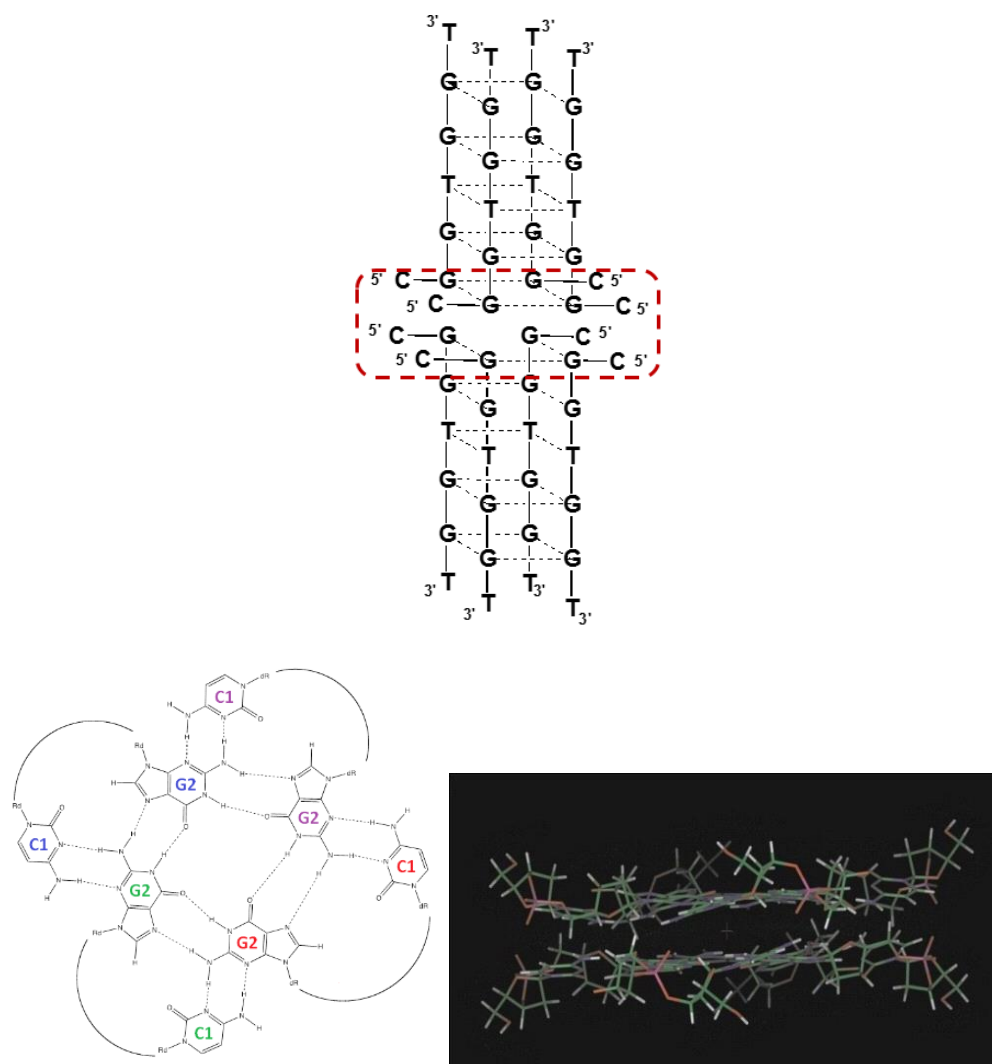


Figure 1: Structural model for the (dCGGTGGT)₈ octamer and proposed structure of the G₂(:C₁):G₂(:C₁):G₂(:C₁):G₂(:C₁) octad.

In another paper, they built a small library of G-rich oligonucleotide strands having the sequence XGTGYGGT and they demonstrated that, as well as in that case, the dimerization occurred and the monomeric quadruplexes formed by d(XGTGYGGT)₄ strands formed stable quadruplex dimer 2Q-like, especially when X= C or T and Y= T or A (14).

The aim of my research work is included in this context. The basic idea is to create a stable monomeric G-quadruplex having two 5'-CG ends able to polymerize using its two 5'-sticky ends and thus to obtain long g-wires like poly-(Q)_n exploiting the 5'-5' π-stacking between G(:C) G(:C) G(:C) G(:C) octads formed by 5'-CG ends. So, the 7-mer d(5'-CGG-3'-3'-TGGC-5') containing a 3'-3' phosphodiester bond that reverse the polarity in the strand thus creating two 5'-ends, has been synthesized. Thanks to several analytical techniques, such as Nuclear Magnetic Resonance (NMR), Size Exclusion Chromatography (SEC analysis), Circular Dichroism (CD) and PAGE, it has been proved that the 7-mer formed the quadruplex monomeric building block that was able to form long G-wires (Fig.2).

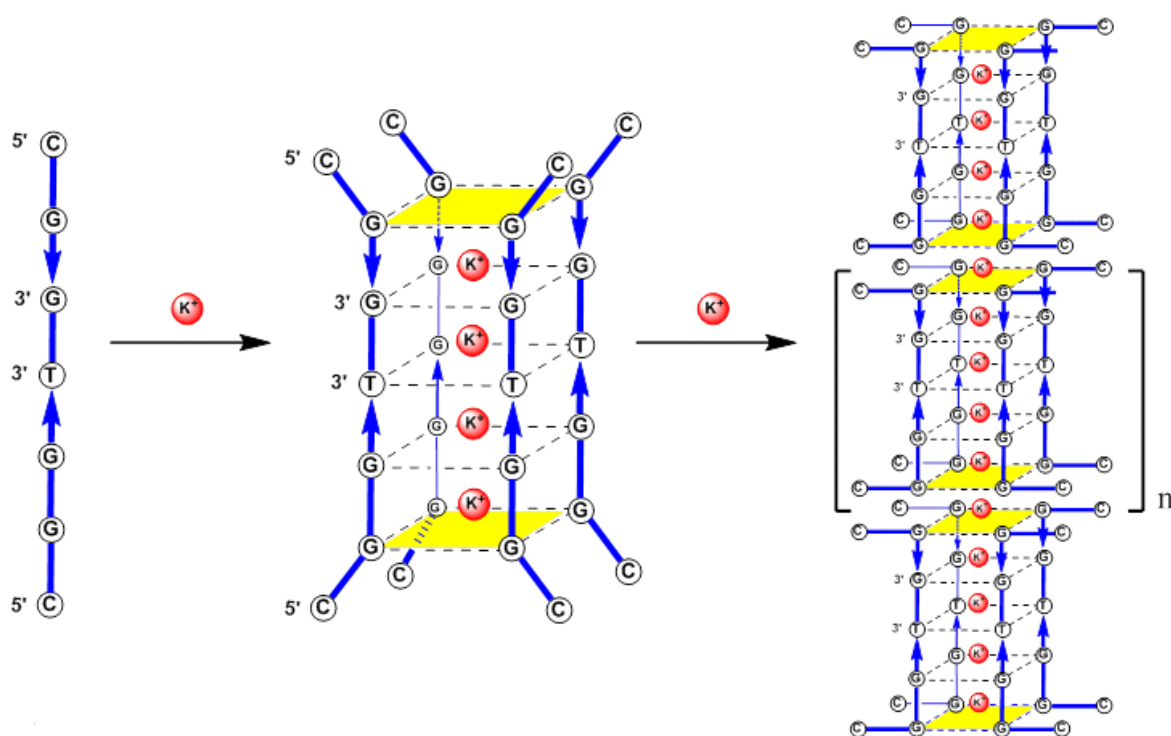


Figure 2: Formation of the G-quadruplex building block Q1 and its multimerization into Qn G-wire polymers starting from the ODN 5'-CGG-3'-3'-TGGC-5'.

2.2 Results and discussion

The first step required the synthesis of the 7-mer d(5'-CGG-3'-3'-TGGC-5') that contains a 3'-3' phosphodiester bond that reverse the polarity in the strand thus creating two 5'-sticky ends. It has been synthesized by using the solid-phase DNA automated synthesis following the standard b-cyanoethyl phosphoroamidite protocols. The inversion of polarity has been realized by using different phosphoramidites: the 5'-phosphoramidites have been used for the first four coupling steps, while the 3'-phosphoramidites have been used for the remaining steps. After the synthesis and the purification, the target sequence has been dissolved in K⁺ 1.0 M and subjected to annealing procedure. Its ability to form G-quadruplex or G-wires superstructure has been so assessed by means of PAGE and SEC-HPLC analysis and spectroscopic techniques.

2.2.1 Page

In order to get information about the propensity of the sequence 5'-CGG-3'-3'-TGGC-5' to fold into a monomeric G-quadruplex (Q1) building block and thus into a polymeric structure poly-Q type, PAGE experiments have been performed.

On the following Table, all the samples loaded in the gel have been reported, while Figure 3 shows the PAGE containing the 7-mer sequence in 1.0 M K⁺ buffer, (lane 3) in comparison with d(TG₄T) (lane 1) in 1.0 M K⁺ buffer, used as the size marker of a tetramolecular monomeric quadruplex, and d(CGGTGGT) (lane 2) in 1.0 M K⁺ buffer, used as the size marker of a dimeric quadruplex. The 7-mer sequence (lane 3) migrated like a ladder of bands in which the fastest moving band showed the same rate of migration as the monomeric in

lane 1 and the 2nd fastest band migrated with the same mobility as the dimeric quadruplex in lane 2. The remaining slower bands, in lane 3, pointed to the presence of multimeric species the size of which can be approximately evaluated by comparison with single strand oligonucleotides used as the size markers (lane 8).

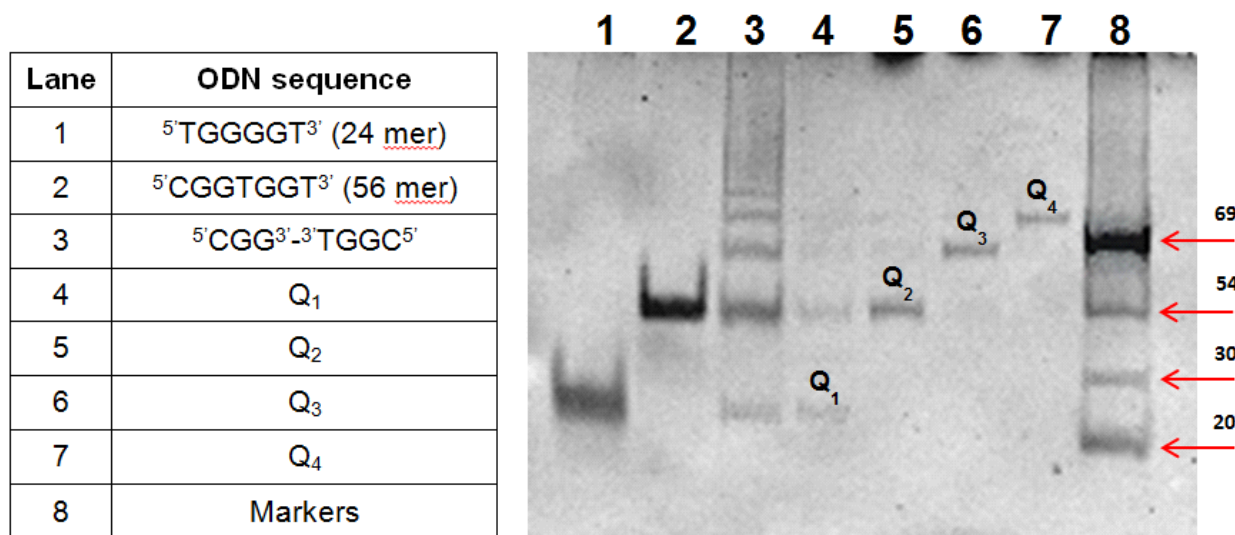


Table 1: List of all the samples loaded on the PAGE.

Figure 3: Electrophoretic mobility of the ODNs under study annealed in 1.0M K⁺ buffer.

It should be noted that the distance between the two fastest bands of the multimeric mixture in lane 3 corresponded to about 32-24 nucleotides (nts) considering the nucleotide composition of the markers in lanes 1 and 2 and the oligonucleotide ladder in lane 8. These data should exclude the formation of G-wire multimers formed by slipped G-rich strands. In fact, in that case the sequential addition of the G-rich 7-mer sequence, would have produced closer bands having only 7 nucleotides in migration distance.

The lanes 4-7 contained the multimeric species isolated by HPLC Size Exclusion Chromatography (Figure 5 and related discussion). In particular, the products in lanes 4-7 corresponded respectively with the monomeric quadruplex (Q₁, lane 4), dimeric quadruplex (Q₂, lane 5), trimeric quadruplex (Q₃, lane 6), and tetrameric quadruplex (Q₄, lane 7).

The whole PAGE data suggested that the 7-mer sequence, could self-assemble in multimeric species, like poly-Q_n, due to the sequential aggregation of a quadruplex building block by using its two “adhesive” 5'-CG terminal faces.

2.2.2 SEC analysis

The 7-mer, annealed in 1.0 M of K⁺ buffer at single strand concentration of 0.1 mM has been analyzed by Size Exclusion Chromatography (SEC-200 Column) and the HPLC profile has been reported in Figure 5. The annealed 7-mer migrated as a distribution of product-peaks in the range 15-22 min in which the species of low molecular weight (m.w.) had greater retention times. To obtain information on the m.w. of the analyzed species, the single strand dT7, the monomeric quadruplex d(TG₄T) and the dimeric quadruplex d[(CGGTGGT)₄]₂ have

been used as size markers (Fig.5). On the basis of the retention times it appeared that in the profile of multimerization products the wide peak at higher retention time could be attributed to the single strand 7-mer and the two peaks before could be assigned to a monomeric and dimeric quadruplex (Q_1 and Q_2). The slight difference in retention time between the quadruplex $d(TG_4T)_4$ and Q_1 could be attributed to the lower m.w. of the former (24 nts) compared to the Q_1 containing 28 nts.

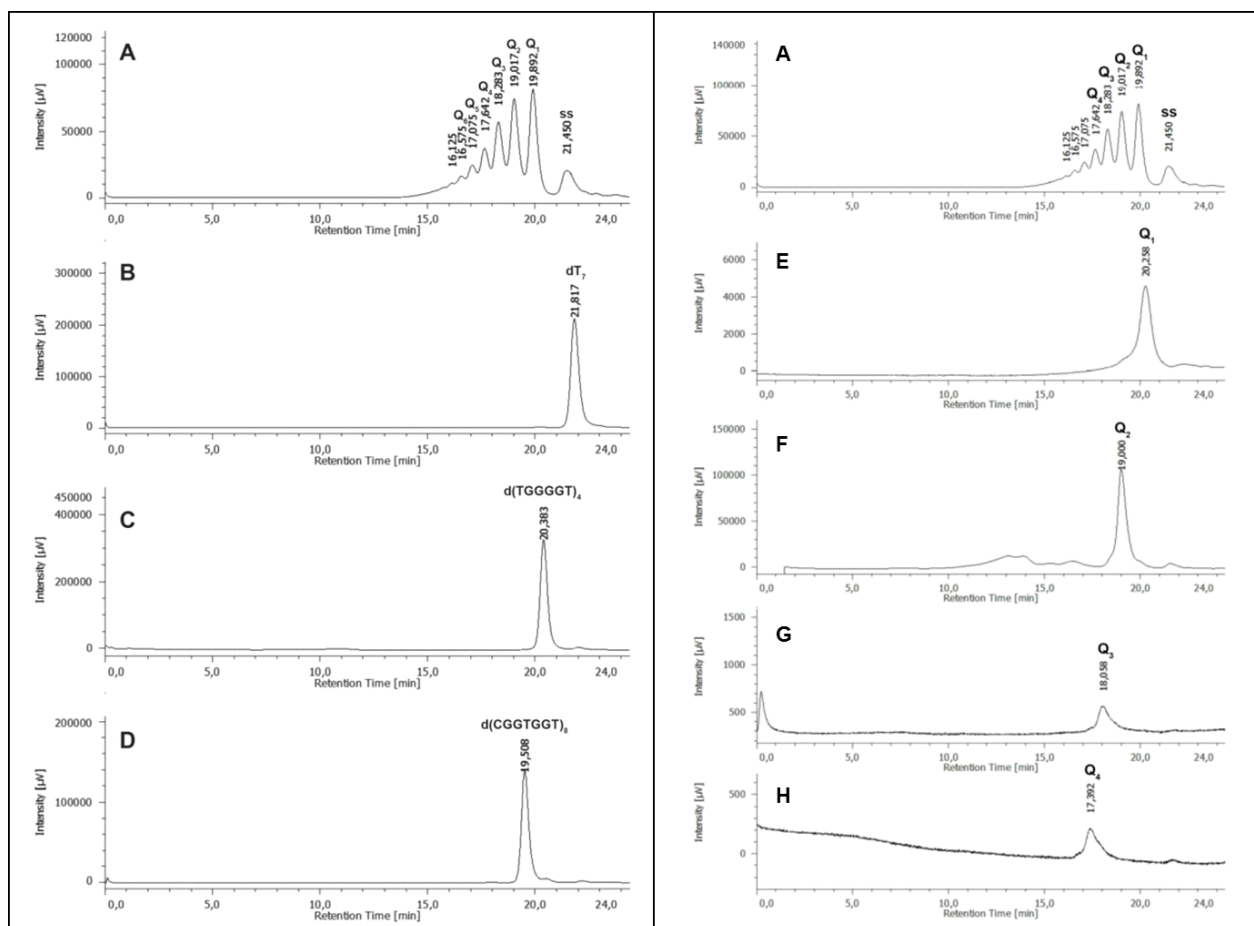


Figure 5: HPLC-SEC profiles of 0.1 mM 1 (A), dT7 (B), dTGGGGT (C) and dCGGTGGT (D) annealed in 1.0 M K⁺ buffer and stored at 4 °C for 24 h. ss = single strand (left panel); HPLC-SEC profiles of 0.1 mM annealed in 1.0 M K⁺ buffer and stored at 4 °C for 24 h and of Q_1 , Q_2 , Q_3 and Q_4 injected 24 h after their recovering from profile A (profiles E-H, respectively).

From these data, it was reasonable to hypothesize that each peak in the HPLC-SEC profile was due to a species which differed from those of the adjacent peaks in m.w. corresponding to a quadruplex formed by four DNA strands 7 nts long (formed by 28 nts). The HPLC-SEC profile of the multimerization of 7-mer was strongly reminiscent of its PAGE ladder profile thus further supporting the hypothesis that the 7-mer in K⁺ buffer forms G-wires species like poly-Qn due to the aggregation G-quadruplex building blocks.

Exploiting the good separation of the peak-species on SEC-200 column, the latest species attributed to Q_1 - Q_4 have been isolated and their purity and PAGE mobility checked (Figure 3, PAGE). The chromatographic analyses on the same SEC column confirmed that the product peaks Q_1 - Q_4 resulted almost pure with very low contamination from the adjacent

product peaks. Furthermore, the PAGE analyses of Q₁-Q₄ confirmed their purity and the correspondence between the ladder bands of the PAGE with the HPLC-SEC product peaks distribution of the 7-mer multimerization.

SEC analysis also revealed a strong connection between the ODN concentration and the possibility to form longer G-wires. In particular, at higher concentration (1.6 mM in single strand) it was possible to observe more polymeric species (Q_n, with n<8) that appeared like distinguishable and almost equally populated peaks, while the intense envelope peak at higher retention time (Rt = 13.6 min) could be attributable to longer G-wire (Fig.6).

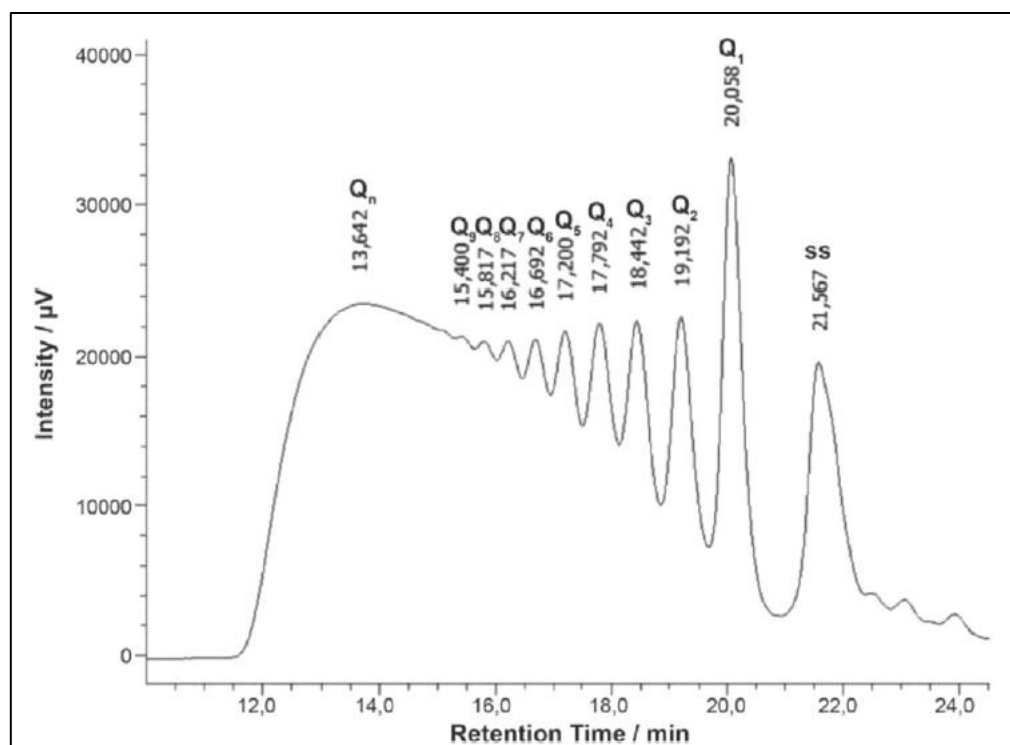


Figure 6: HPLC-SEC profile of Q_n distribution obtained by annealing 1.6 mM in 1.0m K⁺ containing buffer. ss=single-stranded.

The HPLC-SEC analysis has been also performed to have an insight on the dependence of polymerization from temperature. For this reason, samples have been injected at different temperatures (25°C, 45°C, 65°C, 85°C) 30 minutes after heating and equilibration. As the figure below shows (Fig.7), the profile analyzed at 25°C shows the same distribution of that analyzed at 4°C, with the only difference that the species Q₂ was the most abundant among the others. This means that at room temperature the most favorite species in solution was the dimeric species. By heating the samples at 45°C, the situation changed, bringing to an increase of the single-strand species and the contextual reduction of multimeric species Q_n; furthermore, in the peak distribution, the trimeric species became more abundant than the dimeric one at this temperature. When the temperature reached 65°C, the profile suggested the presence of the single-strand species as the more copious in solution, while it became the only species in solution at higher temperature. This suggested that the melting of the polymer Q_n represented a cooperative event and confirmed the high stability of this

supramolecular structures, respect to the G-quadruplex building block, as confirmed through CD melting experiments.

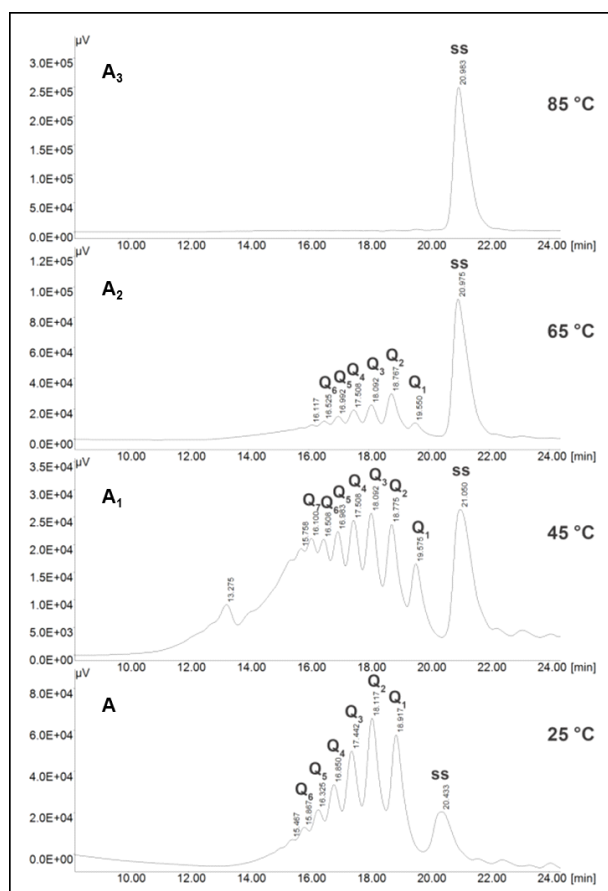


Figure 7: HPLC-SEC profiles of 0.1 mM 1 annealed in 1.0 M K⁺ buffer and stored at 4 °C for 24 h before being injected 30 min after heating at 25 (A), 45 (A₁), 65 (A₂) and 85 °C (A₃).

2.2.3 Circular Dichroism

CD spectroscopy provides essential information about conformational properties of DNA, including the B, A and Z-form of DNA, guanine quadruplexes, cytosine quadruplexes, triplexes and other less characterized structures.

In the simple case of parallel G-quadruplexes, generated by the association of four independent G-rich strands (intermolecular) in which the glycosidic bonds are all *anti* conformation are characterized by a positive ellipticity maximum at 264 nm and a negative minimum at 240 nm. The anti-parallel (intramolecular) complexes – containing both *syn* and *anti* glycosidic - bonds usually possess a positive maximum at 295 nm and a negative minimum at 265 nm(15, 16). However, recent studies reported that the structural variability of G-quadruplexes could be increased by introducing modifications on the structure, such as on the base, sugar backbone, but also by introducing an inversion of polarity site (17, 18).

In Figure 8, the CD spectra of our species has been reported. All the structures, from the polymer Q_n to the isolated species Q_1 , Q_2 , Q_3 , Q_4 , showed the same profile, characterized by positive signals at 246 nm and 300 nm and a negative one at 270 nm.

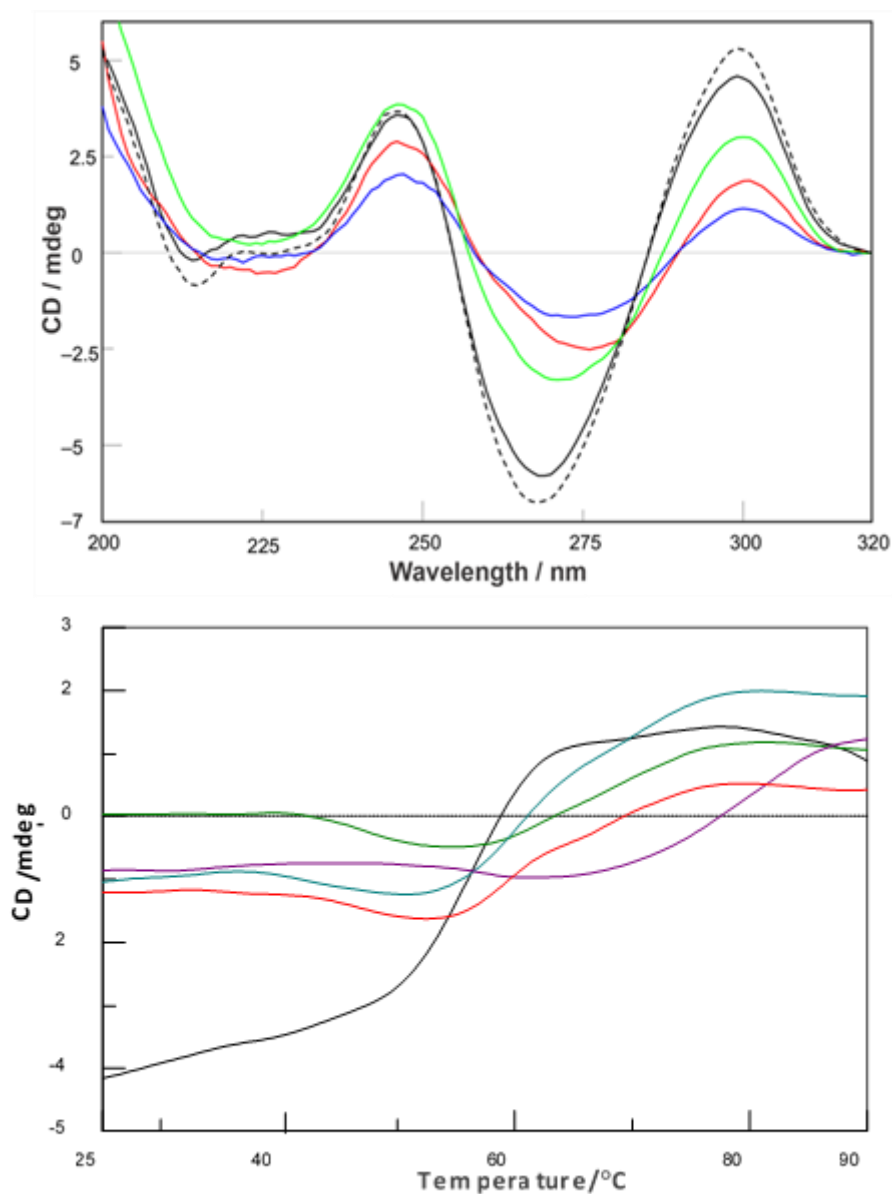


Figure 8: CD spectra of Q_n distribution (dashed curve) and isolated Q_1 (black curve), Q_2 (green curve), Q_3 (red curve) and Q_4 (blue curve) G-quadruplexes. CD denaturation profiles of 0.1 mM annealed in 1.0 M K^+ buffer (Q_n , purple), and of the G-quadruplexes Q_1 (black), Q_2 (green), Q_3 (red), Q_4 (cyan) isolated by HPLC-SEC from Q_n . All curves were recorded at 268 nm, 24 h after isolation (for Q_{1-4}) and storage at 4 °C.

As demonstrated, the CD profiles did not match literature data regarding parallel and antiparallel quadruplex so far reported. This was not quite surprising, considering the structural features presented in the novel complexes that could be ascribed to the presence of the inversion of polarity site. Indeed, despite PAGE and HPLC-SEC data demonstrated the exclusive formation of tetra-stranded G-Q building block, the occurrence of the inversion of polarity site altered the standard tetrads stacking typical of a parallel quadruplex and

generated an opposite (clockwise and anticlockwise) disposal of the two tetrads comprising the inversion of polarity site.

Furthermore, in our previous study, it has been demonstrated that for the 2Q-forming sequences, the negative minimum at about 290 nm was diagnostic of the presence of a head-to-head stacking between the G-Q building block (13). Unfortunately, in this case, the strong positive signal at 300 nm didn't allow us to observe it.

The thermal stability of the species has been also explored by means of CD-melting experiments and results have been reported in Figure 8. The data confirmed the extraordinary stability of such complexes, since the thermal stability of the polymeric species was higher than that of G-Q building block.

2.2.4 NMR

NMR spectroscopy has a unique strength in studying DNA G-quadruplex secondary structures (19, 20). For this reason, the imino peaks associated with guanines in G-tetrad formation give rise to characteristic chemical shifts, around 10.5-12 ppm attributable to the exchange-protected imino protons involved in the formation of Hoogsteen Hydrogen bonds of G-tetrads (Fig.9). This chemical shift region is completely separated from imino chemical shifts from any other DNA conformations, such as duplex DNA, single-stranded DNA, or other secondary DNA structures.

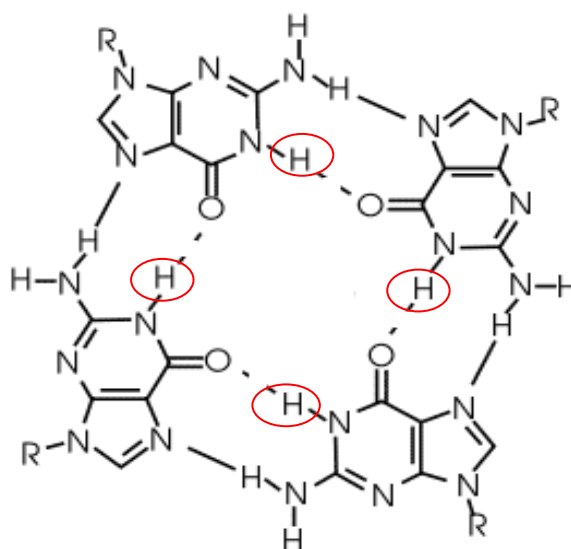


Figure 9: N-1 imino protons of guanine bases and the Hoogsteen bond with O-6 carbonyl atom of the near guanine.

In the paper previously published by the research group of Professor Piccialli, aimed at the study of dimeric G-quadruplexes (2Q), the ^1H -NMR spectra show well-resolved imino protons (11.0-12.0 ppm) and intense anomeric protons signals (5.5-6.5 ppm) visible even at high temperature (65°C). In our case, instead, the ^1H -NMR spectrum of Q_n in 1 M K^+ buffer at 25°C was characterized by the presence of four less-defined imino and anomeric signals compared to those shown for 2Q; furthermore, the spectra at higher temperatures have been

recorded, and as noticed from the overlapping of the spectra, the imino protons disappeared at 65°C (Fig.10).

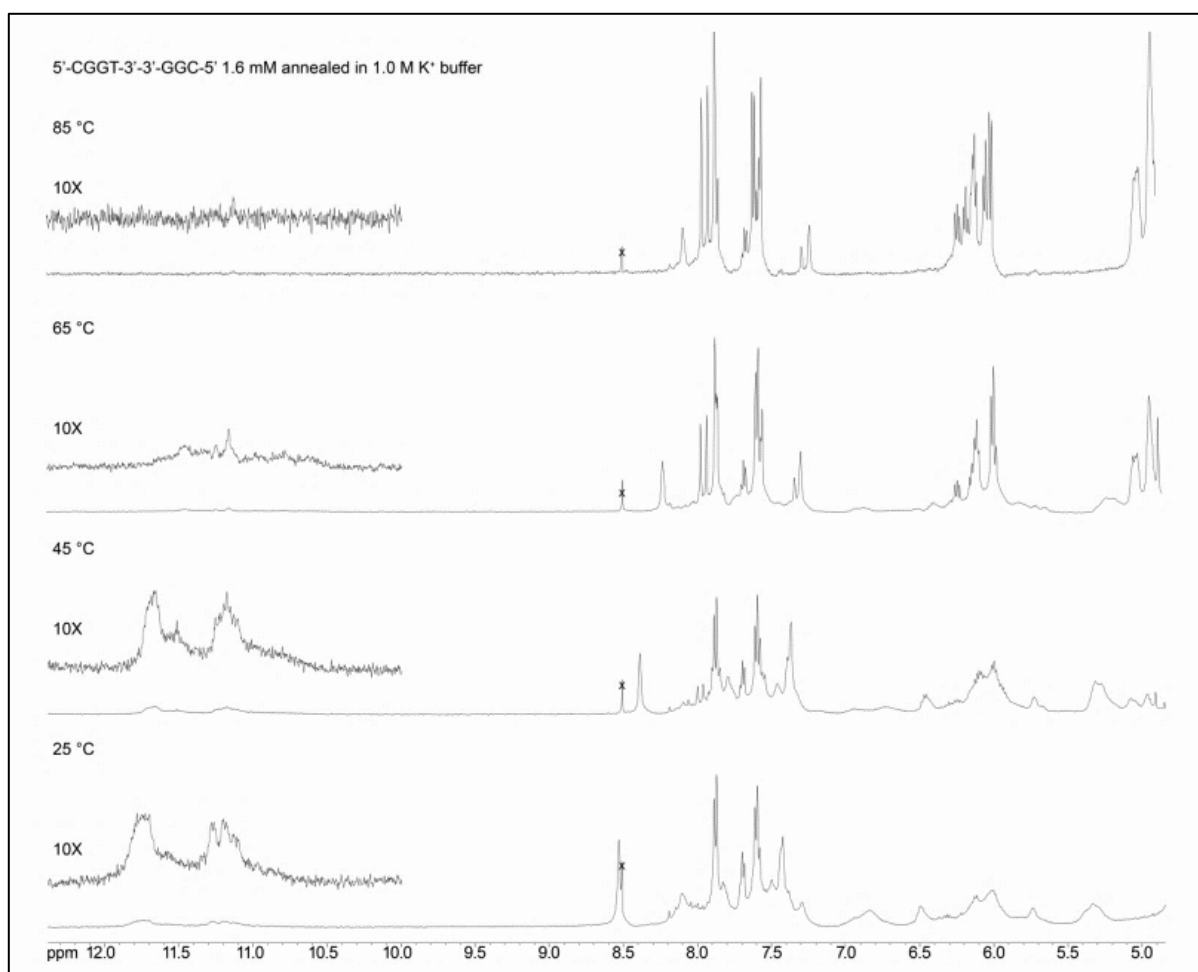


Figure 10: imino, aromatic and anomeric protons regions of ^1H -NMR spectra of the 7-mer 1.6 mM annealed in 1 M K^+ buffer and recorded at 25,45,65 and 85°C. The insets show the imino proton regions at 10x magnification.

The presence of this imino-protons broadened signal could be ascribed to the presence of the inversion of polarity site that created an asymmetric structure that destabilized the G-Quadruplex structure: the imino-protons were more exposed to the solvent and this speeded up the exchange. Furthermore, side-by-side aggregation of G-quadruplex units participating in the Q_n G-wire distribution could be responsible for the observed anomeric signal broadening.

2.2.5 AFM analysis

AFM spectroscopy has been used to obtain information about the morphology of the polymers formed by the 7-mer sequence when annealed in potassium buffer. Figure 11 and 12 show AFM images of the obtained G-wires grown on muscovite mica. From these images

it is possible to note that Q_n quadruplexes interact and self-assemble on mica surfaces in different ways depending on their concentration in the starting solution, as previously reported in literature (4, 8, 21). In particular, analyzing the 1.6 mM solution (Fig.11), AFM images revealed the formation of rod-like shaped aggregates of different lengths (from 21 up to 166 nm) and widths (not more than 100 nm), whereas their heights were always around 2 nm. In particular, the rod-like shaped aggregates showed a preferential direction of alignment (panel B). The preferred orientation can be ascribed to the interaction between G-quadruplexes and the mica surface. The homogeneous values of heights recorded suggested the formation of self-assembled monolayers in the x,y plane owing to the evaporation of the buffer solution, which promoted lateral and longitudinal aggregation of G-quadruplexes, the first one being favored by side-packing. On the other hand, analyzing the 1.6 μ M solution (Fig.12), AFM images suggested the formation of thinly distributed aggregates, even if the orientation was preserved. The aggregates showed the same length of those shown in the concentrated solution, whereas the widths were smaller, never exceeding 30 nm. The heights were always about 2 nm as before. This result confirmed a side-packing mechanism in the assembly of G-structures during evaporation of the solution and confirmed the hypothesis of spontaneous formation of a monolayer. Furthermore, the longitudinal aggregation was competitive compared with the lateral one, owing to steric conditions during the evaporation.

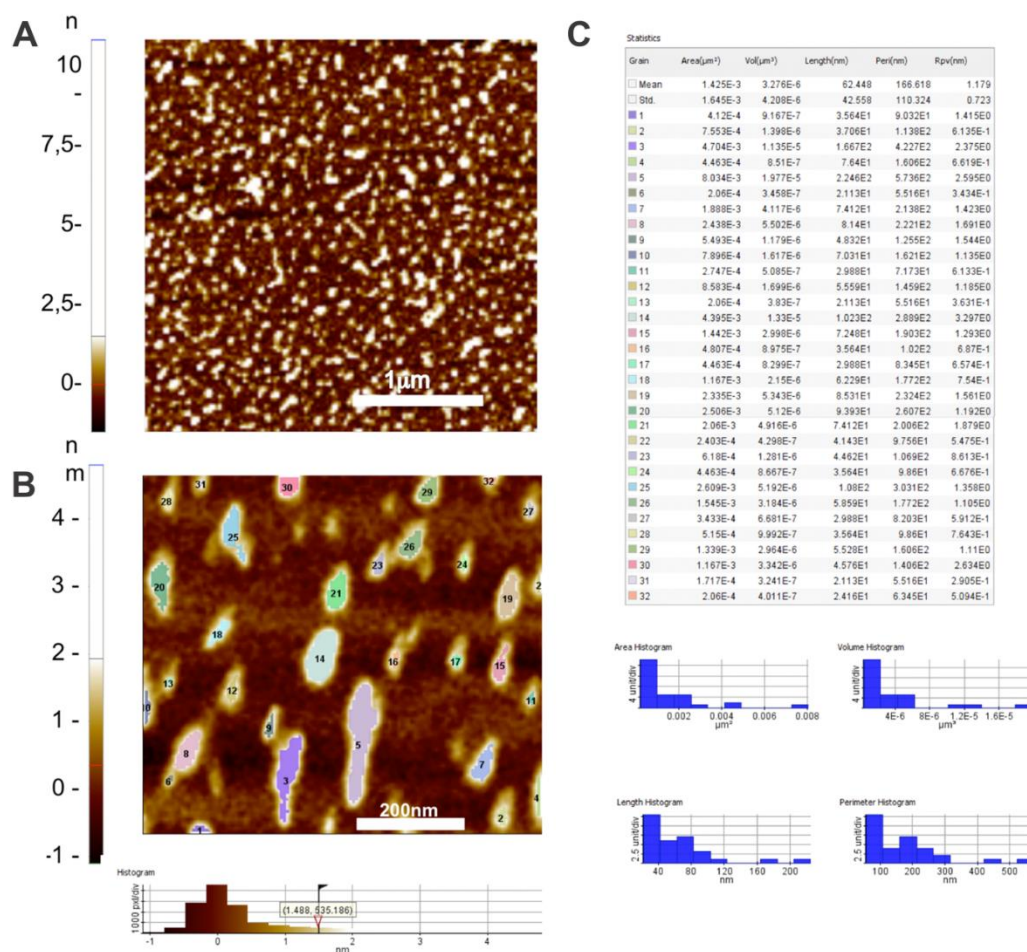


Figure 11. AFM topography images of dried samples at 1.6 mM concentration deposited on a freshly cleaved mica surface: panel A shows a dense population with heights all lower than 10 nm (the scale bar is 1 μ m);

panel B shows a magnified AFM image of the same sample; the colored areas underline the structures with heights higher than 1.488 nm (the scale bar is 200 nm); panel C shows statistics referred to image in panel B.

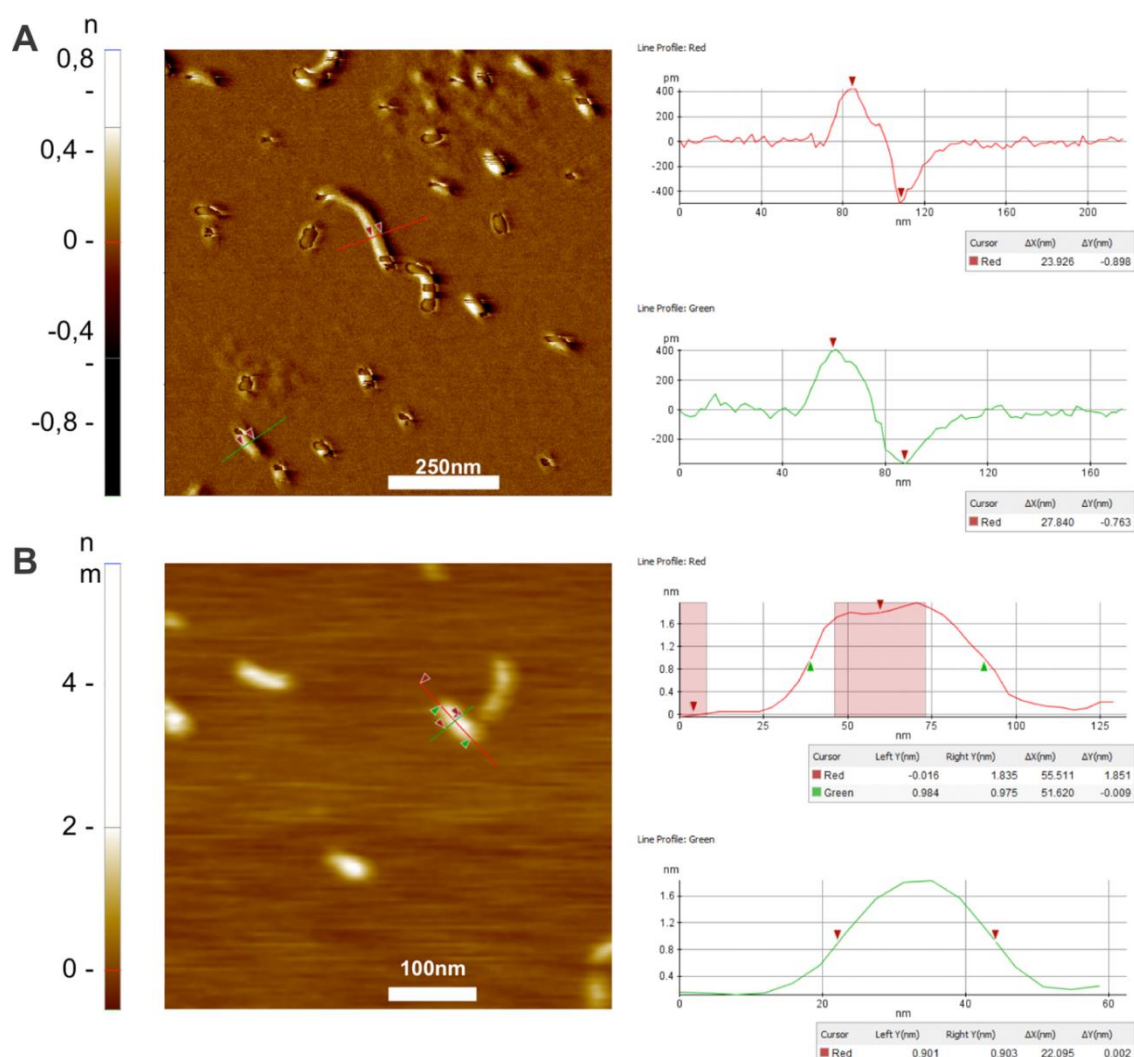


Figure 12. AFM images of dried samples at 16 μM concentration deposited on a freshly cleaved mica surface: panel A shows topographic image of a population sparser than in Figure S7 with heights lower than 6 nm (the scale bar is 250 nm); panel B shows the AFM error signal deflection of the same sample, the minimum and maximum deflection in the measurements in the side panel show structure widths of 24 nm and 28 nm, compatible with a tip radius of about 10 nm (scale bar is 250 nm); panel C shows a magnified topographic image of panel A, measurements shows that structure is 52 nm long, 22 nm wide and 1.8 nm high (scale bar is 250 nm). Also in this case a tip radius of curvature of about 10 nm must be taken in account.

2.3 Conclusions

The present study demonstrates that the formation of a DNA based nanostructure consisting of polymer of a tetramolecular G-quadruplexes can occur when the DNA sequence $\text{CGGT}^{3'}\text{-}^{3'}\text{GGC}$ bearing two 5'CG-ends is annealed in the presence of K^+ ions. The two 5'-ends can be obtained by simply incorporating a 3'-3' inversion of polarity. By means of PAGE, HPLC, CD, NMR and AFM analyses it is possible to demonstrate that DNA polymers could be obtained. This findings adds further possibilities for the design of novel quadruplex-based

DNA functional nanostructures, and further complexity to the mechanism of folding and assembly of G-rich sequences.

However, the structuring of polymeric species from G-quadruplexes remain a big challenge in the field of self-assembly, so further studies will be still performed in order to better control process of multimerization of the G-quadruplex building block.

2.4 Experimental Methods

2.4.1 DNA synthesis and Purification

DNA sequences d(TGGGGT) and d(CGGTGGT) were chemically synthesized with an Expedite 8909 DNA synthesizer (PerSeptive Bio systems, USA) using a universal CPG support purchased from Glen Research. The syntheses were performed by adopting the standard β -cyanoethyl phosphoramidite chemistry at 10–15 mM scale and the products were purified as previously described (22). The synthesis of d(5'-CGGT-3'-3'-GGC-5') was performed with the same DNA synthesizer. The inversion of polarity site within the sequence was achieved by initially assembling the 5'-CGGT-3' tract by using 5'-phosphoramidites and then the 3'-GGC-5' tract with standard 3'- phosphoramidites. After completion of the ODN sequence, the support was treated with concentrated aqueous ammonia at 55°C for 15 h. The combined filtrates and washings were concentrated under reduced pressure and purified through HPLC (JASCO PU2089 pumps equipped with the JASCO 2075 UV detector) with an anion exchange column (Macherey–Nagel, 1000-8/46, 4.4V 50 mm, 5 mm) using a linear gradient from 0 to 100% B in 30 min, flow rate = 1 mLmin⁻¹ and detection at 260 nm (buffer A: 20 mM NaH₂PO₄ aq. solution pH 7.0, containing 20% (v/v) CH₃CN; buffer B: 20 mM NaH₂PO₄ aq. solution pH 7.0, containing 1M NaCl and 20% (v/v) CH₃CN).

2.4.2 Annealing Procedure

The ODN concentrations were determined in water by measuring the absorbance at 260 nm at 90°C by using the nearest-neighbor calculated molar extinction coefficient of 5'-CGGTGGC-3' ($\epsilon = 63100 \text{ m}^{-1} \text{ cm}^{-1}$). The 0.1 and 1.6 mM solutions of 1 were obtained by dissolving the lyophilized sample in 900 mM KCl and 100 mM KH₂PO₄. The samples were annealed by heating at 90°C for 10 min and then quickly cooling to 4°C. After the annealing procedure, the samples were stored at 4°C before measurements.

2.4.3 PAGE

Native gel electrophoresis experiments were performed on 20% polyacrylamide gels containing TBE (8.9 mM Tris, 8.9 mM borate, 0.2 mM EDTA, from BIORAD) and 30 mM KCl, at room temperature, 120 V for 2 h. The ODN samples, annealed at 1.6 mM single strand concentration in 1.0M K⁺ buffer, were diluted at 0.6 mM loading concentration just before the PAGE runs. Glycerol was added (10% final) to facilitate sample loading in the wells. The bands were finally visualized by ethidium bromide staining in a Bio-Rad Laboratories Gel Doc™ XR+ image system.

2.4.4 HPLC-SEC analyses and isolation of Qn species

HPLC-SEC analyses and purifications were performed with a ReproSil 200 SEC column operating in the MW range of 2000–70000 Dalton (Dr. Maisch GmbH, 300V8 mm, 5 mm)

eluted with 90 mM KCl and 10 mM $\text{KH}_2\text{PO}_4/\text{CH}_3\text{CN}$ (80:20, v/v), flow rate 0.5 mLmin⁻¹, detector at 260 nm. The analyses were performed at room temperature.

2.4.5 Circular Dichroism

CD spectra and CD melting profiles were recorded with a Jasco 715 CD spectrophotometer (Jasco, Tokyo, Japan) equipped with a Jasco JPT423S Peltier temperature controller in 1 mm optical path quartz cuvettes (100 nmmin⁻¹ scanning speed, 1 s response time). The spectra were recorded in triplicate at 4°C from 220 to 320 nm. CD samples were prepared in potassium buffer (90 mM KH_2PO_4 and 10 mM KCl) at 20 mM final single strand concentration. The buffer baseline was subtracted from each spectrum and the spectra were normalized to have zero at 320 nm. CD melting curves were registered at 268 nm, 1°Cmin⁻¹ heating rate, temperature range 5–90°C.

2.4.6 NMR spectroscopy

NMR data were recorded with a Varian ^{UNITY}INOVA 500 MHz spectrometer equipped with a broadband inverse probe with z-field gradient. The data were processed by using the iNMR software package (<http://www.inmr.net>). One-dimensional NMR spectra were acquired as 16384 data points with a recycle delay of 1.0 s at 25, 45, 65, and 85°C and the spectra were apodized with a shifted sine bell squared window function. Water suppression was achieved by including a double pulsed-field gradient spin-echo (DPFGSE) module in the pulse sequence prior to acquisition. NMR samples were prepared at the concentration of 1.6 mM single strand in 200 mL of $\text{H}_2\text{O}/\text{D}_2\text{O}$ 9:1 containing 900 mM KCl and 100 mM KH_2PO_4 .

2.4.7 AFM

A XE-100 Park Systems instrument was used for the AFM imaging of Qn G-wires. Surface imaging was obtained in non-contact mode by using 125 mm long silicon/aluminium-coated cantilevers (PPPNCr 10m; Park Systems; tip radius lower than 10 nm), with a resonance frequency of 200 to 400 kHz and nominal force constant of 42 Nm@1. The scan frequency was typically 0.5 Hz per line. When necessary, the AFM images were processed by flattening to remove the background slope, and the contrast and brightness were adjusted. Muscovite mica of about 1 cm² surface was used as the substrate in the AFM study. Muscovite mica surfaces are typically used as AFM substrates owing to their perfect cleavage along a <001> plane, yielding large atomically flat areas. Mica consists of layers of an aluminium phyllosilicate lattice ionically bonded through interstitial K⁺ ions. Upon cleavage, the K⁺ ions are highly mobile and are readily exchanged with divalent cation species at the solid–liquid interface. This exchange results in a positive overcharging of the mica surface, which enables the deposition of molecules that hold a net negative charge, such as DNA. Moreover, the positive charge distribution after cleavage enables a super-hydrophilic surface that guarantees a lower interaction between suspended biomolecules during the evaporation of aqueous solvent. Mica was freshly cleaved by using adhesive tape prior to each deposition to establish its cleanliness. Aliquots (2 mL) of the DNA/imaging buffer were directly deposited by casting onto freshly cleaved muscovite mica. After 2 min, every sample was gently washed with deionized water and then dried by evaporation at room temperature under a ventilated fume hood.

2.5 References

1. Bixon, M., Giese, B., Wessely, S., Langenbacher, T., Michel-Beyerle, M.E. and Jortner, J. (1999) Long-range charge hopping in DNA. *PNAS*, 96, 11713–11716.
2. Kumar, A., Hwang, J.-H., Kumar, S. and Nam, J.-M. (2013) Tuning and assembling metal nanostructures with DNA. *Chem. Commun. Chem. Commun*, 49, 2597–2609.
3. Astakhova, T.Y., Likhachev, V.N. and Vinogradov, G.A. (2012) Long-range charge transfer in biopolymers. *Russ. Chem. Rev.*, 81, 994–1010.
4. Marsh, T.C., Vesenska, J. and Henderson, E. (1995) A new DNA nanostructure, the G-wire, imaged by scanning probe microscopy. *Nucleic Acids Res.*, 23, 696–700 ST-A new DNA nanostructure, the G-wire,.
5. Dai, T.Y., Marotta, S.P. and Sheardy, R.D. (1995) Self-Assembly of DNA Oligomers into High Molecular Weight Species. *Biochemistry*, 34, 3655–3662.
6. Tóthová, Petra; Krafčíková, Petra; Viglaský, V. (2014) Formation of highly ordered multimers in G-quadruplexes. *Biochemistry*, 53, 7013–7027.
7. Marchand, A. and Gabelica, V. (2016) Folding and misfolding pathways of G-quadruplex DNA. *Nucleic Acids Res.*, 44, 10999–11012.
8. Kotlyar, A.B., Borovok, N., Molotsky, T., Cohen, H., Shapir, E. and Porath, D. (2005) Long, monomolecular guanine-based nanowires. *Adv. Mater.*, 17, 1901–1905.
9. Liu, S.P., Weisbrod, S.H., Tang, Z., Marx, A., Scheer, E. and Erbe, A. (2010) Direct measurement of electrical transport through G-quadruplex DNA with mechanically controllable break junction electrodes. *Angew. Chemie - Int. Ed.*, 49, 3313–3316.
10. Hu, D., Ren, J. and Qu, X. (2011) Metal-mediated fabrication of new functional G-quartet-based supramolecular nanostructure and potential application as controlled drug release system. *Chem. Sci.*, 2, 1356.
11. Krishnan-Ghosh, Y., Liu, D. and Balasubramanian, S. (2004) Formation of an interlocked quadruplex dimer by d(GGGT). *J. Am. Chem. Soc.*, 126, 11009–11016.
12. Sun, H., Xiang, J., Zhou, Q., Yang, Q., Xu, G. and Tang, Y. (2010) Temperature-sensitive supramolecules self-assembled by G-quadruplex DNA. *Int. J. Biol. Macromol.*, 46, 123–125.
13. Borbone, N., Amato, J., Oliviero, G., D'Atri, V., Gabelica, V., De Pauw, E., Piccialli, G. and Mayol, L. (2011) D(CGCTGGT) forms an octameric parallel G-quadruplex via stacking of unusual G(C):G(C):G(C):G(C) octads. *Nucleic Acids Res.*, 39, 7848–7857.
14. D'Atri, V., Borbone, N., Amato, J., Gabelica, V., D'Errico, S., Piccialli, G., Mayol, L. and Oliviero, G. (2014) DNA-based nanostructures: The effect of the base sequence on octamer formation from d(XGGYGGT) tetramolecular G-quadruplexes. *Biochimie*, 99, 119–128.
15. Randazzo, A., Spada, G.P. and Webba, M. (2012) Circular Dichroism of Quadruplex Structures. 10.1007/128.
16. Vorlíčková, M., Kejnovská, I., Sagi, J., Renčíuk, D., Bednářová, K., Motlová, J. and Kypr, J. (2012) Circular dichroism and guanine quadruplexes. *Methods*, 57, 64–75.
17. Esposito, V., Virgilio, A., Randazzo, A., Galeone, A. and Mayol, L. (2005) A new class of DNA quadruplexes formed by oligodeoxyribonucleotides containing a 3'-3' or 5'-5' inversion of polarity site. *Chem. Commun. (Camb)*, 10.1039/b504455c.
18. Esposito, V., Virgilio, A., Pepe, A., Oliviero, G., Mayol, L. and Galeone, A. (2009) Effects of the introduction of inversion of polarity sites in the quadruplex forming oligonucleotide TGGGT. *Bioorganic Med. Chem.*, 17, 1997–2001.
19. Adrian, M., Heddi, B. and Phan, A.T. (2012) NMR spectroscopy of G-quadruplexes. *Methods*, 57, 11–24.
20. Burge, S., Parkinson, G.N., Hazel, P., Todd, A.K. and Neidle, S. (2006) Quadruplex DNA: sequence, topology and structure. *Nucleic Acids Res.*, 34, 5402–5415.

21. Lee,A.J., Szymonik,M., Hobbs,J.K. and Wälti,C. (2015) Tuning the translational freedom of DNA for high speed AFM. *Nano Res.*, 8, 1811–1821.
22. Oliviero,G., Borbone,N., Amato,J., D’Errico,S., Galeone,A., Piccialli,G., Varra,M. and Mayol,L. (2009) Synthesis of quadruplex-forming tetra-end-linked oligonucleotides: Effects of the linker size on quadruplex topology and stability. *Biopolymers*, 91, 466–477.

Chapter 3

Target Protector PNA as a new tool in the treatment of Cystic Fibrosis

3.1 Introduction

Cystic fibrosis (CF) is one of the most common serious genetic diseases (1, 2). A person suffering from CF produces thick, sticky mucus, which clogs the lungs (3), causes repeated infection and difficulty breathing. In addition to breathing problems, pancreas does not produce the enzymes (4) resulting in a lack of food digestion, diarrhea, malabsorption, growth retardation in children and poor nutritional status in adults. The progression of pancreatic damage with age often leads to a form of diabetes. Other events may involve the intestines, liver, nasal cavity and, in males, vas deferens (5). For these reasons it is a life-threatening disorder.

CF is due to a defect in the CFTR gene. This gene has been identified and localized on the Chromosome 7. The most common mutation, $\Delta F508$, is a deletion of three nucleotides resulting in the loss of one phenylalanine at position 508. This gene expresses the CFTR protein that controls the movement of salt and water in and out of body's cells. In people who suffer from CF, the malfunctioning of the CFTR protein prevents the chloride ions and water from escaping the epithelial cells and this leads to the formation of a dense and dehydrated mucus that obstructs all internal ducts (especially in the lungs and the pancreas) (6).

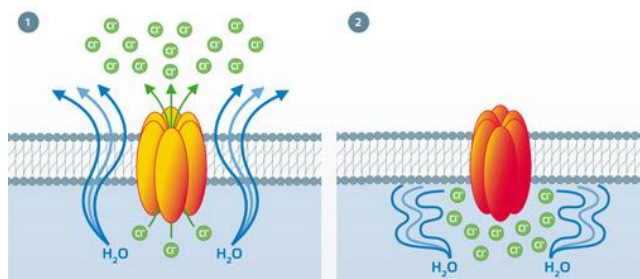


Figure 1: CFTR protein functions.

A child affected by cystic fibrosis inherited a defective gene from both the father and the mother who are silent carriers of the mutated gene. In Italy there is one healthy carrier every 25 people. When a mother and father are both CF carriers, each pregnancy has a 1 in 4 (or 25%) chance for the baby to have cystic fibrosis (1).

CF has not had cure yet, even if treatments have greatly improved life expectancy in the past decades. They included rehydration of the airway surface, mucolytic, anti-inflammatory agents, anti-infective agents; All these approaches are symptomatic, and do not directly target CFTR protein activity and/or the defective gene. Among all these strategies, only the gene therapy targeting the mutated CFTR protein has shown meaningful efficiency to provide hope to the patients. A CFTR potentiator (Ivacaftor) has been developed by Vertex Pharmaceuticals and has been recently approved for the treatment of patients carrying the

p.Gly 551Asp mutation (2-5% of all patients). To date, Ivacaftor in combination with Lumacaftor provided a benefit for patients with cystic fibrosis homozygous for the Phe508del CFTR (7).

In this context, the discovery of new therapies for the treatment of cystic fibrosis has become a challenge for many researchers. Since many CF patients retain a residual channel activity, an approach could be the stabilization of the CFTR messenger RNA (mRNA), by increasing the amount of the protein and resulting in a net chloride channel increase (8). Thus, several groups have suggested miRNA-targeted therapies.

miRNAs are small (20 to 24 nucleotides) noncoding RNAs that regulate post-transcriptional gene expression; miRNAs predominantly down-regulate the expression of their target genes by pairing with the 3'-untranslated regions (UTRs) of target mRNAs, thereby inducing mRNA degradation or translation inhibition (9).

Since CF has been associated with the deregulation of specific microRNAs, many approaches involve the use of oligonucleotide (ON) analogues which being complementary to miRNAs are able to reduce or inhibit their activity (10).

In this context, Yin and coworkers have explored the ability of a PNA sequence to selectively inhibit miRNA-4661-3p (11).

The promising results reported in this kind of approach, led the group of Professor Piccialli to propose the use of peptide nucleic acids (PNAs) as inhibitors of a miRNA involved in the pathological progress of Cystic Fibrosis (12, 13).

This approach arises from the discovery made by the research group of Professor Castaldo of a mutation in the 3'-UTR of CFTR responsible for the down regulation of CFTR because of its enhanced affinity towards a miRNA, the miR-509-3p(14).

Starting from this finding, in these previous works, two negatively charged PNAs, 14 and 7 bases long, conveniently modified at their termini, in order to allow their delivery and individuation within the cells, and complementary to the 5'-terminus of miR-509-3p, were proposed for the selective inhibition of the miRNA. The in vitro studies demonstrated that both PNAs were able to recognize the target within the cells.

Notwithstanding the successful results, this approach gives as a side effect to prevent miRNA from playing other biological roles. Since they regulate multiple genes, microRNA inhibitors will have pleiotropic effects.

In literature, the target protector approach has already been reported; it describes the use of target protector oligonucleotides for the treatment of CF. The oligonucleotides work by masking microRNA binding sites in the 3'UTR of the CFTR messenger with the aim to depress CFTR expression specifically. With target site blockers addressing this site they are able in adult lung cells to achieve 3-6 fold increase in luciferase activity (15).

Starting from this idea, our approach involves the replacement of the target protector oligonucleotides with the PNA. Once identified the seed region of mi-509-3p in the CFTR 3'UTR region, two PNA sequences, 13 and 7 bases long that were complementary to a sequence within the promoter of the CFTR gene have been synthesized.

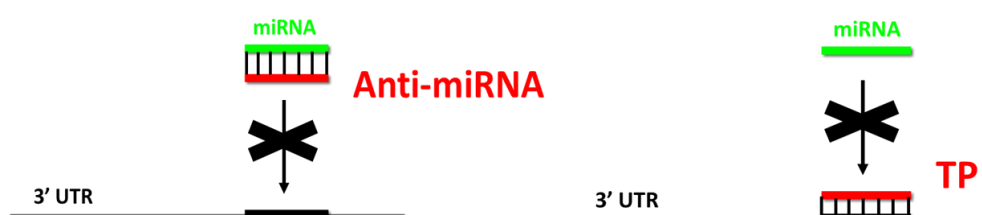


Figure 2: The two approaches for the treatment of CF; on the left the anti-miRNA approach and, on the right, our proposed approach.

3.2 Results and Discussion

The first step required the synthesis and characterization of new PNA sequences, 13 and 7 bases long, complementary to a sequence within the promoter of the CFTR gene. The sequences were synthesized through the Fmoc-solid phase protocol on a Rink amide resin and were equipped with a peptide tail composed by two glycines and two negatively charged serines at the C end with the aim of improving both the water solubility and the cellular uptake of the PNA molecules. After the synthesis, the oligomers were detached from the support, lyophilized and characterized by mass spectrometry; thereafter, the PNAs sequences were dissolved in phosphate buffered saline (PBS) and subjected to annealing procedure. Their ability to interact with the target sequence on the CFTR mRNA was assessed by means of spectroscopic techniques and molecular dynamics studies.

Since DNA is more resistant against nucleases and does not require any chemical modification for handling that could alter its recognition properties, the spectroscopic studies were performed using the corresponding 13-mer DNA model sequence (ODN in Table 1); furthermore, considering the higher binding affinity of RNA strands compared to DNA strands towards complementary PNAs, the stability data obtained by using the ODN model were probably underestimated (16).

Name	Sequence
3' UTR of CFTR mRNA	G-A-A-G-A-A-G-C-A-C-C-A-A-U-C-A-U-G-A-
DNA model sequence (ODN)	G-A-A-G-C-A-C-C-A-A-T-C-A
PNA 1 (C -> N)	G-S(P)-S(P)-G-c-t-t-c-g-t-g-g-t-t-a-g-t
PNA 2 (C -> N)	G-S(P)-S(P)-G-g-g-t-t-a-g-t
PNA 3 (C -> N)	G-S(P)-S(P)-G-c-a-g-t-t-g-t-c-t-g-t-g-t
PNA 4 (C -> N)	G-S(P)-S(P)-G-t-t-g-g-a-g-t

Table 1: Sequences of CFTR messenger RNA, DNA model sequence and PNA synthesized for the studies.

3.2.1 CD and CD melting analyses

Circular dichroism measurements are useful in the characterization of nucleic acid secondary structure and in the study of hybridization events (17). In fact, information about the secondary structure could be obtained since CD measurements are sensitive to the base-pair geometry in the helix (18)

In this case, CD spectra of each component alone and of the mixture were reported in Figure 3, and confirmed the capability of the PNA to bind the target: the dichroic profile of the mixture was typical of an antiparallel DNA/PNA heteroduplex, showing maxima around 220 and 270 nm and minima at 245 nm. As expected, the CD melting analysis revealed the greater stability of the longer PNA1/ODN heteroduplex relative to that of the shorter one (PNA2/ODN), confirming, in both cases, the interaction between the molecules. In particular,

the T_m values of the PNA1/ODN and the PNA2/ODN were of 66°C and 35°C respectively (Fig.4).

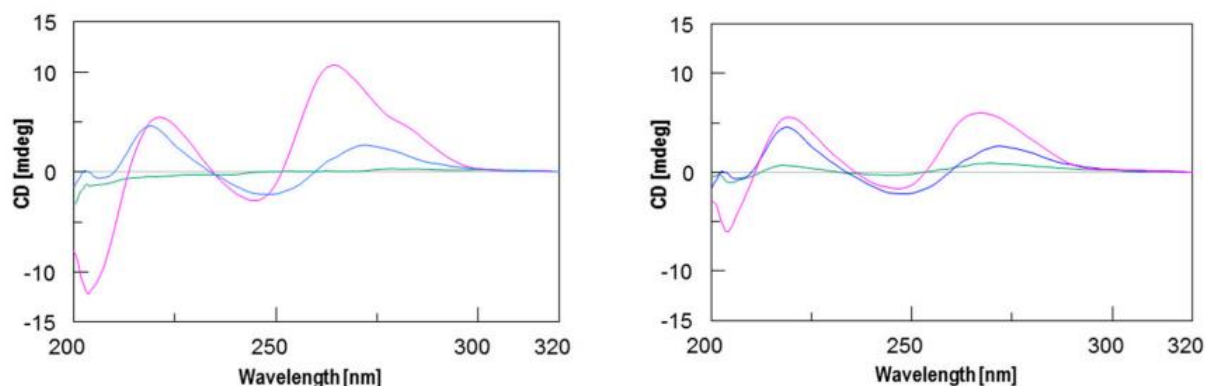


Figure 3: On the left, CD spectra of PNA 1 (green line), ODN (blue line) and 1/ODN mixture (1.5:1) (violet line) and on the right, CD spectra of PNA 2 (green line), ODN (blue line) and 2/ODN mixture (1.5:1) (violet line).

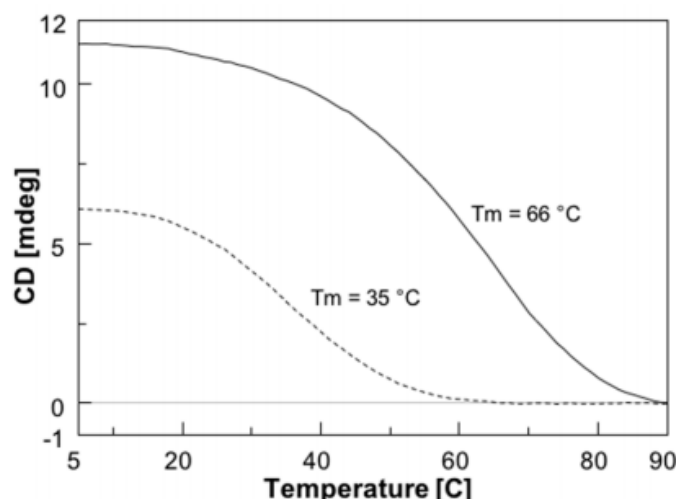


Figure 4: CD melting profile of 1/ODN mixture (1.5:1) (violet dashed line) and 2/ODN mixture (1.5:1) (violet dotted line). The curves were obtained by monitoring the variation of absorbance at 266 nm for 1/ODN mixture and at 264 nm for 2/ODN mixture at a heating rate of 0.5 °C/min.

3.2.2 UV studies

UV experiments were performed to get information about the propensity of the PNAs to form heteroduplexes with the ODN sequence, by exploiting the hypochromic effect resulting from the formation of the PNA/ODN heteroduplexes. Both spectra were characterized by a maximum at around 260 nm, typical of nucleobases; but in the case of the PNA1/ODN complex (violet curve in Figure 5), lower values of absorbance than the arithmetic sum of each component alone (black curve in Figure 5) were recorded, thus confirming the occurrence of stacking interactions and the formation of the heteroduplex. Instead, in the case of the shorter PNA 2, the UV spectrum of its complex with the ODN (violet curve in Figure 5) recorded the same values of absorbance than the arithmetic sum of its

components was recorded, in agreement with the experimental lower stability of the shorter PNA 2/ODN heteroduplex.

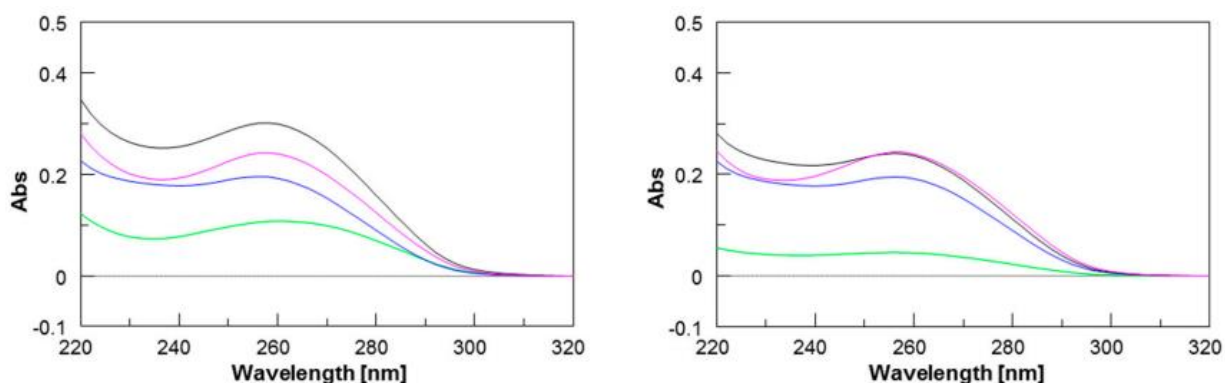


Figure 5: on the left, UV spectra of PNA 1 (green line), ODN (blue line), 1/ODN mixture (1.5:1) (violet line) and the arithmetical sum (black line); on the right, UV spectra of PNA 2 (green line), ODN (blue line), 2/ODN mixture (1.5:1) (violet line) and the arithmetical sum (black line).

A possible explanation to this behaviour could be found in the lower number of bases involved in the Watson-Crick (W-C) base pairing for the 2/ODN complex relative to the total number of bases in the two strands (PNA + ODN).

3.2.3 Molecular Dynamics

Molecular dynamic calculations were performed to check and to obtain information about the structural features of the heteroduplexes PNA1/RNA and PNA2/RNA. The structural analyses revealed low RMSD values and the convergence into a main structure for either 1/RNA or 2/RNA simulations (Fig.6).

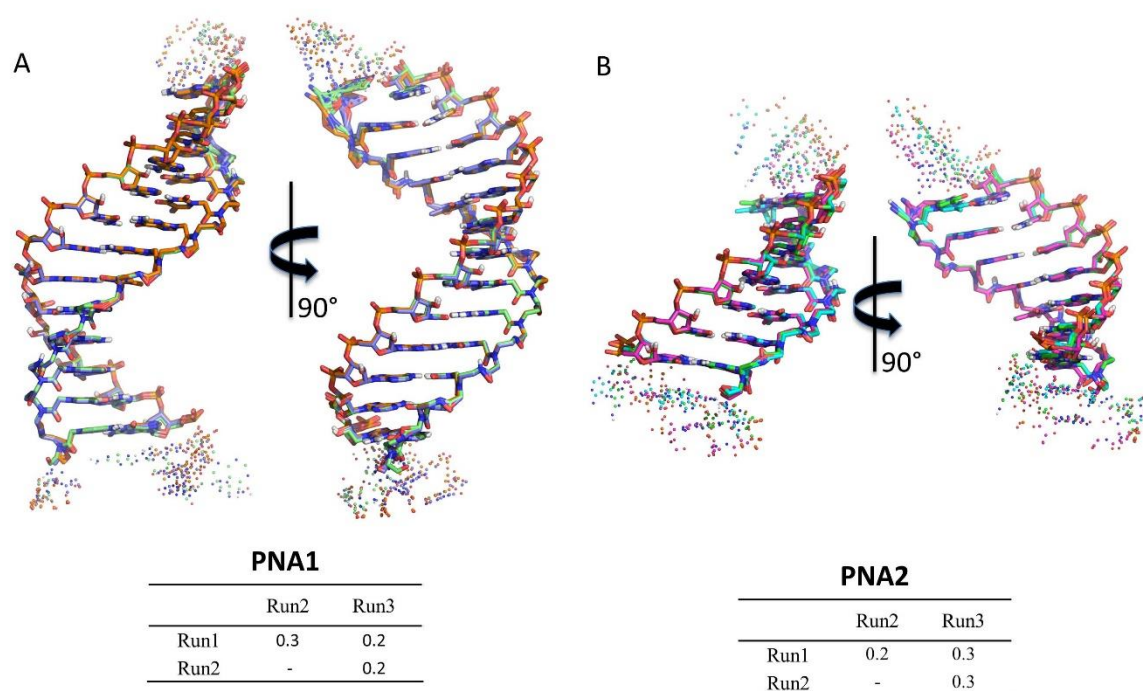


Figure 6. Superposition of average structures of the main represented cluster for 1/RNA (A) and 2/RNA (B), with relative RMSD in Å calculated on heavy atoms. Duplexes regions are represented in licorice colored by atom type with carbon colored by MD run (PNA 1: Blue, Run 1; Orange, Run 2; Light green, Run 3. PNA2: Green, Run 1; Cyan, Run 2; Magenta, Run 3) and other atoms by standard convention (Oxygen in red, Nitrogen in blue, Phosphate in orange and Hydrogens in white). RNA single strand flanking regions and the tetrapeptide Gly-SerP-SerP-Gly are represented in spheres coloured by MD run.

Detailed analysis of the local base pair step parameters (twist, roll, tilt, shift, slide and rise), helical parameters (inclination) and the torsion angles of RNA and PNA monomers reported high similarity with PNA/RNA heteroduplexes structures determined by NMR (PDB ID 176D (19)) and by XRAY (PDB ID 5EME and 5EMF) (20), with few noticeable deviations (Table 2).

Name	Shift	Slide	Rise	Tilt	Roll	Twist
1/RNA	-0.7 (0.2)	-1.9 (0.2)	3.3 (0.2)	1.0 (1.4)	2.4 (1.9)	23.6 (1.7)
2/RNA	-0.9 (0.3)	-1.7 (0.2)	3.3 (0.1)	1.3 (1.5)	3.9 (1.9)	22.6 (1.3)
PNA/RNA (NMR)	0.3 (0.3)	-1.4 (0.6)	3.2 (0.4)	-2.8 (1.3)	4.6 (4.3)	29.4 (3.8)
PNA/RNA (MD)	-	-	-	-	-	24
PNA/RNA (X-RAY)	-0.8 (0.4)	-2.1 (0.3)	3.3 (0.1)	0.1 (1.3)	6.9 (3.5)	25.0 (1.6)
A-RNA	-	-	2.8	-	-	32.7

Table 2: Helicoidal parameters of the average structure of the more representative cluster of 1/RNA and 2/RNA MD simulations. Standard deviations are reported in brackets.

In particular, PNA 1- and 2-containing helices were slightly unwound and less bent with respect to the experimentally determined structures of PNA/RNA heteroduplexes, as indicated by the lower twist values. On the other side, the helices appeared slightly less bent than both NMR and XRAY derived structures because of lower roll values. The roll

parameter, indeed, indicated the degree of rotation with respect to the main helical axis, and, therefore, higher roll values are associated to higher perturbation of the coplanarity of bases, inducing the bending of the helix. The analysis of torsion angles of RNA and PNA backbones confirmed structural features very similar to those of reference experimental structures. RNA strand torsion angles closely resembled those found in the reference PNA/RNA NMR structure and in the canonical A-RNA structure. On the other side, as previously reported (21), (22)(23, 24), the PNA strand showed higher flexibility, particularly in torsion angles α and ϵ , that may assume two sets of values -100° and 100° and -20° and 180° , respectively. Taken together, these results indicated that the negatively charged tetrapeptide slightly affects the structural features of the heteroduplexes with respect to experimentally determined PNA/RNA heteroduplexes.

3.2.4 Biological Assays

Once demonstrated the ability of PNA to form a stable heteroduplex with the DNA, we examined its potential of being a miR-509-3p competitor in a biological context, by binding the seed region of the miRNA in the CFTR gene. Thus, we co-transfected different combinations of pLuc-CFTR-3'UTR vector, (a reporter luciferase construct sensitive to the miR-509-3p mimic action due to the presence of the 3'UTR of the *CFTR* gene), PNA strands, miR-509-3p mimic and corresponding PNA scrambled controls. The co-transfection of miR-509-3p in the presence of the scrambled PNA **3** reduced luciferase expression leading to a residual activity up to 35%. The co-transfection of PNA **1** in the presence of miR-509-3p rescued the luciferase activity by up to 70% (Figure 8), thus indicating that PNA**1** could counteract the inhibitory effects of miR509-3p. As expected, the addition of the PNA**1** alone did not produce any effect on the luciferase expression, thus confirming that the binding of PNA**1** to the 3'UTR of CFTR mRNA did not interfere with the expression of the CFTR protein. A different behavior was observed for the PNA**2**: while spectroscopic and MD data revealed that it was able to form a stable heteroduplex with the ODN, from a biological point of view, it was not able to rescue the luciferase activity.

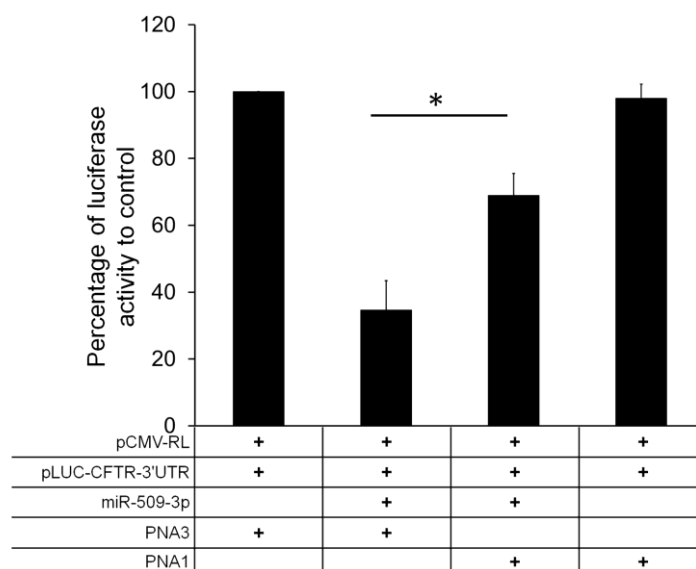


Figure 8: Effect of PNA **1** on miR-509-3p activity. A significant rescue of the luciferase expression was observed using **1**. Contrary, any rescue was observed using the scrambled PNA **3**. *P values < 0.006

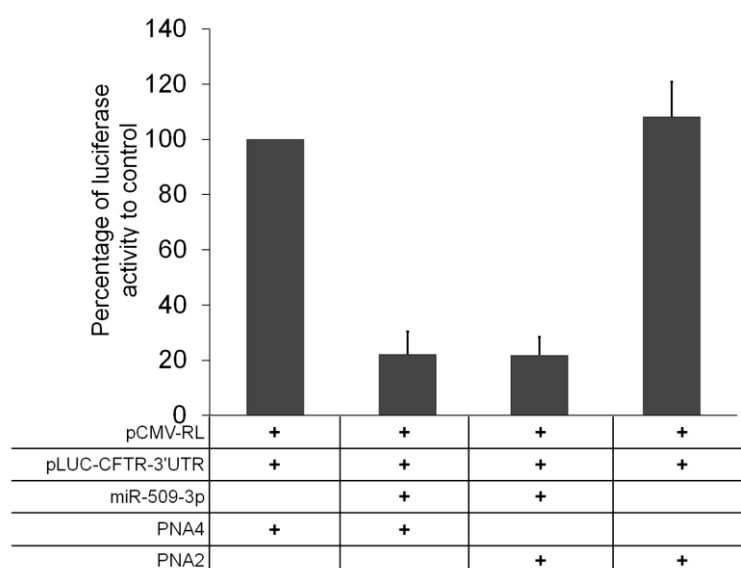


Figure 9: Effect of PNA 2 on miR-509-3p activity. No significant rescue of the luciferase expression was observed using 2. And as expected, any rescue was observed using the scrambled PNA 4.

3.3 Conclusions

In this work, we presented the use of PNA sequences as target protector agent. The chemical features of PNA make it a versatile tool in the field of gene modulation and, to date, several works have witnessed its potency in this context. However, beyond the classical and consolidated application as antigene, antisense and anti-miRNA agent, another interesting and less explored field can benefit from its properties, the miRNA target protectors, with the aim to increase the expression of CFTR in CF. The negatively charged PNAs **1** and **2**, conveniently modified at their C-ends and fully complementary to the 3'UTR region of the CFTR mRNA recognized by the seed region of miR-509-3p, were synthesized and characterized. To demonstrate the sequence dependent activity of **1** and **2**, two other PNAs (**3** and **4**, Table 1), containing scrambled sequences of **1** and **2** respectively, were designed and synthesized. A combination of spectroscopic techniques was firstly used to explore the capability of our PNA to bind the RNA target and the successful findings obtained were then confirmed by the biological assays. Furthermore, this type of approach has the advantage of being relatively mutation-independent. For this reason, it would be sufficient to increase the expression of a protein, even if mutated, to exceed the threshold of minimal activity needed to obtain an optimal clinical phenotype.

3.4 Materials and Methods

3.4.1. General Methods

All reagents and solvents were obtained from commercial sources and used without further purification. Phosphoramidites for DNA syntheses were purchased from Glen Research (Sterling, VA, USA). The ODNs were assembled by using the PerSeptive Biosystems Expedite DNA/RNA 8909 synthesizer using phosphoramidite chemistry. Peptide nucleic acid monomers were purchased from Link technologies (Bellshill, Lanarkshire, UK). Fmoc-L-Ser[PO(OBzl)OH]-OH was purchased from Iris Biotech GmbH (Marktredwitz, Germany).

Fmoc-Gly-OH and the MBHA resin (1% divinylbenzene, 200–400 mesh, 0.5 mmol/g loading) were purchased from Sigma-Aldrich (Saint Louis, MO, USA). The reactions on solid phase were performed using ISOLUTE® single fritted reservoirs (SG), 20 µm PE (polyethylene), equipped with tube caps and luer tip caps Biotage (Uppsala, Sweden) which were shaken in a Multi-reax vibrating shaker Heidolph (Schwabach, Germany). High performance liquid chromatography (HPLC) analyses and purifications were carried out on a Jasco UP-2075 Plus pump equipped with a Jasco (Easton, MD, USA) UV-2075 Plus UV detector using a 4.8 × 150 mm C-18 reverse-phase column (particle size 5 µm) eluted with a linear gradient of CH₃CN containing 0.1% (v/v) trifluoroacetic acid (TFA) in H₂O containing 0.1% (v/v) TFA (from 0 to 100% in 45 min, flow 1.2 mL/min). UV spectra were recorded on a Jasco V-530 spectrophotometer (Jasco). CD spectra were performed on a Jasco 1500 spectropolarimeter (Jasco) equipped with a Jasco PTC-348 WI Peltier-type temperature controller in a 0.1 cm path length cuvette. ESI-MS experiments were performed on an Applied Biosystems (Warrington, Cheshire, UK) 4000 QTRAP mass spectrometer in positive ion electrospray mode, dissolving the compounds in H₂O containing 0.1% (v/v) formic acid.

3.4.2. DNA Synthesis and Analysis

The oligonucleotide 5'GAAGCACCAATCA3' was synthesized using solid phase β-cyanoethyl phosphoramidite chemistry. After the synthesis, the oligomers were detached from the support and deprotected by treatment with concentrated aqueous ammonia at 55° C for 12 h. The combined filtrates and washings were concentrated under reduced pressure, redissolved in H₂O, and analyzed and purified by HPLC on a Macherey Nagel (Düren, Germany) Nucleogel SAX column 1000-8/46 using buffer A: 20 mM NaH₂PO₄ aqueous solution, pH 7.0, containing 20% (v/v) CH₃CN; buffer B: 1 M NaCl, 20 mM NaH₂PO₄ aqueous solution, pH 7.0, containing 20% (v/v) CH₃CN; a linear gradient from 0% to 100% B in 30 min and flow rate 1.2 mL/min were used. The oligomers were collected and successively desalted by Sep-Pak cartridges (C18). The isolated oligomers were >99% pure (NMR). The ODN concentration was determined spectrophotometrically at λ = 260 nm and 90° C, using the molar extinction coefficient ε = 200.9 cm⁻¹ · mM⁻¹ calculated by the nearest neighbor mode.

3.4.3. PNA Synthesis and Analysis

PNA sequences were synthesized using the Fmoc-solid-phase strategy. Fifty milligrams of MBHA resin (0.5 mmol/g), after swelling in CH₂Cl₂ for 30 min and DMF washings, were treated with a solution of 20% piperidine in DMF for 10 min. After washings in DMF (×5), the resin was reacted with Fmoc-Gly (5 eq. in NMP 0.2 M), 1-[Bis(dimethylamino)methylene]-1H-1,2,3-triazolo[4,5-b]pyridinium 3-oxid hexafluorophosphate (HATU) (5 eq. in DMF 0.2 M) and N,N-Diisopropylethylamine (DIPEA) (5 eq.)/lutidine (7.5 eq.) for 45 min at room temperature. Couplings of Fmoc-L-Ser[PO(OBzl)OH]-OH were achieved using the following conditions: Fmoc-Ser monomer (8 eq. in NMP 0.2 M), HATU (8 eq. in DMF 0.4 M), and DIPEA (8 eq.)/lutidine (12 eq.) for 15 h at room temperature. After the serine couplings, a further glycine residue was attached on the N-terminal of the serine tract following the previously described coupling with the glycine monomer. PNA monomers were reacted using the following conditions: monomer building block (10 eq. in NMP 0.2 M), HATU (10 eq. in DMF 0.2 M), and DIPEA (10 eq.)/lutidine (15 eq.), 45 min at room temperature. After each coupling step, capping with Ac₂O in the presence of pyridine was performed for 20 min

at r.t. Fmoc group was removed by a treatment with a 5% 1,8-Diazabicyclo[5,4,0]undec-7-ene (DBU) in DMF solution (5 min). In the case of Fmoc-Ser amino acids, the basic treatment was prolonged (20 min). At the end of synthetic cycles, the PNAs were cleaved from the solid support by treatment with TFA/anisole/ethanedithiol (9:1:1; v/v/v) for 4 h and the products were precipitated with cold diethyl ether. The precipitates were recovered by centrifugation, washed twice with diethyl ether, dissolved in water, and finally lyophilized. PNAs 3 and 4, chosen as the negative control and bearing the same functionalization of PNAs 1 and 2, were synthesized using the same standard Fmoc-solid-phase strategy. The PNAs were obtained with a 48–50% overall yield (94–95% medium yield for each coupling as estimated by Fmoc spectrophotometric measurements). The crude sample was purified by semipreparative reverse phase HPLC (see General methods). The collected fractions were lyophilized and the final pure product was characterized by ESI-MS (positive mode): ESI-MS (m/z) calcd. for PNAs 1 and 3 4003.4; found $[M+^3H]^3+$ 1335.5, $[M+^4H]^4+$ 1002.0; PNAs 2 and 4 2411.8; found $[M+^2H]^2+$ 1206.9, $[M+^3H]^3+$ 805.0. The amount of each PNA sample dissolved in pure water was estimated by quantitative UV at 90° C using the following molar extinction coefficients: PNAs 1 and 3 $\epsilon = 126.5 \text{ mL} \cdot \mu\text{mol}^{-1} \cdot \text{cm}^{-1}$; PNAs 2 and 4 $\epsilon = 75.2 \text{ mL} \cdot \mu\text{mol}^{-1} \cdot \text{cm}^{-1}$ and DNA $\epsilon = 134.2 \text{ mL} \cdot \mu\text{mol}^{-1} \cdot \text{cm}^{-1}$.

3.4.4. Preparation of DNA/PNA Heteroduplexes (Annealing Procedure)

The PNA/ODN heteroduplexes (1.5:1) were obtained by dissolving the mixture of the samples at the concentration of $2.0 \times 10^{-5} \text{ M}$ in 100 mM PBS and by heating the solution to 90° C for 5 min and then slowly cooling to room temperature over 12 h.

3.4.5. UV

The UV spectra were recorded with a Jasco V-530 UV spectrophotometer, in 100 mM PBS buffer at the concentration of 20 μM . They were recorded at 20 °C ($\lambda = 220\text{--}310 \text{ nm}$, 400 nm/min scanning speed, 2.0 nm bandwidth).

3.4.6. CD and CD Melting Studies

The CD spectra were recorded with a Jasco 1500 spectropolarimeter equipped with a Peltier-type temperature controller (PTC-348 WI) in a 0.1 cm cuvette, in 100 mM PBS buffer at the concentration of 20 μM . They were recorded at 5 °C ($\lambda = 220\text{--}310 \text{ nm}$, 200 nm/min scanning speed, 2.0 nm bandwidth) and averaged over three repetitions. A buffer baseline was subtracted from the CD spectra and the spectra were normalized to have zero at 320 nm. Thermal denaturation experiments were also carried out in the temperature range of 5–90 °C by monitoring the CD values at 266 nm for PNA 1/ODN and at 264 nm for PNA 2/ODN at a heating rate of 1.0 °C/min.

3.4.7. Molecular Dynamics (MD) Simulations

The initial structures were built following the same procedure described in (13), starting from the NMR structure of the RNA(GAGUUC)/PNA(GAACTC) duplex (PDB-ID 176D) (18). The correct sequence was obtained by mutating the bases using the X3DNA software (25). Each heteroduplex was built including three flanking bases on both the 30 and 50 ends of the

RNA segment. Thermalization of the duplex and production of MD trajectories were obtained using Amber 15 suite. The leap module of Ambergtools 15 was used to perform the parameterization of the systems, using the ff14SB force field (AMBER99SB and frcmod.ff14SB for peptide + ff99bsc0_chiOL3 for RNA) (26–28), and the Sanders et al. parameters for PNA (24), whereas the parameters for serine phosphate were taken from (24). TIP3P water molecules were added with at least a minimum spacing of 14.0 Å between the edge of the box and the molecules. Na⁺ counterions were added to neutralize the system. The system was geometrically minimized in three steps: (i) optimization of hydrogen atoms with 2000 steps of steepest descent algorithm and 8000 steps of conjugate gradient algorithm, (ii) optimization of water molecules and counterions with 2000 steps of steepest descent and 18,000 steps of conjugate gradient, and (iii) optimization of the whole system with 2000 steps of steepest descent and 8000 steps of conjugate gradient. The equilibration of the system was performed using the protocol described in (25). Briefly: (i) the system was thermalized in 240 ps, raising the temperature from 10 K to 298 K with a time step of 1 fs, and applying inter and intra-strand constraints of 20 kcal·mol⁻¹ ·Å⁻² in order to preserve, respectively, the W-C base pairs and the torsional angles of the RNA sugar; ii) the constraints were gradually removed from 20 kcal·mol⁻¹ ·Å⁻² to 0.1 kcal·mol⁻¹ ·Å⁻² in 240 ps at constant pressure (1 bar) and temperature (298 K). Finally, an equilibration step of 500 ps was run without constraints. Production runs were performed using a time step of 2 fs. The SHAKE algorithm was used for all hydrogen atoms in conjunction with periodic boundary conditions at constant pressure and temperature. Particle mesh Ewald was used for the treatment of long range electrostatic interactions, and a cut-off of 9 Å was used for non-bonded interactions. Each system was studied by means of 300 ns MD simulation runs in triplicate with random seeding for the initial velocities. To investigate more deeply the stability of the PNA 1/RNA system, we extended one run to 600 ns, for a total of 1200 ns for the PNA 1/RNA and 900 ns for the PNA 2/RNA. The analysis of the structure was carried out using the software Curves+ (29). The visualization of the trajectories and related snapshots were performed with Pymol andVMD, while the trajectory post-processing analysis was performed using Ambergtools15. Cluster analysis was performed through a hierarchical agglomerative (bottom-up) approach using a root-mean-square (RMS) metric comparing the heavy atoms in the central duplex base-pairs. Correlation analysis was performed calculating the Pearson correlation coefficient on torsion angles sampled each 0.01 ns.

3.4.8. Cell Line, Construct, and Transfections

A549 human lung carcinoma cells were purchased from ATCC (Manassas, VA, USA). The cells were maintained in Dulbecco's modified Eagle's medium (Gibco Invitrogen, North Andover, MA, USA) with 10% heat inactivated fetal bovine serum (HyClone Laboratories, South Logan, UT, USA) without the addition of antibiotics. A Luciferase construct bearing the 3'UTR of the CFTR gene was used as the miR-509-3p sensitive reporter system. The transfection of the A549 cells with miRNA-mimics (Qiagen, Hilden, Germany) or PNAs was performed with the Attractene Transfection Reagent (Qiagen). Briefly, the cells seeded in 96-well plates were cotransfected with the luciferase reporter construct, miR-509-3p mimic and the PNAs. The luciferase activity level was measured 24 h after transfection using the Dual-Glo Luciferase Assay System (Promega Corporation, Madison, WI, USA). The EnSpire Multimode Plate Reader (Perkin Elmer, Waltham, MA, USA) was used for the luminescence

assay using 96-multiwell black plates. The relative reporter activity was obtained by normalization to the Renilla luciferase activity.

3.5 Bibliography

1. Elborn, J.S. (2016) Cystic fibrosis. *Lancet*, 388, 2519–2531.
2. O'Sullivan, B.P. and Freedman, S.D. (2009) Cystic fibrosis. *Lancet*, 373, 1891–1904.
3. McCarty, N.A. (2000) Permeation Through The CFTR Chloride Channel. *J. Exp. Biol.*, 203, 1947–1962.
4. Gray, M.A., Winpenny, J.P., Verdon, B., Mcalroy, H. and Argent, B.E. (1995) Chloride Channels and Cystic Fibrosis of the Pancreas. *Biosci. Rep.*, 15.
5. Kaplan, E., Shwachman, H., Perlmutter, A.D., Rule, A., Khaw, K.-T. and Holsclaw, D.S. (1968) Reproductive Failure in Males with Cystic Fibrosis. *N. Engl. J. Med.*, 279, 65–69.
6. Cant, N., Pollock, N. and Ford, R.C. (2014) CFTR structure and cystic fibrosis. *Int. J. Biochem. Cell Biol.*, 52, 15–25.
7. Wainwright, C.E. and Elborn, J. et al. (2015) Lumacaftor–Ivacaftor in Patients with Cystic Fibrosis Homozygous for Phe508del CFTR. *N Engl J Med*, 3373, 220–31.
8. Heda, G.D. and Marino, C.R. (2000) Surface expression of the cystic fibrosis transmembrane conductance regulator mutant DeltaF508 is markedly upregulated by combination treatment with sodium butyrate and low temperature. *Biochem. Biophys. Res. Commun.*, 271, 659–664.
9. Griffiths-Jones, S., Saini, H.K., Van Dongen, S. and Enright, A.J. (2008) miRBase: tools for microRNA genomics. *Nucleic Acids Res.*, 36.
10. McKiernan, P.J. and Greene, C.M. (2015) MicroRNA Dysregulation in Cystic Fibrosis. *Mediators Inflamm.*, 2015, 529642.
11. Brown, P.N. and Yin, H. (2013) PNA-based microRNA inhibitors elicit anti-inflammatory effects in microglia cells. *Chem. Commun. Chem. Commun.*, 49, 4415–4417.
12. Amato, F., Tomaiuolo, R., Borbone, N., Elce, A., Amato, J., D'errico, S., De Rosa, G., Mayol, L., Piccialli, G., Oliviero, G., et al. Design, synthesis and biochemical investigation, by in vitro luciferase reporter system, of peptide nucleic acids as new inhibitors of miR-509-3p involved in the regulation of cystic fibrosis disease- gene expression. 10.1039/c3md00257h.
13. Amato, F., Tomaiuolo, R., Nici, F., Borbone, N., Elce, A., Catalanotti, B., D'Errico, S., Morgillo, C.M., De Rosa, G., Mayol, L., et al. (2014) Exploitation of a very small peptide nucleic acid as a new inhibitor of miR-509-3p involved in the regulation of cystic fibrosis disease-gene expression. *Biomed Res. Int.*, 2014.
14. Amato, F., Seia, M., Giordano, S., Elce, A., Zarrilli, F., Castaldo, G. and Tomaiuolo, R. (2013) Gene Mutation in MicroRNA Target Sites of CFTR Gene: A Novel Pathogenetic Mechanism in Cystic Fibrosis? *PLoS One*, 8, 1–6.
15. Viart, V., Bergougnoux, A., Bonini, J., Varilh, J., Chiron, R., Tabary, O., Molinari, N., Claustres, M. and Taulan-Cadars, M. (2015) Transcription factors and miRNAs that regulate fetal to adult CFTR expression change are new targets for cystic fibrosis. *Eur. Respir. J.*, 45, 116–128.
16. Kilså Jensen, K., Ørum, H., Nielsen, P.E. and Nordén, B. (1997) Kinetics for hybridization of peptide nucleic acids (PNA) with DNA and RNA studied with the BIAcore technique. *Biochemistry*, 36, 5072–5077.
17. Armitage, B.A. et al (2013) Strand Invasion of DNA Quadruplexes by PNA: Comparison of Homologous and Complementary Hybridization. *ChemBioChem*, 14, 1–21.
18. Nielsen, P.E. et al. (1993) PNA hybridizes to complementary oligonucleotides obeying the Watson-Crick hydrogen-bonding rules. *Nature*, 363, 566–568.
19. Brown, S.C., Thomson, S.A. and James M. Veal, D. (1993) NMR Solution Structure of a Peptide Nucleic Acid Complexed with RNA. *Science (80-.)*, 265, 777–780.
20. Kiliszek, A., Banaszak, K., Dauter, Z. and Rypniewski, W. (2016) The first crystal structures

of RNA–PNA duplexes and a PNA–PNA duplex containing mismatches—toward anti-sense therapy against TREDs. *Nucleic Acids Res.*, 44, 1937–1943.

21. Amato,F., Tomaiuolo,R., Nici,F., Borbone,N., Elce,A., Catalanotti,B., D'Errico,S., Morgillo,C.M., De Rosa,G., Mayol,L., *et al.* (2014) Exploitation of a very small peptide nucleic acid as a new inhibitor of miR-509-3p involved in the regulation of cystic fibrosis disease-gene expression. *Biomed Res. Int.*, 2014, 68–71.
22. Verona,M.D., Verdolino,V., Palazzesi,F. and Corradini,R. (2017) Focus on PNA Flexibility and RNA Binding using Molecular Dynamics and Metadynamics. *Sci. Rep.*, 7, 42799.
23. Autiero,I., Saviano,M. and Langella,E. (2014) Molecular dynamics simulations of PNA–PNA and PNA–DNA duplexes by the use of new parameters implemented in the GROMACS package: a conformational and dynamics study. *Phys. Chem. Chem. Phys.*, 16, 1868–1874.
24. Sanders,J.M., Wampole,M.E., Chen,C.-P., Sethi,D., Singh,A., Dupradeau,ois-Y., Wang,F., Gray,B.D., Thakur,M.L. and Wickstrom,E. (2013) Effects of Hypoxanthine Substitution in Peptide Nucleic Acids Targeting KRAS2 Oncogenic mRNA Molecules: Theory and Experiment. *J. Phys. Chem. B*, 117, 11584–11595.
25. Lu,X.-J. and Olson,W.K. (2003) 3DNA: a software package for the analysis, rebuilding and visualization of three-dimensional nucleic acid structures. *Nucleic Acids Res*, 31, 5108–5121.
26. Zgarbov,M., Otyepka,M., Sponer,J.R., St,A., Adek,M., Ban,P., Cheatham,T.E. and Jure,P. (2011) Refinement of the Cornell et al. Nucleic Acids Force Field Based on Reference Quantum Chemical Calculations of Glycosidic Torsion Profiles. *J. Chem. Theory Comput*, 7, 2886–2902.
27. Pé,A., Marchá,I.N., Svozil,D., Sponer,J., Cheatham Iii,T.E., Laughton,C.A. and Orozco,M. (2007) Refinement of the AMBER Force Field for Nucleic Acids: Improving the Description of a/g Conformers. *Biophys. J.*, 92, 3817–3829.
28. Maier,J.A., Martinez,C., Kasavajhala,K., Wickstrom,L., Hauser,K.E. and Simmerling,C. (2015) ff14SB: Improving the Accuracy of Protein Side Chain and Backbone Parameters from ff99SB. *J. CHEM. THEORY Comput.*, 11, 3696–3713.
29. Lavery,R., Moakher,M., Maddocks,J.H., Petkeviciute,D. and Zakrzewska,K. (2009) Conformational analysis of nucleic acids revisited: Curves+. *Nucleic Acids Res.*, 37, 5917–5929.

Chapter 4

Synthesis and Label Free Characterization of a Bimolecular PNA Homo Quadruplex for the construction of new K⁺ sensing probes

4.1 Introduction

One of the most interesting features of nucleic acids forming G-quadruplexes is the high polymorphism (1, 2). In fact, G-quadruplexes can give rise to a number of architectures, that depend on alternate strand orientations, loop connectivity, and syn-anti distribution of guanine bases around G-tetrads (3); this polymorphism makes them versatile scaffolds for creating new nanomaterials such as mechanical devices, templates, and biosensors (4,5). First of all, G-quadruplexes demonstrate a potentially high conductance (6) making them appropriate for applications in electronic nanodevices. Furthermore, the use of oligonucleotides for the assembly of inorganic nanocrystals has already been reported: in this case the hybridization properties of oligonucleotides led to the assembly of gold nanoparticles at distances given by the length of the oligonucleotides and led also to the formation of three-dimensional networks (7, 8).

Recently, it has been demonstrated that suitable G-rich ONs can be considered versatile scaffolds for the construction of oligonucleotide-based analytical sensing platforms (9). For example, as reported in literature, by connecting AuNPs (as probes) and suitable G-rich fragments (as the recognition element) is possible to obtain a rapid, simple, high sensitive and excellent selective sensor for the determination of K⁺, exploiting the conformation change from the “random coil” to a compact rigid G-quadruplex formed by the aggregation of the nanoparticles in solution (10).

However, the ability to control the assembly of nanomaterials from stable and well-defined building blocks represents a key step for the exploitation of the technological potential of these materials.

Several studies demonstrated that the formation of four-stranded (or tetramolecular) G-quadruplexes is slow and requires high oligonucleotide concentration (11). These unfavourable kinetic parameters could be disadvantageous in view of their potential use in the field of therapeutic but also of nanotechnology. The synthesis of modified quadruplexes could overcome these problems, and could help researcher in developing new building blocks with improved chemical-physical properties to be used in biotechnology.

For all these reasons, the research group of Professor Piccialli, some years ago, proposed the use of tetra-end linker (TEL) oligonucleotides. These modified oligonucleotides form very stable TEL-quadruplex structures (Fig.1).

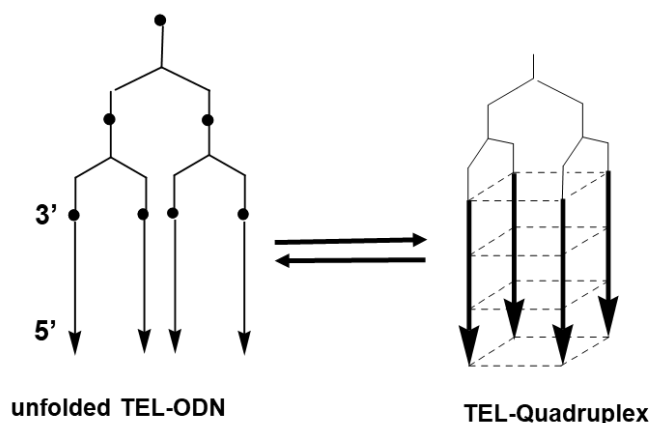


Figure 1: Schematic representation of unfolded (left) and folded (right) TEL-ODNs.

These new kind of quadruplex is formed by a cluster of four d(TG4T) hexanucleotides linked together by their 3'-ends (or 5'-ends) through a tetra-branched linker. Subsequently, the new structure has been proven to possess a remarkable thermal stability compared to its natural counterpart (12–14). Furthermore, TEL-quadruplexes have been shown to possess a high antiviral (HIV) activity acting as an aptamer that binds selectively the HIV-1 glycoprotein gp120 (15–17).

Since ODNs are susceptible to nucleases, and so unstable in biological fluids, their use has been often limited. For this reason, researchers realized the necessity for inclusion of chemical modifications to develop ODNs with improved features. In this context, one of the most promising ON analogue is Peptide Nucleic Acid (PNA). The first report concerning the design and properties of PNA was published in 1991 by Nielsen (18). PNA is a synthetic DNA mimic, in which the phosphodiester backbone of DNA/RNA is replaced with a polyamide–(2-aminoethyl) glycine–skeleton to which nucleobases are attached via a methylene carbonyl linker. By strict chemical means, PNA, is neither a peptide nor a nucleic acid, since its backbone is achiral uncharged polyamide. However, this atypical backbone gives PNA most appreciated advantages over other DNA analogues like phosphorothioates etc. PNA oligonucleotides are not recognized by proteases or nucleases and are therefore extremely stable in biological fluids (19)(20).

To date, the ability of PNA to form stable G-quadruplexes hasn't been so much investigated and, at the best of our knowledge, only tetramolecular PNA G-quadruplexes have been so far reported, despite their unfavourable kinetic and thermodynamic parameters (21).

In this context, exploiting our experience in the synthesis of branched linkers, the aim of my research work was to synthesize an unprecedented non-DNA bifunctional linker functionalized with two PNA strands (*bis-end-linker* PNA or *bel*-PNA), and to evaluate its ability to form quadruplexes.

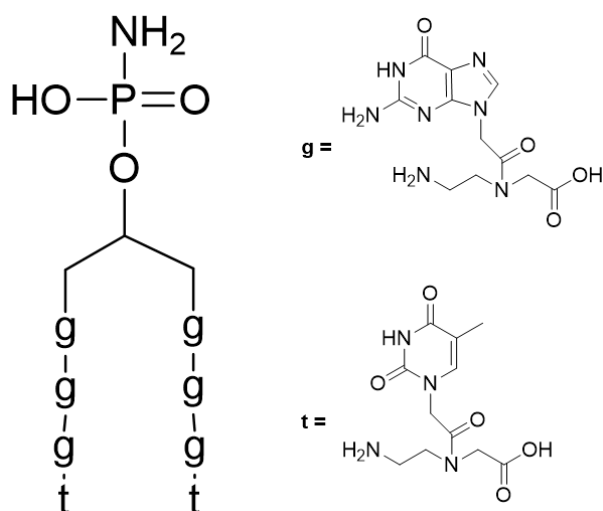


Figure 2: Structure of the *bel*-PNA.

Thanks to CD, CD melting and SERS experiments, it was proved that, in presence of K^+ , the *bel*-PNA could form a bimolecular PNA G-quadruplex structure.

The present study aimed at the design of a new PNA G-Q based sensor: in fact, once demonstrated the ability of the *bel*-PNA to form G-quadruplexes, further studies will be devoted to the realization of nanoparticles decorated with the *bel*-PNA to obtain lattice through quadruplexes connections.

4.2 Results and Discussion

My research work has been addressed on such targets:

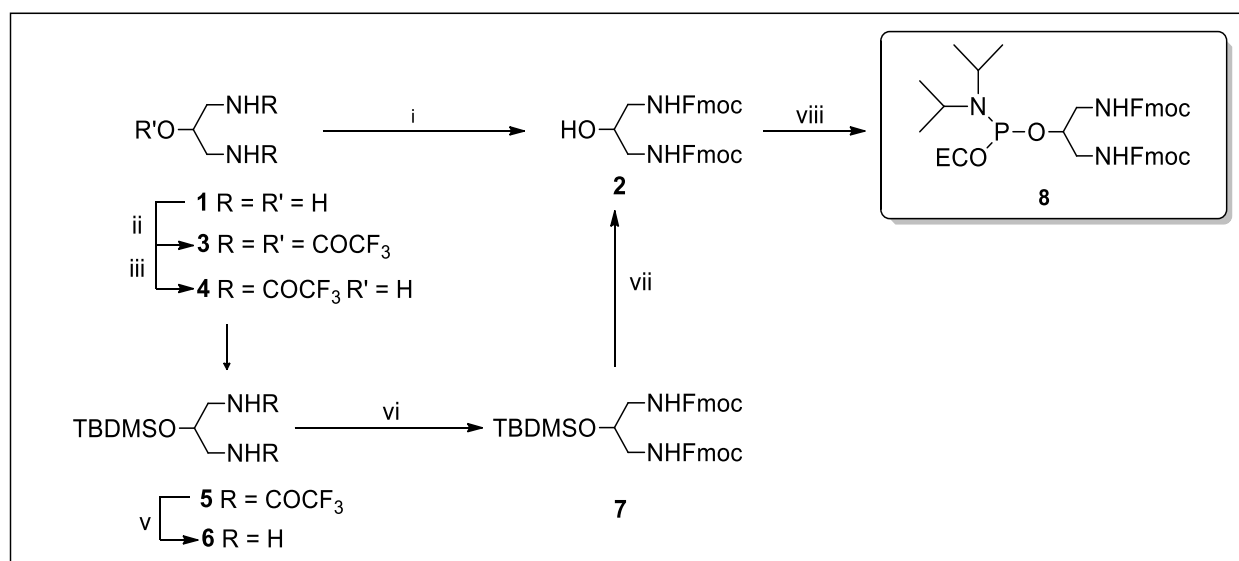
- 1) Synthesis of the non-nucleotidic linker;
- 2) Functionalization of the linker with PNA strands to form the *bel*-PNA;
- 3) Evaluation of the ability of the *bel*-PNA to form a PNA-based quadruplex.

4.2.1 Synthesis of the non-nucleotidic linker.

The first step for the preparation of the target compound contemplated the synthesis of the non-nucleotidic linker **8**.

The key reaction step was the selective Fmoc protection of the primary amino functions of **1**. In literature was reported that the selective Fmoc NH_2 protection in the presence of OH groups could be performed by using Fmoc-*N*-hydroxy succinimide ester or Fmoc-Cl reagents (22), but these procedures allowed us to obtain the target bis-Fmoc derivative **2** only in low yield, together with other variously protected by-products. The inability of modulating the nucleophilicity of the functional groups in the compound **1** towards Fmoc reagents forced us to explore an alternative synthetic route for the preparation of compound **2**, exploiting the protection of the OH group during the synthetic steps. Starting with the full protection of the three functional groups in **1** with an excess of CF_3COOEt , we obtained the

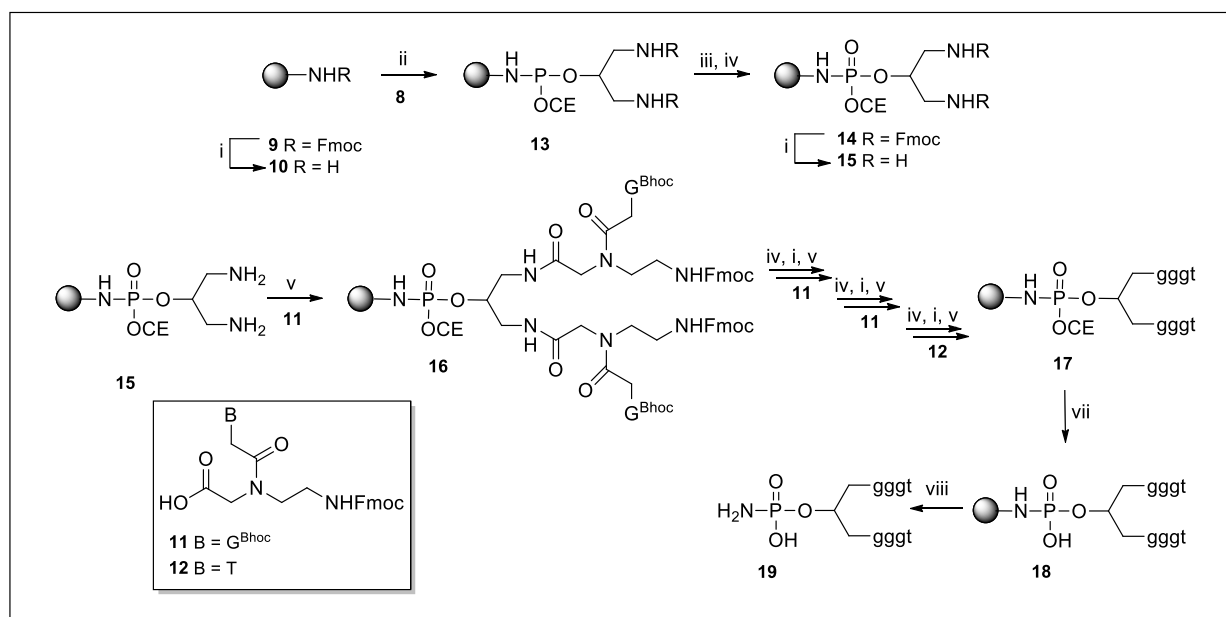
tri-protected derivative **3** in 97% yield. At this stage, we explored the selective deprotection of the OH group. Pleasingly, the treatment of the compound **3** with methanol afforded the derivative **4** by selective methanolysis of the trifluoroacetic ester. The alcohol **4** was then silylated, affording the derivative **5** in 62% yield. The quantitative deprotection of both amino groups in **5** was accomplished with saturated NH_3 in MeOH, to give compound **6** that was successfully transformed in its bis-Fmoc derivative **7** in 90% yield by reaction with Fmoc-Cl. Next, compound **7** was desilylated by treatment with the $3\text{HF}^+\text{TEA}$ complex and the free OH group of compounds **2** reacted with $(i\text{Pr})_2\text{NP}(\text{OCE})\text{Cl}$ to afford the phosphoramidite derivative **8**.



Scheme 1. i) Fmoc-*N*-hydroxy succinimide ester, Py, r.t., 16 h, or Fmoc-Cl, $\text{NaHCO}_3(\text{aq})$, CH_2Cl_2 , r.t., 16 h; ii) 1) CF_3COOEt , DCM, r.t., 1 h, iii) MeOH, r.t., 30 min; iv) TBDMSCl, Hym, DMF, r.t., 16 h; v) sat. NH_3 in MeOH, r.t., 16 h; vi) Fmoc-Cl, Py, r.t., 16 h; vii) $3\text{HF}^+\text{TEA}$, THF, r.t. 16 h; viii) 2-cyanoethyl-*N,N*-diisopropylchlorophosphoramidite, DIPEA, CH_2Cl_2 , THF, r.t., 1 h.

4.2.2 Functionalization of the linker with PNA strands to form the *bel*-PNA.

Thereafter, solid support **10**, after reaction with **8** in the presence of 1-*H*-tetrazole and oxidation with $t\text{BuOOH}$, gave the phosphoramidate containing support **14**. Cleavage of both Fmoc protecting groups on the functionalized resin **14** in basic solution allowed the construction of PNA strands using the standard protocols. At the end of the synthetic cycles, treatment of solid support **17** with concentrated $\text{NH}_4\text{OH}(\text{aq})$ gave the support **18** from which the BEL-PNA **19** was detached.



Scheme 2. Reagents: (i) piperidine/DMF, r.t., 10 min; (ii) **7**, 1-*H*-tetrazole, DCM, THF, r.t., 2 h; (iii) ^tBuOOH, THF, r.t., 30 min; (iv) Ac₂O/Py, r.t., 20 min; (v) **11**, HATU, DIPEA, lutidine, DMF, r.t., 30 min; (vi) **12**, HATU, DIPEA, lutidine, DMF, r.t., 30 min; (vii) conc. aq NH₄OH, MeOH, r.t., 2 h; (viii) *m*-cresole, TFA, r.t., 4 h.

The obtainment of pure compound **19** was assessed by ESI-MS analyses. Purified sample was dissolved in K⁺ buffer and subjected to the annealing procedure. The propensity of **19** to fold into the target bimolecular PNA quadruplex was then supported by means of spectroscopic techniques.

4.2.3 Evaluation of the ability of the *bel*-PNA to form a PNA-based quadruplex.

To investigate whether the *bel*-PNA adopted a quadruplex structure and, in case, to determine its nature and stability, CD studies, including CD thermal denaturation experiments, were carried out (23). The sample was analysed K⁺ buffer after the annealing procedure. The *bel*-PNA showed a CD profiles characterized by positive and negative bands centred around 283 and 260 nm, respectively, which are indicative of a bimolecular antiparallel stranded G-quadruplex structure. Upon the basis of these findings, it was reasonable to hypothesize that the antiparallel orientation of PNA strands could be due to the steric hindrance and charge repulsion of the negatively charged phosphate linker moieties. Furthermore, the apparent melting temperature of the PNA-based bimolecular quadruplex was to be estimated at around 25°C (Fig.3).

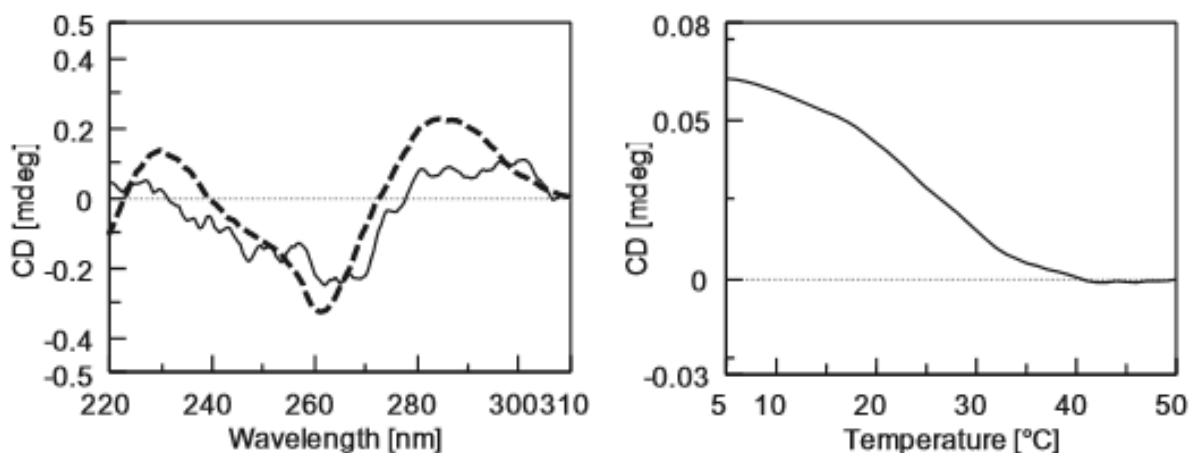


Figure 3: (left) CD spectra of BEL-PNA 19 (2.0×10^{-5} M) dissolved in pure water (solid line) or annealed in 0.1 M K⁺ buffer (dotted line), pH 7; (right) CD melting at 283 nm of 19 dissolved in K⁺ buffer.

It was to be noted that the backbone of PNAs is inherently achiral, so PNA G-Qs show a weak CD spectrum in comparison to their DNA analogues, as previously demonstrated by Balasumanian (21). The formation of such CD-unfriendly complexes could be monitored by using other spectroscopic techniques.

Among all, Surface-enhanced Raman scattering (SERS) has recently emerged as a unique technique to be used for the structural analysis of biomolecules. Since its discovery in 1977, SERS has received a huge interest from researchers because of its high sensitivity and the minimal required sample volume, making it an ideal tool for the investigation of precious biological samples (24). The high sensitivity of this technique derives from the strong enhancement of the Raman cross section when the analyte is close to metallic nanostructures. The metallic surface (typically silver or gold) is usually in the form of a thin layer of metallic film or a suspension of aqueous metallic colloidal nanoparticles. Several studies demonstrated the effectiveness of this technique for the detection of DNA bases or short DNA sequences (25).

Starting from these findings, recently, the research group of Professor Piccialli proposed, for the first time, the use of the SERS technique for having an insight of the formation of G-quadruplexes in solution (26). Furthermore, they also evaluate the stability of different kind of quadruplexes. In the proposed model, they also suggested that quadruplexes adopted a perpendicular or “standing-up” orientation with respect to the silver colloidal substrate, therefore exposing the guanine tetrad to the metallic surface. In doing so, this produced a favorable configuration for investigating the intrastrand bonding.

In this context, the aim of the work was to extend the applicability of this label-free technique to ascertain the formation of the bimolecular PNA-based quadruplex. SERS analysis of *bel*-PNA 19 annealed in K⁺ buffer was performed by acquiring the signals in 100 randomly selected points. Figure 5 shows the average SERS signal for *bel*-PNA molecules in the K⁺ buffer. To better highlight the SERS features a forth order baseline was removed and the spectrum was normalized to the height of the prominent peak at 1572 cm⁻¹. On the other hand, Table 1 summarizes the main SERS bands observed and their assignment. SERS spectra of PNA molecules (single strands) were firstly reported by Colaianni et al. (28); in this case, the spectra were mainly characterized by single nucleobase contributions as well as Amide I band due to the PNA backbone. Differently, our *bel*-PNA 19 in K⁺ annealed SERS

signals are dominated in the 1300-1600 cm^{-1} region by spectral features clearly due to guanine residues, also exhibiting some clear similarities with the spectral features observed in both spontaneous Raman scattering of telomeric DNA quadruplexes (29) and in SERS spectra of guanine-rich DNA sequences (26). Notably, the SERS spectrum shows a strong band at 1484 cm^{-1} easily assignable to the C8=N7-H2 deformation of the guanine tetrad, being therefore diagnostic of the Hoogsteen hydrogen bonding of the G.G pairs (28, 30). To the best of our knowledge, this outcome constitutes the first SERS-based evidence of PNA-quadruplex formation. This also confirms the outcome provided by CD-measurements, which reveals the arrangement of BEL-PNA 19 K^+ annealed in an antiparallel folded quadruplex structure. The other intense SERS peak at 1572 cm^{-1} can be identified with the C2=N3 guanine band appearing in the spontaneous Raman spectrum of quadruplexes around 1580 cm^{-1} . The $\sim 8 \text{ cm}^{-1}$ shift of this band for the SERS case has been previously observed by Pagba et al. (31) in the analysis of quadruplex-folded DNA and is likely due to the specific surface-induced selection rules of SERS. The band around 1220 cm^{-1} can be assigned to PO_2^- bonds (32), which are present in the *bel* linker. Numerous other bands of the spectrum in Figure 5 are clearly due to the peptide components of the molecule and to single unpaired components. For instance, the peak at 1165 cm^{-1} is likely due to a combination of $\nu(\text{C-N})$ and $\delta(\text{C-H})$ vibrations with some contributions of unpaired thymine residues (33), while the band at 791 cm^{-1} is certainly a ring mode from the moieties (28). Moreover, many protein-related Raman bands can be observed in the Amide III (1200-1310 cm^{-1}), Amide II (1540-1560 cm^{-1}) and Amide I (1610-1700 cm^{-1}) regions, the latter band mainly involving the C=O vibration. In particular, the Amide I band probably masks the presence of guanosine N1H bands which, being sensitive of the N1H environment, is usually a valuable indicator of the guanine interbase interaction strength. Importantly, a significant number of the acquired signals (more than 80%) exhibited a quite reproducible spectral pattern, the relative height of each feature being constant within 15% of its mean value. These spectra were dominated by features due to guanine residues, with only some contributions from the PNA backbone. The remaining spectra exhibited numerous bands associated with the CH vibration bands in the region 1350–1650 cm^{-1} , whose partial overlapping gave rise to a broad background in the same region. As it is well known, enhanced bands in SERS spectra are generally due to vibrational modes occurring in molecular moieties in close contact with the silver colloids. Therefore, the substantial reproducibility of spectra could be read in terms of a tendency of molecules to assume a well-defined orientation on the SERS substrate (Fig.4). A similar propensity to be ordered, mainly ruled by the electrostatic interaction of charged groups with the colloid surface, was previously observed by our group for DNA-based quadruplexes on Ag-colloids (26) and by Briones et al. for PNA strands on gold colloids (27). The reproducibility of SERS signals, together with the favourable exposure of guanines in PNA strands to the SERS substrate, revealed in most of SERS spectra, allowed us to get precious information on their structural arrangement.

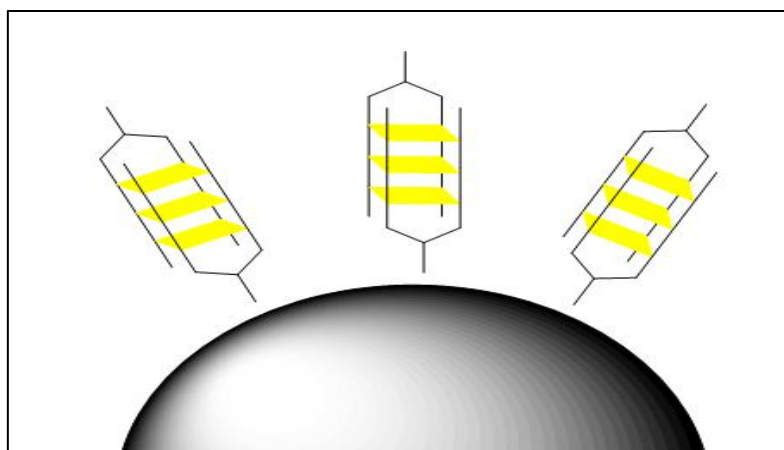


Figure 4: Schematic representation for the interaction between PNA-based quadruplex and the silver colloidal microparticle. G-tetrads are reported in yellow.

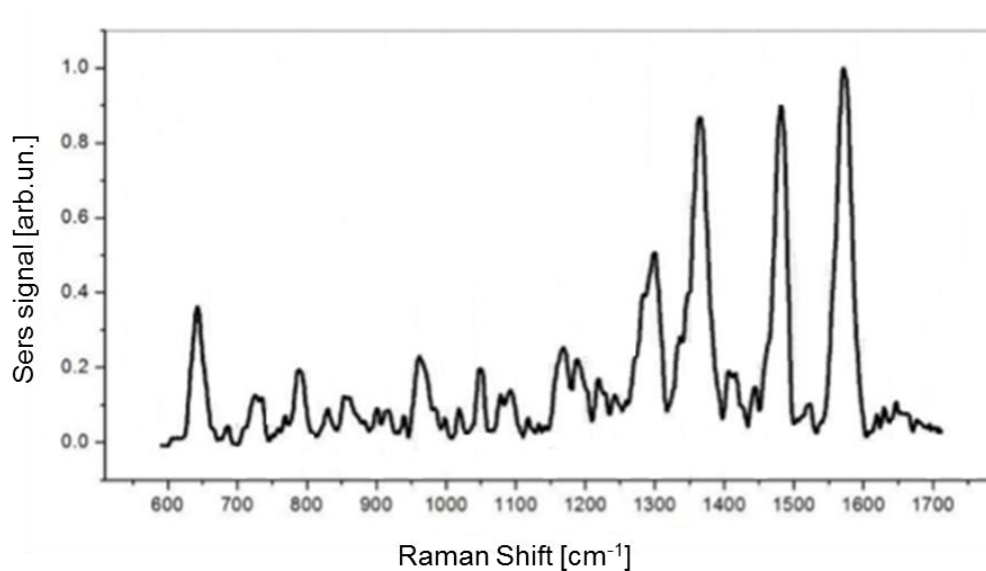


Figure 5: Average SERS signal from *bel*-PNA molecules in a K^+ buffer. This spectrum exhibits the typical band around 1484 cm^{-1} diagnostic of quadruplex formation.

Observed position (cm^{-1})	Assignment
785	Guanine ring
966	$\nu(\text{C-C})$
1160	$\nu(\text{C-N}) + \delta(\text{C-H}), \text{T}$
1220	PO_2^-
1300	Amide III
1484	$\text{C8}=\text{N7-H2}$
1542	Amide II

1572	C2=N3 of Guanine
1630	Amide III
1650	Amide III, $\nu(\text{CO}_2)$, $\nu(\text{C6O6})$

Table 1: Assignment of the prominent SERS features observed in this work.

4.3 Conclusions

The results, described in this work, confirm the potential of the *bel*-PNA, a new type of ON analogue, to form a bimolecular PNA-based quadruplex. In particular, it has been demonstrated that by tethering two G-rich PNA strands to the two ends of a suitable bifunctional linker it is possible to obtain bimolecular PNA homo quadruplexes after annealing in K^+ -containing buffers. Moreover, the formation of such CD-unfriendly complexes can be monitored, even at low concentrations, by using the SERS technique. Once demonstrated the ability of *bel*-PNA to fold into a new Bimolecular G-Q structure, the next step will be the functionalization of nanoparticles with the aim to obtain new sensing probes.

Given the importance of DNA G-quadruplexes in medicine and nanotechnology, the obtainment of G-quadruplex analogues provided with enhanced enzymatic stability, and their monitoring by highly sensitive label-free techniques, are of the highest importance.

4.4 Experimental section

All reagents and solvents were obtained from commercial sources and used without further purification. MBHA resin (1% divinylbenzene, 200–400 mesh, 0.5 mmol/g loading) was purchased from Sigma-Aldrich. The reactions on solid phase were performed using ISOLUTE® single fritted reservoirs (SG), 20 μm PE, equipped with tube caps and luer tip caps (Biotage) which were shaken in a Multi-reax vibrating shaker (Heidolph). High performance liquid chromatography (HPLC) analyses and purifications were carried out on a Jasco UP-2075 Plus pump equipped with a Jasco UV-2075 Plus UV detector using a 4.8 \times 150 mm C-18 reverse-phase column (particle size 5 μm) eluted with a linear gradient of CH_3CN containing 0.1% (v/v) TFA in H_2O containing 0.1% (v/v) TFA (from 0 to 100% in 45 min, flow 1.2 mL/min). UV spectra were recorded on a Jasco V-530 spectrophotometer. CD spectra were performed on a Jasco 1500 spectropolarimeter in a 0.1 cm path length cuvette. ^1H NMR experiments were performed using Varian Mercury Plus 400 MHz and Varian UNITYINOVA 500 MHz spectrometers in CD_3OD , D_2O , and acetone- d_6 solvents. Chemical shifts are reported in parts per million (δ) relative to residual solvents signals – CD_2HOD 3.31, $(\text{CD}_3)(\text{CD}_2\text{H})\text{CO}$ 2.09 – and assigned by $^1\text{H}/^1\text{H}$ COSY experiments. ^{31}P NMR experiments were performed on a Varian UNITYINOVA 500 MHz spectrometer using 85% H_3PO_4 as an external standard (0 ppm). Data were processed using the Varian VNMR software package. The abbreviations s, d, dd, m, bs, bd, bt represent singlet, doublet, doublet of doublets, multiplet, broad singlet, broad doublet and broad triplet, respectively. ESI-MS experiments were performed on a AB Sciex 4000 QTRAP mass spectrometer in positive ion electrospray mode. Column chromatography was performed on silica gel 60

(70–230 mesh ASTM, Merck) and analytical TLC analyses were performed on F₂₅₄ silica gel plates (0.2 mm thick, Merck) with TLC spots being detected under UV light (λ = 254 nm).

4.4.1. Synthesis of Fmoc protected *be*-linker 8

2.2.1. N,N'-(2-hydroxypropane-1,3-diyl)bis(2,2,2-trifluoroacetamide) (4) To an ice-cooled solution of 1,3-diamino-2-propanol 1 (0.10 g, 1.1 mmol) in CH₂Cl₂ (1 mL), CF₃COOEt (0.6 mL, 5.0 mmol) was added dropwise. The mixture was stirred at 0 °C for 60 min (TLC monitoring: CH₂Cl₂/CH₃OH = 95:5) and then quenched with CH₃OH at r.t. for 30 min. Volatiles were removed by rotary evaporation, thus obtaining 4 (0.302 g, 97% yield) as an amorphous solid that was used for the next reaction step without purification. ¹H NMR (400 MHz, CD₃OD) δ 3.92–3.84 (m, 1H, CH), 3.37 (dd, *J* = 4.7, 13.7 Hz, 2H, 2 × Ha), 3.28 (dd, *J* = 7.2, 13.7 Hz, 2H, 2 × Hb). ESI-MS (*m/z*) calcd. for C₇H₈F₆N₂NaO₃ [*M* + Na]⁺ 305; found 305.

4.4.2 N,N'-(2-((tert-butyldimethylsilyl)oxy)propane-1,3-diyl)bis(2,2,2-trifluoroacetamide) (5)

tert-butyldimethylsilyl chloride (0.96 g, 0.6 mmol) and imidazole (0.06 g, 1.0 mmol) were dissolved in dry DMF and the solution cooled at 0 °C in an ice-bath. Compound 4 (0.150 g, 0.53 mmol), dissolved in dry DMF (2 mL), was added dropwise and the mixture was stirred for 24 h (TLC monitoring: CH₂Cl₂/CH₃OH = 95:5). The reaction was quenched by adding CH₃OH and the mixture was diluted with AcOEt (30 mL) and washed with Brine (3 × 30 mL). The organic phase was dried over Na₂SO₄ and evaporated. The crude was purified over a silica gel column eluted with increasing amounts of CH₃OH in CH₂Cl₂ (up to 3%) giving pure 5 (0.13 g, 62% yield) as a white foam. ¹H NMR (400 MHz, CD₃OD) δ 4.06–3.98 (m, 1H, CH), 3.38–3.26 (m, 4H, 2 × CH₂), 0.89 (s, 9H, ^tBu), 0.089 (s, 6H, 2 × CH₃). ESI-MS (*m/z*) calcd. for C₁₃H₂₂F₆N₂NaO₃Si [*M* + Na]⁺ 419; found 419.

4.4.3. 2-((tert-butyldimethylsilyl)oxy)propane-1,3-diamine (6)

Compound 5 (0.13 g, 0.33 mmol) was dissolved in sat. NH₃ in CH₃OH (1 mL) and kept at r.t. for 16 h (TLC monitoring: CH₂Cl₂/CH₃OH/ NH₃(aq)=7:3:0.2). The solvents were removed under reduced pressure and the crude was purified over a silica gel column eluted with increasing amounts of CH₃OH in CH₂Cl₂ (up to 30%), giving pure 6 (0.07 g, 99% yield) as an oil. ¹H NMR (400 MHz, CD₃OD) δ 4.22–4.15 (m, 1H, CH), 3.12–3.02 (m, 4H, 2 × CH₂), 0.94 (s, 9H, ^tBu), 0.18 (s, 6H, 2 × CH₃). ESI-MS (*m/z*) calcd. for C₉H₂₅N₂O₃Si [*M* + Na]⁺ 205; found 205.

4.4.4. bis((9H-fluoren-9-yl)methyl) (2-((tert-butyldimethylsilyl)oxy)propane-1,3-diyl)dicarbamate (7)

To a solution of 6 (0.05 g, 0.25 mmol) in dry pyridine (5 mL), Fmoc-Cl (0.14 g, 0.54 mmol) was added and the mixture was shaken at r.t. for 16 h (TLC monitoring: CHCl₃/CH₃OH = 95:5). The reaction was quenched by addition of CH₃OH, solvents were removed under reduced pressure and the crude purified over a silica gel column eluted with increasing amounts of CH₃OH in CHCl₃ (up to 2%), affording pure 7 (0.11 g, 90% yield) as an amorphous white solid. ¹H NMR (400 MHz, CD₃OD) δ 7.76–7.19 (complex signal, 16H, arom. Fmoc), 4.30 (d, *J* = 6.6 Hz, 4H, 2 × CH₂ Fmoc), 4.13 (t, *J* = 6.5 Hz, 2H, 2 × CH Fmoc), 3.05 (d, *J* = 5.5 Hz, 4H, 2 × CH₂), 0.82 (s, 9H, ^tBu), 0.00 (s, 6H, 2 × CH₃). ESI-MS (*m/z*) calcd. for C₃₉H₄₄N₂NaO₅Si [*M* + Na]⁺ 671; found 671.

4.4.5. bis((9H-fluoren-9-yl)methyl) (2-hydroxypropane-1.3-diyl) dicarbamate (2)

Compound 7 (0.08 g, 0.12 mmol) was dissolved in THF (8 mL) and treated with TEA*3HF (196 μ L, 1.2 mmol) at r.t. for 16 h (TLC monitoring: CHCl₃/CH₃OH, 95:5). Volatiles were removed under reduced pressure and the crude purified over a silica gel column eluted with increasing amounts of CH₃OH in CHCl₃ (up to 5%), giving pure 2 (0.06 g, 90% yield) as an amorphous white solid. ¹H NMR (400 MHz, CD₃OD) δ 7.90–7.20 (complex signal, 16H, arom. Fmoc), 4.35 (bd, 4H, 2 \times CH₂ Fmoc), 4.23 (bt, 2H, 2 \times CH Fmoc), 3.73–3.61 (m, 1H, CH), 3.05–3.23 (complex signal, 4H, 2 \times CH₂). ESI-MS (m/z) calcd. For C₃₃H₃₁N₂O₅ [M + H]⁺ 535; found 535.

4.4.6. bis((9H-fluoren-9-yl)methyl)(2-(((2-cyanoethoxy)(diisopropylamino)phosphino)oxy)propane-1.3-diyl)dicarbamate (8)

2 (0.06 g, 0.11 mmol) was dissolved in a 1:1 (v/v) mixture of dry CH₂Cl₂/THF (3 mL), DIPEA was added (60 μ L, 0.33 mmol) followed by addition of 2-cyanoethyl-N,N-diisopropylchlorophosphoramidite (40 μ L, 0.18 mmol). The mixture was stirred for 1 h at r.t. (TLC monitoring: n-hexane/AcOEt/DIPEA = 6:4:0.1) then diluted with AcOEt (30 mL) and washed with brine (4 \times 30 mL). The organic phase was dried over Na₂SO₄ and evaporated under reduced pressure. The crude was purified over a silica gel column eluted with increasing amounts of AcOEt in n-hexane (up to 40%), giving pure 8 (0.048 g, 59% yield) as a white foam. ¹H NMR (500 MHz, acetone-d₆) δ 7.86–7.25 (complex signal, 16H, arom. Fmoc), 4.36 (d, J = 8.6 Hz, 2H, CH₂ Fmoc), 4.33 (d, J = 8.6 Hz, 2H, CH₂ Fmoc), 4.26–4.17 (m, 2H, 2 \times CH Fmoc), 4.01–3.93 (m, 1H, CHO), 3.90–3.70 (complex signal, 2H, CH₂O), 3.67–3.59 (m, 1H, CHN), 3.36–3.28 (m, 4H, 2 \times CH₂N), 2.71–2.65 (m, 2H, CH₂CN), 1.18–1.13 (two overlapped doublets, J = 6.5 and 6.6 Hz, 12H, 4 \times CH₃). ³¹P NMR (202 MHz, acetone-d₆) δ 149.5 (s). ESI-MS (m/z) calcd. For C₄₂H₄₇N₄NaO₆P [M + Na]⁺ 757; found 757.

4.4.7. Synthesis of *beI*-PNA 19

beI-PNA 19 was synthesized using the Fmoc-solid-phase strategy. In particular, 50 mg of MBHA resin 9 (0.5 mmol/g), after swelling in CH₂Cl₂ for 30 min and DMF washings, was treated with a solution of 20% piperidine in DMF for 10 min, giving solid support 10. After washings with DMF, the resin 10 was swelled in a 1:1 solution of CH₂Cl₂/THF (1 mL) and reacted with compound 8 (74 mg, 0.1 mmol) in the presence of 1-H-tetrazole (13 mg, 0.19 mmol) for 2 h at r.t., affording, after washings with a 1:1 solution of CH₂Cl₂/THF, the solid support 13. The last was swelled in THF (1 mL) and treated with ^tBuOOH (5.5 M in decane, 50 μ L, 0.25 mmol) for 30 min at r.t. giving, after washings with THF and then CH₂Cl₂, the solid support 14. The resin 14 was swelled in CH₂Cl₂ for 30 min, washed with DMF and treated with a solution of 20% piperidine in DMF for 10 min, thus obtaining solid support 15. The eluate was collected, and the coupling yield was estimated by Fmoc spectrophotometric measurements (98%). PNA chains were assembled by reacting PNA monomers (11 or 12, 5 equiv.) in the presence of HATU (5 equiv), DIPEA (5 equiv) and lutidine (6 equiv.), for 30 min at r.t. After each coupling step, capping with Ac₂O in the presence of pyridine was performed by shaking the corresponding support with the reagents mixture for 20 min at r.t. At the end of synthetic cycles, cyanoethyl groups were removed suspending the resin 17 in conc. NH₄OH(aq) for 2 h at r.t., affording solid support 18. Next, the synthesized *beI*-PNA was cleaved off suspending the resin 18 in a TFA/m-cresol (4:1, v/v) solution for 4 h at r.t. and precipitated with cold diethyl ether. The precipitates were recovered by centrifugation, washed twice with diethyl ether, dissolved in water and finally lyophilized. *beI*-PNA 19 was obtained with a 48–50% overall yield (94% average yield for each coupling). The crude sample was purified by semipreparative RP-HPLC. The collected fractions were lyophilized,

and the final pure product was characterized by ESI-MS (positive mode): ESI-MS (m/z) calcd. for $C_{91}H_{123}N_{53}O_{29}P$ $[M + H]^+$ 2453; found 2453.

4.4.8. Obtainment of quadruplexes (annealing)

The target dimeric PNA G-Q was obtained by dissolving the *beI*-PNA 19 at the concentration of 2.0×10^{-5} M in 100 mM K^+ buffer (KH_2PO_4 10 mM, KCl 90 mM, pH 7.0) and by heating the solution at 90 °C for 10 min and then slow cooling to room temperature over 3 h. The solution was equilibrated at 4 °C for 72 h before characterizations.

4.4.9. UV and CD studies

The concentration of 19, dissolved in pure water, was determined by UV measurements at 260 nm at 90 °C using the nearest-neighbor calculated molar extinction coefficient of the gggt PNA strand multiplied by 2 (the number of PNA strands linked to *beI*) (calculated $\epsilon = 43.9 \text{ mL cm}^{-1} \mu\text{mol}^{-1}$). The CD spectra were recorded both in pure water and in the 100 mM K^+ buffer at final single strand concentration of 20 μM . The spectra were recorded at 5 °C ($\lambda=220\text{--}310$ nm, 200 nm/min scanning speed, 2.0 nm bandwidth) and averaged over 50 repetitions. A buffer baseline was subtracted from the CD spectra and the spectra were normalized to have zero at 320 nm. Thermal denaturation experiments on 19 were also carried out in the temperature range of 5–90 °C by monitoring CD values at 282 nm at a heating rate of 1.0 °C/min.

4.4.10 SERS studies

Ag colloids were used as the SERS substrate; briefly, $AgNO_3$ (90 mg) was dissolved in 500 mL of H_2O and brought to the boil. Next, a sodium citrate solution (1%w/w) was added under vigorous stirring and then the resulting mixture was kept boiling for 1 h. All chemicals were purchased from Sigma- Aldrich. Before use, the silver solution was appropriately diluted with distilled water. SERS spectra were recorded using the WiTec Alpha 300 system, a confocal Raman system endowed with a Raman probe at 532 nm focused on the sample through a Nikon 60 \times dry objective ($NA = 0.8$ and $WD = 300 \mu\text{m}$). The back-scattered light from the sample, after proper filtering to remove the pump radiation, was sent to a high throughput spectrometer equipped with two diffraction gratings with 600 and 1800 gmm^{-1} , providing a resolution, respectively, of 3.6 and 1.5 cm^{-1} . Photons were detected by a back-illuminated Andor CCD camera (DV401A-BV-352, 1024 \times 400 pixels) operating at -60 °C. The confocal conditions were imposed by the 25 μm core (acting as a pin-hole) of the multimode fibre delivering the signal to the spectrometer. SERS analysis was performed on samples at a concentration of 20 μM . For the measurements, a proper diluted aliquot of the silver colloid solution was added to the sample and the analyte was allowed to bind for 2 h at room temperature prior to spectrum acquisition. To avoid any photochemical-induced effect, the Raman probe power impinging on the sample was limited to 50 μW while the integration time was 5 s. Under this condition, SERS spectra were comparatively stable and the signal-to-noise ratio was higher than 100 on the single acquisition.

4.5 References

1. Marchand, A. and Erie Gabelica, V. (2016) Folding and misfolding pathways of G-quadruplex DNA. *Nucleic Acids Res.*, 44, 10999–11012.
2. Burge, S., Parkinson, G.N., Hazel, P., Todd, A.K. and Neidle, S. (2006) Quadruplex DNA: sequence, topology and structure. *Nucleic Acids Res.*, 34, 5402–5415.
3. Burge, S., Parkinson, G.N., Hazel, P., Todd, A.K. and Neidle, S. (2006) Quadruplex DNA: Sequence, topology and structure. *Nucleic Acids Res.*, 34, 5402–5415.
4. Dutta, K., Fujimoto, T., Inoue, M., Miyoshi, D. and Sugimoto, N. (2010) Development of new functional nanostructures consisting of both DNA duplex and quadruplex. *Chem. Commun.*, 46, 7772–7774.
5. Tintoré, M., Eritja, R. and Fábrega, C. (2014) DNA nanoarchitectures: Steps towards biological applications. *ChemBioChem*, 15, 1374–1390.
6. Liu, S.P., Weisbrod, S.H., Tang, Z., Marx, A., Scheer, E. and Erbe, A. (2010) Direct measurement of electrical transport through G-quadruplex DNA with mechanically controllable break junction electrodes. *Angew. Chemie - Int. Ed.*, 49, 3313–3316.
7. Alivisatos, A.P., Johnsson, K.P., Peng, X., Wilson, T.E., Loweth, C.J., Bruchez, M.P. and Schultz, P.G. (1996) Organization of 'nanocrystal molecules' using DNA. *Nature*, 382, 609–611.
8. Mirkin, C.A., Letsinger, R.L., Mucic, R.C. and Storhoff, J.J. (1996) A DNA-based method for rationally assembling nanoparticles into macroscopic materials. *Nature*, 382, 607–609.
9. Ruttkay-Nedecky, B., Kudr, J., Nejd, L., Maskova, D., Kizek, R. and Adam, V. (2013) G-quadruplexes as sensing probes. *Molecules*, 18, 14760–14779.
10. Chen, Z.B., Guo, J.X., Ma, H., Zhou, T. and Li, X.X. (2014) A simple colorimetric sensor for potassium ion based on DNA G-quadruplex conformation and salt-induced gold nanoparticles aggregation. *Anal. Methods*, 6, 8018–8021.
11. Mergny, J.L., De Cian, A., Ghelab, A., Saccà, B. and Lacroix, L. (2005) Kinetics of tetramolecular quadruplexes. *Nucleic Acids Res.*, 33, 81–94.
12. Oliviero, G., Amato, J., Borbone, N., Galeone, A., Petraccone, L., Varra, M., Piccialli, G. and Mayol, L. (2006) Synthesis and characterization of monomolecular DNA G-quadruplexes formed by tetra-end-linked oligonucleotides. *Bioconjug. Chem.*, 17, 889–898.
13. Oliviero, G., Borbone, N., Amato, J., D'Errico, S., Galeone, A., Piccialli, G., Varra, M. and Mayol, L. (2009) Synthesis of quadruplex-forming tetra-end-linked oligonucleotides: Effects of the linker size on quadruplex topology and stability. *Biopolymers*, 91, 466–477.
14. Oliviero, G., Amato, J., Borbone, N., Galeone, A., Varra, M., Piccialli, G. and Mayol, L. (2006) Synthesis and Characterization of DNA Quadruplexes Containing T-Tetrads Formed by Bunch-Oligonucleotides. *Biophys. Chem.*, 81, 194–201.
15. Tsuzuki, T., Sakaguchi, N., Kudoh, T., Takano, S., Uehara, M., Murayama, T., Sakurai, T., Hashii, M., Higashida, H., Weber, K., et al. (2013) Design and synthesis of cyclic ADP-4-thioribose as a stable equivalent of cyclic ADP-ribose, a calcium ion-mobilizing second messenger. *Angew. Chemie - Int. Ed.*, 52, 6633–6637.
16. Oliviero, G., Amato, J., Borbone, N., D'Errico, S., Galeone, A., Mayol, L., Haider, S., Olubiyi, O., Hoorelbeke, B., Balzarini, J., et al. (2010) Tetra-end-linked oligonucleotides forming DNA G-quadruplexes: a new class of aptamers showing anti-HIV activity. *Chem. Commun.*, 46, 8971.
17. D'Atri, V., Oliviero, G., Amato, J., Borbone, N., D'Errico, S., Mayol, L., Piccialli, V., Haider, S., Hoorelbeke, B., Balzarini, J., et al. (2012) New anti-HIV aptamers based on tetra-end-linked DNA G-quadruplexes: effect of the base sequence on anti-HIV activity. *Chem. Commun.*, 48, 9516.

18. Nielsen, P., Egholm, M., Berg, R. and Buchardt, O. (1991) Sequence-selective recognition of DNA by strand displacement with a thymine-substituted polyamide. *Science* (80-.), 254.
19. Pooga, M., Land, T., Bartfai, T. and Langel, Ü. (2001) PNA oligomers as tools for specific modulation of gene expression. *Biomol. Eng.*, 17, 183–192.
20. Pooga Margus, Land Tiit, Bartfai Tamas, L.U. (2001) PNA oligomers as tools for specific modulation of gene expression. *Biomol. Eng.*, 17, 183–192.
21. Krishnan-Ghosh, Y., Stephens, E. and Balasubramanian, S. (2004) A PNA 4 Quadruplex. *J. AM. CHEM. SOC.*, 126, 5944–5945.
22. Crestey, F., Ottesen, L.K., Jaroszewski, J.W., Franzyk, H., Nhfmoc, H., Nhfmoc, H.R., R 'r 'n, R.R., R ', F., Nhfmoc, R., Ho, H., *et al.* (2008) Efficient loading of primary alcohols onto a solid phase using a trityl bromide linker. *Tetrahedron Lett.*, 49, 5890–5893.
23. Karsisiotis, A.I., Hessari, N.M.A., Novellino, E., Spada, G.P., Randazzo, A. and Webba Da Silva, M. (2011) Topological characterization of nucleic acid G-quadruplexes by UV absorption and circular dichroism. *Angew. Chemie - Int. Ed.*, 50, 10645–10648.
24. Cialla, D., Pollok, S., Steinbrücker, C., Weber, K. and Popp, J. (2014) SERS-based detection of biomolecules. *Nanophotonics*, 3, 383–411.
25. Xu, L.-J., Lei, Z.-C., Li, J., Zong, C., James Yang, C. and Ren, B. (2015) Label-Free Surface-Enhanced Raman Spectroscopy Detection of DNA with Single-Base Sensitivity. *J. Am. Soc.*, 137, 5149–5154.
26. Rusciano, G., Luca, A.C. De, Pesce, G., Sasso, A., Oliviero, G., Amato, J., Borbone, N., Errico, S.D., Piccialli, V., Piccialli, G., *et al.* (2011) Label-Free Probing of G-Quadruplex Formation by Surface-Enhanced Raman Scattering. *Anal. Chem.*, 83, 6849–6855.
27. Briones, C., Mateo-Martí, E., Gómez-Navarro, C., Parro, V., Román, E. and Martín-Gago, J.A. (2004) Ordered Self-Assembled Monolayers of Peptide Nucleic Acids with DNA Recognition Capability. *Phys. Rev. Lett.*, 93.
28. May Colaianni, S.E., Aubard, J., Høime Hansen, S. and Faurskov Nielsen, O. (1995) Raman spectroscopic studies of some biochemically relevant molecules. *Vib. Spectrosc.*, 9, 111–120.
29. Krafft, C., Benevides, J.M. and Thomas, G.J. (2002) Secondary structure polymorphism in Oxytricha nova telomeric DNA. *Nucleic Acids Res.*, 30, 3981–3991.
30. Miura, T. and Thomas, G.J. (1994) Structural Polymorphism of Telomere DNA: Interquadruplex and Duplex-Quadruplex Conversions Probed by Raman Spectroscopy. *Biochemistry*, 33, 7848–7856.
31. Pagba, C. V., Lane, S.M. and Wachsmann-Hogiu, S. (2009) Raman and surface-enhanced Raman spectroscopic studies of the 15-mer DNA thrombin-binding aptamer. *J. Raman Spectrosc.*, 41, n/a-n/a.
32. Arrondo, J.L.R. and Goñi, F.M. (1998) Infrared studies of protein-induced perturbation of lipids in lipoproteins and membranes. *Chem. Phys. Lipids*, 96, 53–68.
33. Mateo-Martí, E., Briones, C., Pradier, C.M. and Martín-Gago, J.A. (2007) A DNA biosensor based on peptide nucleic acids on gold surfaces. *Biosens. Bioelectron.*, 22, 1926–1932.

Chapter 5

Concluding Remarks and Future Perspectives

The present thesis has been devoted to exploring the most promising and fascinating applications of nucleic acids. Hereafter, the most important results of my research.

The first part of my research was focused on the use of oligonucleotides in supramolecular chemistry. In this context, I synthesized and characterized a novel G-rich ODN sequence for the development of long G-wires; The basic idea has been to create a stable monomeric G-quadruplex having two 5'-CG ends able to polymerize using its two 5'-sticky ends and thus to obtain long g-wires like poly-(Q)_n exploiting the 5'-5' π -stacking between G(:C) G(:C) G(:C) G(:C) octads formed by 5'-CG ends. So, the 7-mer d(5'-CGG-3'-3'-TGGC-5') containing a 3'-3' phosphodiester bond that reverse the polarity in the strand thus creating two 5'-ends, has been synthesized. Particularly, once annealed our sample in potassium buffer, it has been possible to visualize, according to their different electrophoretic mobility, a distribution of objects, starting from the monomeric G-quadruplex species (fastest species) through to an indistinct mixture of higher order objects (slowest species). The SEC-HPLC analysis has been particularly interesting: the obtained chromatograms have allowed us to identify, by analysing the retention times, all the multimers formed by the examined species and to isolate those objects. In addition, by varying the experimental conditions, it was possible to demonstrate that the pattern of the peaks was concentration/temperature-dependent. Furthermore, circular dichroism and NMR spectroscopies have contributed to further characterizing these higher order structures, while AFM analysis has allowed to visualize these structures and define their dimensions.

An interesting development of this work could be aimed at the study of the interaction of these higher order structures with ligands in order to obtain further information about the self-assembly process, in particular by studying the effect of such molecules on the multimerization.

The second part of my research was focused on the use of the most intriguing oligonucleotide analogue, the Peptide Nucleic Acid, and, in particular I synthesized and characterized four PNA sequences to be used in a novel approach for the treatment of Cystic Fibrosis (target protector strategy), in which the basic idea was to mask the miRNA binding region of 3'UTR region of the CFTR gene by the action of miRNA, with the effect to increase the production of CFTR protein. In this context, we have synthesized and characterized 2 PNA sequences (and related scramble sequences used as a negative control) and through spectroscopic studies, such as circular dichroism and UV, their ability to form structures hybrids with the target has been evaluated: from such experiments it emerged that both PNA sequences are able to form anti-parallel heteroduplex with the target, whose thermal stability has been evaluated through CD melting analysis. Such results have been supported by molecular dynamics studies. Finally, preliminary biological assays performed on the luciferase construct have highlighted that the action of the PNA is able to significantly restore luciferase activity.

As future perspective, we hope to complete all the set of biological assays with the aim to fully understand all the mechanisms that control this kind of approach.

Encouraged by the positive results obtained from the use of PNA in a biological context the third part of my research has been focused on the use of PNAs from a nanotechnological point of view; so my work was focused on the synthesis and characterization of a short sequence of PNA conjugated to a novel bifunctional linker aimed at the obtainment of PNA-based quadruplex. In this context, the goal of my work was to continue investigating the infinite potential of PNA by evaluating its ability to form new G-quadruplex structures, useful for the construction of new nanomaterials. Exploiting as the starting point the expertise of the research group of Prof. Piccialli in the synthesis of branched linkers, the approach has provided first the synthesis of a new type of linker, and, secondly, its functionalization by guanine-rich PNA sequences. Thus, the obtained molecule, named *bis-end-linked* PNA, (or *bel*-PNA), was then suspended in potassium buffer and the ability to form a G-quadruplex structure was evaluated by spectroscopic studies. In particular, through the preliminary circular dichroism analysis, it was possible to demonstrate that the *bel*-PNA gave rise to a G-quadruplex structure; however, since the PNA is an achiral molecule, CD analysis requires the support of another type of technique. In this context, SERS spectroscopy has been included, and has proved to be an indispensable instrument for the structural characterization of CD-unfriendly type of molecule.

An interesting development of this work could be aimed at the functionalization of nanoparticles with the aim to obtain new sensing probes with enhanced enzymatic stability to be used in the field of nano-biotechnology.

APPENDIX

❖ List of Publications

- 1) Zarrilli, F., Amato, F., Morgillo, C.M., **Pinto, B.**, Santarpia, G., Borbone, N., D'Errico, S., Catalanotti, B., Piccialli, G., Castaldo, G., Oliviero, G., Peptide Nucleic Acids as miRNA Target Protectors for the Treatment of Cystic Fibrosis, *Molecules* 2017, Accepted, in press.
- 2) Oliviero, G., D'Errico, S., **Pinto, B.**, Nici, F., Dardano, P., Rea, I., De Stefano, L., Mayol, L., Piccialli, G., and Borbone, N., Self-Assembly of a G-Rich Oligonucleotide Incorporating a 3'-3' Inversion of Polarity Site: A New Route Towards G-Wire Nanostructures, *ChemistryOpen*, 2017, Accepted, in press.
- 3) **Pinto, B.**, Rusciano, G., D' Errico, S., Borbone, N., Sasso, A., Piccialli, V., Mayol, L., Oliviero, G., Piccialli, G. Synthesis and Label Free Characterization of a Bimolecular PNA Homo Quadruplex, *Biochimica et Biophysica Acta (BBA)*, 2016, 1861, 5, 1222-1228.
- 4) Mahal, A., D' Errico, S., Borbone, N., **Pinto, B.**, Costantino, V., Oliviero, G., Secondo, A., Tedeschi, V., Piccialli, V., Piccialli, G. Synthesis of cyclic N (1)-pentylinosine phosphate, a new structurally reduced cADPR analogue with calcium-mobilizing activity on PC12 cells, *Beilstein Journal of Organic Chemistry*, 2015, 11, 2689-95.
- 5) D' Errico, S., Oliviero, G., Borbone, N., Nici, F., Piccialli, V., **Pinto, B.**, D'Alonzo, D., Mayol, L. and Piccialli, G. Synthesis of C6-Pyridylpurine Nucleosides by Reaction of Nebularine N1-Oxidewith Pyridinyl Grignard Reagents, *Eur. J. Org. Chem.* 2015, 2244–2249.
- 6) D' Errico, S., Oliviero, G., Borbone, N., Piccialli, V., **Pinto, B.**, De Falco, F., Maiuri, M.C., Carnuccio, R., Costantino, V., Nici, F. and Piccialli, G. Synthesis and Pharmacological Evaluation of Modified Adenosines Joined to Mono-Functional Platinum Moieties, *Molecules* 2014, 19, 9339-9353.

❖ PhD activities spent in the following laboratories:

01/11/2014 – 31/10/2017: Department of Pharmacy, University of Naples “Federico II”. Tutor: Prof. Gennaro Piccialli.







11/03/2016 – 08/06/2016: Visiting Scholar at the University of Southern California, Los Angeles (USA). Tutor: Prof. Peter Z. Qin.

❖ Congress Communications

- 1) 9th International Symposium on Nano and Supramolecular Chemistry, Naples, September 4-7, 2017.
- 2) International Summer School on Natural Products (ISSNP 2017), Naples, July 4-7, 2017. **Poster Communication:** "Design and Synthesis of a new bifunctional linker for the obtainment of biological active dipeptides", Oliviero, G., D'Errico, S., Borbone, N., Piccialli, G., Pinto, B.
- 3) XVII International Summer School of Organic Synthesis, Gargnano (BS), June 18-22, 2017. **Oral Communication:** "Synthesis of a non-nucleotidic linker for the construction of a bimolecular pna homo quadruplex", B. Pinto, S. D'Errico, N. Borbone, G. Piccialli and G. Oliviero.
- 4) 16° Edizione "Giornate Scientifiche Borsisti" CINMPIS, Arcavacata di Rende, December 16-17, 2016. **Oral Communication:** "Synthesis of a new structurally reduced cIDPR analogue", Pinto, B., Oliviero, G., D' Errico, S., Borbone, N., Piccialli, G.
- 5) Ischia Advanced School of Organic Chemistry (IASOC 2016), Ischia (Na), September 25-29, 2016. **Poster Communication:** "Synthesis, characterization and preliminary biological evaluation of negatively-charged PNAs as new promising tools for the treatment of Cystic Fibrosis", Pinto B., Oliviero, G., Borbone, N., D'Errico, S., Nici F., Santarpia, G., Morgillo, C.M., Catalanotti, B., Amato, F., Castaldo G., Piccialli G.
- 6) Convegno Nazionale della Divisione di Chimica dei Sistemi Biologici, Verona, September 21-23, 2016. **Oral and Poster Communication:** "Target Protector PNA: a new tool in Cystic Fibrosis treatment", Pinto B., Oliviero, G., Borbone, N., D'Errico, S., Nici F., Santarpia, G., Morgillo, C.M., Catalanotti, B., Amato, F., Castaldo G., Piccialli G.
- 7) XV Convegno Scuola della Chimica dei Carboidrati (CSCC 2016), Certosa di Pontignano, Siena, June 19-22, 2016.
- 8) 15° Edizione "Giornate Scientifiche Borsisti" CINMPIS, Napoli, December 11-12, 2015.
- 9) International Summer School On Natural Products (ISSNP 2015), Naples, July 6-10, 2015. **Oral Communication:** "Synthesis Of A Novel cADPR Derivative Modified At The Base And Pyrophosphate Bridge", G. Oliviero, A. M. Salem, V. Costantino, S. D'Errico, A. Caso, N. Borbone, G. Piccialli, B. Pinto.
- 10) Fuctional DNA Nanotechnology, Rome, June 19-20, 2014. **Poster Communication:** "Synthesis of new anti-HIV aptamers based on tetra-end-linked DNA Gquadruplexes and investigation of the effects of the base sequence on anti-HIV activity", B. Pinto, F. Nici, V. D'Atri, G. Oliviero, S. D'Errico, L. Mayol, V. Piccialli, S. Haider, B. Hoorelbeke, J. Balzarini and N. Borbone.

Article

Peptide Nucleic Acids as miRNA Target Protectors for the Treatment of Cystic Fibrosis

Federica Zarrilli ^{1,2} , Felice Amato ^{2,3} , Carmine Marco Morgillo ⁴ , Brunella Pinto ⁴,
Giuliano Santarpia ⁴, Nicola Borbone ⁴ , Stefano D'Errico ⁴ , Bruno Catalanotti ⁴ ,
Gennaro Piccialli ⁴, Giuseppe Castaldo ^{2,3} and Giorgia Oliviero ^{3,*}

¹ Department of Biosciences and Territory, University of Molise, 86170 Isernia, Italy; zarrillif@gmail.com

² CEINGE–Advanced Biotechnologies Scarl, 80131 Napoli, Italy; felice.amato@unina.it (F.A.);
giuseppe.castaldo@unina.it (G.C.)

³ Department of Molecular Medicine and Medical Biotechnologies, University of Naples Federico II,
80131 Napoli, Italy

⁴ Department of Pharmacy, University of Naples Federico II, 80131 Napoli, Italy;
carminemarco.morgillo@unina.it (C.M.M.); brunella.pinto87@gmail.com (B.P.);
santarpiajuliano@gmail.com (G.S.); nicola.borbone@unina.it (N.B.); stefano.derrico@unina.it (S.D.);
brucatal@unina.it (B.C.); picciall@unina.it (G.P.)

* Correspondence: golivier@unina.it; Tel.: +39-081-679-896

Received: 31 May 2017; Accepted: 4 July 2017; Published: 8 July 2017

Abstract: Cystic Fibrosis (CF) is one of the most common life shortening conditions in Caucasians. CF is caused by mutations in the CF Transmembrane Conductance Regulator (CFTR) gene which result in reduced or altered CFTR functionality. Several microRNAs (miRNAs) downregulate the expression of CFTR, thus causing or exacerbating the symptoms of CF. In this context, the design of anti-miRNA agents represents a valid functional tool, but its translation to the clinic might lead to unpredictable side effects because of the interference with the expression of other genes regulated by the same miRNAs. Herein, for the first time, is proposed the use of peptide nucleic acids (PNAs) to protect specific sequences in the 3'UTR (untranslated region) of the CFTR messenger RNA (mRNA) by action of miRNAs. Two PNAs (7 and 13 bases long) carrying the tetrapeptide Gly-SerP-SerP-Gly at their C-end, fully complementary to the 3'UTR sequence recognized by miR-509-3p, have been synthesized and the structural features of target PNA/RNA heteroduplexes have been investigated by spectroscopic and molecular dynamics studies. The co-transfection of the pLuc-CFTR-3'UTR vector with different combinations of PNAs, miR-509-3p, and controls in A549 cells demonstrated the ability of the longer PNA to rescue the luciferase activity by up to 70% of the control, thus supporting the use of suitable PNAs to counteract the reduction in the CFTR expression.

Keywords: cystic fibrosis; CFTR; miRNA; miRNA target protectors; miR-509-3p; peptide nucleic acid; PNA

1. Introduction

One in every 3000 newborn Caucasians is affected by Cystic Fibrosis (CF), an autosomal recessive genetic disorder caused by mutations in a gene that encodes the cystic fibrosis transmembrane conductance regulator (CFTR) protein, a chloride-conducting transmembrane channel expressed in most epithelial and blood cells. Individuals who have inherited two mutated copies of the CFTR gene produce an altered CFTR protein (with decreased or absent CFTR chloride channel activity) that inhibits the flow of water and chloride ions across the cellular membranes and triggers the onset of clinical phenotypes characterized by an altered sweat test, pancreatic insufficiency, and pulmonary infections that gradually lead to respiratory insufficiency [1,2]. CF patients with at least one mutation

that retains a residual channel activity could be treated with a strategy that aims to stabilize the CFTR messenger RNA (mRNA), thus increasing the amount of the protein and resulting in a net chloride flux increase [3]. Recently, it has been demonstrated that microRNAs (miRNAs) are also involved in the negative regulation of CFTR expression and consequently in the development and manifestations of CF lung disease [4–10]. MicroRNAs are evolutionarily conserved single-stranded non-coding RNAs, 18–25 nucleotides in length, that regulate the expression of specific genes at a post-transcriptional level, inhibiting the protein production [11–13]. In this context, the anti-miRNA strategy represents a valid tool within basic research and clinical applications. Indeed, our group used Peptide Nucleic Acids (PNAs) as anti-miRNA agents [14,15]. PNAs are mimics of DNA in which the sugar-phosphate backbone of the nucleic acid is replaced by a synthetic achiral peptide backbone. They emerged as one of the most promising candidates for gene therapeutics in antisense strategies and anti-miRNA approaches, showing a high affinity towards nucleic acid targets and generating very stable heteroduplex complexes. Moreover, PNAs and their complexes are not recognized by nucleases [16–25]. In a previous study, using an in vitro system based on the luciferase reporter system, we demonstrated that PNAs can inhibit miRNA activity and rescue the CFTR expression [14,15]. Although effective, the anti-miRNA approach suffers from a main limitation, i.e., it may interfere with other miRNA targets leading to unpredictable side effects. To overcome this problem and to counteract the effects of miRNAs binding to the CFTR mRNA [26], we propose the use of PNAs as miRNAs target protectors (TPs). This approach differs from the anti-miRNAs one because the PNAs block the miRNAs activity only for the specific gene of interest by competing with the miRNAs for the target mRNA. In the case of CF, the increased expression of the CFTR protein could lead to clinical benefit for all patients who retain residual activity of the CFTR channel. Furthermore, it has been shown that the expression of CFTR decreases during the development from embryo to adulthood. Therefore, an increase of the CFTR protein, and consequently of the flow of chloride through the membranes, could help those patients with at least one mutation that maintains some residual activity of the protein. In this study, we have synthesized and investigated, based on their ability to protect the CFTR mRNA, two PNA strands of different lengths (**1** and **2**, thirteen and seven bases in length, respectively, Table 1) that are fully complementary to the mRNA sequence recognized by the seed region of mir-509-3p. In addition, two other PNAs sharing the same base composition as **1** and **2**, but in random order (**3** and **4**, respectively, Table 1), have been designed and synthesized to confirm the sequence dependent activity of **1** and **2**. The negatively charged tetra-peptide Gly-SerP-SerP-Gly was installed at the C-end of all PNAs to improve their water solubility. The ability of **1** and **2** to recognize the mRNA was investigated by Circular Dichroism (CD) and UV studies on the corresponding PNA/DNA models and molecular modelling studies were performed to further confirm the structure and stability of the target PNA/mRNA complexes. We show that **1** proved effective in rescuing the luciferase expression by up to 70% of control in A549 cell culture model.

2. Results

2.1. Synthesis of PNAs 1–4

PNA **1–4** (Table 1) were synthesized using the standard Fmoc-solid phase strategy on a 4-methylbenzhydrylamine (MBHA) resin. In the synthetic approach, the peptide tract was assembled at first, followed by the construction of the PNA portion. After the synthesis, the oligomers were detached from the support and lyophilized. The purification and analysis of the crude products were carried out using HPLC as outlined in the Materials and Methods. The electrospray mass spectrometry (ESI-MS) analyses confirmed the structure of the synthesized PNAs (Table 1).

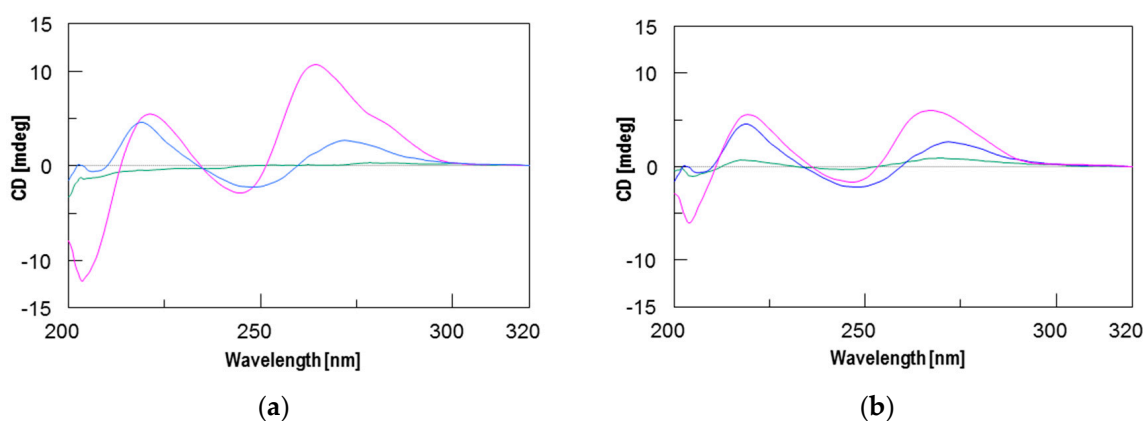
Table 1. Sequences of the cystic fibrosis (CF) transmembrane conductance regulator (CFTR) messenger RNA (mRNA) and of peptide nucleic acids (PNAs) 1–4. UTR = untranslated region.

Name	Sequence ^{1,2}
3'UTR of CFTR mRNA (RNA)	G-A-A-G-A-A-G-C-A- C-C-A-A-U-C-A -U-G-A
DNA model sequence (ODN)	G-A-A-G-C-A-C-C-A-A-T-C-A
PNA 1 (C → N)	G-S(P)-S(P)-G-c-t-t-c-g-t-g-g-t-t-a-g-t
PNA 2 (C → N)	G-S(P)-S(P)-G-g-g-t-t-a-g-t
PNA 3 (C → N)	G-S(P)-S(P)-G-c-a-g-t-t-g-t-c-t-g-t-g-t
PNA 4 (C → N)	G-S(P)-S(P)-G-t-t-g-g-a-g-t

¹ The tetrapeptide tail at PNAs C-end is written in *italics*. ² Target of miR-509-3p seed region is in red.

2.2. Circular Dichroism (CD) and CD Melting Analyses

To assess the interaction between the new PNAs and the target sequence on the CFTR mRNA strand and the stability of the resulting PNA/RNA heteroduplexes, we used CD and CD melting analyses. However, because DNA is more resistant against nucleases and does not require any chemical modification for handling that could alter its recognition properties, the spectroscopic studies were performed using the corresponding 13-mer DNA model sequence (ODN in Table 1). Furthermore, considering the higher binding affinity of RNA strands relative to DNA strands towards complementary PNAs [27], the stability data obtained using the ODN model are probably underestimated. The formation of PNA/ODN heteroduplexes for **1** and **2** was assessed by recording the CD spectra of PNAs/ODN mixtures (1.5:1) in comparison with the CD spectra of PNAs and ODN alone. Each spectrum was recorded in phosphate buffered saline (PBS) buffer at 5 °C after the annealing procedure. Different from the CD spectra of PNAs and ODN alone, the spectra of both PNA/ODN mixtures showed the typical CD profile of antiparallel PNA/DNA heteroduplexes [28], characterized by maxima around 260 nm and 220 nm, and minima around 245 nm and 200 nm, thus confirming the formation of the target heteroduplexes **1**/ODN and **2**/ODN (Figure 1). The CD melting curves of both complexes are shown in Figure 2 and confirm, as expected, the greater stability of the longer **1**/ODN heteroduplex relative to that of the shorter one (T_m values of 66 °C and 35 °C, respectively).

**Figure 1.** Circular dichroism (CD) spectra of: (a) PNA 1 (green), ODN (blue), and 1.5:1 **1**/ODN mixture (magenta); (b) PNA 2 (green), ODN (blue), and 1.5:1 **2**/ODN mixture (magenta). ODN is the DNA model sequence.

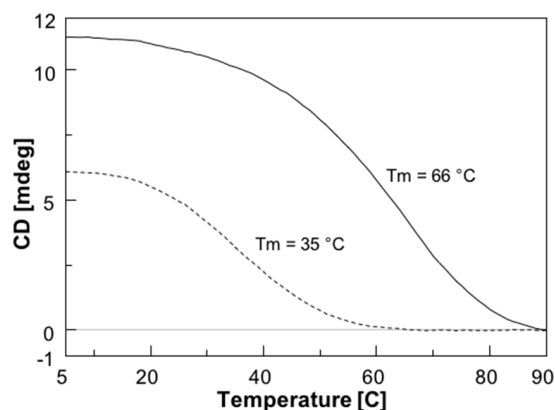


Figure 2. CD melting profiles of 1.5:1 PNA/ODN mixtures of **1** (solid line) and **2** (dashed line). The curves were obtained by monitoring the absorbance at 266 or 264 nm, respectively, for **1**/ODN or **2**/ODN, at a heating rate of 0.5 °C/min.

2.3. UV Studies

The formation of PNAs/ODN heteroduplexes was also monitored by UV spectroscopy by exploiting the hypochromic effect resulting from the formation of the heteroduplexes. The UV spectrum of each component alone and those of the mixtures are reported in Figure 3. All spectra were characterized by a maximum at around 260 nm, typical of nucleobases. The UV spectrum of the **1**/ODN complex (magenta curve in Figure 3a) showed lower values of absorbance than the arithmetic sum of each component alone (black curve in Figure 3a), thus confirming the occurrence of stacking interactions and the formation of the heteroduplex. In the case of the shorter PNA **2**, the UV spectrum of its complex with the ODN (violet curve in Figure 3b) showed almost the same values of absorbance as the arithmetic sum of its components, in agreement with the experimental lower stability of the shorter **2**/ODN heteroduplex.

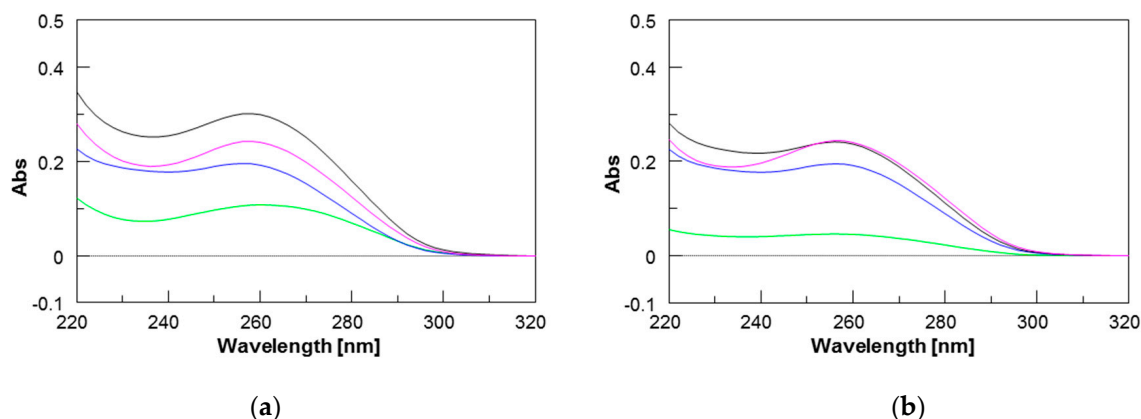


Figure 3. UV spectra of: (a) PNA **1** (green), ODN (blue), 1.5:1 **1**/ODN mixture (magenta), and the arithmetical sum of **1** and ODN (black); (b) PNA **1** (green), ODN (blue), 1.5:1 **1**/ODN mixture (magenta), and the arithmetical sum of **1** and ODN (black).

2.4. Molecular Modelling Studies

Molecular dynamics was used to check the structural features of the heteroduplexes **1**/RNA and **2**/RNA (Supplementary Materials, Table S1). The heteroduplexes were built starting from the NMR structure of the RNA(GAGUUC)/PNA(GAACTC) duplex (PDB-ID 176D) [29] as described in the Material and Methods section. The heteroduplexes were analyzed by means of three independent runs of molecular dynamics, for a total simulation time of 1200 ns for **1**/RNA system and of 900 ns

for **2/RNA**. The chemical-physical properties of the systems, such as temperature, pressure, volume, density, and energy were fairly constant during the whole simulation for all the systems (data not shown). All the simulations were characterized by low root-mean-square deviation (RMSD) values and low fluctuations in the central duplex region (Supplementary Materials, Figure S1), thus indicating the presence of a stable structure. To evaluate the convergence between the independent runs of each system, a hierarchical clusterization of the molecular dynamics (MD) run was performed using Ambertools 15 [30]. The clusterization yielded in both cases one main cluster, accounting for more than 77% of frames for each run of PNA **1** and for more than 90% for PNA **2** runs (Supplementary Materials, Table S2 for details). Superposition of the average structure of the main cluster of each run showed very low RMSD values, thus indicating the convergence of the run to the same main structure (Figure 4; Supplementary Materials, Tables S3 and S4).

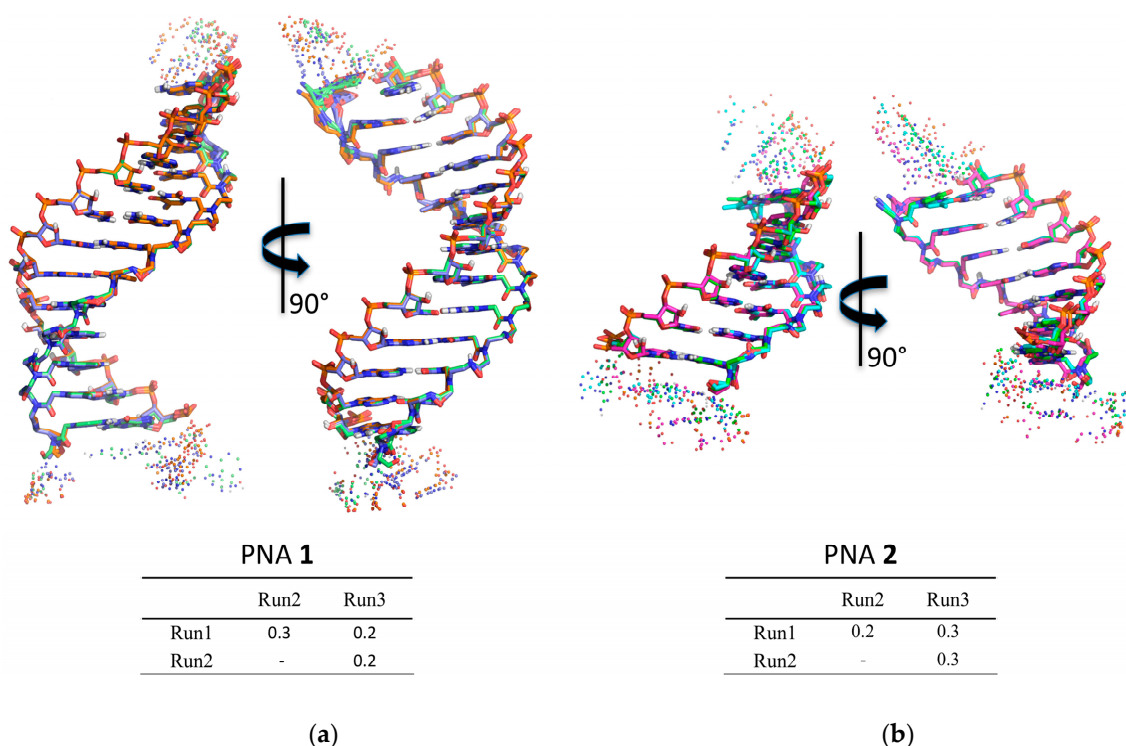


Figure 4. Superposition of average structures of the main represented cluster for **1/RNA** (a) and **2/RNA** (b), with relative root-mean-square deviation (RMSD) in Å calculated on heavy atoms. Duplex regions are represented in licorice, with carbons colored by molecular dynamics (MD) run (PNA **1**: Blue, Run 1; Orange, Run 2; Light green, Run 3. PNA **2**: Green, Run 1; Cyan, Run 2; Magenta, Run 3) and other atoms by standard convention (Oxygen in red, Nitrogen in blue, Phosphate in orange, and Hydrogen in white). RNA single strand flanking regions and the tetrapeptide Gly-SerP-SerP-Gly are represented in spheres coloured by MD run.

To characterize the structural properties of the **1/RNA** and **2/RNA** heteroduplexes, local base pair step parameters (twist, roll, tilt, shift, slide, and rise), helical parameters (inclination), and the torsion angles of RNA and PNA monomers were calculated with the program Curves+ [31]. To limit the influence of the sterically less restricted terminal base pairs, the analysis was limited to the central 11 and 5 base pairs for the heteroduplexes formed by **1** and **2**, respectively. The results are reported in Tables 2 and 3. All the heteroduplexes showed high similarity with the PNA/RNA heteroduplex experimental structures determined by NMR (PDB ID 176D [29]) and by XRAY (PDB ID 5EME and 5EMF) [32], with few noticeable deviations. In particular, **1/RNA** and **2/RNA** heteroduplexes showed

lower values of twist and roll with respect to the experimentally determined structures, assuming values similar to those reported in previous MD studies [33].

Table 2. Helicoidal parameters of the average structure of the more representative cluster of **1/RNA** and **2/RNA** MD simulations. Standard deviations are reported in brackets.

Name	Shift	Slide	Rise	Tilt	Roll	Twist
1/RNA	−0.7 (0.2)	−1.9 (0.2)	3.3 (0.2)	1.0 (1.4)	2.4 (1.9)	23.6 (1.7)
2/RNA	−0.9 (0.3)	−1.7 (0.2)	3.3 (0.1)	1.3 (1.5)	3.9 (1.9)	22.6 (1.3)
PNA/RNA (NMR) ¹	0.3 (0.3)	−1.4 (0.6)	3.2 (0.4)	−2.8 (1.3)	4.6 (4.3)	29.4 (3.8)
PNA/RNA (MD) ²	−	−	−	−	−	24
PNA/RNA (X-RAY) ³	−0.8 (0.4)	−2.1 (0.3)	3.3 (0.1)	0.1 (1.3)	6.9 (3.5)	25.0 (1.6)
A-RNA ⁴	−	−	2.8	−	−	32.7

¹ Calculated on the average structure of PDB 176D, from [29]; ² from [33]; ³ calculated on the average structure of PDBs 5EME and 5EMF, from [32]; ⁴ from [34].

The analysis of RNA torsion angles (Table 3) confirmed their close similarity with respect to the reference NMR PNA/RNA heteroduplex [29] and a strict consistence with the canonical A-RNA structure [34]. PNA angles, on the contrary, as previously reported [15,35–38], showed higher deviation and flexibility, particularly pronounced in the case of α and ϵ torsion angles, assuming values around -100° and 180° , respectively, in both PNA/RNA heteroduplexes (Supplementary Materials, Figure S1).

Table 3. Average torsion angle values of the average structure of the more representative cluster of **1/RNA** and **2/RNA** MD simulations. Standard deviations are reported in brackets. The torsion angle definition is given in Figure 5.

Torsional PNA Angles									
Name	α	β	γ	δ	ϵ	ω	χ_1	χ_2	χ_3
1/RNA	−120 (46.0)	78 (10.6)	71 (2.5)	95 (1.8)	−177 (42.9)	−146 (10.0)	−2 (1.2)	−164 (2.2)	84 (2.8)
2/RNA	−136 (43.2)	76 (4.1)	79 (3.9)	96 (2.0)	−162 (56.6)	−172 (10.6)	−3 (1.6)	−152 (18.0)	77 (12.6)
PNA/RNA (NMR) ¹	160 (10.1)	68 (2.4)	81 (5.0)	59 (16.1)	−104 (6.7)	−177 (3.2)	12 (3.3)	−118 (8.6)	49 (10.2)
PNA/RNA (XRAY) ²	−177 (83.5)	68 (8.8)	71 (7.5)	95 (5.2)	−123 (81.0)	−178 (10.5)	5 (5.1)	−173 (4.0)	82 (6.6)
Torsional RNA Angles									
Name	α	β	γ	δ	ϵ	ζ	χ		
1/RNA	−77 (1.5)	172 (1.7)	68 (1.5)	79 (0.9)	−162 (2.7)	−72 (2.9)	−160 (3.1)		
2/RNA	−78 (1.6)	173 (1.9)	67 (1.6)	79 (1.3)	−164 (2.7)	−73 (2.4)	−156 (2.8)		
PNA/RNA (NMR) ¹	−68 (6.7)	171 (13.8)	58 (1.2)	79 (3.6)	−149 (23.8)	−73 (11.6)	−168 (4.4)		
PNA/RNA (X-RAY) ²	−80 (4.9)	177 (5.4)	63 (4.9)	79 (6.2)	−158 (5.5)	−71 (6.6)	−164 (4.9)		
A-RNA ³	−79 (43.5)	172 (19.9)	64 (34.7)	80 (9.53)	−152 (17.6)	−76 (24.7)	−162 (9.76)		

¹ Calculated on the average structure of PDB 176D, from Ref. [29]; ² calculated on the average structure of PDBs 5EME and 5EMF, from Ref. [32]; ³ from Ref. [34].

Interestingly, the analysis of the correlation between the torsion angle ε of the residue i and the torsion $\alpha_{(i+1)}$ of the subsequent base, showed the lack of consistent correlation between ε_i and $\alpha_{(i+1)}$. Moreover, to further explore structural features of PNAs/RNA heteroduplexes, we also evaluated the correlation between the pseudo-torsion angle ν_i , defined as the angle between C8'-N4'-C'-O1' (Figure 5, red circles), and the torsion angle $\alpha_{(i+1)}$ of the subsequent base, as a pointer of the orientation of the backbone carbonyl with respect to the strand terminus. The high Pearson correlation coefficients calculated revealed that there is a strong anti-correlation between the pseudo torsion angle ν_i and $\alpha_{(i+1)}$ of the subsequent base, thus revealing a prevalent orientation of the carbonyl group toward the N-terminus (Supplementary Materials, Table S5). A detailed discussion of the torsion angle behavior is given in Supplementary Materials (Text S1).

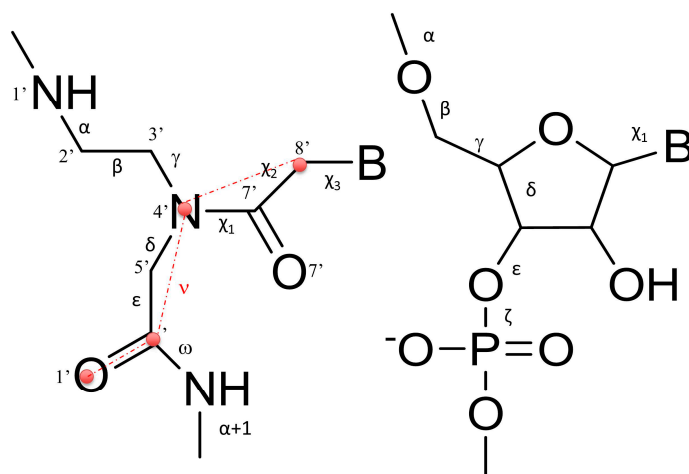
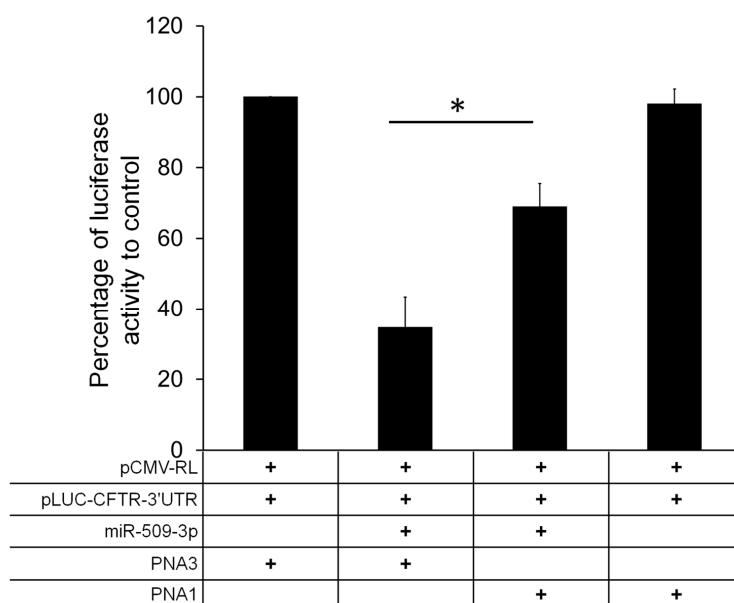


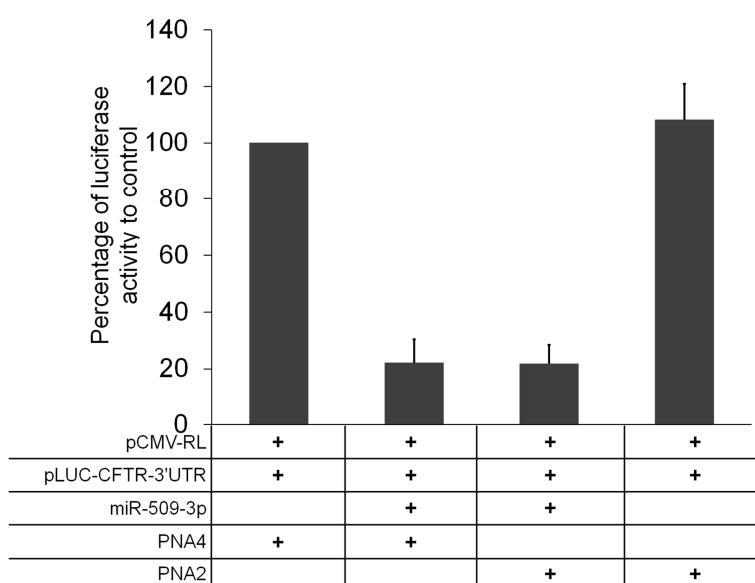
Figure 5. Schematic representation of the PNA (**left**) and RNA (**right**) backbones showing the definition of the torsion angles analyzed in Table 3. B stands for Base.

2.5. Biological Activity

Next, we tested the ability of PNAs **1** and **2** to block the inhibitor activity of miR-509-3p in a biological context. For this purpose, we tested the ability of the two PNA strands to rescue the reduction of luciferase activity induced by the transfection of miR-509-3p in A549 cells. Thus, we co-transfected different combinations of pLuc-CFTR-3'UTR (untranslated region) vector (a reporter luciferase construct sensitive to the miR-509-3p mimic action due to the presence of the 3'UTR of the CFTR gene), PNA strands, miR-509-3p mimic, and corresponding PNA scrambled controls. The co-transfection of miR-509-3p in the presence of the scrambled PNA **3** reduced luciferase expression leading to a residual activity up to 35%. The co-transfection of PNA **1** in the presence of miR-509-3p rescued the luciferase activity by up to 70% (Figure 6a). On the contrary, the addition of **1** alone did not produce any effect on the luciferase expression, thus indicating that **1** counteracts the inhibitory effects of miR509-3p by selectively competing for its binding on the 3'UTR of CFTR mRNA. Conversely, despite the spectroscopic and molecular dynamics evidence, the co-transfection of **2** in similar experimental conditions did not rescue the luciferase activity (Figure 6b).



(a)



(b)

Figure 6. Effect of PNAs 1 (a) and 2 (b) on miR-509-3p activity. A significant rescue of the luciferase expression was observed using 1. No significant activity was observed using 2. * p values < 0.006.

3. Discussion

CFTR gene regulation by miRNAs plays an important role in lowering CFTR levels in CF patients. Therefore, much effort has been made to modulate miRNA control on CFTR. In a recent paper, we demonstrated that the activity of miR-509-3p miRNA, one of the miRNAs involved in the post-transcriptional regulation of the CFTR gene, could be inhibited using 14 or 7 bases long PNAs [14,15]. However, this type of strategy, as evidenced by some authors [26,39], has enormous off-target effects, because every miRNA regulates hundreds or thousands of mRNA targets.

Alternatively, the use of miRNA Target Protectors (TPs) has been proposed as a promising option for the development of effective tools for the correction of CFTR expression in people with CF. In this context, we have here investigated the use of PNA strands as miRNA TPs. This strategy has the advantage of protecting the CFTR mRNA from binding with the miRNAs, which remain free to interact with their physiological mRNA targets. For this purpose, we have designed and synthesized two negatively charged PNAs, PNAs **1** and **2** (Table 1), functionalized at the C-end with the negatively charged tetrapeptide Gly-SerP-SerP-Gly to improve the water solubility and cellular uptake. The chemico-physical characterization of PNA/nucleic acid heterocomplexes was performed through CD, CD melting and UV experiments. To ease the nucleic acid handling during the CD and UV investigations, all spectroscopic investigations were performed using the 3'UTR mRNA DNA mimic (ODN in Table 1) rather than the corresponding RNA strand. This approach allowed us to avoid the use of a nucleases-resistant chemically-modified RNA strand, which could have affected the binding affinity with the studied PNAs. Circular dichroism measurements are useful in the characterization of the secondary structure of nucleic acids and in the study of hybridization events. In this case, the CD studies confirmed the capability of PNAs **1** and **2** to bind the target ODN strand and form the corresponding heteroduplexes, whose melting temperatures were determined by derivatization of the resulting CD melting curves (64 °C and 35 °C, respectively; Figure 3). In addition, the comparison of the UV spectra shown in Figure 4 revealed a lower absorbance than the arithmetic sum of each component alone for the **1**/ODN heteroduplex. This confirms the occurrence of strong stacking interactions between the DNA strand and **1**. The same behavior was not observed for the UV spectra of **2**/ODN complex (Figure 5), even if the formation of the heteroduplex was supported by CD and molecular dynamics studies. A possible explanation for this behavior could be found in the lower number of bases involved in the Watson-Crick (W-C) base pairing for the **2**/ODN complex relative to the total number of bases in the two strands (PNA + ODN). Furthermore, the MD simulations of **2**/RNA complex showed high fluctuations for the terminal base pairs (Supplementary Materials, Figure S1C), indicating that only four or five bases could be involved in stable W-C interactions in the heteroduplex. Finally, we also performed MD simulations of **1**/RNA and **2**/RNA (1200 and 900 ns, respectively) to characterize the structural features of these heteroduplexes conjugated to a negatively charged tetrapeptide tail. The analysis of helicoidal parameters and torsion angles (Tables 2 and 3) revealed that both MD derived PNA/RNA heteroduplexes showed similar structural features. PNA **1**- and **2**-containing helices were slightly unwound and less bent with respect to the experimentally determined structures of PNA/RNA heteroduplexes, as indicated by the lower twist values. On the other side, the helices appeared slightly less bent than both NMR and XRAY derived structures because of lower roll values. The roll parameter, indeed, indicated the degree of rotation with respect to the main helical axis, and, therefore, higher roll values are associated to higher perturbation of the coplanarity of bases, inducing the bending of the helix. The analysis of torsion angles of RNA and PNA backbones confirmed structural features very similar to those of reference experimental structures. RNA strand torsion angles closely resembled those found in the reference PNA/RNA NMR structure and in the canonical A-RNA structure. On the other side, as previously reported [15,35–38], the PNA strand showed higher flexibility, particularly in torsion angles α and ϵ , that may assume two sets of values -100° and 100° and -20° and 180° , respectively (Supplementary Materials, Figure S2 and Text S1). Taken together, these results indicated that the negatively charged tetrapeptide slightly affects the structural features of the heteroduplexes with respect to experimentally determined PNA/RNA heteroduplexes.

The ability of PNAs **1** and **2** to protect the miR-509-3p target site in the 3'UTR of CFTR gene was evaluated by testing the effects on the expression of the luciferase gene cloned upstream. The results have shown clearly that the transfection of the 7 bases long PNA **2** in A549 cells co-transfected with miR-509-3p did not increase significantly the luciferase gene expression (Figure 6b), whereas the co-transfection with the longer PNA **1** reduced the miR-509-3p gene inhibition by up to 70% (Figure 6a). These results are apparently in contradiction with the results of our previous paper on the efficacy of 7 and 14 bases long anti-miRNA PNAs to rescue the luciferase expression in the presence of

miR-509-3p [15] (which showed almost the same potency for the two PNAs). A possible explanation for the observed different behavior may be found in the different mechanism of action of the two approaches. The anti-miRNA mechanism is based on the competition of PNAs with the miRNAs for the mRNA target, whereas the activity of miRNA TPs is indeed the result of the formation of heteroduplexes between PNAs and the target mRNA. In the latter case, the length of PNAs directly correlates with the binding affinity for the target mRNA, due to the increasing number of base pairs involved in longer duplexes. On the other side, the anti-miRNA approach requires that the PNAs interact with miRNAs integrated in the RNA-induced silencing complexes, which result from the association of miRNAs with proteins of the argonaute family [40]. Hence, the interaction of longer PNAs with the miRNA-protein complex rather than with the free miRNA could be disfavored relative to the interaction of shorter PNAs.

4. Materials and Methods

4.1. General Methods

All reagents and solvents were obtained from commercial sources and used without further purification. Phosphoramidites for DNA syntheses were purchased from Glen Research (Sterling, VA, USA). The ODNs were assembled by using the PerSeptive Biosystems Expedite DNA/RNA 8909 synthesizer using phosphoramidite chemistry. Peptide nucleic acid monomers were purchased from Link technologies (Bellshill, Lanarkshire, UK). Fmoc-L-Ser[PO(OBzl)OH]-OH was purchased from Iris Biotech GmbH (Marktredwitz, Germany). Fmoc-Gly-OH and the MBHA resin (1% divinylbenzene, 200–400 mesh, 0.5 mmol/g loading) were purchased from Sigma-Aldrich (Saint Louis, MO, USA). The reactions on solid phase were performed using ISOLUTE® single fritted reservoirs (SG), 20 µm PE (polyethylene), equipped with tube caps and luer tip caps Biotage (Uppsala, Sweden) which were shaken in a Multi-reax vibrating shaker Heidolph (Schwabach, Germany). High performance liquid chromatography (HPLC) analyses and purifications were carried out on a Jasco UP-2075 Plus pump equipped with a Jasco (Easton, MD, USA) UV-2075 Plus UV detector using a 4.8 × 150 mm C-18 reverse-phase column (particle size 5 µm) eluted with a linear gradient of CH₃CN containing 0.1% (v/v) trifluoroacetic acid (TFA) in H₂O containing 0.1% (v/v) TFA (from 0 to 100% in 45 min, flow 1.2 mL/min). UV spectra were recorded on a Jasco V-530 spectrophotometer (Jasco). CD spectra were performed on a Jasco 1500 spectropolarimeter (Jasco) equipped with a Jasco PTC-348 WI Peltier-type temperature controller in a 0.1 cm path length cuvette. ESI-MS experiments were performed on an Applied Biosystems (Warrington, Cheshire, UK) 4000 QTRAP mass spectrometer in positive ion electrospray mode, dissolving the compounds in H₂O containing 0.1% (v/v) formic acid.

4.2. DNA Synthesis and Analysis

The oligonucleotide 5'GAAGCACCAATCA3' was synthesized using solid phase β-cyanoethyl phosphoramidite chemistry. After the synthesis, the oligomers were detached from the support and deprotected by treatment with concentrated aqueous ammonia at 55 °C for 12 h. The combined filtrates and washings were concentrated under reduced pressure, redissolved in H₂O, and analyzed and purified by HPLC on a Macherey Nagel (Düren, Germany) Nucleogel SAX column 1000-8/46 using buffer A: 20 mM NaH₂PO₄ aqueous solution, pH 7.0, containing 20% (v/v) CH₃CN; buffer B: 1 M NaCl, 20 mM NaH₂PO₄ aqueous solution, pH 7.0, containing 20% (v/v) CH₃CN; a linear gradient from 0% to 100% B in 30 min and flow rate 1.2 mL/min were used. The oligomers were collected and successively desalted by Sep-Pak cartridges (C18). The isolated oligomers were >99% pure (NMR). The ODN concentration was determined spectrophotometrically at λ = 260 nm and 90 °C, using the molar extinction coefficient ε = 200.9 cm^{−1}·mM^{−1} calculated by the nearest neighbor mode.

4.3. PNA Synthesis and Analysis

PNA sequences were synthesized using the Fmoc-solid-phase strategy. Fifty milligrams of MBHA resin (0.5 mmol/g), after swelling in CH_2Cl_2 for 30 min and DMF washings, was treated with a solution of 20% piperidine in DMF for 10 min. After washings in DMF ($\times 5$), the resin was reacted with Fmoc-Gly (5 eq. in NMP 0.2 M), 1-[Bis(dimethylamino)methylene]-1*H*-1,2,3-triazolo[4,5-*b*]pyridinium 3-oxid hexafluorophosphate (HATU) (5 eq. in DMF 0.2 M) and *N,N*-Diisopropylethylamine (DIPEA) (5 eq.)/lutidine (7.5 eq.) for 45 min at room temperature. Couplings of Fmoc-L-Ser[PO(OBzl)OH]-OH were achieved using the following conditions: Fmoc-Ser monomer (8 eq. in NMP 0.2 M), HATU (8 eq. in DMF 0.4 M), and DIPEA (8 eq.)/lutidine (12 eq.) for 15 h at room temperature. After the serine couplings, a further glycine residue was attached on the N-terminal of the serine tract following the previously described coupling with the glycine monomer. PNA monomers were reacted using the following conditions: monomer building block (10 eq. in NMP 0.2 M), HATU (10 eq. in DMF 0.2 M), and DIPEA (10 eq.)/lutidine (15 eq.), 45 min at room temperature. After each coupling step, capping with Ac_2O in the presence of pyridine was performed for 20 min at r.t. Fmoc group was removed by a treatment with a 5% 1,8-Diazabicyclo[5,4,0]undec-7-ene (DBU) in DMF solution (5 min). In the case of Fmoc-Ser amino acids, the basic treatment was prolonged (20 min). At the end of synthetic cycles, the PNAs were cleaved from the solid support by treatment with TFA/anisole/ethanedithiol (9:1:1; *v/v/v*) for 4 h and the products were precipitated with cold diethyl ether. The precipitates were recovered by centrifugation, washed twice with diethyl ether, dissolved in water, and finally lyophilized. PNAs 3 and 4, chosen as the negative control and bearing the same functionalization of PNAs 1 and 2, were synthesized using the same standard Fmoc-solid-phase strategy. The PNAs were obtained with a 48–50% overall yield (94–95% medium yield for each coupling as estimated by Fmoc spectrophotometric measurements). The crude sample was purified by semipreparative reverse phase HPLC (see General methods). The collected fractions were lyophilized and the final pure product was characterized by ESI-MS (positive mode): ESI-MS (*m/z*) calcd. for PNAs 1 and 3 4003.4; found $[\text{M} + 3\text{H}]^{3+}$ 1335.5, $[\text{M} + 4\text{H}]^{4+}$ 1002.0; PNAs 2 and 4 2411.8; found $[\text{M} + 2\text{H}]^{2+}$ 1206.9, $[\text{M} + 3\text{H}]^{3+}$ 805.0. The amount of each PNA sample dissolved in pure water was estimated by quantitative UV at 90 °C using the following molar extinction coefficients: PNAs 1 and 3 $\epsilon = 126.5 \text{ mL} \cdot \mu\text{mol}^{-1} \cdot \text{cm}^{-1}$; PNAs 2 and 4 $\epsilon = 75.2 \text{ mL} \cdot \mu\text{mol}^{-1} \cdot \text{cm}^{-1}$ and DNA $\epsilon = 134.2 \text{ mL} \cdot \mu\text{mol}^{-1} \cdot \text{cm}^{-1}$.

4.4. Preparation of DNA/PNA Heteroduplexes (Annealing Procedure)

The PNA/ODN heteroduplexes (1.5:1) were obtained by dissolving the mixture of the samples at the concentration of $2.0 \times 10^{-5} \text{ M}$ in 100 mM PBS and by heating the solution to 90 °C for 5 min and then slowly cooling to room temperature over 12 h.

4.5. UV

The UV spectra were recorded with a Jasco V-530 UV spectrophotometer, in 100 mM PBS buffer at the concentration of 20 μM . They were recorded at 20 °C ($\lambda = 220\text{--}310 \text{ nm}$, 400 nm/min scanning speed, 2.0 nm bandwidth).

4.6. CD and CD Melting Studies

The CD spectra were recorded with a Jasco 1500 spectropolarimeter equipped with a Peltier-type temperature controller (PTC-348 WI) in a 0.1 cm cuvette, in 100 mM PBS buffer at the concentration of 20 μM . They were recorded at 5 °C ($\lambda = 220\text{--}310 \text{ nm}$, 200 nm/min scanning speed, 2.0 nm bandwidth) and averaged over three repetitions. A buffer baseline was subtracted from the CD spectra and the spectra were normalized to have zero at 320 nm. Thermal denaturation experiments were also carried out in the temperature range of 5–90 °C by monitoring the CD values at 266 nm for PNA 1/ODN and at 264 nm for PNA 2/ODN at a heating rate of 1.0 °C/min.

4.7. Molecular Dynamics (MD) Simulations

The initial structures were built following the same procedure described in [15], starting from the NMR structure of the RNA(GAGUUC)/PNA(GAACTC) duplex (PDB-ID 176D) [28]. The correct sequence was obtained by mutating the bases using the X3DNA software [41]. Each heteroduplex was built including three flanking bases on both the 3' and 5' ends of the RNA segment (Supplementary Materials, Table S1). Thermalization of the duplex and production of MD trajectories were obtained using Amber 15 suite [30]. The leap module of Ambertools 15 was used to perform the parameterization of the systems, using the ff14SB force field (AMBER99SB and frcmod.ff14SB for peptide + ff99bsc0_chiOL3 for RNA) [42–44], and the Sanders et al. parameters for PNA [37], whereas the parameters for serine phosphate were taken from [45]. TIP3P water molecules were added with at least a minimum spacing of 14.0 Å between the edge of the box and the molecules. Na⁺ counterions were added to neutralize the system. The system was geometrically minimized in three steps: (i) optimization of hydrogen atoms with 2000 steps of steepest descent algorithm and 8000 steps of conjugate gradient algorithm, (ii) optimization of water molecules and counterions with 2000 steps of steepest descent and 18,000 steps of conjugate gradient, and (iii) optimization of the whole system with 2000 steps of steepest descent and 8000 steps of conjugate gradient. The equilibration of the system was performed using the protocol described in [15]. Briefly: (i) the system was thermalized in 240 ps, raising the temperature from 10 K to 298 K with a time step of 1 fs, and applying inter- and intra-strand constraints of 20 kcal·mol^{−1}·Å^{−2} in order to preserve, respectively, the W-C base pairs and the torsional angles of the RNA sugar; (ii) the constraints were gradually removed from 20 kcal·mol^{−1}·Å^{−2} to 0.1 kcal·mol^{−1}·Å^{−2} in 240 ps at constant pressure (1 bar) and temperature (298 K). Finally, an equilibration step of 500 ps was run without constraints. Production runs were performed using a time step of 2 fs. The SHAKE algorithm was used for all hydrogen atoms in conjunction with periodic boundary conditions at constant pressure and temperature. Particle mesh Ewald was used for the treatment of long range electrostatic interactions, and a cut-off of 9 Å was used for non-bonded interactions. Each system was studied by means of 300 ns MD simulation runs in triplicate with random seeding for the initial velocities. In order to investigate more deeply the stability of the PNA 1/RNA system, we extended one run to 600 ns, for a total of 1200 ns for the PNA 1/RNA and 900 ns for the PNA 2/RNA. The analysis of the structure was carried out using the software Curves+ [31]. The visualization of the trajectories and related snapshots were performed with Pymol [46] and VMD [47], while the trajectory post-processing analysis was performed using Ambertools15 [30]. Cluster analysis was performed through a hierarchical agglomerative (bottom-up) approach using a root-mean-square (RMS) metric comparing the heavy atoms in the central duplex base-pairs. Correlation analysis was performed calculating the Pearson correlation coefficient on torsion angles sampled each 0.01 ns.

4.8. Cell Line, Construct, and Transfections

A549 human lung carcinoma cells were purchased from ATCC (Manassas, VA, USA). The cells were maintained in Dulbecco's modified Eagle's medium (Gibco Invitrogen, North Andover, MA, USA) with 10% heat inactivated fetal bovine serum (HyClone Laboratories, South Logan, UT, USA) without the addition of antibiotics. A Luciferase construct bearing the 3'UTR of the CFTR gene was used as the miR-509-3p sensitive reporter system. The transfection of the A549 cells with miRNA-mimics (Qiagen, Hilden, Germany) or PNAs was performed with the Attractene Transfection Reagent (Qiagen). Briefly, the cells seeded in 96-well plates were cotransfected with the luciferase reporter construct, miR-509-3p mimic and the PNAs. The luciferase activity level was measured 24 h after transfection using the Dual-Glo Luciferase Assay System (Promega Corporation, Madison, WI, USA). The EnSpire Multimode Plate Reader (Perkin Elmer, Waltham, MA, USA) was used for the luminescence assay using 96-multiwell black plates. The relative reporter activity was obtained by normalization to the Renilla luciferase activity.

5. Conclusions

In this paper, we have proposed for the first time the use of PNAs as miRNA target protectors to increase the expression of CFTR in CF. The negatively charged PNAs **1** and **2**, conveniently modified at their C-ends and fully complementary to the 3'UTR region of the CFTR mRNA recognized by the seed region of miR-509-3p, were synthesized and characterized. To demonstrate the sequence dependent activity of **1** and **2**, two other PNAs (**3** and **4**, Table 1), containing scrambled sequences of **1** and **2**, respectively, were designed and synthesized. Spectroscopic data confirmed the ability of **1** and **2** to bind their complementary ODN target by forming stable PNA/ODN heteroduplexes. The structural features of **1**/RNA and **2**/RNA heteroduplexes were also determined through molecular dynamics simulations. The results indicated that the presence of the negatively charged tetra peptide at the C-end of **1** and **2** slightly affected the structural features of the resulting PNA/RNA heteroduplexes (with respect to the experimentally determined PNA/RNA heteroduplexes). Biological studies show that the PNA molecules are suitable to counteract the action of miR-509-3p (in this case) as miRNA target protectors. These data confirm, once again, that a mRNA-targeted approach of a gene to increase the expression of the protein could be a good therapeutic strategy (that, of course, could be also used in other monogenic diseases). Moreover, the PNAs, showing a high affinity towards nucleic acid targets and forming stable heteroduplex complexes, represent excellent candidates to be used for this approach. Furthermore, this type of approach has the advantage of being relatively mutation-independent. For this reason, it would be sufficient to increase the expression of a protein, even if mutated, to exceed the threshold of minimal activity needed to obtain an optimal clinical phenotype.

Supplementary Materials: Supplementary materials are available online.

Acknowledgments: This work was supported by Ministero della Salute (Rome, Italy) L. 548/93 for the regional research funding quote of years 2009–2012. B.C. gratefully acknowledges the support of NVIDIA Corporation with the donation of the Tesla K40 GPU used for this research. G.S. also acknowledges the CINECA (ISCRA C projects ID HP10CIL4P9) for access to high performance computing resources.

Author Contributions: G.O., G.P. and G.C. conceived and designed the experiments; F.Z. and F.A. performed and analyzed the biological experiments; S.D. and B.P. performed the synthesis and purification of DNA and PNA molecules; N.B., G.O. and B.P. performed the CD, UV and MS experiments; C.M.M., G.S. and B.C. performed the MD studies; G.O., F.A., B.C. and N.B. wrote the paper.

Conflicts of Interest: The authors declare no conflict of interest. The founding sponsors had no role in the design of the study; in the collection, analyses, or interpretation of data; in the writing of the manuscript, and in the decision to publish the results.

References

1. Elborn, J.S. Cystic fibrosis. *Lancet* **2016**, *388*, 2519–2531. [[CrossRef](#)]
2. O'Sullivan, B.P.; Freedman, S.D. Cystic fibrosis. *Lancet* **2009**, *373*, 1891–1904. [[CrossRef](#)]
3. Heda, G.D.; Marino, C.R. Surface expression of the cystic fibrosis transmembrane conductance regulator mutant deltaF508 is markedly upregulated by combination treatment with sodium butyrate and low temperature. *Biochem. Biophys. Res. Commun.* **2000**, *271*, 659–664. [[CrossRef](#)] [[PubMed](#)]
4. Amato, F.; Seia, M.; Giordano, S.; Elce, A.; Zarrilli, F.; Castaldo, G.; Tomaiuolo, R. Gene mutation in microRNA target sites of CFTR gene: A novel pathogenetic mechanism in cystic fibrosis? *PLoS ONE* **2013**, *8*, e60448. [[CrossRef](#)] [[PubMed](#)]
5. Gillen, A.E.; Gosalia, N.; Leir, S.H.; Harris, A. MicroRNA regulation of expression of the cystic fibrosis transmembrane conductance regulator gene. *Biochem. J.* **2011**, *438*, 25–32. [[CrossRef](#)] [[PubMed](#)]
6. Ramachandran, S.; Karp, P.H.; Osterhaus, S.R.; Jiang, P.; Wohlford-Lenane, C.; Lennox, K.A.; Jacobi, A.M.; Praek, K.; Rose, S.D.; Behlke, M.A.; et al. Post-transcriptional Regulation of CFTR Expression and Function by MicroRNAs. *Am. J. Respir. Cell. Mol. Biol.* **2013**, *49*, 544–551. [[CrossRef](#)]
7. Oglesby, I.K.; Chotirmall, S.H.; McElvaney, N.G.; Greene, C.M. Regulation of Cystic Fibrosis Transmembrane Conductance Regulator by MicroRNA-145, -223, and -494 Is Altered in $\Delta F508$ Cystic Fibrosis Airway Epithelium. *J. Immunol.* **2013**, *190*, 3354–3362. [[CrossRef](#)] [[PubMed](#)]

8. Hassan, F.; Nuovo, G.J.; Crawford, M.; Boyaka, P.N.; Kirkby, S.; Nana-Sinkam, S.P.; Cormet-Boyaka, E. MiR-101 and miR-144 Regulate the Expression of the CFTR Chloride Channel in the Lung. *PLoS ONE* **2012**, *7*, e50837. [[CrossRef](#)] [[PubMed](#)]
9. Ramachandran, S.; Karp, P.H.; Jiang, P.; Ostedgaard, L.S.; Walz, A.E.; Fisher, J.T.; Keshavjee, S.; Lennox, K.A.; Jacobi, A.M.; Rose, S.D.; et al. A microRNA network regulates expression and biosynthesis of wild-type and F508 mutant cystic fibrosis transmembrane conductance regulator. *Proc. Natl. Acad. Sci. USA* **2012**, *109*, 13362–13367. [[CrossRef](#)] [[PubMed](#)]
10. Megiorni, F.; Cialfi, S.; Dominici, C.; Quattrucci, S.; Pizzuti, A. Synergistic Post-Transcriptional Regulation of the Cystic Fibrosis Transmembrane conductance Regulator (CFTR) by miR-101 and miR-494 Specific Binding. *PLoS ONE* **2011**, *6*, e26601. [[CrossRef](#)] [[PubMed](#)]
11. Griffiths-Jones, S.; Saini, H.K.; van Dongen, S.; Enright, A.J. Mirbase: Tools for microRNA genomics. *Nucleic Acids Res.* **2008**, *36*, D154–D158. [[CrossRef](#)] [[PubMed](#)]
12. He, L.; Hannon, G.J. MicroRNAs: Small RNAs with a big role in gene regulation. *Nat. Rev. Genet.* **2004**, *5*, 522–531. [[CrossRef](#)] [[PubMed](#)]
13. Selbach, M.; Schwanhaussner, B.; Thierfelder, N.; Fang, Z.; Khanin, R.; Rajewsky, N. Widespread changes in protein synthesis induced by microRNAs. *Nature* **2008**, *455*, 58–63. [[CrossRef](#)] [[PubMed](#)]
14. Amato, F.; Tomaiuolo, R.; Borbone, N.; Elce, A.; Amato, J.; D'Errico, S.; De Rosa, G.; Mayol, L.; Piccialli, G.; Oliviero, G.; et al. Design, synthesis and biochemical investigation, by in vitro luciferase reporter system, of peptide nucleic acids as new inhibitors of miR-509–3p involved in the regulation of cystic fibrosis disease-gene expression. *Med. Chem. Commun.* **2014**, *5*, 68–71. [[CrossRef](#)]
15. Amato, F.; Tomaiuolo, R.; Nici, F.; Borbone, N.; Elce, A.; Catalanotti, B.; D'Errico, S.; Morgillo, C.M.; De Rosa, G.; Mayol, L.; et al. Exploitation of a very small peptide nucleic acid as a new inhibitor of miR-509–3p involved in the regulation of cystic fibrosis disease-gene expression. *Biomed. Res. Int.* **2014**, *2014*, 610718. [[CrossRef](#)] [[PubMed](#)]
16. Amato, J.; Oliviero, G.; De Pauw, E.; Gabelica, V. Hybridization of short complementary PNAs to G-quadruplex forming oligonucleotides: An electrospray mass spectrometry study. *Biopolymers* **2009**, *91*, 244–255. [[CrossRef](#)] [[PubMed](#)]
17. Amato, J.; Pagano, B.; Borbone, N.; Oliviero, G.; Gabelica, V.; Pauw, E.D.; D'Errico, S.; Piccialli, V.; Varra, M.; Giancola, C.; et al. Targeting G-quadruplex structure in the human c-kit promoter with short PNA sequences. *Bioconj. Chem.* **2011**, *22*, 654–663. [[CrossRef](#)] [[PubMed](#)]
18. Amato, J.; Stellato, M.I.; Pizzo, E.; Petraccone, L.; Oliviero, G.; Borbone, N.; Piccialli, G.; Orecchia, A.; Bellei, B.; Castiglia, D.; et al. PNA as a potential modulator of col7a1 gene expression in dominant dystrophic epidermolysis bullosa: A physico-chemical study. *Mol. Biosyst.* **2013**, *9*, 3166–3174. [[CrossRef](#)] [[PubMed](#)]
19. Avitabile, C.; Saviano, M.; D'Andrea, L.; Bianchi, N.; Fabbri, E.; Brognara, E.; Gambari, R.; Romanelli, A. Targeting pre-miRNA by peptide nucleic acids: A new strategy to interfere in the miRNA maturation. *Artif. DNA: PNA&XNA* **2012**, *3*, 88–96.
20. Brognara, E.; Fabbri, E.; Montagner, G.; Gasparello, J.; Manicardi, A.; Corradini, R.; Bianchi, N.; Finotti, A.; Breveglieri, G.; Borgatti, M.; et al. High levels of apoptosis are induced in human glioma cell lines by co-administration of peptide nucleic acids targeting miR-221 and miR-222. *Int. J. Oncol.* **2016**, *48*, 1029–1038. [[CrossRef](#)] [[PubMed](#)]
21. Hyrup, B.; Nielsen, P.E. Peptide nucleic acids (PNA): Synthesis, properties and potential applications. *Bioorg. Med. Chem.* **1996**, *4*, 5–23. [[CrossRef](#)]
22. Nielsen, P.E.; Egholm, M.; Berg, R.H.; Buchardt, O. Sequence-selective recognition of DNA by strand displacement with a thymine-substituted polyamide. *Science* **1991**, *254*, 1497–1500. [[CrossRef](#)] [[PubMed](#)]
23. Roviello, G.N.; Musumeci, D.; De Cristofaro, A.; Capasso, D.; Di Gaetano, S.; Bucci, E.M.; Pedone, C. Alternate dab-aegPNAs: Synthesis, nucleic acid binding studies and biological activity. *Mol. Biosyst.* **2010**, *6*, 199–205. [[CrossRef](#)] [[PubMed](#)]
24. Roviello, G.N.; Ricci, A.; Bucci, E.M.; Pedone, C. Synthesis, biological evaluation and supramolecular assembly of novel analogues of peptidyl nucleosides. *Mol. Biosyst.* **2011**, *7*, 1773–1778. [[CrossRef](#)] [[PubMed](#)]
25. Pinto, B.; Rusciano, G.; D'Errico, S.; Borbone, N.; Sasso, A.; Piccialli, V.; Mayol, L.; Oliviero, G.; Piccialli, G. Synthesis and label free characterization of a bimolecular PNA homo quadruplex. *BBA-Gen. Subj.* **2016**, *1861*, 1222–1228. [[CrossRef](#)] [[PubMed](#)]

26. Viart, V.; Bergougoux, A.; Bonini, J.; Varilh, J.; Chiron, R.; Tabary, O.; Molinari, N.; Claustres, M.; Taulan-Cadars, M. Transcription factors and miRNAs that regulate fetal to adult CFTR expression change are new targets for cystic fibrosis. *Eur. Respir. J.* **2014**, *45*, 116–128. [[CrossRef](#)] [[PubMed](#)]
27. Jensen, K.K.; Orum, H.; Nielsen, P.E.; Norden, B. Kinetics for hybridization of peptide nucleic acids (PNA) with DNA and RNA studied with the BIAcore technique. *Biochemistry* **1997**, *36*, 5072–5077. [[CrossRef](#)] [[PubMed](#)]
28. Egholm, M.; Buchardt, O.; Christensen, L.; Behrens, C.; Freier, S.M.; Driver, D.A.; Berg, R.H.; Kim, S.K.; Norden, B.; Nielsen, P.E. PNA hybridizes to complementary oligonucleotides obeying the watson-crick hydrogen-bonding rules. *Nature* **1993**, *365*, 566–568. [[CrossRef](#)] [[PubMed](#)]
29. Brown, S.C.; Thomson, S.A.; Veal, J.M.; Davis, D.G. NMR solution structure of a peptide nucleic acid complexed with RNA. *Science* **1994**, *265*, 777–780. [[CrossRef](#)] [[PubMed](#)]
30. Case, D.A.; Babin, J.T.; Berryman, J.T.; Betz, R.M.; Cai, Q.; Cerutti, D.S.; Cheatham, T.E., III; Darden, T.A.; Duke, R.E.; Giese, T.J.; et al. *Amber 14*; University of California: San Francisco, CA, USA, 2015.
31. Lavery, R.; Moakher, M.; Maddocks, J.H.; Petkeviciute, D.; Zakrzewska, K. Conformational analysis of nucleic acids revisited: Curves+. *Nucleic Acids Res.* **2009**, *37*, 5917–5929. [[CrossRef](#)] [[PubMed](#)]
32. Kiliszek, A.; Banaszak, K.; Dauter, Z.; Rypniewski, W. The first crystal structures of RNA-PNA duplexes and a PNA-PNA duplex containing mismatches-toward anti-sense therapy against TREDs. *Nucleic Acids Res.* **2016**, *44*, 1937–1943. [[CrossRef](#)] [[PubMed](#)]
33. Soliva, R.; Sherer, E.; Luque, F.J.; Laughton, C.A.; Orozco, M. Molecular dynamics simulations of PNA-DNA and PNA-RNA duplexes in aqueous solution. *J. Am. Chem. Soc.* **2000**, *122*, 5997–6008. [[CrossRef](#)]
34. Tanaka, Y.; Fujii, S.; Hiroaki, H.; Sakata, T.; Tanaka, T.; Uesugi, S.; Tomita, K.; Kyogoku, Y. A'-form RNA double helix in the single crystal structure of r (UGAGCUUCGGCUC). *Nucleic Acids Res.* **1999**, *27*, 949–955. [[CrossRef](#)]
35. Autiero, I.; Saviano, M.; Langella, E. Molecular dynamics simulations of PNA-PNA and PNA-DNA duplexes by the use of new parameters implemented in the GROMACS package: A conformational and dynamics study. *Phys. Chem. Chem. Phys.* **2014**, *16*, 1868–1874. [[CrossRef](#)] [[PubMed](#)]
36. He, W.; Hatcher, E.; Balaeff, A.; Beratan, D.N.; Gil, R.R.; Madrid, M.; Achim, C. Solution structure of a peptide nucleic acid duplex from NMR data: Features and limitations. *J. Am. Chem. Soc.* **2008**, *130*, 13264–13273. [[CrossRef](#)] [[PubMed](#)]
37. Sanders, J.M.; Wampole, M.E.; Chen, C.P.; Sethi, D.; Singh, A.; Dupradeau, F.Y.; Wang, F.; Gray, B.D.; Thakur, M.L.; Wickstrom, E.; et al. Effects of hypoxanthine substitution in peptide nucleic acids targeting kras2 oncogenic mRNA molecules: Theory and experiment. *J. Phys. Chem. B* **2013**, *117*, 11584–11595. [[CrossRef](#)] [[PubMed](#)]
38. Sen, S.; Nilsson, L. Molecular dynamics of duplex systems involving PNA: Structural and dynamical consequences of the nucleic acid backbone. *J. Am. Chem. Soc.* **1998**, *120*, 619–631. [[CrossRef](#)]
39. Greene, C.M.; Hartl, D. Developmental control of CFTR: From bioinformatics to novel therapeutic approaches. *Eur. Respir. J.* **2015**, *45*, 18–20. [[CrossRef](#)] [[PubMed](#)]
40. Hasuwa, H.; Ueda, J.; Ikawa, M.; Okabe, M. MiR-200b and miR-429 function in mouse ovulation and are essential for female fertility. *Science* **2013**, *341*, 71–73. [[CrossRef](#)] [[PubMed](#)]
41. Lu, X.J.; Olson, W.K. 3DNA: A software package for the analysis, rebuilding and visualization of three-dimensional nucleic acid structures. *Nucleic Acids Res.* **2003**, *31*, 5108–5121. [[CrossRef](#)] [[PubMed](#)]
42. Maier, J.A.; Martinez, C.; Kasavajhala, K.; Wickstrom, L.; Hauser, K.E.; Simmerling, C. Ff14sb: Improving the accuracy of protein side chain and backbone parameters from ff99sb. *J. Chem. Theory Comput.* **2015**, *11*, 3696–3713. [[CrossRef](#)] [[PubMed](#)]
43. Perez, A.; Marchan, I.; Svozil, D.; Sponer, J.; Cheatham, T.E., 3rd; Laughton, C.A.; Orozco, M. Refinement of the amber force field for nucleic acids: Improving the description of alpha/gamma conformers. *Biophys. J.* **2007**, *92*, 3817–3829. [[CrossRef](#)] [[PubMed](#)]
44. Zgarbova, M.; Otyepka, M.; Sponer, J.; Mladek, A.; Banas, P.; Cheatham, T.E., 3rd; Jurecka, P. Refinement of the Cornell et al. nucleic acids force field based on reference quantum chemical calculations of glycosidic torsion profiles. *J. Chem. Theory Comput.* **2011**, *7*, 2886–2902. [[CrossRef](#)] [[PubMed](#)]
45. Craft, J.W., Jr.; Legge, G.B. An AMBER/DYANA/MOLMOL phosphorylated amino acid library set and incorporation into NMR structure calculations. *J. Biomol. NMR* **2005**, *33*, 15–24. [[CrossRef](#)] [[PubMed](#)]

46. *The PyMol Molecular Graphics System*; Version 1.8; Schrödinger, LLC: New York, NY, USA.
47. Humphrey, W.; Dalke, A.; Schulten, K. VMD: Visual Molecular Dynamics. *J. Mol. Graph.* **1996**, *14*, 27–38. [[CrossRef](#)]

Sample Availability: Samples of the DNA and PNA molecules reported in this study are available from the authors.



© 2017 by the authors. Licensee MDPI, Basel, Switzerland. This article is an open access article distributed under the terms and conditions of the Creative Commons Attribution (CC BY) license (<http://creativecommons.org/licenses/by/4.0/>).

Self-Assembly of G-Rich Oligonucleotides Incorporating a 3′–3′ Inversion of Polarity Site: A New Route Towards G-Wire DNA Nanostructures

Giorgia Oliviero,^[b] Stefano D'Errico,^[a] Brunella Pinto,^[a] Fabrizia Nici,^[a] Principia Dardano,^[c] Ilaria Rea,^[c] Luca De Stefano,^[c] Luciano Mayol,^[a] Gennaro Piccialli,^[a] and Nicola Borbone^{*,[a]}

Obtaining DNA nanostructures with potential applications in drug discovery, diagnostics, and electronics in a simple and affordable way represents one of the hottest topics in nanotechnology and medical sciences. Herein, we report a novel strategy to obtain structurally homogeneous DNA G-wire nanostructures of known length, starting from the short unmodified G-rich oligonucleotide d(5′-CGGT-3′–3′-GGC-5′) (1) incorporat-

ing a 3′–3′ inversion of polarity site. The reported approach allowed us to obtain long G-wire assemblies through 5′–5′ π – π stacking interactions in between the tetramolecular G-quadruplex building blocks that form when 1 is annealed in the presence of potassium ions. Our results expand the repertoire of synthetic methodologies to obtain new tailored DNA G-wire nanostructures.

1. Introduction

In the development of new nanotechnologies and biomaterials, the possibility of assembling ordered supramolecular structures starting from small building blocks and the exploitation of self-assembly driving forces are very important and much studied topics.^[1–3] In the bottom-up approach, DNA strands have been demonstrated to be very useful building blocks for the assembly of supramolecular structures of various dimensions and shapes. For example, the DNA nanotechnology known as DNA origami allows the design and the construction of tailored three-dimensional superstructures by exploiting the Watson–Crick base-pairing scheme.^[4–7] Besides the Watson–Crick base-pairing scheme, also the Hoogsteen hydrogen bonding one, which allows the formation of G-quadruplex DNA, can be exploited to obtain DNA supramolecular struc-

tures. G-Quadruplexes are unusual secondary structures of DNA, which form when guanine-rich DNA strands are annealed in the presence of suitable monovalent or divalent cations.

The building block of G-quadruplexes is the G-quartet (Figure 1 A), a planar arrangement of four guanines held together by a cyclic array of eight Hoogsteen hydrogen bonds.^[8–10] The onset of π – π interactions among the stacked G-quartets greatly stabilizes the G-quadruplex assembly, which is generally more stable than a DNA duplex of the same length. A G-quadruplex can be formed by one, two, or four G-rich DNA strands and can be classified as either parallel, antiparallel, or hybrid type depending on the mutual orientation of the strands in-

[a] Dr. S. D'Errico, Dr. B. Pinto, Dr. F. Nici, Prof. Dr. L. Mayol, Prof. Dr. G. Piccialli, Dr. N. Borbone
Department of Pharmacy
Università degli Studi di Napoli Federico II
Via D. Montesano 49, 80131 Napoli (Italy)
E-mail: nicola.borbone@unina.it

[b] Prof. Dr. G. Oliviero
Department of Molecular Medicine and Medical Biotechnologies
Via S. Pansini 5, 80131 Napoli (Italy)

[c] Dr. P. Dardano, Dr. I. Rea, Dr. L. De Stefano
Institute for Microelectronics and Microsystems
Consiglio Nazionale delle Ricerche
Via P. Castellino 111, 80131 Napoli (Italy)

Supporting Information and the ORCID identification number(s) for the author(s) of this article can be found under <https://doi.org/10.1002/open.201700024>.

© 2017 The Authors. Published by Wiley-VCH Verlag GmbH & Co. KGaA. This is an open access article under the terms of the Creative Commons Attribution-NonCommercial-NoDerivs License, which permits use and distribution in any medium, provided the original work is properly cited, the use is non-commercial and no modifications or adaptations are made.

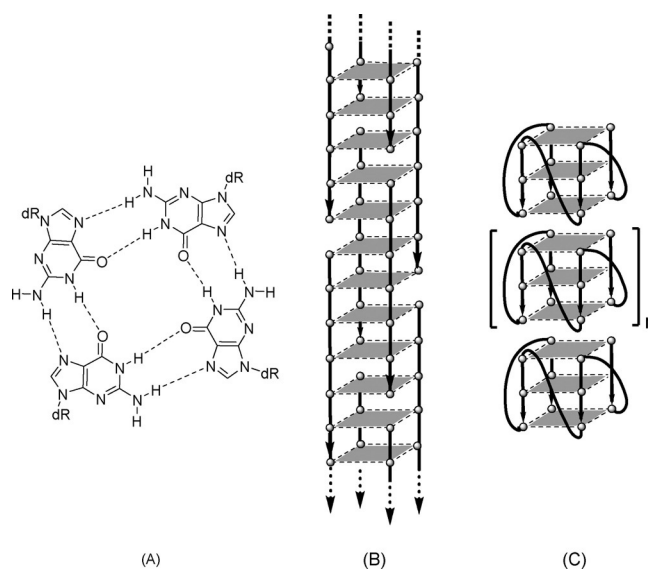


Figure 1. Schematic representations of a G-tetrad (A) and of interlocked (B) and stacked (C) G-wire polymers.

involved in the G-quartets formation.^[11,12] Further factors that contribute to the wide polymorphism of G-quadruplexes are the length and the base composition of the loops (when present), as well as the nature of the cations used to stabilize the quadruple helix structure.^[13–15] The biological implications of G-quadruplexes in cellular processes^[16–18] and their use as promising drugs^[19–22] or in drugs delivery^[23] and diagnostics^[23–25] are well known. In addition, G-quadruplexes possess greater conductivity than DNA duplexes, thus suggesting their use for the obtainment of electronic nano-biomaterials and nanodevices.^[26–28] These properties indicate the G-quadruplex scaffold as a useful structural motif to obtain supramolecular self-assemblies, including the so-called G-wires.^[29–32] G-wire superstructures can reach the length of thousands of nanometers along the axis perpendicular to the G-tetrad planes. Depending on the topological arrangement of the G-rich strands participating in their formation, G-wires can be classified into two categories: i) *interlocked G-wires*, characterized by the cooperative assembly of interlocked slipped strands (Figure 1B) and ii) *stacked G-wires*, characterized by the multimerization of G-quadruplex building blocks held together by end-to-end π - π stacking (Figure 1C). Besides the well-known interlocked G-wires^[29–35] and G-wires containing both topological motifs,^[36–38] only a few examples of exclusively stacked G-wires have been reported so far.^[39–41]

In a previous study, we reported that in the presence of K^+ cations the 7-mer d(CGGTGGT) can assemble into the octameric higher-ordered G-quadruplex complex d(CGGTGGT)₈ (Figure S1 in the Supporting Information) through π - π stacking of two unusual G(C):G(C):G(C):G(C) planar octads belonging to two identical tetramolecular parallel G-quadruplexes.^[42] Later, we demonstrated that the same dimerization pathway is also possible for all the other d(CGGXGGT) DNA strands, with X = A, G, or C.^[43] Herein, we report on the achievement of a new type of stacked G-wire, here indicated as Q_n (Figure 2) obtained by exploiting the 5'-5' π - π stacking interactions between the G(C):G(C):G(C):G(C) octads formed at both ends of the tetramolecular G-quadruplex building block Q_1 (Figure 2). The last

forms when the d(5'-CGGT-3'-3'-GGC-5') DNA strand (1, Figure 2), incorporating a 3'-3' inversion of polarity site, is annealed in the presence of K^+ ions. The resulting G-wires were obtained as a distribution of quadruplex multimers of different length.

The n subscript in Q_n indicates the number of tetramolecular G-quadruplex building blocks participating in the G-wires elongation. The actual formation of the target G-wires was confirmed by polyacrylamide gel electrophoresis (PAGE), HPLC size exclusion chromatography (HPLC-SEC), circular dichroism (CD), ¹H nuclear magnetic resonance (NMR) spectroscopy, and atomic force microscopy (AFM) studies. The analytical results allowed us also to gather information on the G-wires assembly and stability, and to isolate and characterize the three shortest Q_n species ($n = 2-4$).

2. Results and Discussion

2.1. Synthesis of d(5'-CGGT-3'-3'-GGC-5') and G-Wires

The d(5'-CGGT-3'-3'-GGC-5') (1) incorporating a 3'-3' inversion of polarity site was synthesized by using a solid-phase automated DNA synthesizer as described in the Experimental Section. The inversion of polarity site was achieved by performing the first four coupling cycles with 5'-phosphoramidites and the remaining three with standard 3'-phosphoramidites. The Q_n species were obtained by heating 1—dissolved in 1.0 M K^+ containing buffer at the single strand concentration of 0.1 or 1.6 mM—at 90 °C for 10 min and then rapidly cooling it to 4 °C (fast annealing procedure). All samples were stored at 4 °C for 24 h before further investigation.

2.2. PAGE Studies

The annealed 1.6 mM 1 was analyzed by PAGE to obtain information on its propensity to form the tetramolecular G-quadruplex building block Q_1 and/or the target Q_n multimers. For this purpose, we compared the electrophoretic mobility of 1 (lane 3 in Figure 3) with those of the G-quadruplexes d(TGGGGT)₄ (lane 1) and d(CGGTGGT)₈ (lane 2), used as size

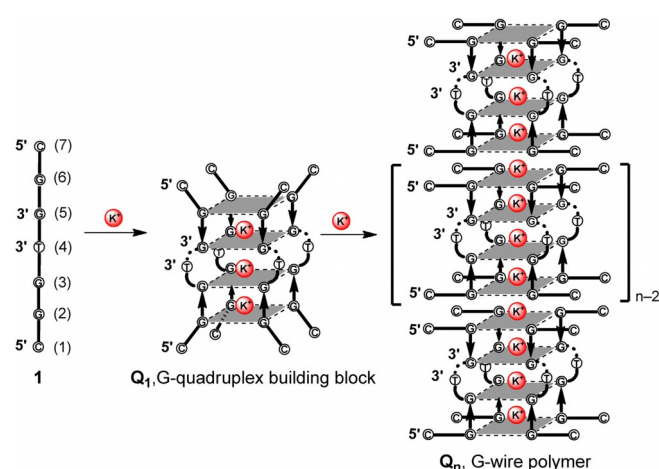


Figure 2. Formation of the G-quadruplex building block Q_1 and its multimerization into Q_n G-wire polymers starting from the ODN 1. The expected stabilizing K^+ ions are shown as red spheres.

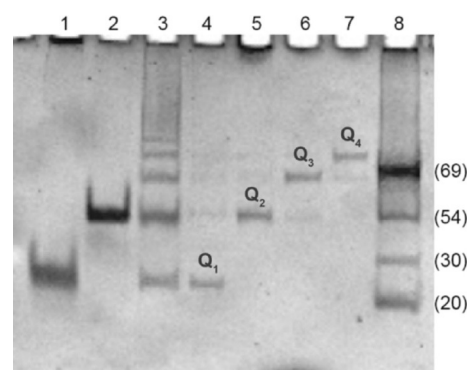


Figure 3. Electrophoretic mobility of the ODNs under study annealed in 1.0 M K^+ buffer. Lane 1: d(TGGGGT)₄; lane 2: d(CGGTGGT)₈; lane 3: ODN 1; lanes 4–7: isolated peaks from the HPLC-SEC fractionation of annealed 1; lane 8: single-stranded DNA reference ladder.

markers for the tetramolecular G-quadruplex building block Q_1 and for its eight-stranded dimer Q_2 , respectively. At the studied conditions, the annealed **1** migrated as a ladder of bands, thus confirming its propensity to form G-quadruplex multimers. The electrophoretic mobility of the two fastest bands matched almost perfectly with that of the size markers in lanes 1 and 2, thus confirming the formation of a tetra-stranded Q_1 and octa-stranded Q_2 ; whereas the remaining slower bands in lane 3 were likely a result of longer Q_n species ($n \geq 3$). The electrophoretic mobility of the isolated Q_{1-4} species, obtained by HPLC-SEC fractionation (see the following section), was also assessed (lanes 4–7). Taken together, the PAGE data suggested that the oligodeoxynucleotide (ODN) **1** in the presence of K^+ ions is capable of self-assembling in a distribution of G-wire species of different lengths (Q_n) obtained by the sequential stacking of the tetramolecular G-quadruplex building block Q_1 presenting two “sticky” G(C):G(C):G(C):G(C) planar octads at both 5'-ends.

2.3. SEC Studies

The Q_n G-wire population was analyzed by HPLC-SEC at room temperature on a ReproSil 200 SEC column 24 h after annealing and storage at 4 °C. The HPLC profile of the annealed 0.1 mM **1** showed a distribution of peaks in which low molecular weight species had greater retention times (Figure S2A in the Supporting Information). To obtain information on the M_w of the observed product peaks, we used the same HPLC-SEC conditions (see the Experimental Section) to determine the retention times (R_t) of i) the single-stranded dT₇ (panel B), ii) the tetramolecular quadruplex d(TGGGGT)₄ (panel C), and iii) the dimeric quadruplex d(CG GTGGT)₈ (panel D). Based on the HPLC-SEC data, the peak at the highest retention time ($R_t = 21.45$ min) was attributed to the single-stranded **1**, whereas the two preceding peaks (at $R_t = 19.89$ and 19.02 min) were assigned to the G-quadruplex building block Q_1 and to its dimer Q_2 , respectively. From these data, it was reasonable to hypothesize that each peak in the HPLC-SEC profile belongs to a species differing from those of the adjacent peaks for a M_w corresponding to the tetramolecular G-quadruplex building block Q_1 (i.e. 28 nucleotides). Exploiting the good peak resolution on the HPLC-SEC column, the species likely corresponding to Q_{1-4} were recovered and their purity and electrophoretic mobility assessed by PAGE (Figure 3, lanes 4–7). PAGE results confirmed the purity and allowed us to match the species responsible for the four fast-moving bands in the PAGE (i.e. Q_4 , Q_3 , Q_2 , and Q_1 from the slowest to the fastest band in Figure 3) with the four corresponding peaks in the HPLC-SEC distribution (i.e. Q_4 , Q_3 , Q_2 , and Q_1 from the least to the most retained in Figure S2A in the Supporting Information). Furthermore, HPLC-SEC re-injection of the isolated Q_{1-4} species, performed 24 h after their isolation and storage at 4 °C (Figure S3 in the Supporting Information), disclosed that the G-quadruplex building block Q_1 and the first three Q_n species (Q_{2-4}) do not interconvert each other and can be stored as single G-wire segments of known length for at least 24 h. However, considering the contribution of entropy to the formation of Q_n G-wires,

different behaviors could be anticipated for samples of **1** annealed at different ODN concentrations. Thus, we exploited the good chromatographic separation of Q_n species to assess the effect of the ODN annealing concentration on the formation and size distribution of Q_n species. As expected, the HPLC-SEC profile of Q_n obtained 24 h after the annealing of **1** at 1.6 mM concentration (Figure 4) confirmed that the formation of

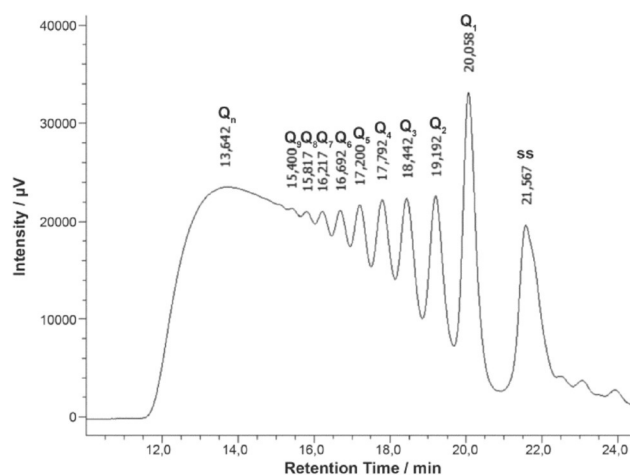


Figure 4. HPLC-SEC profile of Q_n distribution obtained by annealing 1.6 mM **1** in 1.0 M K^+ containing buffer. ss = single-stranded **1**.

longer G-wires is strongly dependent on the ODN concentration during the annealing procedure. Indeed, in Figure 4 all Q_n species with $n \leq 8$ are clearly distinguishable and almost equally populated, and an intense envelope peak attributable to longer G-wires is present at $R_t = 13.6$ min. Conversely, in the HPLC-SEC profile obtained from the sample annealed at 0.1 mM ODN concentration (Figure S2A in the Supporting Information), the envelope peak is absent and only the Q_n species with $n \leq 3$ are significantly populated.

The effect of the temperature on the distribution of Q_n species was investigated by HPLC-SEC 24 h after the annealing of 0.1 mM **1** in 1.0 M K^+ buffer. HPLC-SEC analyses were performed by injecting the sample 30 min after heating and equilibration at 25, 45, 65, and 85 °C (Figure S4 in the Supporting Information). The profile obtained from the sample injected at 25 °C showed almost the same Q_n distribution as the sample injected at 4 °C, but showed that at room temperature the dimeric Q_2 species not only is more abundant than the building block Q_1 (whereas the opposite was observed in the sample stored and injected at 4 °C), but represents the most abundant species. The progressive heating of the sample determined the reduction of the amount of Q_n species and the contextual increase of the single-stranded **1**, which resulted in the only observable peak at 85 °C. However, two significant outcomes emerged from the profiles obtained at 45 and 65 °C: 1) at 45 °C, although the most abundant species was represented by the single-stranded **1**, we observed that the distribution of Q_n species shifted towards longer G-wires, with the appearance of a new peak at $R_t = 13.3$ min and with the Q_3 species being even more abundant than Q_2 ; 2) the analysis of the pro-

file obtained at 65 °C suggested that the Q_n species melt through a cooperative process, which drives directly to the random coil **1** (the peak of the G-quadruplex building block Q_1 was even less abundant than that of Q_5 species). The higher thermal stability of Q_n species relative to Q_1 was also confirmed by CD melting data (see the following section).

2.4. CD Studies

CD is a well-established diagnostic technique to provide preliminary information about the topology of G-quadruplexes in solution. Generally, the CD profile of parallel G-quadruplexes, in which all guanines in the G-tetrads are in the *anti* glycosidic bond conformation (Type 1 stem), is characterized by a positive signal at around 264 nm and a negative signal at around 240 nm; whereas that of antiparallel G-quadruplexes with alternating *syn-anti* glycosidic bonds along the stem (Type 3 stem) shows a positive signal at 245 nm, a trough at around 260 nm, and a second positive signal at 290 nm.^[41,44–46] Considering the formation of stacking interactions between the terminal G-tetrads of Q_1 building blocks (required to obtain the Q_n G-wires) and the presence of the 3'–3' inversion of polarity site within the stem of Q_1 and its multimers, the CD profile obtained for the annealed **1** (containing a mixture of Q_n of different lengths), showing positive signals at 246 nm and 300 nm and a negative signal at 270 nm (Figure 5, dashed line), was somewhat unexpected. In fact, although the latter structural features anticipated for a Type 2 CD profile,^[44] the experimental result resembled that of a Type 3 stem. A Type 3 stem could be obtainable from **1** only if the thymines of two ODN **1** strands would participate in the formation of a propeller loop, thus allowing the formation of a bimolecular antiparallel quadruplex stem. However, this structural hypothesis has been ruled out by PAGE and HPLC-SEC evidence, which indicated the exclusive formation of the tetra-stranded quadruplex building block and its multimers.

Indeed, the CD profile of Q_n resembles those reported for the G-quadruplexes formed by $d(5'TG3'-3'GGT)_4$ ^[47] and $d(TGG3'-3'GGT)_4$ ^[48] incorporating a 3'–3' inversion of polarity

site and characterized by the presence of all *anti* G-tetrads. The occurrence of the same system of uninterrupted stacked G-tetrads, including both clockwise and counter-clockwise directionality, in Q_1 and Q_n could explain the CD profiles shown in Figure 5. The resulting structural hypothesis requires that the thymines are projected outside the quadruplex stem to form bulge loops,^[49] as depicted in Figure 2. Unfortunately, the strong positive signal at 300 nm induced by the presence of the 3'–3' inversion of polarity site precluded the observation of the negative band at 290 nm, which, in our previous studies, proved diagnostic for the formation of higher-ordered G-quadruplex assemblies obtained by non-covalent π – π stacking of planar G(C):G(C):G(C):G(C) octads.^[42,43] Similar CD profiles were obtained for the isolated Q_{1-4} (Figure 5, colored lines), thus confirming that the CD profile of Q_n was the result of the presence of quadruplex assemblies of different lengths incorporating the 3'–3' inversion of polarity site. The overall thermal stability of the species populating the Q_n distribution and that of the isolated Q_{1-4} complexes was assessed by means of CD denaturation experiments (Figure S5 in the Supporting Information). The resulting apparent melting curves clearly provided evidence that the thermal stability of the quadruplex multimers was higher than that of the parent quadruplex building block Q_1 .

2.5. NMR Spectroscopy

The formation of G-quadruplex assemblies from suitable G-rich ODN sequences is usually confirmed by water-suppressed ¹H NMR spectroscopy. When the N-1 imino protons of guanine bases are engaged in Hoogsteen-type hydrogen bonding with the O-6 carbonyl oxygen atoms of flanking guanines in each G-tetrad, they are protected from exchange with the hydrogen atoms of the solvent and are thus visible in the ¹H NMR spectrum as quadruplex-diagnostic slightly broad signals resonating between 10 and 12 ppm.^[50,51] Depending on the orientation of the strands and on the glycosidic torsion angle of guanines participating in G-tetrads, the four imino protons in each G-tetrad resonate as one, two, or four NMR signals.^[52] The downfield region of the water-suppressed ¹H NMR spectra of the Q_n distribution—obtained by annealing **1** in 1 M K⁺ buffer at 1.6 mM single strand concentration—recorded at 25, 45, 65, and 85 °C are shown in Figure S6 in the Supporting Information. In agreement with the CD evidence, the observation of the G-quadruplex diagnostic imino protons signals in the 11–12 ppm region confirmed the presence in solution of G-quadruplex species at temperatures lower than 65 °C. However, the intensity and the shape of imino and anomeric protons signals differed significantly from those we observed in the ¹H NMR spectra of the dimeric higher-ordered G-quadruplexes formed by CGGTGGT^[42] and CGGAGGT.^[43] In the two latter, four well-resolved imino protons (11.0–12.0 ppm) and intense anomeric protons signals (5.5–6.5 ppm) were visible at temperatures up to 65 °C. Conversely, in the NMR spectra of **1** recorded at 25 and 45 °C, all imino and anomeric signals appeared severely broadened, thus suggesting the involvement of imino and anomeric protons in chemical or conformational exchange

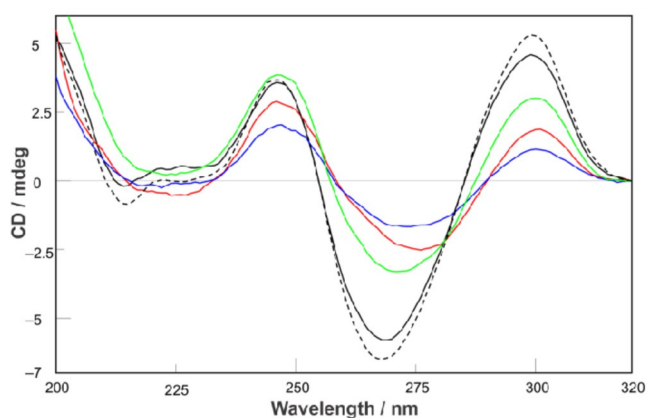


Figure 5. CD spectra of Q_n distribution (dashed curve) and isolated Q_1 (black curve), Q_2 (green curve), Q_3 (red curve), Q_4 (blue curve) G-quadruplexes.

phenomena. The line broadening of the imino protons was so intense as to require 10× software amplification for signal observation (see insets in Figure S6 in the Supporting Information). As far as the low intensity of the imino proton signals is concerned, we hypothesize that the presence of the bulge loops connecting the stacked G3 and G5 tetrads destabilizes the G-quadruplex stem, thus speeding up the imino proton exchange with water. The anomeric proton signal broadening, instead, could be the result of side-by-side aggregation of G-quadruplex units, as seen by Hu et al. in G-wire assemblies formed by dGMP annealed in the presence of Sr^{2+} .^[53] As we have shown in our previous papers,^[42,43] the anomeric protons are located at the outer shell of 2Q-like quadruplexes, thus it is conceivable that lateral contacts between flanking G-quadruplex structures participating in the Q_n G-wire distribution could be responsible for the observed anomeric signal broadening. As we will see in the following section, AFM evidence supports the formation of extended quadruplex layers by lateral aggregation of quadruplex units. Although AFM gives us a picture of quadruplex aggregates deposited on mica surfaces, we believe that such aggregates could also form in solution considering the relatively high ODN concentration used for the preparation of the NMR samples (6.0 mM). In the light of this hypothesis, the comparison of the NMR spectra recorded in the 25–85 °C temperature range indicates that the breakdown of quadruplex aggregates and the melting of quadruplex units to the random coil 1 are cooperative processes, which start at temperatures between 45 and 65 °C and complete at temperatures lower than 85 °C.

2.6. AFM Studies

Q_n quadruplexes interact and self-assemble on mica surfaces in different ways depending on their concentration in the starting solution. The morphology of the obtained films has been investigated by AFM by using 1.6 mM and 16 μM solutions of 1 in 0.1 M phosphate buffer, at pH 7.0. Muscovite mica was used as the AFM support both for the super-hydrophilic property of its surface, which guarantees a lower interaction between suspended molecules in aqueous solution during the evaporation of the solvent, and for its flatness, with less than 0.5 nm of root mean-square (r.m.s.) roughness for a 1000 × 1000 nm² surface area. The AFM images of the G-quadruplexes spontaneously adsorbed from 1.6 mM ODN freshly prepared solutions showed a densely populated surface (Figure S7 in the Supporting Information), characterized by aggregates of different lengths and widths (*x,y* coordinates on panels A–C), whereas their heights (*z* coordinate) are always around 2 nm. These structures are due to the formation, after adsorption on the mica surface, of rod-like shaped quadruplex aggregates grown during the evaporation of a 2 μL drop of 1.6 mM solution (panel A, scale bar = 1 μm). The preferential direction of alignment of the G-rodlets is well evident in panel B—the scale bar is 200 nm—where aggregates with lengths from 21 up to 166 nm (average value of 60 ± 40 nm) are shown; widths are in the tenths of nanometers range and are always less than 100 nm; heights are almost all about 2 nm (see the statistics

panels reported in Figure S7 in the Supporting Information). The AFM results are compatible with reported SEC results considering that, differently from height measurements, the length and width measurements are affected by the curvature radius of the AFM tip. The preferred orientation can be ascribed to the interaction between G-quadruplexes and the mica surface. The homogeneous values of heights recorded suggested the formation of self-assembled monolayers in the *x,y* plane owing to the evaporation of the buffer solution, which promoted lateral and longitudinal aggregation of G-quadruplexes, the first one being favored by side-packing.

A 100-times diluted solution gave different results, as can be noted in Figure S8 in the Supporting Information. Even if a preferred orientation could still be envisaged, the structures seemed sparser and less ordered (see panel A); lengths are in the same interval as before, whereas the widths are smaller, never exceeding 30 nm, as evident from the measurements in panel B. Also in this case, a tip radius of curvature of about 10 nm must be taken in account. This result confirmed a side-packing mechanism in the assembly of G-structures during evaporation of the solution. The heights are always about 2 nm as before (see measurements in panel C), again endorsing the hypothesis of spontaneous formation of a monolayer. In the case of diluted starting solution, the longitudinal aggregation is competitive compared with the lateral one, owing to steric conditions during the evaporation.

3. Conclusions

In this paper, we reported the successful results of our study aimed at the obtainment of a new kind of G-wire DNA by exploitation of π – π stacking interactions between tetramolecular G-quadruplex building blocks incorporating a 3'–3' inversion of polarity site and exposing G(C):G(C):G(C):G(C) planar “sticky” octads at both 5'-ends. The main findings of the study can be summarized as follows: 1) the obtained G-wires are unprecedented and are achievable by using the short 5'CGGT3'–3'GGC5' G-rich ODN as the starting material in a facile and affordable way; 2) the use of a tetramolecular G-quadruplex building block to obtain DNA G-wire polymers represents a major improvement over the use of monomolecular G-quadruplexes, which, possessing different end-faces and lateral nucleotide loops, could induce the formation of different kinds of aggregates thus reducing the amount of target G-wires; 3) the reported G-wires can be easily monitored in their formation and length-growth by PAGE and HPLC-size exclusion chromatography. We also demonstrated that the HPLC-SEC technique can be used to determine the number of quadruplex building blocks in each Q_n G-wire, as well as to isolate and recover the three shortest Q_n species ($n = 2$ –4).

Experimental Section

DNA Synthesis and Purification

DNA sequences d(TGGGGT) and d(CG GTGGT) were chemically synthesized with an Expedite 8909 DNA synthesizer (PerSeptive Bio-

systems, USA) using a universal CPG support purchased from Glen Research. The syntheses were performed by adopting the standard β -cyanoethyl phosphoramidite chemistry at 10–15 μM scale and the products were purified as previously described.^[54] The synthesis of d(5'-CGGT-3'-3'-GGC-5') (1) was performed with the same DNA synthesizer. The inversion of polarity site within the sequence was achieved by initially assembling the 5'-CGGT-3' tract by using 5'-phosphoramidites and then the 3'-GGC-5' tract with standard 3'-phosphoramidites. After completion of the ODN sequence, the support was treated with concentrated aqueous ammonia at 55 °C for 15 h. The combined filtrates and washings were concentrated under reduced pressure and purified through HPLC (JASCO PU2089 pumps equipped with the JASCO 2075 UV detector) with an anion exchange column (Macherey–Nagel, 1000-8/46, 4.4 \times 50 mm, 5 μm) using a linear gradient from 0 to 100% B in 30 min, flow rate = 1 mL min⁻¹ and detection at 260 nm (buffer A: 20 mM NaH₂PO₄ aq. solution pH 7.0, containing 20% (v/v) CH₃CN; buffer B: 20 mM NaH₂PO₄ aq. solution pH 7.0, containing 1 M NaCl and 20% (v/v) CH₃CN).

Annealing Procedure

The ODN concentrations were determined in water by measuring the absorbance at 260 nm at 90 °C by using the nearest-neighbor calculated molar extinction coefficient of 5'-CGGTGGC-3' ($\epsilon = 63\,100\text{ M}^{-1}\text{ cm}^{-1}$). The 0.1 and 1.6 mM solutions of 1 were obtained by dissolving the lyophilized sample in 900 mM KCl and 100 mM KH₂PO₄. The samples were annealed by heating at 90 °C for 10 min and then quickly cooling to 4 °C. After the annealing procedure, the samples were stored at 4 °C before measurements.

PAGE

Native gel electrophoresis experiments were performed on 20% polyacrylamide gels containing TBE (8.9 mM Tris, 8.9 mM borate, 0.2 mM EDTA, from BIORAD) and 30 mM KCl, at room temperature, 120 V for 2 h. The ODN samples, annealed at 1.6 mM single strand concentration in 1.0 M K⁺ buffer, were diluted at 0.6 mM loading concentration just before the PAGE runs. Glycerol was added (10% final) to facilitate sample loading in the wells. The bands were finally visualized by ethidium bromide staining in a Bio-Rad Laboratories Gel DocTM XR+ image system.

HPLC-SEC Analyses and Isolation of Q_n Species

HPLC-SEC analyses and purifications were performed with a Repro-Sil 200 SEC column operating in the M_w range of 2000–70 000 Dalton (Dr. Maisch GmbH, 300 \times 8 mm, 5 μm) eluted with 90 mM KCl and 10 mM KH₂PO₄/CH₃CN (80:20, v/v), flow rate 0.5 mL min⁻¹, detector at 260 nm. The analyses were performed at room temperature.

CD

CD spectra and CD melting profiles were recorded with a Jasco 715 CD spectrophotometer (Jasco, Tokyo, Japan) equipped with a Jasco JPT4235 Peltier temperature controller in 1 mm optical path quartz cuvettes (100 nm min⁻¹ scanning speed, 1 s response time). The spectra were recorded in triplicate at 4 °C from 220 to 320 nm. CD samples were prepared in potassium buffer (90 mM KH₂PO₄ and 10 mM KCl) at 20 μM final single strand concentration. The buffer baseline was subtracted from each spectrum and the

spectra were normalized to have zero at 320 nm. CD melting curves were registered at 268 nm, 1 °C min⁻¹ heating rate, temperature range 5–90 °C.

NMR Spectroscopy

NMR data were recorded with a Varian ^{UNITY}INOVA 500 MHz spectrometer equipped with a broadband inverse probe with z-field gradient. The data were processed by using the iNMR software package (<http://www.inmr.net>). One-dimensional NMR spectra were acquired as 16384 data points with a recycle delay of 1.0 s at 25, 45, 65, and 85 °C and the spectra were apodized with a shifted sine bell squared window function. Water suppression was achieved by including a double pulsed-field gradient spin-echo (DPFGSE) module^[55,56] in the pulse sequence prior to acquisition. NMR samples were prepared at the concentration of 1.6 mM single strand in 200 μL of H₂O/D₂O 9:1 containing 900 mM KCl and 100 mM KH₂PO₄.

AFM

A XE-100 Park Systems instrument was used for the AFM imaging of Q_n G-wires. Surface imaging was obtained in non-contact mode by using 125 μm long silicon/aluminium-coated cantilevers (PPP-NCHR 10 M; Park Systems; tip radius lower than 10 nm), with a resonance frequency of 200 to 400 kHz and nominal force constant of 42 N m⁻¹. The scan frequency was typically 0.5 Hz per line. When necessary, the AFM images were processed by flattening to remove the background slope, and the contrast and brightness were adjusted. Muscovite mica of about 1 cm² surface was used as the substrate in the AFM study. Muscovite mica surfaces are typically used as AFM substrates owing to their perfect cleavage along a <001> plane, yielding large atomically flat areas. Mica consists of layers of an aluminium phyllosilicate lattice ionically bonded through interstitial K⁺ ions. Upon cleavage, the K⁺ ions are highly mobile and are readily exchanged with divalent cation species at the solid–liquid interface. This exchange results in a positive overcharging of the mica surface, which enables the deposition of molecules that hold a net negative charge, such as DNA.^[57] Moreover, the positive charge distribution after cleavage enables a super-hydrophilic surface that guarantees a lower interaction between suspended biomolecules during the evaporation of aqueous solvent. Mica was freshly cleaved by using adhesive tape prior to each deposition to establish its cleanliness. Aliquots (2 μL) of the DNA/imaging buffer were directly deposited by casting onto freshly cleaved muscovite mica. After 2 min, every sample was gently washed with deionized water and then dried by evaporation at room temperature under a ventilated fume hood.

Acknowledgments

The authors are grateful to Dr Maria Marzano for her technical assistance in the processing of HPLC-SEC data.

Conflict of Interest

The authors declare no conflict of interest.

Keywords: DNA nanostructures • G-quadruplexes • G-wires • inversion of polarity sites • self-assembly

- [1] G. A. Ozin, K. Hou, B. V. Lotsch, L. Cademartiri, D. P. Puzzo, F. Scotognella, A. Ghadimi, J. Thomson, *Mater. Today* **2009**, *12*, 12–23.
- [2] E. Busseron, Y. Ruff, E. Moulin, N. Giuseppone, *Nanoscale* **2013**, *5*, 7098–7140.
- [3] J. K. Kim, S. Y. Yang, Y. Lee, Y. Kim, *Prog. Polym. Sci.* **2010**, *35*, 1325–1349.
- [4] P. W. K. Rothmund, *Nature* **2006**, *440*, 297–302.
- [5] A. E. Marras, L. Zhou, H.-J. Su, C. E. Castro, *Proc. Natl. Acad. Sci. USA* **2015**, *112*, 713–718.
- [6] V. Linko, H. Dietz, *Curr. Opin. Biotech.* **2013**, *24*, 555–561.
- [7] D. Yang, M. J. Campolongo, T. N. Nhi Tran, R. C. H. Ruiz, J. S. Kahn, D. Luo, *Wiley Interdiscip. Rev. Nanomed. Nanobiotechnol.* **2010**, *2*, 648–669.
- [8] A. T. Phan, V. Kuryavyy, K. N. Luu, D. J. Patel, in *Quadruplex Nucleic Acids* (Eds.: S. Neidle, S. Balasubramanian), Royal Society of Chemistry, Cambridge, **2006**, pp. 81–99.
- [9] T. Simonsson, *Biol. Chem.* **2001**, *382*, 621–628.
- [10] G. N. Parkinson, in *Quadruplex Nucleic Acids* (Eds.: S. Neidle, S. Balasubramanian), Royal Society of Chemistry, Cambridge, **2006**, pp. 1–30.
- [11] M. S. Searle, H. E. L. Williams, C. T. Gallagher, R. J. Grant, M. F. G. Stevens, *Org. Biomol. Chem.* **2004**, *2*, 810–812.
- [12] A. Guédin, A. De Cian, J. Gros, L. Lacroix, J.-L. Mergny, *Biochimie* **2008**, *90*, 686–696.
- [13] A. Risitano, K. R. Fox, *Nucleic Acids Res.* **2004**, *32*, 2598–2606.
- [14] P. A. Rachwal, I. S. Findlow, J. M. Werner, T. Brown, K. R. Fox, *Nucleic Acids Res.* **2007**, *35*, 4214–4222.
- [15] P. Hazel, J. Huppert, S. Balasubramanian, S. Neidle, *J. Am. Chem. Soc.* **2004**, *126*, 16405–16415.
- [16] N. Maizels, *Nat. Struct. Mol. Biol.* **2006**, *13*, 1055–1059.
- [17] H. J. Lipps, D. Rhodes, *Trends Cell Biol.* **2009**, *19*, 414–422.
- [18] G. Biffi, D. Tannahill, J. McCafferty, S. Balasubramanian, *Nat. Chem.* **2013**, *5*, 182–186.
- [19] N. Borbone, M. Bucci, G. Oliviero, E. Morelli, J. Amato, V. D'Atri, S. D'Errico, V. Vellecco, G. Cirino, G. Piccialli, C. Fattorusso, M. Varra, L. Mayol, M. Persico, M. Scuto, *J. Med. Chem.* **2012**, *55*, 10716–10728.
- [20] E. W. Choi, L. V. Nayak, P. J. Bates, *Nucleic Acids Res.* **2010**, *38*, 1623–1635.
- [21] V. D'Atri, G. Oliviero, J. Amato, N. Borbone, S. D'Errico, L. Mayol, V. Piccialli, S. Haider, B. Hoorelbeke, J. Balzarini, G. Piccialli, *Chem. Commun.* **2012**, *48*, 9516–9518.
- [22] E. M. Reyes-Reyes, Y. Teng, P. J. Bates, *Cancer Res.* **2010**, *70*, 8617–8629.
- [23] D. Musumeci, G. Piccialli, G. Oliviero, G. N. Roviello, E. M. Bucci, *Bioconjugate Chem.* **2012**, *23*, 382–391.
- [24] L. Lv, Z. Guo, J. Wang, E. Wang, *Curr. Pharm. Des.* **2012**, *18*, 2076–2095.
- [25] X. Lin, Q. Chen, W. Liu, H. Li, J. M. Lin, *Biosens. Bioelectron.* **2014**, *56*, 71–76.
- [26] G. I. Livshits, A. Stern, D. Rotem, N. Borovok, G. Eidelstein, A. Migliore, E. Penzo, S. J. Wind, R. Di Felice, S. S. Skourtis, J. C. Cuevas, L. Gurevich, A. B. Kotlyar, D. Porath, *Nat. Nanotechnol.* **2014**, *9*, 1040–1046.
- [27] S.-P. Liu, S. H. Weisbrod, Z. Tang, A. Marx, E. Scheer, A. Erbe, *Angew. Chem. Int. Ed.* **2010**, *49*, 3313–3316; *Angew. Chem.* **2010**, *122*, 3385–3388.
- [28] H. Cohen, T. Sapir, N. Borovok, T. Molotsky, R. Di Felice, A. B. Kotlyar, D. Porath, *Nano Lett.* **2007**, *7*, 981–986.
- [29] T. C. Marsh, J. Vesenska, E. Henderson, *Nucleic Acids Res.* **1995**, *23*, 696–700.
- [30] J. Vesenska, E. Henderson, T. Marsh, in *DNA-Based Molecular Construction, International Workshop on DNA-Based Molecular Construction* (Ed.: W. Fritzsche), Jena, **2002**, pp. 109–122.
- [31] T. C. Marsh, E. Henderson, *Biochemistry* **1994**, *33*, 10718–10724.
- [32] A. B. Kotlyar, N. Borovok, T. Molotsky, H. Cohen, E. Shapir, D. Porath, *Adv. Mater.* **2005**, *17*, 1901–1905.
- [33] T.-Y. Dai, S. P. Marotta, R. D. Sheardy, *Biochemistry* **1995**, *34*, 3655–3662.
- [34] M. A. Batalia, E. Protozanova, R. B. Macgregor, D. A. Erie, *Nano Lett.* **2002**, *2*, 269–274.
- [35] Y. Krishnan-Ghosh, D. Liu, S. Balasubramanian, *J. Am. Chem. Soc.* **2004**, *126*, 11009–11016.
- [36] T. Ilc, P. Šket, J. Plavec, M. Webba da Silva, I. Drevenšek-Olenik, L. Spindler, *J. Phys. Chem. C* **2013**, *117*, 23208–23215.
- [37] N. M. Hessari, L. Spindler, T. Troha, W.-C. Lam, I. Drevenšek-Olenik, M. Webba da Silva, *Chem. Eur. J.* **2014**, *20*, 3626–3630.
- [38] P. Tóthová, P. Krafčíková, V. Víglašký, *Biochemistry* **2014**, *53*, 7013–7027.
- [39] Y. Shi, H. Q. Luo, N. B. Li, *Chem. Commun.* **2013**, *49*, 6209–6211.
- [40] C. Saintomé, S. Amrane, J.-L. Mergny, P. Alberti, *Nucleic Acids Res.* **2016**, *44*, 2926–2935.
- [41] N. Smargiasso, F. Rosu, W. Hsia, P. Colson, E. S. Baker, M. T. Bowers, E. De Pauw, V. Gabelica, *J. Am. Chem. Soc.* **2008**, *130*, 10208–10216.
- [42] N. Borbone, J. Amato, G. Oliviero, V. D'Atri, V. Gabelica, E. De Pauw, G. Piccialli, L. Mayol, *Nucleic Acids Res.* **2011**, *39*, 7848–7857.
- [43] V. D'Atri, N. Borbone, J. Amato, V. Gabelica, S. D'Errico, G. Piccialli, L. Mayol, G. Oliviero, *Biochimie* **2014**, *99*, 119–128.
- [44] A. I. Karsiotis, N. M. Hessari, E. Novellino, G. P. Spada, A. Randazzo, M. Webba da Silva, *Angew. Chem. Int. Ed.* **2011**, *50*, 10645–10648; *Angew. Chem.* **2011**, *123*, 10833–10836.
- [45] M. Vorlíčková, I. Kejnovská, J. Sagi, D. Renčíuk, K. Bednárová, J. Motlová, J. Kypr, *Methods* **2012**, *57*, 64–75.
- [46] A. Marchand, V. Gabelica, *Nucleic Acids Res.* **2016**, *44*, 10999–11012.
- [47] V. Esposito, A. Virgilio, A. Pepe, G. Oliviero, L. Mayol, A. Galeone, *Bioorg. Med. Chem.* **2009**, *17*, 1997–2001.
- [48] V. Esposito, A. Virgilio, A. Randazzo, A. Galeone, L. Mayol, *Chem. Commun.* **2005**, 3953–3955.
- [49] V. T. Mukundan, A. T. Phan, *J. Am. Chem. Soc.* **2013**, *135*, 5017–5028.
- [50] R. Jin, B. L. Gaffney, C. Wang, R. A. Jones, K. J. Breslauer, *Proc. Natl. Acad. Sci. USA* **1992**, *89*, 8832–8836.
- [51] J. Feigon, K. M. Koshlap, F. W. Smith, *Methods Enzymol.* **1995**, *261*, 225–255.
- [52] M. Adrian, B. Heddi, A. T. Phan, *Methods* **2012**, *57*, 11–24.
- [53] D. Hu, J. Ren, X. Qu, *Chem. Sci.* **2011**, *2*, 1356–1361.
- [54] G. Oliviero, N. Borbone, J. Amato, S. D'Errico, A. Galeone, G. Piccialli, M. Varra, L. Mayol, *Biopolymers* **2009**, *91*, 466–477.
- [55] T. L. Hwang, A. J. Shaka, *J. Magn. Reson. Ser. A* **1995**, *112*, 275–279.
- [56] C. Dalvit, *J. Biomol. NMR* **1998**, *11*, 437–444.
- [57] A. J. Lee, M. Szymonik, J. K. Hobbs, C. Wälti, *Nano Res.* **2015**, *8*, 1811–1821.

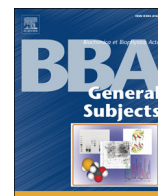
Received: February 6, 2017

Version of record online June 13, 2017



Contents lists available at ScienceDirect

Biochimica et Biophysica Acta

journal homepage: www.elsevier.com/locate/bbagen

Synthesis and label free characterization of a bimolecular PNA homo quadruplex☆

Brunella Pinto ^a, Giulia Rusciano ^b, Stefano D'Errico ^a, Nicola Borbone ^a, Antonio Sasso ^b, Vincenzo Piccialli ^c, Luciano Mayol ^a, Giorgia Oliviero ^{d,*}, Gennaro Piccialli ^{a,e,**}

^a Dipartimento di Farmacia, Università degli Studi di Napoli Federico II, 80131 Napoli, Italy

^b Dipartimento di Scienze Fisiche, Università degli Studi di Napoli Federico II, 80126 Napoli, Italy

^c Dipartimento di Scienze Chimiche, Università degli Studi di Napoli Federico II, 80126 Napoli, Italy

^d Dipartimento di Medicina Molecolare e Biotecnologie Mediche, Università degli Studi di Napoli Federico II, 80131 Napoli, Italy

^e CNR, Institute of Protein Biochemistry, 80131 Napoli, Italy

ARTICLE INFO

Article history:

Received 19 October 2016

Received in revised form 25 November 2016

Accepted 26 November 2016

Available online xxxx

Keywords:

PNA

G-quadruplex

Surface enhanced Raman scattering

SERS

Label free monitoring

ABSTRACT

Background: G-quadruplex DNA is involved in many physiological and pathological processes. Both clinical and experimental studies on DNA G-quadruplexes are slowed down by their enzymatic instability. In this frame, more stable chemically modified analogs are needed.

Methods: The bis-end-linked-(gggt)₂ PNA molecule (BEL-PNA) was synthesized using in solution and solid phase synthetic approaches. Quadruplex formation was assessed by circular dichroism (CD) and surface enhanced Raman scattering (SERS).

Results: An unprecedented bimolecular PNA homo quadruplex is here reported. To achieve this goal, we developed a bifunctional linker that once functionalized with gggt PNA strands and annealed in K⁺ buffer allowed the obtainment of a PNA homo quadruplex. The identification of the strong SERS band at ~1481 cm⁻¹, attributable to vibrations involving the quadruplex diagnostic Hoogsteen type hydrogen bonds, confirmed the formation of the PNA homo quadruplex.

Conclusions: By tethering two G-rich PNA strands to the two ends of a suitable bifunctional linker it is possible to obtain bimolecular PNA homo quadruplexes after annealing in K⁺-containing buffers. The formation of such CD-unfriendly complexes can be monitored, even at low concentrations, by using the SERS technique.

General significance: Given the importance of DNA G-quadruplexes in medicine and nanotechnology, the obtainment of G-quadruplex analogs provided with enhanced enzymatic stability, and their monitoring by highly sensitive label-free techniques are of the highest importance. This article is part of a Special Issue entitled "G-quadruplex" – guest edited by Dr. Concetta Giancola and Dr. Daniela Montesarchio.

© 2016 Elsevier B.V. All rights reserved.

1. Introduction

G-rich oligonucleotide (ON) sequences have a natural propensity to fold into unusual secondary structures, named G-Quadruplexes (G-Qs), whose fundamental units are planar arrangements of four guanine bases held together by Hoogsteen hydrogen bonds (G-quartets) and stabilized by monovalent cations. Despite the G-Q core is always the same – two or more stacked G-tetrads – G-Qs are characterized by extremely high variability in regards to the folding topology, loop

orientation, molecularity and glycosidic bonds orientation [1–5]. Owing to the evidence of G-Qs formation within the vertebrate genomes [6–7], G-Qs have attracted great interest since their discovery. It is well known that G-Qs are involved in a number of key biological processes, including gene regulation [8–14] and protein activity modulation [15–16]. Furthermore, the propensity of suitable G-rich ONs to self-assemble into highly ordered supramolecular G-Qs indicates the former as useful structural elements for the construction of nanoscale assemblies to be used in nanotechnology and biosensing [17–20]. However, the use of natural G-rich ONs as G-Q building blocks is hampered by their enzymatic instability towards the ubiquitous exonucleases and endonucleases. Hence, much efforts have been devoted to the development of quadruplex-forming ON analogs provided with improved chemical and enzymatic resistance [21–25].

Among the most interesting DNA analogs are peptide nucleic acids (PNAs), first reported by P. E. Nielsen in 1991 [26]. PNAs are DNA

☆ This article is part of a Special Issue entitled "G-quadruplex" Guest Editor: Dr. Concetta Giancola and Dr. Daniela Montesarchio.

* Corresponding author.

** Corresponding author at: Dipartimento di Farmacia, Università degli Studi di Napoli Federico II, 80131 Napoli, Italy.

E-mail addresses: giorgia.oliviero@unina.it (G. Oliviero), gennaro.piccialli@unina.it (G. Piccialli).

mimics in which the sugar-phosphate backbone is replaced by a 2-aminoethyl-glycine chain. PNAs are resistant to enzymatic hydrolysis and recognize – by formation of standard Watson-Crick hydrogen bonds – with high affinity and specificity complementary fragments of DNA or RNA to give the resulting PNA/DNA or PNA/RNA hetero duplexes [27–35], triplexes [36–40] and quadruplexes [41–44], respectively. Notwithstanding the stronger binding affinity of PNA strands with complementary ONs and the remarkable stability of PNA/DNA hetero triplex and quadruplex structures, only few papers have reported about the formation of stable PNA homo G-Qs [45–46]. Indeed, to the best of our knowledge, only tetramolecular PNA homo G-Qs have been reported so far; despite their unfavorable kinetic and thermodynamic parameters [46]. In trying to fill this gap, we have undertaken a series of studies aimed at the obtainment of stable PNA homo G-Qs, exploiting the standard PNA solid phase synthetic strategy and our experience in the preparation of bis- and tetra-end linkers (BEL and TEL, respectively) [47].

Herein, we report the results of our study aimed at the design and structural characterization by Circular Dichroism (CD) and Surface Enhanced Raman Scattering (SERS) of an unprecedented bimolecular PNA homo G-Quadruplex obtained by annealing the BEL- g_3t (g = guanine PNA monomer; t = thymine PNA monomer) building block **19** (Scheme 2) synthesized using the suitable protected tri-functionalized linker **8** (Scheme 1).

CD spectroscopy is the technique most widely used to investigate G-quadruplex topologies. The main attraction of CD spectroscopy is its ability to discriminate between parallel and anti-parallel strands orientation, although some exceptions to the general rules have been reported [48–49].

As it is well known, Raman Scattering (RS) is a quite useful analytical tool for the structural analysis of biomolecules [50]. It has recently emerged as a formidable alternative to fluorescence technique, usually considered the spectroscopic gold-standard in biology, thanks to its intrinsic label-free character and to the low Raman cross section of water, which makes RS ideally suited for the analysis of samples in aqueous solution. The Raman spectrum of a molecule consists of numerous discrete bands associated with its specific normal modes of vibration and, as such, can be used as a sensitive and selective fingerprint of three-dimensional structure and intermolecular interactions. Thus, RS has been widely used for the analysis of DNA, starting from single nucleobases to the complex architecture of DNA occurring in telomeres [51]. In particular, RS has been widely used to reveal DNA folding in quadruplexes. Indeed, specific Raman markers have been identified to probe the hydrogen bonding at guanine N7 sites, therefore being diagnostic of quadruplexes formation [52]. Moreover, Raman spectra allow to probe the conformation of both the phosphodiester backbone and

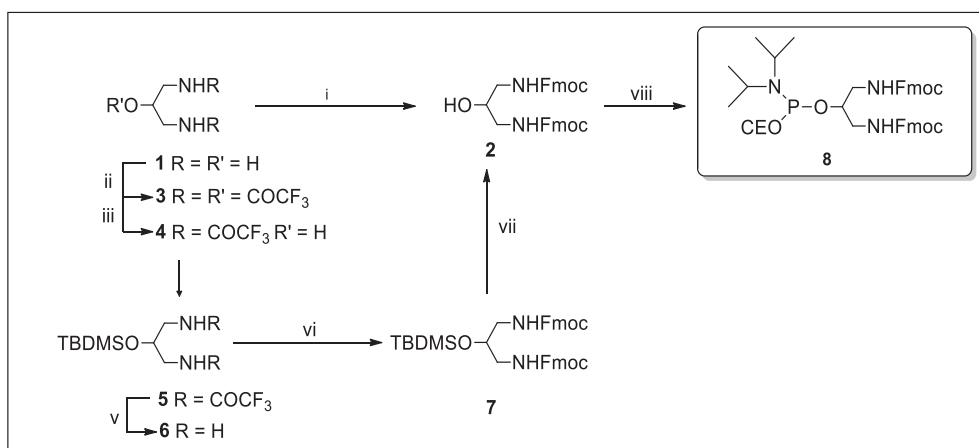
the glycosidic bonds of quadruplexes, being therefore sensitive to their parallel or antiparallel arrangement. The other side of the coin of RS is its very low efficiency, associated with the small cross-section of the inelastic scattering process, typically up to 12 orders of magnitude smaller than fluorescence. This makes Raman detection of low-concentrated samples prohibitive. SERS has recently emerged as a technique suitable for overcoming this limitation. As a matter of facts, the huge enhancement (up to 12 orders of magnitude) of the Raman signal associated with this technique has constituted a huge step forward to the concrete use of Raman spectroscopy for the analysis of precious, low-concentrated samples such as DNA. The signal enhancement observed in SERS spectra occurs when the analyte is reasonably close (within a few nanometres) to a proper metallic nanostructure, and derives from the coupling of the Raman probe with the Localized Plasmon Resonance (LPR) of the metal surface. Recently, we have demonstrated that SERS is a suitable tool for revealing the arrangement of guanine-rich DNA strands in quadruplexes, also providing information on the relative stability of G-quadruplex structures with different numbers of G-tetrads [53].

In the light of these observations, in this paper we have for the first time explored the application of SERS to monitor the formation of PNA-based quadruplexes. In particular, our spectra clearly revealed the presence of a band (around 1484 cm^{-1}) associated with hydrogen bonding at guanine N7 sites, which, being diagnostic for the Hoogsteen hydrogen bonding in G-tetrads, confirmed the formation of the target bimolecular PNA homo quadruplex.

2. Materials and methods

2.1. General methods

All reagents and solvents were obtained from commercial sources and used without further purification. MBHA resin (1% divinylbenzene, 200–400 mesh, 0.5 mmol/g loading) was purchased from Sigma-Aldrich. The reactions on solid phase were performed using ISOLUTE® single fritted reservoirs (SG), 20 μm PE, equipped with tube caps and luer tip caps (Biotage) which were shaken in a Multi-reax vibrating shaker (Heidolph). High performance liquid chromatography (HPLC) analyses and purifications were carried out on a Jasco UP-2075 Plus pump equipped with a Jasco UV-2075 Plus UV detector using a $4.8 \times 150\text{ mm}$ C-18 reverse-phase column (particle size $5\text{ }\mu\text{m}$) eluted with a linear gradient of CH_3CN containing 0.1% (v/v) TFA in H_2O containing 0.1% (v/v) TFA (from 0 to 100% in 45 min, flow 1.2 mL/min). UV spectra were recorded on a Jasco V-530 spectrophotometer. CD spectra were performed on a Jasco 1500 spectropolarimeter in a 0.1 cm path length cuvette. ^1H NMR experiments were performed using Varian Mercury



Scheme 1. i) Fmoc-*N*-hydroxy succinimide ester, Py, r.t., 16 h, or Fmoc-Cl, $\text{NaHCO}_3(\text{aq})$, CH_2Cl_2 , r.t., 16 h; ii) 1) CF_3COOEt , DCM, r.t., 1 h, iii) MeOH, r.t., 30 min; iv) TBDMSCl, imidazole, DMF, r.t., 16 h; v) sat. NH_3 in MeOH, r.t., 16 h; vi) Fmoc-Cl, Py, r.t., 16 h; vii) $3\text{HF}^+\text{TEA}$, THF, r.t. 16 h; viii) 2-cyanoethyl-*N,N*-diisopropylchlorophosphoramidite, DIPEA, CH_2Cl_2 , THF, r.t., 1 h.

Plus 400 MHz and Varian ^{UNITY}INOVA 500 MHz spectrometers in CD₃OD, D₂O, and acetone-*d*₆ solvents. Chemical shifts are reported in parts per million (δ) relative to residual solvents signals – CD₂HOD 3.31, (CD₃)(CD₂H)CO 2.09 – and assigned by H–H COSY experiments. ³¹P NMR experiments were performed on a Varian ^{UNITY}INOVA 500 MHz spectrometer using 85% H₃PO₄ as an external standard (0 ppm). Data were processed using the Varian VNMR software package. The abbreviations s, d, dd, m, bs, bd, bt represent singlet, doublet, doublet of doublets, multiplet, broad singlet, broad doublet and broad triplet, respectively. ESI-MS experiments were performed on an AB Sciex 4000 QTRAP mass spectrometer in positive ion electrospray mode. Column chromatography was performed on silica gel 60 (70–230 mesh ASTM, Merck) and analytical TLC analyses were performed on F₂₅₄ silica gel plates (0.2 mm thick, Merck) with TLC spots being detected under UV light (λ = 254 nm).

2.2. Synthesis of Fmoc protected BEL-linker **8**

2.2.1. *N,N'*-(2-hydroxypropane-1,3-diyl)bis(2,2,2-trifluoroacetamide) (**4**)

To an ice-cooled solution of 1,3-diamino-2-propanol **1** (0.10 g, 1.1 mmol) in CH₂Cl₂ (1 mL), CF₃COOEt (0.6 mL, 5.0 mmol) was added dropwise. The mixture was stirred at 0 °C for 60 min (TLC monitoring: CH₂Cl₂/CH₃OH = 95:5) and then quenched with CH₃OH at r.t. for 30 min. Volatiles were removed by rotary evaporation, thus obtaining **4** (0.302 g, 97% yield) as an amorphous solid that was used for the next reaction step without purification. ¹H NMR (400 MHz, CD₃OD) δ 3.92–3.84 (m, 1H, CH), 3.37 (dd, *J* = 4.7, 13.7 Hz, 2H, 2 \times H_A), 3.28 (dd, *J* = 7.2, 13.7 Hz, 2H, 2 \times H_B). ESI-MS (*m/z*) calcd. for C₇H₈F₆N₂NaO₃ [M + Na]⁺ 305; found 305.

2.2.2. *N,N'*-(2-((*tert*-butyldimethylsilyl)oxy)propane-1,3-diyl)bis(2,2,2-trifluoroacetamide) (**5**)

tert-butyldimethylsilyl chloride (0.96 g, 0.6 mmol) and imidazole (0.06 g, 1.0 mmol) were dissolved in dry DMF and the solution cooled at 0 °C in an ice-bath. Compound **4** (0.150 g, 0.53 mmol), dissolved in dry DMF (2 mL), was added dropwise and the mixture was stirred for 24 h (TLC monitoring: CH₂Cl₂/CH₃OH = 95:5). The reaction was quenched by adding CH₃OH and the mixture was diluted with AcOEt (30 mL) and washed with Brine (3 \times 30 mL). The organic phase was dried over Na₂SO₄ and evaporated. The crude was purified over a silica gel column eluted with increasing amounts of CH₃OH in CH₂Cl₂ (up to 3%) giving pure **5** (0.13 g, 62% yield) as a white foam. ¹H NMR (400 MHz, CD₃OD) δ 4.06–3.98 (m, 1H, CH), 3.38–3.26 (m, 4H, 2 \times CH₂), 0.89 (s, 9H, ^tBu), 0.089 (s, 6H, 2 \times CH₃). ESI-MS (*m/z*) calcd. for C₁₃H₂₂F₆N₂NaO₃Si [M + Na]⁺ 419; found 419.

2.2.3. 2-((*tert*-butyldimethylsilyl)oxy)propane-1,3-diamine (**6**)

Compound **5** (0.13 g, 0.33 mmol) was dissolved in sat. NH₃ in CH₃OH (1 mL) and kept at r.t. for 16 h (TLC monitoring: CH₂Cl₂/CH₃OH/NH_{3(aq)} = 7:3:0.2). The solvents were removed under reduced pressure and the crude was purified over a silica gel column eluted with increasing amounts of CH₃OH in CH₂Cl₂ (up to 30%), giving pure **6** (0.07 g, 99% yield) as an oil. ¹H NMR (400 MHz, CD₃OD) δ 4.22–4.15 (m, 1H, CH), 3.12–3.02 (m, 4H, 2 \times CH₂), 0.94 (s, 9H, ^tBu), 0.18 (s, 6H, 2 \times CH₃). ESI-MS (*m/z*) calcd. for C₉H₂₅N₂O₃Si [M + Na]⁺ 205; found 205.

2.2.4. bis((9H-fluoren-9-yl)methyl) (2-((*tert*-butyldimethylsilyl)oxy)propane-1,3-diyl)dicarbamate (**7**)

To a solution of **6** (0.05 g, 0.25 mmol) in dry pyridine (5 mL), Fmoc-Cl (0.14 g, 0.54 mmol) was added and the mixture was shaken at r.t. for 16 h (TLC monitoring: CHCl₃/CH₃OH = 95:5). The reaction was quenched by addition of CH₃OH, solvents were removed under reduced pressure and the crude purified over a silica gel column eluted with increasing amounts of CH₃OH in CHCl₃ (up to 2%), affording pure **7** (0.11 g, 90% yield) as an amorphous white solid. ¹H NMR (400 MHz, CD₃OD) δ 7.76–7.19 (complex signal, 16H, arom. Fmoc), 4.30 (d, *J* =

6.6 Hz, 4H, 2 \times CH₂ Fmoc), 4.13 (t, *J* = 6.5 Hz, 2H, 2 \times CH Fmoc), 3.05 (d, *J* = 5.5 Hz, 4H, 2 \times CH₂), 0.82 (s, 9H, ^tBu), 0.00 (s, 6H, 2 \times CH₃). ESI-MS (*m/z*) calcd. for C₃₉H₄₄N₂NaO₅Si [M + Na]⁺ 671; found 671.

2.2.5. bis((9H-fluoren-9-yl)methyl) (2-hydroxypropane-1,3-diyl) dicarbamate (**2**)

Compound **7** (0.08 g, 0.12 mmol) was dissolved in THF (8 mL) and treated with TEA⁺3HF[−] (196 μ L, 1.2 mmol) at r.t. for 16 h (TLC monitoring: CHCl₃/CH₃OH, 95:5). Volatiles were removed under reduced pressure and the crude purified over a silica gel column eluted with increasing amounts of CH₃OH in CHCl₃ (up to 5%), giving pure **2** (0.06 g, 90% yield) as an amorphous white solid. ¹H NMR (400 MHz, CD₃OD) δ 7.90–7.20 (complex signal, 16H, arom. Fmoc), 4.35 (bd, 4H, 2 \times CH₂ Fmoc), 4.23 (bt, 2H, 2 \times CH Fmoc), 3.73–3.61 (m, 1H, CH), 3.05–3.23 (complex signal, 4H, 2 \times CH₂). ESI-MS (*m/z*) calcd. for C₃₃H₃₁N₂O₅ [M + H]⁺ 535; found 535.

2.2.6. bis((9H-fluoren-9-yl)methyl)(2-(((2-cyanoethoxy)(diisopropylamino)phosphino)oxy)propane-1,3-diyl)dicarbamate (**8**)

2 (0.06 g, 0.11 mmol) was dissolved in a 1:1 (v/v) mixture of dry CH₂Cl₂/THF (3 mL), DIPEA was added (60 μ L, 0.33 mmol) followed by addition of 2-cyanoethyl-*N,N*-diisopropylchlorophosphoramidite (40 μ L, 0.18 mmol). The mixture was stirred for 1 h at r.t. (TLC monitoring: *n*-hexane/AcOEt/DIPEA = 6:4:0.1) then diluted with AcOEt (30 mL) and washed with brine (4 \times 30 mL). The organic phase was dried over Na₂SO₄ and evaporated under reduced pressure. The crude was purified over a silica gel column eluted with increasing amounts of AcOEt in *n*-hexane (up to 40%), giving pure **8** (0.048 g, 59% yield) as a white foam. ¹H NMR (500 MHz, acetone-*d*₆) δ 7.86–7.25 (complex signal, 16H, arom. Fmoc), 4.36 (d, *J* = 8.6 Hz, 2H, CH₂ Fmoc), 4.33 (d, *J* = 8.6 Hz, 2H, CH₂ Fmoc), 4.26–4.17 (m, 2H, 2 \times CH Fmoc), 4.01–3.93 (m, 1H, CHO), 3.90–3.70 (complex signal, 2H, CH₂O), 3.67–3.59 (m, 1H, CHN), 3.36–3.28 (m, 4H, 2 \times CH₂N), 2.71–2.65 (m, 2H, CH₂CN), 1.18–1.13 (two overlapped doublets, *J* = 6.5 and 6.6 Hz, 12H, 4 \times CH₃). ³¹P NMR (202 MHz, acetone-*d*₆) δ 149.5 (s). ESI-MS (*m/z*) calcd. for C₄₂H₄₇N₄NaO₆P [M + Na]⁺ 757; found 757.

2.2.7. Synthesis of BEL-PNA **19**

BEL-PNA **19** was synthesized using the Fmoc-solid-phase strategy. In particular, 50 mg of MBHA resin **9** (0.5 mmol/g), after swelling in CH₂Cl₂ for 30 min and DMF washings, was treated with a solution of 20% piperidine in DMF for 10 min, giving solid support **10**. After washings with DMF, the resin **10** was swelled in a 1:1 solution of CH₂Cl₂/THF (1 mL) and reacted with compound **8** (74 mg, 0.1 mmol) in the presence of 1-*H*-tetrazole (13 mg, 0.19 mmol) for 2 h at r.t., affording, after washings with a 1:1 solution of CH₂Cl₂/THF, the solid support **13**. The last was swelled in THF (1 mL) and treated with ^tBuOOH (5.5 M in decane, 50 μ L, 0.25 mmol) for 30 min at r.t. giving, after washings with THF and then CH₂Cl₂, the solid support **14**. The resin **14** was swelled in CH₂Cl₂ for 30 min, washed with DMF and treated with a solution of 20% piperidine in DMF for 10 min, thus obtaining solid support **15**. The eluate was collected and the coupling yield was estimated by Fmoc spectrophotometric measurements (98%). PNA chains were assembled by reacting PNA monomers (**11** or **12**, 5 equiv.) in the presence of HATU (5 equiv), DIPEA (5 equiv) and lutidine (6 equiv.), for 30 min at r.t. After each coupling step, capping with Ac₂O in the presence of pyridine was performed by shaking the corresponding support with the reagents mixture for 20 min at r.t. At the end of synthetic cycles, cyanoethyl groups were removed suspending the resin **17** in conc. NH₄OH_(aq) for 2 h at r.t., affording solid support **18**. Next, the synthesized BEL-PNA was cleaved off suspending the resin **18** in a TFA/*m*-cresol (4:1, v/v) solution for 4 h at r.t. and precipitated with cold diethyl ether. The precipitates were recovered by centrifugation, washed twice with diethyl ether, dissolved in water and finally lyophilized. BEL-PNA **19** was obtained with a 48–50% overall yield (94% average yield for each coupling). The crude sample was purified by

semipreparative RP-HPLC (see General Methods). The collected fractions were lyophilized and the final pure product was characterized by ESI-MS (positive mode): ESI-MS (m/z) calcd. for $C_{91}H_{123}N_{53}O_{29}P$ $[M + H]^+$ 2453; found 2453.

2.3. Obtainment of G-quadruplexes (annealing)

The target dimeric PNA G-Q was obtained by dissolving the BEL-PNA **19** at the concentration of 2.0×10^{-5} M in 100 mM K^+ buffer (KH_2PO_4 10 mM, KCl 90 mM, pH 7.0) and by heating the solution at 90 °C for 10 min and then slow cooling to room temperature over 3 h. The solution was equilibrated at 4 °C for 72 h before characterizations [46].

2.4. UV and CD studies

The concentration of **19**, dissolved in pure water, was determined by UV measurements at 260 nm at 90 °C using the nearest-neighbor calculated molar extinction coefficient of the gggt PNA strand multiplied by 2 (the number of PNA strands linked to BEL) (calculated $\epsilon = 43.9$ mL cm^{-1} μmol^{-1}). The CD spectra were recorded both in pure water and in the 100 mM K^+ buffer described above at final single strand concentration of 20 μM . The spectra were recorded at 5 °C ($\lambda = 220$ –310 nm, 200 nm/min scanning speed, 2.0 nm bandwidth) and averaged over 50 repetitions. A buffer baseline was subtracted from the CD spectra and the spectra were normalized to have zero at 320 nm. Thermal denaturation experiments on **19** were also carried out in the temperature range of 5–90 °C by monitoring CD values at 282 nm at a heating rate of 1.0 °C/min.

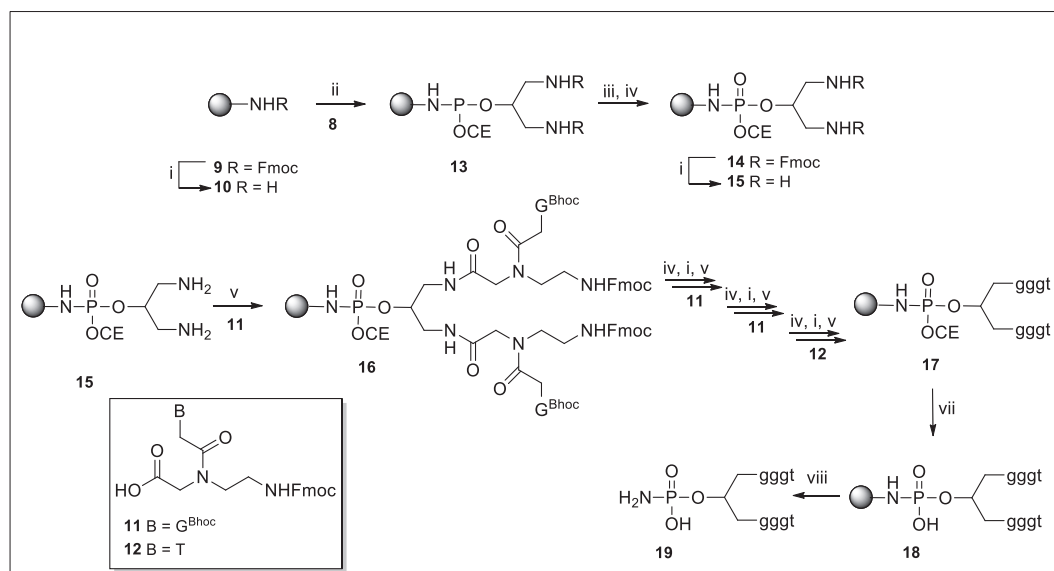
2.5. SERS studies

Ag colloids, used as the SERS substrate, were prepared according to the protocol reported in [54]. Briefly, $AgNO_3$ (90 mg) was dissolved in 500 mL of H_2O and brought to the boil. Next, a sodium citrate solution (1% w/w) was added under vigorous stirring and then the resulting mixture was kept boiling for 1 h. All chemicals were purchased from Sigma-Aldrich. Before use, the silver solution was appropriately diluted with distilled water. SERS spectra were recorded using the WiTec Alpha 300 system [55], a confocal Raman system endowed with a Raman probe at 532 nm focused on the sample through a Nikon 60 \times dry objective (NA = 0.8 and WD = 300 μm). The back-scattered light from the

sample, after proper filtering to remove the pump radiation, was sent to a high throughput spectrometer equipped with two diffraction gratings with 600 and 1800 $g\ mm^{-1}$, providing a resolution, respectively, of 3.6 and 1.5 cm^{-1} . Photons were detected by a back-illuminated Andor CCD camera (DV401A-BV-352, 1024 \times 400 pixels) operating at -60 °C. The confocal conditions were imposed by the 25 μm core (acting as a pin-hole) of the multimode fibre delivering the signal to the spectrometer. SERS analysis was performed on samples at a concentration of 20 μM . For the measurements, a proper diluted aliquot of the silver-colloid solution was added to the sample and the analyte was allowed to bind for 2 h at room temperature prior to spectrum acquisition. To avoid any photochemical-induced effect, the Raman probe power impinging on the sample was limited to 50 μW while the integration time was 5 s. Under this condition, SERS spectra were comparatively stable and the signal-to-noise ratio was higher than 100 on the single acquisition.

3. Results and discussion

The elongation of PNA chains was accomplished by solid-phase synthesis, growing the strands along the two primary amino functions of the resin-bonded bis-end linker **15** (Scheme 2). The last was obtained by connecting the Fmoc-protected BEL **8** to the MBHA resin **10** through a phosphoramidite bond (**13**), which was then oxidized to phosphoramidate **14** before the removal of the Fmoc protecting groups, as shown in Scheme 2. In particular, for the preparation of compound **8** the key reaction step was the selective Fmoc protection of the primary amino functions of **1**. Literature studies [56] reported that a selective Fmoc NH_2 protection in the presence of OH groups could be performed by using Fmoc- N -hydroxy succinimide ester or Fmoc-Cl reagents. Unfortunately, in our case these procedures failed, allowing the recovery of the target bis-Fmoc derivative **2** only in low yield, together with other variously protected by-products. The inability of modulating the nucleophilicity of the functional groups in the compound **1** towards Fmoc reagents forced us to explore an alternative synthetic route for the preparation of compound **2**, exploiting the protection of the OH group during the synthetic steps. Starting with the full protection of the three functional groups in **1** with an excess of CF_3COOEt , we obtained the tri-protected derivative **3** in 97% yield. At this stage, we explored the selective deprotection of the OH group. Pleasingly, the treatment of the compound **3** with methanol afforded the derivative **4** by selective



Scheme 2. Reagents: (i) piperidine/DMF, r.t., 10 min; (ii) **8**, 1-*H*-tetrazole, DCM, THF, r.t., 2 h; (iii) $tBuOOH$, THF, r.t., 30 min; (iv) Ac_2O/Py , r.t., 20 min; (v) **11**, HATU, DIPEA, lutidine, DMF, r.t., 30 min; (vi) **12**, HATU, DIPEA, lutidine, DMF, r.t., 30 min; (vii) conc. aq NH_4OH , MeOH, r.t., 2 h; (viii) *m*-cresol, TFA, r.t., 4 h.

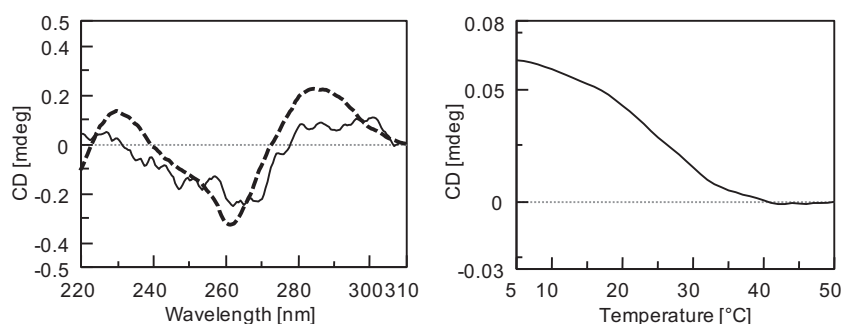


Fig. 1. (left) CD spectra of BEL-PNA **19** (2.0×10^{-5} M) dissolved in pure water (solid line) or annealed in 0.1 M K^+ buffer (dotted line), pH 7; (right) CD melting at 283 nm of **19** dissolved in K^+ buffer.

methanolysis of the trifluoroacetic ester. The alcohol **4** was then silylated, affording the derivative **5** in 62% yield. The quantitative deprotection of both amino groups in **5** was accomplished with saturated NH_3 in MeOH, to give compound **6** that was successfully transformed in its bis-Fmoc derivative **7** in 90% yield by reaction with Fmoc-Cl. Next, compound **7** was desilylated by treatment with the $3HF^*TEA$ complex and the free OH group of compound **2** reacted with $(^iPr)_2NP(OCE)Cl$ to afford the phosphoramidite derivative **8**. Thereafter, solid support **10**, after reaction with **8** in the presence of 1-*H*-tetrazole and oxidation with $tBuOOH$, gave the phosphoramidate containing support **14**. Cleavage of both Fmoc protecting groups on the functionalized resin **14** in basic solution allowed the construction of PNA strands using the standard protocols. At the end of the synthetic cycles, treatment of solid support **17** with concentrated $NH_4OH_{(aq)}$ gave the support **18** from which the BEL-PNA **19** was detached. Purification and analysis of crude product were carried out using HPLC as outlined in General Methods. The obtainment of pure compound **19** was assessed by ESI-MS analyses. Purified sample was dissolved in K^+ buffer and subjected to the annealing procedure. The propensity of **19** to fold into the target bimolecular PNA quadruplex was then supported by CD and SERS experiments.

Typically, parallel and antiparallel G-Qs show CD profiles characterized by positive and negative Cotton effects at distinct wavelengths. Parallel-stranded DNA G-Qs show a negative Cotton effect at 240 nm and a positive one at 260 nm, whereas negative and positive Cotton effects for antiparallel G-Qs are typically at around 260 and 290 nm, respectively [57]. It is to be noted that the backbone of PNAs is inherently achiral, so PNA G-Qs show a weak CD spectrum in comparison to their DNA analogs [46]. As shown in Fig. 1, BEL-PNA **19** when dissolved and annealed in pure water (solid line) does not exhibit a significant CD profile, whereas the same dissolved and annealed in 0.1 M K^+ buffer (dotted

line) shows a negative band at 260 nm and a positive one at 283 nm, suggesting the formation of an antiparallel bimolecular PNA G-Q whose apparent melting temperature was estimated to be around 25 °C by CD thermal denaturation (Fig. 1, right panel). The antiparallel orientation of PNA strands could be the result of steric hindrance and charge repulsion between the phosphate-linker moieties. To support the above structural hypothesis, we decided to ascertain the formation of the target BEL-PNA G-Q by using the SERS technique.

SERS analysis of BEL-PNA **19** annealed in K^+ buffer was performed by acquiring the signals in 100 randomly selected points under the experimental conditions described above. Importantly, a significant number of the acquired spectra (more than 80%) exhibit a quite reproducible spectral pattern, being the relative height of peaks within 15% of their mean value. These spectra are dominated by features due to guanine residues, with only some contributions from the PNA backbone. The remaining spectra (~20%) exhibit numerous bands associated with CH vibration bands in the region $1350\text{--}1650\text{ cm}^{-1}$, whose partial overlapping gives rise to a broad background. As it is well known, enhanced bands in SERS spectra are generally due to vibrational modes occurring in molecular moieties in close contact with the silver colloids. Therefore, the substantial reproducibility of spectra can be read in terms of a tendency of molecules to assume a well-defined orientation on the SERS substrate. A similar propensity to be ordered, mainly ruled by the electrostatic interaction of charged groups with the colloid surface, was previously observed by our group for DNA-based quadruplexes on Ag-colloids [53] and by Briones et al. for PNA strands on gold colloids [58]. The reproducibility of SERS signals, together with the favourable exposure of guanines in PNA strands to the SERS substrate, revealed in most of SERS spectra, allowed us to get precious information on their structural arrangement.

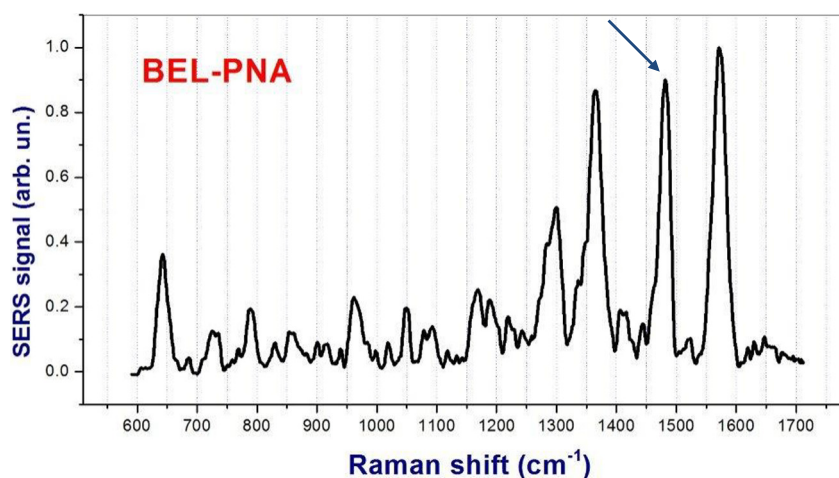


Fig. 2. Average SERS signal from BEL-PNA **19** annealed in 0.1 M K^+ buffer. This spectrum exhibits the typical band around 1484 cm^{-1} (highlighted by the blue arrow) diagnostic of G-quadruplex formation.

Table 1
Assignment of the prominent SERS features observed in this work.

Observed position (cm ⁻¹)	Assignment	References
785	Guanine ring	58
966	$\nu(\text{C}=\text{C})$	63
1160	$\nu(\text{C}=\text{N}) + \delta(\text{C}-\text{H}), \text{T}$	62
1220	PO_2^-	61
1300	Amide III	63
1484	$\text{C8} = \text{N7-H2}$	52, 59, 53
1542	Amide II	63
1572	$\text{C2} = \text{N3}$ of guanine	60
1630	Amide III	63
1650	Amide III, $\nu(\text{CO}_2)$, $\nu(\text{C6O6})$	63

The average SERS signal of BEL-PNA annealed in K^+ buffer, obtained from a subset of spectra described above, is shown in Fig. 2. To better highlight the SERS features a forth order baseline was removed and the spectrum was normalized to the height of the prominent peak at 1572 cm⁻¹. Table 1 summarizes the main SERS bands observed and their assignment. SERS spectra of unstructured PNA molecules (single strands) were firstly reported by Colaiaanni et al. [59]; in this case, the spectra were mainly characterized by single nucleobase contributions as well as Amide I band due to the PNA backbone. Differently, the SERS signals of BEL-PNA **19** annealed in K^+ buffer are dominated in the 1300–1600 cm⁻¹ region by spectral features clearly due to guanine residues, also exhibiting some clear similarities with the spectral features observed in both spontaneous Raman scattering of telomeric DNA quadruplexes [60] and in SERS spectra of guanine-rich DNA sequences [53]. Notably, the SERS spectrum shows a strong band at ~1484 cm⁻¹ easily attributable to the $\text{C8} = \text{N7-H2}$ deformation of the guanine tetrad, being therefore diagnostic for the Hoogsteen hydrogen bonding of G. G pairs in G-tetrads [52–53,59]. To the best of our knowledge, this outcome constitutes the first SERS-based evidence of PNA-quadruplex formation and confirms the indications provided by CD-measurements, which suggested the formation of G-Q assemblies due to the antiparallel arrangements of BEL-PNA **19** when annealed in K^+ containing buffer.

The other intense SERS peak at 1572 cm⁻¹ can be identified with the $\text{C2} = \text{N3}$ guanine band appearing in the spontaneous Raman spectrum of quadruplexes around 1580 cm⁻¹. The ~8 cm⁻¹ shift of this band for the SERS case has been previously observed by Pagba et al. [61] in the analysis of quadruplex-folded DNA and is likely due to the specific surface-induced selection rules of SERS. The band around 1220 cm⁻¹ can be assigned to PO_2^- bonds [62], which are present in the BEL linkers.

Numerous other bands of the spectrum in Fig. 2 are clearly due to the peptide components of the molecule and to single unpaired components. For instance, the peak at 1165 cm⁻¹ is likely due to a combination of $\nu(\text{C}=\text{N})$ and $\delta(\text{C}-\text{H})$ vibrations with some contributions of unpaired thymine residues [63], while the band at 791 cm⁻¹ is certainly a ring mode from the moieties [59]. Moreover, many protein-related Raman bands can be observed in the Amide III (1200–1310 cm⁻¹), Amide II (1540–1560 cm⁻¹) and Amide I (1610–1700 cm⁻¹) regions, the latter band mainly involving the $\text{C}=\text{O}$ vibration [64]. In particular, the Amide I band probably masks the presence of guanosine N1H bands which, being sensitive for the N1H environment, is usually a valuable indicator of the guanine interbase interaction strength [52,60].

4. Conclusions

In summary, we have reported the unprecedented obtainment of a PNA bimolecular homo quadruplex. This goal was accomplished by growing two gggt PNA strands to the ends of the solid support-bonded bis-end linker **15** to obtain, after detachment from the solid support, the corresponding BEL-(gggt)₂ (**19**). The annealing of **19** in K^+ containing buffer gave the target bimolecular PNA quadruplex, which was characterized by CD and SERS spectroscopies. Importantly, these results

constitute a robust basis for the introduction of SERS as a label-free analytical technique, complementary to CD, to monitor the formation of PNA quadruplexes.

Transparency Document

The Transparency document associated with this article can be found, in the online version.

References

- [1] S. Neidle, S. Balasubramanian, Quadruplex Nucleic Acids, 2006.
- [2] J.T. Davis, G-quartets 40 years later: from 5'-GMP to molecular biology and supra-molecular chemistry, *Angew. Chem. Int. Ed.* 43 (2004) 668–698.
- [3] S. Burge, G.N. Parkinson, P. Hazel, A.K. Todd, S. Neidle, Quadruplex DNA: sequence, topology and structure, *Nucleic Acid Res.* 34 (2006) 5402–5415.
- [4] V. Esposito, A. Virgilio, A. Pepe, G. Oliviero, L. Mayol, A. Galeone, Effects of the introduction of inversion of polarity sites in the quadruplex forming oligonucleotide TGGGT, *Bioorg. Med. Chem.* 17 (2009) 1997–2001.
- [5] G. Oliviero, N. Borbone, J. Amato, S. D'Errico, A. Galeone, G. Piccialli, M. Varra, L. Mayol, Synthesis of quadruplex-forming tetra-end-linked oligonucleotides: effects of the linker size on quadruplex topology and stability, *Biopolymers* 91 (2009) 466–477.
- [6] E.Y. Lam, D. Beraldi, D. Tannahill, S. Balasubramanian, G-quadruplex structures are stable and detectable in human genomic DNA, *Nat. Commun.* 4 (2013) 1796.
- [7] S. Cogoi, L.E. Xodo, G4 DNA in ras genes and its potential in cancer therapy, *Biochim. Biophys. Acta* 1859 (2016) 663–674.
- [8] D. Rhodes, H.J. Lipps, G-quadruplexes and their regulatory roles in biology, *Nucl. Acid Res.* 43 (2015) 8627–8637.
- [9] S. Balasubramanian, L.H. Hurley, S. Neidle, Targeting G-quadruplexes in gene promoters: a novel anticancer strategy? *Nat. Rev. Drug Discov.* 10 (2011) 261–275.
- [10] T. Agarwal, S. Roy, S. Kumar, T.K. Chakraborty, S. Maiti, In the sense of transcription regulation by G-quadruplexes: asymmetric effects in sense and antisense strands, *Biochemistry* 53 (2014) 3711–3718.
- [11] I.T. Holder, J.S. Hartig, A matter of location: influence of G-quadruplexes on *Escherichia coli* Gene expression, *Chem. Biol.* 21 (2014) 1511–1521.
- [12] S.L. Cree, M.A. Kennedy, Relevance of G-quadruplex structures to pharmacogenetics, *Front. Pharmacol.* 5 (2014) 160.
- [13] Y.J. Shin, V. Kumarasamy, D. Camacho, D. Sun, Involvement of G-quadruplex structures in regulation of human RET gene expression by small molecules in human medullary thyroid carcinoma TT cells, *Oncogene* 34 (2015) 1292–1299.
- [14] J. Bidzinska, G. Cimino-Reale, N. Zaffaroni, M. Folini, G-quadruplex structures in the human genome as novel therapeutic targets, *Molecules* 18 (2013) 12368–12395.
- [15] V. D'Atri, G. Oliviero, J. Amato, N. Borbone, S. D'Errico, L. Mayol, V. Piccialli, S. Haider, B. Hoorelbeke, J. Balzarini, G. Piccialli, New anti-HIV aptamers based on tetra-end-linked DNA G-quadruplexes: effect of the base sequence on anti-HIV activity, *Chem. Commun.* 48 (2012) 9516–9518.
- [16] V. Brázda, L. Hároníková, J.C.C. Liao, M. Fojta, DNA and RNA quadruplex-binding proteins, *Int. J. Mol. Sci.* 15 (2014) 17493–17517.
- [17] N. Borbone, J. Amato, G. Oliviero, V. D'Atri, V. Gabelica, E. De Pauw, G. Piccialli, L. Mayol, d(CGGTGGT) forms an octameric parallel G-quadruplex via stacking of unusual G(C):G(C):G(C):G(C) octads, *Nucleic Acids Res.* 39 (2011) 7848–7857.
- [18] G.W. Collier, G.N. Parkinson, The application of DNA and RNA G-quadruplexes to therapeutic medicines, *Chem. Soc. Rev.* 40 (2011) 5867–5892.
- [19] G.I. Livshits, A. Stern, D. Rotem, N. Borovok, G. Eidelstein, A. Migliore, E. Penzo, S.J. Wind, R. Di Felice, S.S. Skourtis, J.C. Cuevas, L. Gurevich, A.B. Kotlyar, D. Porath, Long-range charge transport in single G-quadruplex DNA molecules, *Nat. Nanotechnol.* 9 (2014) 1040–1046.
- [20] L. De Stefano, G. Oliviero, J. Amato, N. Borbone, G. Piccialli, L. Mayol, I. Rendina, M. Terracciano, I. Rea, Aminosilane functionalizations of mesoporous oxidized silicon for oligonucleotide synthesis and detection, *J. R. Soc. Interface* 10 (2013) 1–7.
- [21] J. Gros, F. Rosu, S. Amrane, A. De Cian, V. Gabelica, L. Lacroix, J.L. Mergny, Guanines are a quartet's best friend: impact of base substitutions on the kinetics and stability of tetramolecular quadruplexes, *Nucleic Acids Res.* 35 (2007) 3064–3075.
- [22] C.J. Lech, J.K.C. Lim, J.M.W. Lim, S. Amrane, B. Heddi, A.T. Phan, Effects of site-specific guanine C8-modifications on an intramolecular DNA G-quadruplex, *Biophys. J.* 101 (2011) 1987–1998.
- [23] J. Sagi, G-quadruplexes incorporating modified constituents: a review, *J. Biomol. Struct. Dyn.* 32 (2014) 477–511.
- [24] A. Avino, C. Fabrega, M. Tintore, R. Eritja, Thrombin binding aptamer, more than a simple aptamer: chemically modified derivatives and biomedical applications, *Curr. Pharm. Des.* 18 (2012) 2036–2047.
- [25] N. Borbone, M. Bucci, G. Oliviero, E. Morelli, J. Amato, V. D'Atri, S. D'Errico, V. Vellecco, G. Cirino, G. Piccialli, C. Fattorusso, M. Varra, L. Mayol, M. Persico, M. Scuto, Investigating the role of T7 and T12 residues on the biological properties of thrombin-binding aptamer: enhancement of anticoagulant activity by a single nucleobase modification, *J. Med. Chem.* 55 (2012) 10716–10728.
- [26] P.E. Nielsen, M. Egholm, R.H. Berg, O. Buchardt, Sugar-modified G-quadruplexes: effects of LNA-, 2'-F-RNA- and 2'-F-ANA-guanosine chemistries on G-quadruplex structure and stability, *Science* 6 (1991) 1497–1500.
- [27] T.N. Grossmann, S. Sasaki, M. Ritzefeld, S.W. Choi, A. Maruyama, O. Seitz, Inducing the replacement of PNA in DNA*PNA duplexes by DNA, *Bioorganic Med. Chem.* 16 (2008) 34–39.

- [28] G.N. Roviello, D. Musumeci, A. De Cristofaro, D. Capasso, S. Di Gaetano, E.M. Bucci, C. Pedone, Alternate dab-aegPNAs: synthesis, nucleic acid binding studies and biological activity, *Mol. Biosyst.* 6 (2010) 199–205.
- [29] G.N. Roviello, A. Ricci, E.M. Bucci, C. Pedone, Synthesis, biological evaluation and supramolecular assembly of novel analogues of peptidyl nucleosides, *Mol. Biosyst.* 7 (2011) 1773–1778.
- [30] B. Armitage, T. Koch, H. Frydenlund, H. Ørum, G.B. Schuster, Peptide nucleic acid (PNA)/DNA hybrid duplexes: intercalation by an internally linked anthraquinone, *Nucleic Acids Res.* 26 (1998) 715–720.
- [31] L. Moggio, L. De Napoli, B. Di Blasio, G. Di Fabio, J. D'Onofrio, D. Montesarchio, A. Messere, Solid-phase synthesis of cyclic PNA and PNA-DNA chimeras, *Org. Lett.* 8 (2006) 2015–2018.
- [32] N. Sugimoto, N. Satoh, K. Yasuda, S.I. Nakano, Stabilization factors affecting duplex formation of peptide nucleic acid with DNA, *Biochemistry* 40 (2001) 8444–8451.
- [33] T.J. Griffin, L.M. Smith, An approach to predicting the stabilities of peptide nucleic acid:DNA duplexes, *Anal. Biochem.* 260 (1998) 56–63.
- [34] F. Amato, R. Tomaiuolo, N. Borbone, A. Elce, J. Amato, S. D'Errico, G. De Rosa, L. Mayol, G. Piccialli, G. Oliviero, G. Castaldo, Design, synthesis and biochemical investigation, by in vitro luciferase reporter system, of peptide nucleic acids as new inhibitors of miR-509-3p involved in the regulation of cystic fibrosis disease gene expression, *Med. Chem. Commun.* 5 (2014) 68–71.
- [35] F. Amato, R. Tomaiuolo, F. Nici, N. Borbone, A. Elce, B. Catalanotti, S. D'Errico, C.M. Morgillo, G. De Rosa, L. Mayol, G. Piccialli, G. Oliviero, G. Castaldo, Exploitation of a very small peptide nucleic acid as a new inhibitor of miR-509-3p involved in the regulation of cystic fibrosis disease-Gene expression, *Biomed. Res. Int.* 2014 (2014) 1–10.
- [36] M. Egholm, O. Buchardt, L. Christensen, C. Behrens, S.M. Freier, D.A. Driver, R.H. Berg, S.K. Kim, B. Norden, P.E. Nielsen, PNA hybridizes to complementary oligonucleotides obeying the Watson-Crick hydrogen-bonding rules, *Nature* 365 (1993) 566–568.
- [37] L. Betts, J.A. Josey, J.M. Veal, S.R. Jordan, A nucleic acid triple helix formed by a peptide nucleic acid-DNA complex, *Science* 270 (1995) 1838–1841.
- [38] M.P. Knauer, P.M. Glazer, Triplex forming oligonucleotides: sequence-specific tools for gene targeting, *Hum. Mol. Genet.* 10 (2001) 2243–2251.
- [39] P. Wittung, P. Nielsen, B. Nordén, Extended DNA-recognition repertoire of peptide nucleic acid (PNA): PNA-dsDNA triplex formed with cytosine-rich homopyrimidine PNA, *Biochemistry* 36 (1997) 7973–7979.
- [40] P. Wittung, P. Nielsen, B. Nordén, Direct observation of strand invasion by peptide nucleic acid (PNA) into double-stranded DNA, *J. Am. Chem. Soc.* 118 (1996) 7049–7054.
- [41] K.A. Kormuth, J.L. Woolford, B.A. Armitage, Homologous PNA Hybridization to Non-canonical DNA G-Quadruplexes, *Biochemistry* 55 (2016) 1749–1757.
- [42] C.T. Murphy, A. Gupta, B.A. Armitage, P.L. Opresko, Hybridization of G-quadruplex forming peptide nucleic acids to guanine rich DNA templates inhibits DNA polymerase η extension, *Biochemistry* 53 (2014) 5315–5322.
- [43] M.I. Onyshchenko, T.I. Gaynutdinov, E.A. Englund, D.H. Appella, R.D. Neumann, I.G. Panyutin, Stabilization of G-quadruplex in the BCL2 promoter region in double-stranded DNA by invading short PNAs, *Nucleic Acids Res.* 37 (2009) 7570–7580.
- [44] T. Ishizuka, J. Yang, M. Komiyama, Y. Xu, G-rich sequence-specific recognition and scission of human genome by PNA/DNA hybrid G-quadruplex formation, *Angew. Chemie - Int. Ed.* 51 (2012) 7198–7202.
- [45] B. Datta, M.E. Bier, S. Roy, B.A. Armitage, Quadruplex formation by a guanine-rich PNA Oligomer, *J. Am. Chem. Soc.* 127 (2005) 4199–4207.
- [46] Y. Krishnan-Ghosh, E. Stephens, S. Balasubramanian, A PNA4 quadruplex, *J. Am. Chem. Soc.* 126 (2004) 5944–5945.
- [47] G. Oliviero, N. Borbone, A. Galeone, M. Varra, G. Piccialli, L. Mayol, Synthesis and characterization of a bunchy oligonucleotide forming a monomolecular parallel quadruplex structure in solution, *Tetrahedron Lett.* 45 (2004) 4869–4872.
- [48] S. Nagatoishi, Y. Tanaka, K. Tsumoto, Circular dichroism spectra demonstrate formation of the thrombin-binding DNA aptamer G-quadruplex under stabilizing-cation-deficient conditions, *Biochem. Biophys. Res. Commun.* 352 (2007) 812–817.
- [49] J. Kypr, I. Kejnovska, D. Rencuk, M. Vorlickova, Circular dichroism and conformational polymorphism of DNA, *Nucleic Acids Res.* 37 (2009) 1713–1725.
- [50] K. Kneipp, H. Kneipp, I. Itzkan, R. Dasari, M. Feld, Ultrasensitive chemical analysis by Raman spectroscopy, *Chem. Rev.* 99 (1999) 2957–2976.
- [51] G.J. Thomas Jr., Raman spectroscopy of protein and nucleic acid assemblies, *Annu. Rev. Biophys. Biomol. Struct.* 28 (1999) 1–27.
- [52] T. Miura, G. Thomas, Structural polymorphism of telomere DNA: interquadruplex and duplex-quadruplex conversions probed by Raman spectroscopy, *Biochemist* 33 (1994) 7848–7856.
- [53] G. Rusciano, A.C. De Luca, G. Pesce, A. Sasso, G. Oliviero, J. Amato, N. Borbone, S. D'Errico, V. Piccialli, G. Piccialli, L. Mayol, Label-free probing of G-quadruplex formation by surface-enhanced Raman scattering, *Anal. Chem.* 83 (2011) 6849–6855.
- [54] P. Lee, D.J. Meisel, Adsorption and surface-enhanced Raman of dyes on silver and gold sols, *Phys. Chem.* 86 (1982) 3391–3395.
- [55] G. Rusciano, G. Pesce, G. Zito, A. Sasso, R. Gaglione, R. Del Giudice, R. Piccoli, D.M. Monti, A. Arciello, Insights into the interaction of the N-terminal amyloidogenic polypeptide of ApoA-I with model cellular membranes, *BBA - General Subjects* 1860 (2016) 795–801.
- [56] F. Crestey, L.K. Ottesen, J.W. Jaroszewski, H. Franzyk, Efficient loading of primary alcohols onto a solid phase using a trityl bromide linker, *Tetrahedron Lett.* 49 (2008) 5890–5893.
- [57] S. Masiero, R. Trotta, S. Pieraccini, S. De Tito, R. Perone, A. Randazzo, G.P. Spada, A non-empirical chromophoric interpretation of CD spectra of DNA G-quadruplex structures, *Org. Biomol. Chem.* 8 (2010) 2683–2692.
- [58] C. Briones, E. Mateo-Marti, C. Gomez-Rodriguez, V. Parro, E. Roman, J.A. Martin-Gago, Ordered self-assembled monolayers of peptide nucleic acids with DNA recognition capability, *Phys. Rev. Lett.* 93 (2004), 208103.
- [59] S.S.M. Colaanni, J. Aubard, H. Hansen, O.F. Nielsen, Raman spectroscopic studies of some biochemically relevant molecules, *Vibrat. Spectr.* 9 (1995) 111–120.
- [60] C. Krafft, J.M. Benevides, G.J. Thomas, Secondary structure polymorphism in *Oxytricha nova* telomeric DNA, *Nucleic Acids Res.* 30 (2002) 3981–3991.
- [61] C.V. Pagba, S.M. Lane, S.J. Wachsmann-Hogiu, Raman and surface-enhanced Raman spectroscopic studies of the 15-mer DNA thrombin-binding aptamer, *Raman Spectrosc.* 41 (2010) 241–247.
- [62] J.L.R. Arrondo, F.M. Goñi, Infrared studies of protein-induced perturbation of lipids in lipoproteins and membranes, *Chem. Phys. Lipids* 96 (1998) 53–68.
- [63] E. Mateo-Marti, C. Briones, C.M. Pradier, J.A. Martin-Gago, A DNA biosensor based on peptide nucleic acids on gold surfaces, *Biosens. Bioelectron.* 22 (2007) 1926–1932.
- [64] F.S. Parker, Applications of Infrared, Plenum Press, Raman and Resonance Raman spectroscopy in biochemistry, 1983.



Synthesis of cyclic N^1 -pentylinosine phosphate, a new structurally reduced cADPR analogue with calcium-mobilizing activity on PC12 cells

Ahmed Mahal^{‡1}, Stefano D'Errico^{‡1}, Nicola Borbone¹, Brunella Pinto¹, Agnese Secondo², Valeria Costantino¹, Valentina Tedeschi², Giorgia Oliviero^{*1}, Vincenzo Piccialli³ and Gennaro Piccialli^{1,4}

Full Research Paper

[Open Access](#)

Address:

¹Dipartimento di Farmacia, Università degli Studi di Napoli Federico II, Via D. Montesano 49, 80131, Napoli, Italy, ²Dipartimento di Neuroscienze e Scienze Riproduttive ed Odontostomatologiche, Università degli Studi di Napoli Federico II, Via Pansini 5, 80131 Napoli, Italy, ³Dipartimento di Scienze Chimiche, Università degli Studi di Napoli Federico II, Napoli, Italy and ⁴Institute of Protein Biochemistry, National Council Research of Italy, Via Pietro Castellino 111, 80131 Napoli, Italy

Email:

Giorgia Oliviero^{*} - golivier@unina.it

* Corresponding author ‡ Equal contributors

Keywords:

calcium mobilization; cIDPR analogues; cyclic ADP-ribose (cADPR); cyclization

Beilstein J. Org. Chem. **2015**, *11*, 2689–2695.

doi:10.3762/bjoc.11.289

Received: 31 July 2015

Accepted: 04 December 2015

Published: 22 December 2015

Associate Editor: K. N. Ganesh

© 2015 Mahal et al; licensee Beilstein-Institut.

License and terms: see end of document.

Abstract

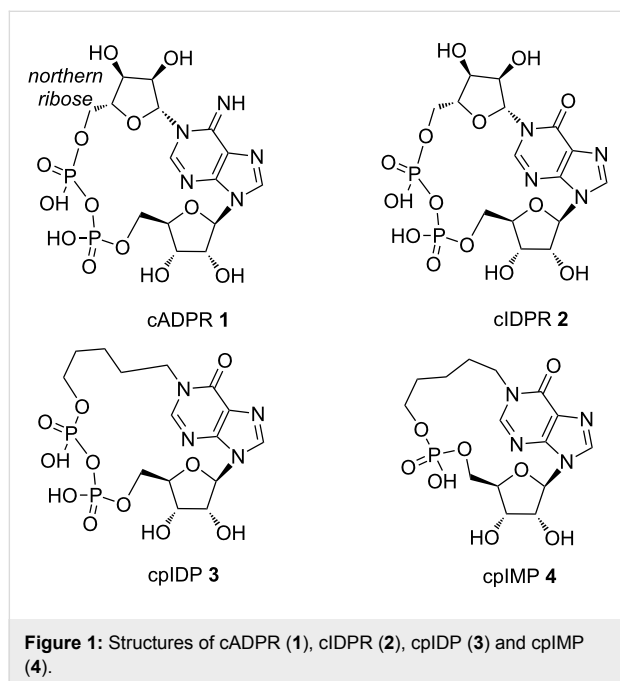
Cyclic N^1 -pentylinosine monophosphate (cpIMP), a novel simplified inosine derivative of cyclic ADP-ribose (cADPR) in which the N^1 -pentyl chain and the monophosphate group replace the northern ribose and the pyrophosphate moieties, respectively, was synthesized. The role played by the position of the phosphate group in the key cyclization step, which consists in the formation of a phosphodiester bond, was thoroughly investigated. We have also examined the influence of the phosphate bridge on the ability of cpIMP to mobilize Ca^{2+} in PC12 neuronal cells in comparison with the pyrophosphate bridge present in the cyclic N^1 -pentylinosine diphosphate analogue (cpIDP) previously synthesized in our laboratories. The preliminary biological tests indicated that cpIMP and cpIDP induce a rapid increase of intracellular Ca^{2+} concentration in PC12 neuronal cells.

Introduction

Nucleosides and nucleotides (NNs) are widely used as key intermediates and important core structures in the field of synthetic medicinal chemistry [1,2]. They represent versatile syn-

thetic building blocks towards the synthesis of biologically relevant compounds such as antiviral and antineoplastic drugs [3-8], antibiotics and antifungal agents [9-11]. Furthermore,

several NNs act as potent second messengers involved in the regulation of key metabolic pathways [12]. Among these NNs there is the cyclic ADP-ribose (cADPR **1**, Figure 1), a metabolite strictly involved in the homeostasis of cellular calcium ions. cADPR is a second messenger that activates the ryanodine receptors of the sarcoplasmic reticulum and mobilizes Ca^{2+} ions in many cell types of protozoa, plants, animals and humans [13].



Furthermore, there is a strong evidence that cADPR is an important second messenger in the nervous system where it is involved in the handling of Ca^{2+} ions that control several functions. Indeed, the administration of cADPR to cell cultures produces three patterns of response in terms of variation of intracellular concentration of calcium ions ($[\text{Ca}^{2+}]_i$): (a) a rapid response after direct microinjection of the messenger into the cells; (b) a slow variation of $[\text{Ca}^{2+}]_i$ when cADPR is added to the cell culture medium; c) a progressive potentiation of $[\text{Ca}^{2+}]_i$ increasing due to a depolarization. In fact, cADPR induces Ca^{2+} release from presynaptic and postsynaptic intracellular stores and plays an important role in the activity-dependent synaptic plasticity, including long-term depression [14]. In addition, enzymes able to catalyze the hydrolysis of cyclic ADP-ribose to ADP-ribose are expressed ubiquitously in the mouse brain. Specifically, wild-type mice show the highest cyclase activity in the hypothalamus, and then in the cerebellum, cerebrum and posterior pituitary [15].

Unfortunately, the lability of the N-1 glycosidic bond of cADPR towards enzymatic and/or non-enzymatic hydrolysis to

ADP-ribose, even in a neutral aqueous solution, greatly hinders the studies aimed at elucidating its physiological role [16]. Several enzymes involved in the metabolism of cADPR have been described. Among them is the ubiquitous ADP-ribosyl cyclase, an enzyme first isolated from *Aplysia Californica* [17]. Using the *Aplysia* ADP-ribosyl cyclase many metabolite analogues of cADPR have been produced starting from NAD^+ and NADP^+ [18–21]. However, the specificity of the enzymatic cyclization mechanism drastically limits its applicability for enzymatic or chemo-enzymatic procedures. For this reason, to obtain new cADPR derivatives the exploitation of chemical synthetic strategies is still necessary. A lot of modifications regarding the northern and southern ribose as well as the purine base of cADPR have been proposed so far [22,23]. Matsuda and co-workers were the first who synthesized new analogues of the cADPR in which the adenine base was replaced by a hypoxanthine ring [24]. This kind of modification produced the cyclic inosine diphosphate ribose (cIDPR) **2** which proved to be stable in hydrolytic physiological conditions and showed significant Ca^{2+} mobilizing activity, thus fostering the synthesis of a variety of cIDPR analogues. In particular, the N1, N9 and C8-substituted cIDPR were the most interesting [24–33]. In the last few years several cIDPR analogues were also synthesized in our laboratory [34–37]. Among these, the N^1 -pentyl analogue cpIDP (**3**, Figure 1) [34] showed interesting activity on the PC12 cell line previously differentiated with the Nerve Growth Factor (NGF) (data not previously published). Starting from these data, we here report the synthesis and the preliminary biological activity of the new cyclic N^1 -pentylinosine monophosphate (cpIMP) (**4**, Figure 1), in which the pyrophosphate group of **3** was replaced by a monophosphate moiety connecting the southern ribose with the N^1 -pentyl chain. The here reported results significantly contribute to the understanding of the role played by the pyrophosphate moiety of cADPR and cIDPR analogues on the mobilization of Ca^{2+} ions. To date, such structure-activity relationship has only been poorly investigated [38–41]. We anticipate here that compounds **3** and **4** induce the same effect on Ca^{2+} mobilization in NGF-differentiated PC12 cells. In particular, both compounds produced a transient increase of intracellular concentration of Ca^{2+} when added to the cells, thus demonstrating their ability to cross the plasma membrane.

Results and Discussion

Chemistry

The key step for the preparation of all cADPR/cIDPR analogues is the macrocyclization via pyrophosphate bond formation, which is usually performed by joining the two phosphate moieties at the end of the multistep synthesis [24–29]. Similarly, the preparation of the new cpIMP derivative **4** could be performed by the cyclization of a monophosphate precursor via

phosphodiester bond formation. For this purpose we investigated both the possible synthetic strategies (pathways A and B, Figure 2) in which the phosphate group (or its synthon) has been attached either on the end of the N^1 -pentyl chain (precursor A) or on the 5'-ribose position (precursor B).

At first, to obtain the cpIMP (**4**) we followed the synthetic pathway A by using the strategy reported in Scheme 1 that

employed the N^1 - ω -hydroxypentylinosine derivative **5** as the starting material [34]. Compound **5** was phosphorylated on the ω -hydroxyalkyl function by using the phosphitylating chloroamidite agent **6**. The reaction of **5** with **6** furnished the sole regioisomer **7** equipped with the reactive phosphorous(III) group. Unfortunately, the activation of the phosphoramidite function with 1*H*-tetrazole aimed at inducing the cyclization on the 5'-OH ribose function produced only a complex mixture.

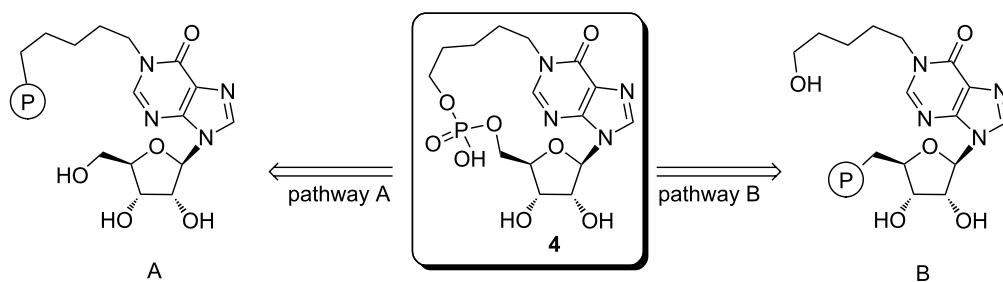
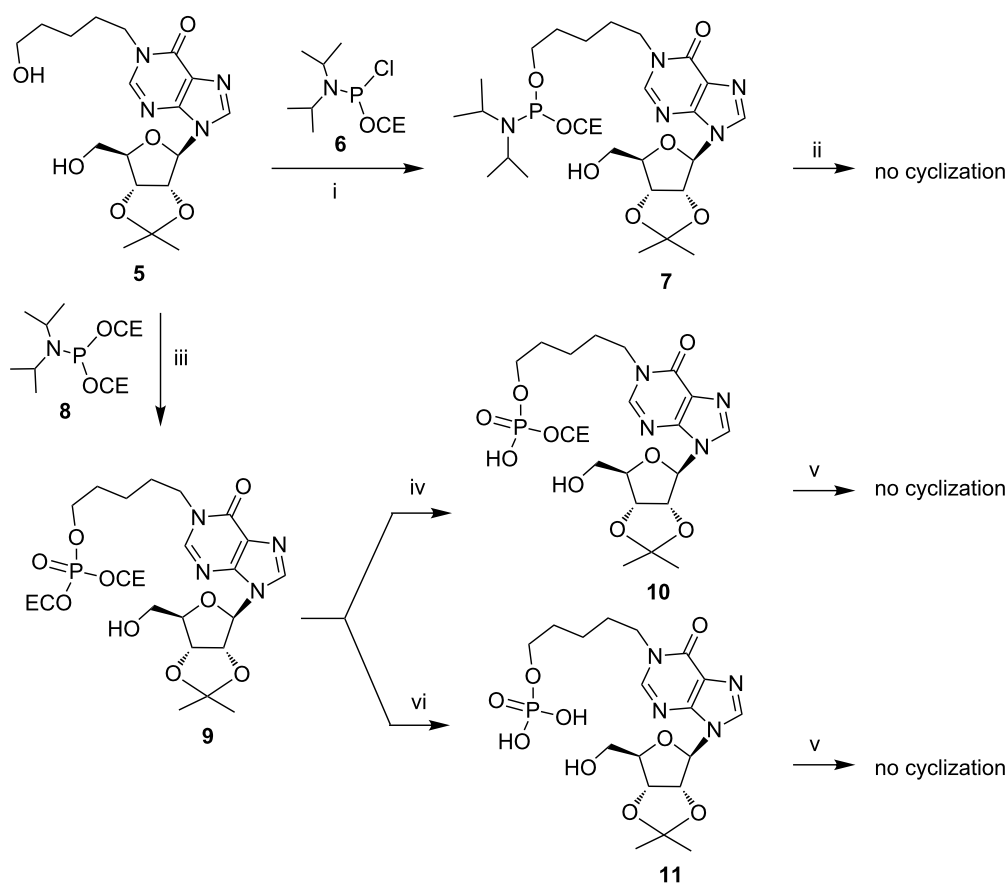


Figure 2: Synthetic strategies explored in the cyclization step via phosphodiester bond formation.



Scheme 1: i) $(i\text{Pr})_2\text{NP}(\text{OCE})\text{Cl}$, DIPEA, THF, 1 h, rt; ii) 1) 1*H*-tetrazole, THF, 2) *t*-BuOOH, 2 h, rt; iii) 1) $(i\text{Pr})_2\text{NP}(\text{OCE})_2$, 1*H*-tetrazole, THF, 2 h, rt, 2) *t*-BuOOH, 2 h, rt; iv) TEA/pyridine, 1:1 v/v, 16 h, rt; v) activating agent (EDC in DMF or DCC in DMF or MSNT in pyridine) 16 h, rt; vi) conc. aq NH_4OH , MeOH, 50 °C, 16 h.

No traces of the target cyclic compound were detected after the usual phosphorous oxidation step.

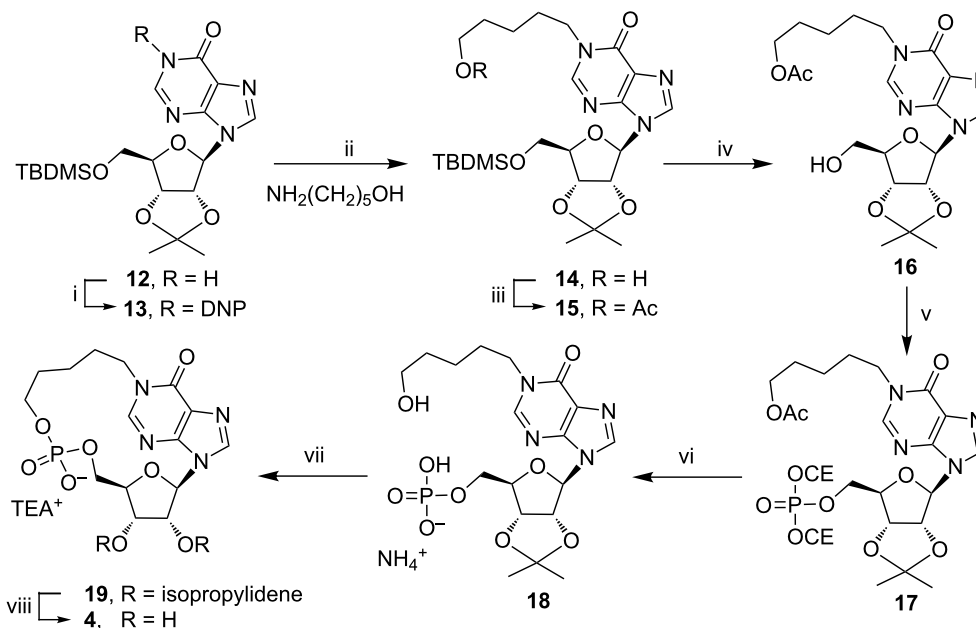
This failure prompted us to use the alternative phosphitylating reagent bis(cyanoethyl)phosphoramidite **8**, which, after the regioselective reaction with the 5'-hydroxyalkyl function of **5** led to the phosphotriester product **9** after the phosphorous oxidation with *t*-BuOOH. Starting from **9** we explored two synthetic routes, differing for the degree of esterification at the phosphate moiety, to achieve the cyclization of the 17-membered ring of **4**. The treatment of **9** with a mixture of triethylamine/pyridine furnished the phosphodiester product **10** in almost quantitative yield. Instead, the complete removal of both 2-cyanoethyl groups of **9** with concentrated aqueous ammonia gave the phosphomonoester **11**. Unfortunately, neither linear precursors **10** nor **11** underwent the expected cyclization step, even when treated with the most common phosphate activating agents (EDC, DCC, MSNT) in very diluted conditions. In our opinion, the target intramolecular cyclizations failed because of the poor mobility of the 5'-OH ribose function, as well as because of the unfavourable *anti* conformation of the N-glycosidic bond induced by the presence at the N1 position of the purine base of the bulky ω -phosphate adduct formed with the activating agent.

For this reason, we decided to switch to the synthetic pathway B (Figure 2), in which the monophosphate group is installed at the 5'-ribose position. This strategy, reported in Scheme 2, used as

the starting material the 5'-TBDMS-2',3'-*O*-isopropylideneinosine (**12**). The protected inosine **12** was initially converted into the *N*¹-dinitrophenyl derivative **13**, which, after reaction with the 5-aminopentan-1-ol, furnished the *N*¹- ω -hydroxypentylino-sine derivative **14** [35]. This compound was acetylated on the ω -hydroxy function (compound **15**) and then deprotected on the 5'-hydroxy function thus obtaining **16**. The phosphorylation of the 5'-OH function of **16**, by using the (iPr)₂NP(OCE)₂/*t*-BuOOH system, already used in the preparation of compound **9**, furnished the 5'-*O*-phosphotriester inosine derivative **17**. The treatment of **17** with concentrated aqueous ammonia allowed the removal of both the OCE phosphate protecting groups together with the acetate function, thus obtaining the key intermediate **18** as triethylammonium salt after HPLC purification. The derivate **18**, dissolved in DMF at the final concentration of 2 mM was treated with EDC (1.2 equiv) and the reaction allowed to stand at room temperature for 48 h. From this mixture it was possible to isolate cyclic compound **19** (30% cyclization yield) whose structure was confirmed by NMR and high-resolution mass analyses. Eventually, the treatment of compound **19** with aqueous 20% TFA afforded the target compound **4**.

Ca²⁺-mobilizing activity of **3** and **4** in PC12 cells

To study the biological activity of compounds **3** and **4**, we evaluated their effect on the mobilization of Ca²⁺ ions in PC12 cells differentiated with NGF. Interestingly, compounds **3** and **4**



Scheme 2: i) DNCB, K₂CO₃, DMF, 4 h, 80 °C; ii) 5-aminopentan-1-ol, DMF, 16 h, 50 °C; iii) Ac₂O, pyridine, 2 h, rt, iv) NH₄F, MeOH, 16 h, reflux; v) 1) (iPr)₂NP(OCE)₂, 1*H*-tetrazole, THF, 2 h, rt, 2) *t*-BuOOH, 2 h, rt; vi) conc. NH₄OH(aq), MeOH, 50 °C, 16 h; vii) EDC, DMF; viii) TFA, H₂O, 16 h, rt.

caused a rapid and transient increase of the intracellular $[\text{Ca}^{2+}]_i$ when added to the medium at the concentration of 100 nM (Figure 3). This pattern of response could be ascribed to the initial release of Ca^{2+} ions from the intracellular organelles followed by a depolarization-induced Ca^{2+} influx. The biological assays also confirmed that the cIDPR analogues **3** and **4** retained the ability to pass the plasma membrane of neuronal cells.

Conclusion

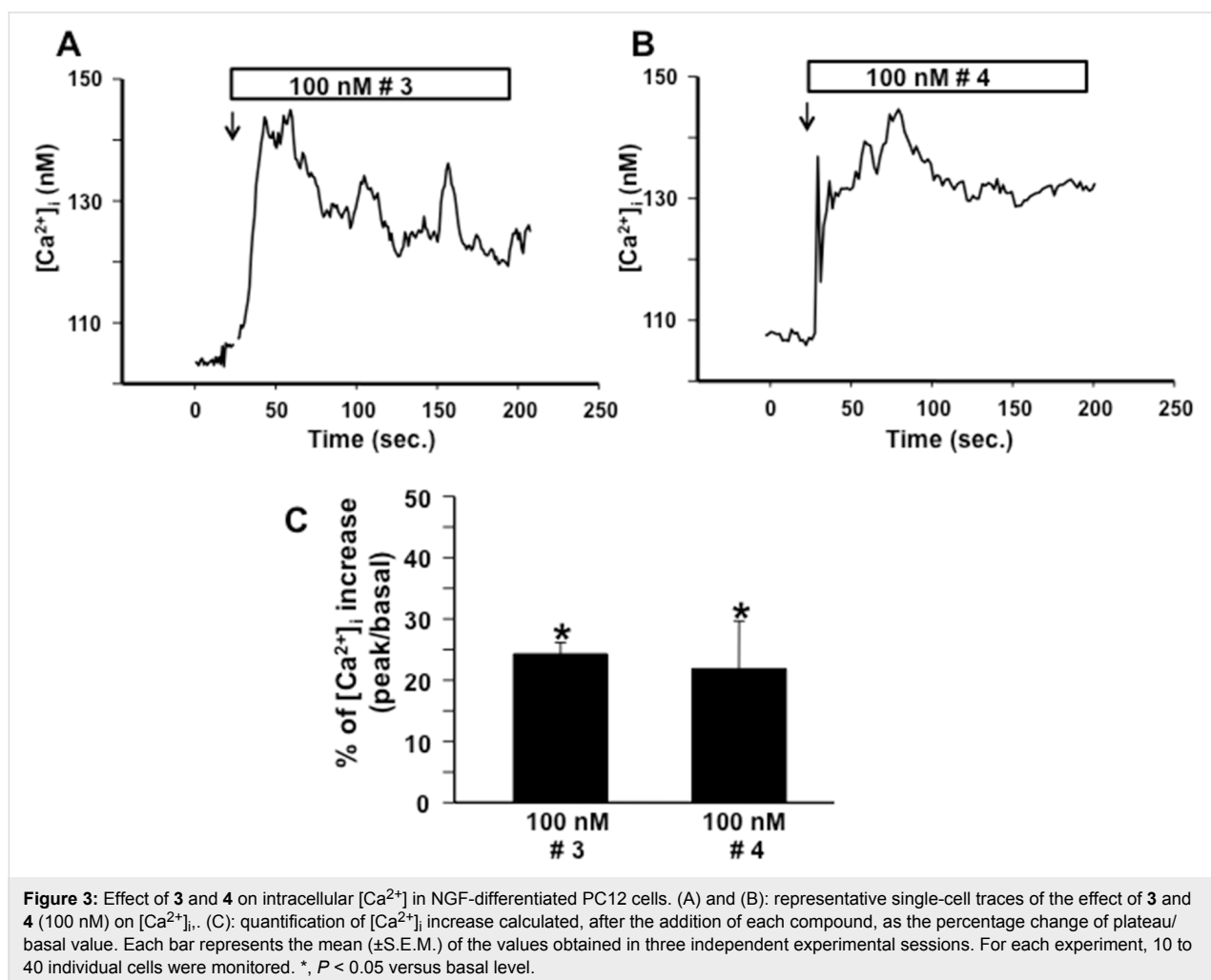
cADPR is a second messenger synthesized by neuronal cells that modulates the Ca^{2+} homeostasis in the nervous system [42]. Unfortunately, cADPR is characterized by a low ability to cross the plasma membranes. This behaviour hinders the studies on the effects of cADPR on cell functions. To overcome this limitation and to understand the role played by the pyrophosphate bridge on the biological activities of cADPR, we synthesized the lipophilic derivative cpIMP (**4**) in which the pyrophosphate group of **3** was replaced by a monophosphate moiety connecting the southern ribose with the N^1 -pentyl chain. We

compared the activity of **4** in modulating the concentration of $[\text{Ca}^{2+}]_i$ with that of the previously synthesized cpIDP (**3**). To study the effect of **3** and **4** on $[\text{Ca}^{2+}]_i$, these compounds were added to PC12 cells previously differentiated with NGF at the concentration of 100 nM. Both compounds caused a fast and transient increase in $[\text{Ca}^{2+}]_i$. This pattern of response could be ascribed to the initial release of Ca^{2+} from intracellular organelles followed by a depolarization-induced Ca^{2+} influx. The reported preliminary results indicate that **3** and **4** possess almost the same activity, thus indicating that the role of the pyrophosphate bridge is not stringent and that the introduction of an alkyl chain in the N1 position of the purine base improves the permeation of the cell membrane by passive diffusion or through an active uptake system expressed on the membrane.

Experimental

General

All solvents were dried by standard methods and all reactions were carried out under inert atmosphere (argon or nitrogen). All reagents were obtained and used from commercial sources



(Sigma-Aldrich, Germany) without further purification. ^1H and ^{13}C NMR experiments were performed using a Varian Mercury Plus 400 MHz spectrometer in CD_3OD , D_2O , CDCl_3 and acetone- d_6 solvents. Chemical shifts are reported in parts per million (δ) relative to residual solvents signals: CD_2HOD 3.31, HOD 4.80, $(\text{CD}_3)(\text{CD}_2\text{H})\text{CO}$ 2.09 for ^1H NMR and CD_3OD 49.0 for ^{13}C NMR. ^{31}P NMR experiments were carried out on a Varian Unity INOVA 500 MHz instrument in CD_3OD solvent using 85% H_3PO_4 as an external standard (0 ppm). High performance liquid chromatography (HPLC) was performed using a Jasco UP-2075 Plus pump equipped with a Jasco UV-2075 Plus UV detector and a 4.8×150 mm C-18 reversed-phase column (particle size 5 μm) eluted with a linear gradient of CH_3CN in 0.1 M triethylammonium bicarbonate (TEAB) buffer (from 0 to 50% in 45 min, flow 1.3 mL/min). UV spectra were recorded on a Jasco V-530 UV spectrophotometer. High-resolution MS spectra were recorded on a Bruker APEX II FT-ICR mass spectrometer using the electrospray ionization (ESI) technique. Column chromatography was carried out on silica gel-60 (Merck, 0.063–0.200 mm) or on C-18 reversed-phase silica gel-60 (Merck, 0.040–0.063 mm). Analytical TLC analyses were performed using F_{254} silica gel plates (0.2 mm thick, Merck). TLC spots were detected under UV light (254 nm).

Cell cultures and $[\text{Ca}^{2+}]_i$ measurements

PC12 cells, grown on plastic dishes in RPMI medium composed of 10% horse serum, 5% FBS, 100 UI/mL penicillin and 100 $\mu\text{g/mL}$ streptomycin, were differentiated in neurons with NGF (50 ng/mL; 7 days). Cells were cultured in an atmosphere of 5% CO_2 . The culture medium was changed every 2 days. For microfluorimetric studies with Fura 2-AM, cells were seeded on glass coverslips (Fisher, Springfield, NJ, USA) coated with poly-L-lysine (5 $\mu\text{g/mL}$) (Sigma, St. Louis, Missouri, USA) and used at least 12 h after seeding. Intracellular Ca^{2+} concentration ($[\text{Ca}^{2+}]_i$) was measured by single cell computer-assisted video QImaging [43]. Briefly, differentiated PC12 cells cultured on poly-L-lysine-coated glass coverslips were loaded with 10 μM Fura-2AM for 1 h at 22 $^\circ\text{C}$ in Krebs–Ringer saline solution containing the following: 5.5 mM KCl, 160 mM NaCl, 1.2 mM MgCl_2 , 1.5 mM CaCl_2 , 10 mM glucose, and 10 mM HEPES-NaOH, pH 7.4. At the end of the loading period, the coverslips were placed in a perfusion chamber (Medical System, Greenvale, NY, USA), mounted on a Zeiss Axiovert 200 microscope (Carl Zeiss, Germany) equipped with a FLUAR 40X oil objective lens. The experiments employed a digital imaging system composed of a MicroMax 512BFT cooled CCD camera (Princeton Instruments, Trenton, NJ, USA), LAMBDA 10-2 filter wheeler (Sutter Instruments, Novato, CA, USA), and Meta-Morph/MetaFluor Imaging System software (Universal Imaging, West Chester, PA, USA). After loading, the cells were illuminated alternately at 340 and 380 nm by a Xenon lamp.

The emitted light was passed through a 512 nm barrier filter. Fura-2AM fluorescence intensity was measured every 3 s. Forty to sixty-five individual cells were selected and monitored simultaneously from each cover slip. Results are presented as the cytosolic Ca^{2+} concentration. Calibrations used the relation of Grynkiewicz et al. [44] assuming that the KD for Fura-2AM was 224 nM.

Supporting Information

Supporting Information File 1

Structural characterizations.

[<http://www.beilstein-journals.org/bjoc/content/supplementary/1860-5397-11-289-S1.pdf>]

Acknowledgments

The research leading to these results was funded by the Seventh Framework Programme (FP7) of the European Union 2007–2013 under grant agreement No. 229893 (BlueGenics) and by Regione Campania under POR Campania FESR 2007–2013 – O.O. 2.1 (FarmaBioNet).

References

1. Chu, C. K. *Antiviral Nucleosides: Chiral Synthesis and Chemotherapy*; Elsevier: Amsterdam, The Netherlands, 2003.
2. Simons, C.; Wu, Q.; Htar, T. T. *Curr. Top. Med. Chem.* **2005**, *5*, 1191–1203. doi:10.2174/156802605774463051
3. Lagoja, I. M. *Chem. Biodiversity* **2005**, *2*, 1–50. doi:10.1002/cbdv.200490173
4. Miura, S.; Izuta, S. *Curr. Drug Targets* **2004**, *5*, 191–195. doi:10.2174/1389450043490578
5. Parker, W. B.; Secrist, J. A.; Waud, W. R. *Curr. Opin. Invest. Drugs* **2004**, *5*, 592–596.
6. D'Errico, S.; Oliviero, G.; Amato, J.; Borbone, N.; Cerullo, V.; Hemminki, A.; Piccialli, V.; Zaccaria, S.; Mayol, L.; Piccialli, G. *Chem. Commun.* **2012**, *48*, 9310–9312. doi:10.1039/c2cc33511e
7. D'Errico, S.; Oliviero, G.; Borbone, N.; Amato, J.; D'Alonzo, D.; Piccialli, V.; Mayol, L.; Piccialli, G. *Molecules* **2012**, *17*, 13036–13044. doi:10.3390/molecules171113036
8. Caso, M. F.; D'Alonzo, D.; D'Errico, S.; Palumbo, G.; Guaragna, A. *Org. Lett.* **2015**, *17*, 2626–2629. doi:10.1021/acs.orglett.5b00982
9. Kimura, K.-i.; Bugg, T. D. H. *Nat. Prod. Rep.* **2003**, *20*, 252–273. doi:10.1039/b202149h
10. Rachakonda, S.; Cartee, L. *Curr. Med. Chem.* **2004**, *11*, 775–793. doi:10.2174/0929867043455774
11. Knapp, S. *Chem. Rev.* **1995**, *95*, 1859–1876. doi:10.1021/cr00038a006
12. Clapper, D. L.; Walseth, T. F.; Dargie, P. J.; Lee, H. C. *J. Biol. Chem.* **1987**, *262*, 9561–9568.
13. Guse, A. H. *Curr. Med. Chem.* **2004**, *11*, 847–855. doi:10.2174/0929867043455602
14. Reyes-Harde, M.; Empson, R.; Potter, B. V. L.; Galione, A.; Stanton, P. K. *Proc. Natl. Acad. Sci. U. S. A.* **1999**, *96*, 4061–4066. doi:10.1073/pnas.96.7.4061

15. Jin, D.; Liu, H.-X.; Hirai, H.; Torashima, T.; Nagai, T.; Lopatina, O.; Shnayder, N. A.; Yamada, K.; Noda, M.; Seike, T.; Fujita, K.; Takasawa, S.; Yokoyama, S.; Koizumi, K.; Shiraishi, S.; Tanaka, Y.; Hashii, M.; Yoshihara, T.; Higashida, K.; Islam, M. S.; Yamada, N.; Hayashi, K.; Noguchi, N.; Kato, I.; Okamoto, H.; Matsushima, A.; Salmina, A.; Munesue, T.; Shimizu, N.; Mochida, S.; Asano, M.; Higashida, H. *Nature* **2007**, *446*, 41–45. doi:10.1038/nature05526
16. Shuto, S.; Matsuda, A. *Curr. Med. Chem.* **2004**, *11*, 827–845. doi:10.2174/0929867043455639
17. Aarhus, R.; Graeff, R. M.; Dickey, D. M.; Walseth, T. F.; Lee, H. C. *J. Biol. Chem.* **1995**, *270*, 30327–30333. doi:10.1074/jbc.270.51.30327
18. Moreau, C.; Ashamu, G. A.; Bailey, V. C.; Galione, A.; Guse, A. H.; Potter, B. V. L. *Org. Biomol. Chem.* **2011**, *9*, 278–290. doi:10.1039/C0OB00396D
19. Inageda, K.; Takahashi, K.; Tokita, K.; Nishina, H.; Kanaho, Y.; Kukimoto, I.; Kontani, K.; Hoshino, S.; Katadat, T. *J. Biochem.* **1995**, *117*, 125–131.
20. De Flora, A.; Guida, L.; Franco, L.; Zocchi, E.; Buzzzone, S.; Benatti, U.; Damonte, G.; Lee, H. C. *J. Biol. Chem.* **1997**, *272*, 12945–12951. doi:10.1074/jbc.272.20.12945
21. Fukushi, Y.; Kato, I.; Takasawa, S.; Sasaki, T.; Ong, B. H.; Sato, M.; Ohsaga, A.; Sato, K.; Shirato, K.; Okamoto, H.; Maruyama, Y. *J. Biol. Chem.* **2001**, *276*, 649–655. doi:10.1074/jbc.M004469200
22. Zhang, L.; Yue, J.; Zhang, L.-H. *Chem. Rec.* **2015**, *15*, 511–523. doi:10.1002/tcr.201402072
23. Guse, A. H. *J. Chin. Pharm. Sci.* **2013**, *22*, 127–136.
24. Fukuoka, M.; Shuto, S.; Minakawa, N.; Ueno, Y.; Matsuda, A. *J. Org. Chem.* **2000**, *65*, 5238–5248. doi:10.1021/jo0000877
25. Wagner, G. K.; Black, S.; Guse, A. H.; Potter, B. V. L. *Chem. Commun.* **2003**, 1944–1945. doi:10.1039/b305660k
26. Gu, X.; Yang, Z.; Zhang, L.; Kunerth, S.; Fliegert, R.; Weber, K.; Guse, A. H.; Zhang, L. *J. Med. Chem.* **2004**, *47*, 5674–5682. doi:10.1021/jm040092t
27. Guse, A. H.; Gu, X.; Zhang, L.; Weber, K.; Krämer, E.; Yang, Z.; Jin, H.; Li, Q.; Carrier, L.; Zhang, L. *J. Biol. Chem.* **2005**, *280*, 15952–15959. doi:10.1074/jbc.M414032200
28. Swarbrick, J. M.; Potter, B. V. L. *J. Org. Chem.* **2012**, *77*, 4191–4197. doi:10.1021/jo202319f
29. Shuto, S.; Shirato, M.; Sumita, Y.; Ueno, Y.; Matsuda, A. *J. Org. Chem.* **1998**, *63*, 1986–1994. doi:10.1021/jo9717797
30. Huang, L.-J.; Zhao, Y.-Y.; Yuan, L.; Min, J.-M.; Zhang, L.-H. *Bioorg. Med. Chem. Lett.* **2002**, *12*, 887–889. doi:10.1016/S0960-894X(02)00033-1
31. Huang, L.-J.; Zhao, Y.-Y.; Yuan, L.; Min, J.-M.; Zhang, L.-H. *J. Med. Chem.* **2002**, *45*, 5340–5352. doi:10.1021/jm010530I
32. Takano, S.; Tsuzuki, T.; Murayama, T.; Sakurai, T.; Fukuda, H.; Arisawa, M.; Shuto, S. *J. Org. Chem.* **2015**, *80*, 6619–6627. doi:10.1021/acs.joc.5b00723
33. Tsuzuki, T.; Sakaguchi, N.; Kudoh, T.; Takano, S.; Uehara, M.; Murayama, T.; Sakurai, T.; Hashii, M.; Higashida, H.; Weber, K.; Guse, A. H.; Kameda, T.; Hirokawa, T.; Kumaki, Y.; Potter, B. V. L.; Fukuda, H.; Arisawa, M.; Shuto, S. *Angew. Chem., Int. Ed.* **2013**, *52*, 6633–6637. doi:10.1002/anie.201302098
34. Galeone, A.; Mayol, L.; Oliviero, G.; Piccialli, G.; Varra, M. *Eur. J. Org. Chem.* **2002**, 4234–4238. doi:10.1002/1099-0690(200212)2002:24<4234::AID-EJOC4234>3.0.CO;2-8
35. Oliviero, G.; D'Errico, S.; Borbone, N.; Amato, J.; Piccialli, V.; Varra, M.; Piccialli, G.; Mayol, L. *Tetrahedron* **2010**, *66*, 1931–1936. doi:10.1016/j.tet.2010.01.013
36. D'Errico, S.; Oliviero, G.; Borbone, N.; Amato, J.; Piccialli, V.; Varra, M.; Mayol, L.; Piccialli, G. *Molecules* **2011**, *16*, 8110–8118. doi:10.3390/molecules16098110
37. D'Errico, S.; Oliviero, G.; Borbone, N.; Amato, J.; Piccialli, V.; Varra, M.; Mayol, L.; Piccialli, G. *Molecules* **2013**, *18*, 9420–9431. doi:10.3390/molecules18089420
38. Qi, N.; Jung, K.; Wang, M.; Na, L. X.; Yang, Z. J.; Zhang, L. R.; Guse, A. H.; Zhang, L. H. *Chem. Commun.* **2011**, *47*, 9462–9464. doi:10.1039/c1cc13062e
39. Aarhus, R.; Gee, K.; Lee, H. C. *J. Biol. Chem.* **1995**, *270*, 7745–7749. doi:10.1074/jbc.270.13.7745
40. Zhang, F.-J.; Yamada, S.; Gu, Q.-M.; Sih, C. J. *Bioorg. Med. Chem. Lett.* **1996**, *6*, 1203–1208. doi:10.1016/0960-894X(96)00207-7
41. Xu, L.; Walseth, T. F.; Slama, J. T. *J. Med. Chem.* **2005**, *48*, 4177–4181. doi:10.1021/jm049469I
42. Higashida, H.; Hashii, M.; Yokoyama, S.; Hoshi, N.; Asai, K.; Kato, T. *J. Neurochem.* **2001**, *76*, 321–331. doi:10.1046/j.1471-4159.2001.00082.x
43. Secondo, A.; Staiano, R. I.; Scorziello, A.; Sirabella, R.; Boscia, F.; Adornetto, A.; Valsecchi, V.; Molinaro, P.; Canzoniero, L. M.; Di Renzo, G.; Annunziato, L. *Cell Calcium* **2007**, *42*, 521–535. doi:10.1016/j.ceca.2007.01.006
44. Gryniewicz, G.; Poenie, M.; Tsien, R. Y. *J. Biol. Chem.* **1985**, *260*, 3440–3450.

License and Terms

This is an Open Access article under the terms of the Creative Commons Attribution License (<http://creativecommons.org/licenses/by/2.0>), which permits unrestricted use, distribution, and reproduction in any medium, provided the original work is properly cited.

The license is subject to the *Beilstein Journal of Organic Chemistry* terms and conditions: (<http://www.beilstein-journals.org/bjoc>)

The definitive version of this article is the electronic one which can be found at:
[doi:10.3762/bjoc.11.289](http://dx.doi.org/10.3762/bjoc.11.289)

Synthesis of C⁶-Pyridylpurine Nucleosides by Reaction of Nebularine N¹-Oxide with Pyridinyl Grignard Reagents

Stefano D'Errico,^[a] Giorgia Oliviero,^{*[a]} Nicola Borbone,^[a] Fabrizia Nici,^[a] Vincenzo Piccialli,^[b] Brunella Pinto,^[a] Daniele D'Alonzo,^[b] Luciano Mayol,^[a] and Gennaro Piccialli^[a]

Keywords: Synthetic methods / Grignard reaction / Transmetallation / Nucleosides / Nucleobases

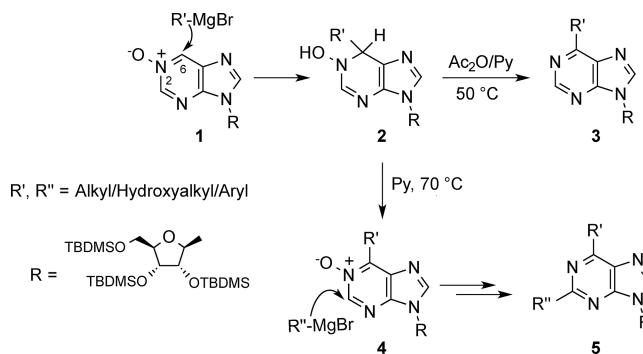
A general synthesis of C⁶-pyridylpurine nucleosides is described. The reported synthetic procedure exploits the regioselective addition of pyridinyl Grignard reagents, obtained by bromine/magnesium exchange between mono- or dihalopyridines and *i*PrMgCl, to the C6–N1–O[−] moiety of nebularine N¹-oxide. The regioselective transmetallation of

unsymmetrical dihalopyridines with *i*PrMgCl allowed C⁶-halopyridylpurine nucleosides to be obtained through the addition of halopyridinyl Grignard reagents. The presence of a halogenated pyridine ring in these nucleosides allows for further useful synthetic transformations.

Introduction

Natural nucleosides and nucleotides play a central role in cell metabolism and in signal transduction, acting as synthetic precursors and regulatory agents. In addition, they are substrates of polymerases and, in some cases, can control the activity of these enzymes so as to regulate nucleic acid construction. Several nucleoside and nucleotide analogues have been approved for the treatment of viral diseases and some of them are in clinical trials for cancer treatment.^[1] Therefore the preparation of modified nucleosides and nucleotides continues to attract the interest of chemical and biomedical research. Modifications of nucleobases can affect the hydrogen-bonding patterns and base-pairing in nucleic acids or confer on them peculiar properties such as fluorescence, which allows monitoring of their fate in cells and analysis of DNA and RNA structures.^[2] Purine nucleosides bearing a C substituent at C-6 represent an important subclass of nucleoside analogues possessing a broad spectrum of biological activities^[3] and this has prompted synthetic efforts towards these substances. The introduction of C substituents at C-6 in the purine nucleus has been mostly accomplished by metal-mediated cross-coupling processes starting from 6-halopurines,^[3b,4] whereas N, O, and S substituents have been introduced by direct nucleophilic aro-

matic substitution.^[5] We have recently discovered a new approach to accessing C⁶-alkyl/aryl nucleosides. In particular, we observed that the sugar-protected nebularine N¹-oxide^[6a] (**1**, Scheme 1) can regioselectively react with Grignard reagents at the more electrophilic C-6 position leading to adduct **2**, which is re-aromatized by treatment with Ac₂O/Py to furnish the C⁶-substituted purine nucleoside **3** in high yields. We have also shown that a second alkyl/aryl substituent can be introduced at C-2 by a similar strategy, that is, by the addition of a Grignard reagent to the C⁶-substituted nebularine N¹-oxides **4** through the opening/re-closing of the pyrimidine ring induced by the Grignard reagent itself. Through this approach we have synthesized new collections of 6-alkyl(aryl)purine nucleosides **3** and 2,6-di-alkyl(aryl)purine nucleosides **5**.^[6]



Scheme 1. Reaction of nebularine N¹-oxide **1** with Grignard reagents. Functionalization of the C-6 and C-2 positions of the purine.

C⁶-Pyridinyl nucleosides are appealing nucleoside analogues because the presence of a nitrogen atom in the C-6 residue can potentially alter the hydrogen-bonding capabilities of the nucleoside as well as promote its coordination to

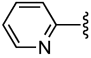
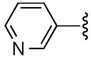
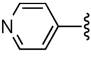
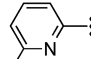
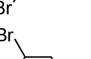
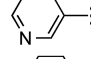
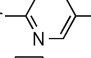
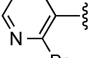
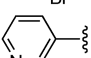
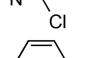
[a] Dipartimento di Farmacia, Università degli Studi di Napoli Federico II,
Via D. Montesano 49, 80131 Napoli, Italy
E-mail: golivier@unina.it
http://www.unina.it

[b] Dipartimento di Scienze Chimiche, Università degli Studi di Napoli Federico II,
Via Cinthia 4, 80126 Napoli, Italy

Supporting information for this article is available on the WWW under <http://dx.doi.org/10.1002/ejoc.201403648>.

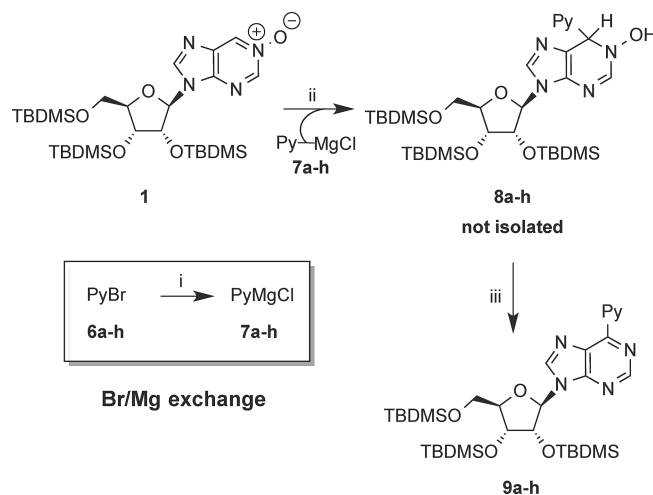
biologically important metals, such as platinum and ruthenium.^[7] In addition, a number of pharmaceuticals, natural products, and active products for agriculture are pyridine derivatives.^[8] However, the introduction of a pyridinyl residue at the C-6 position of purine nucleosides has scarcely been studied. As far as we know, the only known substances of this type are 6-(2-pyridyl)nebularine and the nucleotide corresponding to 6-(5-bromo-3-pyridyl)nebularine (see **9a** and **9e** in Table 1), both displaying interesting biological activities. These compounds were synthesized by the Pd-catalyzed cross-coupling of 6-chloropurine riboside with Rieke organozinc reagents^[9] and 5-bromopyridine-3-boronic acid,^[10] respectively. However, Hocek et al. reported the failure to introduce 3- and 4-pyridyl residues at C-6 by Suzuki–Miyaura coupling with the more reactive catalytic system Pd(OAc)₂/2-(dicyclohexylphosphanyl)biphenyl.^[11] These precedents and the lack of a general synthetic procedure for obtaining C⁶-pyridylpurine nucleosides prompted us to explore the addition of pyridinyl Grignard reagents **7a–h** (Scheme 2) to nebularine N¹-oxide (**1**) by using our procedure. We report here that it can be successfully applied to the synthesis of various C⁶-pyridinyl nucleosides **9a–c** and C⁶-halopyridinyl nucleosides **9d–h** (Table 1) in moderate-to-good yields.

 Table 1. Product yields of compounds **9a–j**.

PyBr	PyMgCl	Py	Product yields (%) from 1
6a	7a		9a (55%)
6b	7b		9b (60%)
6c	7c		9c (55%)
6d	7d		9d (50%)
6e	7e		9e (60%)
6f	7f		9f (55%)
6g	7g		9g (48%)
6h	7h		9h (65%)
6i	7i		9i (20%)
6j	7j		9j no reaction

Results and Discussion

The required pyridinyl Grignard reagents **7a–h** (Table 1) were prepared by bromine/magnesium exchange between bromopyridines **6a–h** and *i*PrMgCl (Scheme 2). This procedure has previously been efficiently employed by Trécourt et al. for the transmetalation of 2-, 3-, and 4-bromopyridines, as well as for the regioselective transmetalation of 2,3-, 2,5-, 2,6-, and 3,5-dibromopyridines to obtain various pyridinyl Grignard reagents.^[12] Our general strategy for the bromine/magnesium exchange makes use of a 1:1 ratio of *i*PrMgCl and bromopyridines **6a–h** (2 h at room temp.). The complexes **7a–h** (5 equiv.) obtained in this way were added in one portion to **1** and the reaction mixtures were left at room temp. for 2 h. After work-up (see the Exp. Sect.), the crude products **8a–h** were treated with Ac₂O/pyridine to form the purine rings **9a–h** by re-aromatization.



Scheme 2. Reagents and conditions: i) *i*PrMgCl, THF, 2 h, room temp., N₂; ii) **7a–h**, THF, 2 h, room temp., N₂; iii) Ac₂O/pyridine (4:6, v/v), 1 h, 50 °C.

Reactions of Bromopyridines **6a–c**

Following our procedure, the 2-pyridyl residue could be easily introduced at the C-6 purine position by the reaction of **1** with 2-pyridylmagnesium chloride (**7a**, Table 1), and compound **9a** was obtained in a yield higher than previously reported (55%, reported 27%).^[9] Compound **9b**, embodying a 3-pyridyl residue, was obtained by treating **1** with 3-pyridylmagnesium chloride (**7b**). The process proceeded smoothly and the product was obtained in 60% yield. In contrast, 4-bromopyridine (**6c**) is an unstable compound and has to be prepared immediately prior to use by neutralization of the corresponding hydrochloride salt (commercially available). Initially we used the recommended procedure in which the hydrochloride salt is treated with a 5% aqueous Na₂CO₃ solution, followed by extraction with Et₂O, and drying with MgSO₄.^[12] Disappointingly, 4-bromopyridine prepared in this way, when treated

with *i*PrMgCl, gave a very low yield of the corresponding Grignard reagent **7c**, as suggested by its unproductive reaction with **1**.

We ascribed this failure to the difficulty in obtaining very dry 4-bromopyridine after aqueous treatment and drying with MgSO₄. On the other hand, bromopyridine is a volatile liquid and it could not be dried effectively under reduced pressure. We succeeded in obtaining 4-bromopyridine suitable for the preparation of the Grignard reagent by treatment of its hydrochloride salt with 1 equiv. of NaH in dry THF. The pyridine **6c** obtained was transmetallated in situ by the addition of *i*PrMgCl to give the 4-bromopyridinyl Grignard reagent **7c**, which was immediately treated with **1**. By this procedure, compound **9c** was obtained in 55% yield, which compares well with the yields of **9a** and **9b**. Therefore the 3- and 4-pyridyl nucleosides **9b** and **9c** could be synthesized by our procedure, whereas the Suzuki–Miyaura coupling reaction was unsuccessful.^[11]

Reactions of Dihalopyridines 6d–h

Halopyridines are known to undergo a number of useful synthetic transformations.^[13] Therefore the introduction of a halopyridine ring at the C-6 position of a purine nucleoside would allow its further synthetic elaboration. Thus, dibromopyridines **6d–g** and the 2-chloro-3-bromopyridine (**6h**) were transmetallated with *i*PrMgCl, as described for bromopyridines **6a–6c**, to furnish the corresponding Grignard reagents **7d–h**. Bromopyridinyl nucleosides **9d** and **9e** were obtained from symmetrical dibromopyridines **6d** and **6e** in yields of 50 and 60%, respectively, on coupling with **1**. The fully ribose-deprotected compound **9e** was recently prepared by the reaction of 6-chloropurine riboside under Suzuki–Miyaura cross-coupling conditions in 40% yield. Interestingly, its nucleotide derivative was active towards human and rat DNHP1 enzymes, showing itself to be a competitive inhibitor of dGMP binding with a micromolar affinity.^[10]

Grignard reagents prepared in the usual manner from unsymmetrical 2,5- and 2,3-dibromopyridines **6f** and **6g** and used in the coupling/aromatization sequence afforded compounds **9f** and **9g**, respectively, which were analyzed by 2D NMR experiments. In particular, the correlations observed in the HMBC spectrum of **9f** between the 2''-H and 4''-H protons of the pyridine ring, which resonate at δ = 10.2 and 8.86 ppm, respectively, and C-6 at δ = 152.2 ppm of the purine nucleus (Figure 1) clearly indicate the formation of the C3''–C6 bond during the coupling step. This confirms the expected preferential transmetallation at C-5 of the 2,5-dibromopyridine ring. On the other hand, in the case of compound **9g**, a significant correlation in the HMBC spectrum was seen between the 4''-H proton at δ = 8.00 ppm and the C-6 purine carbon at δ = 156.5 ppm (Figure 1), which indicates the connection C3''–C6 in this compound and, accordingly, confirms the preferential transmetallation at C-3 of the 2,3-dibromopyridine ring.

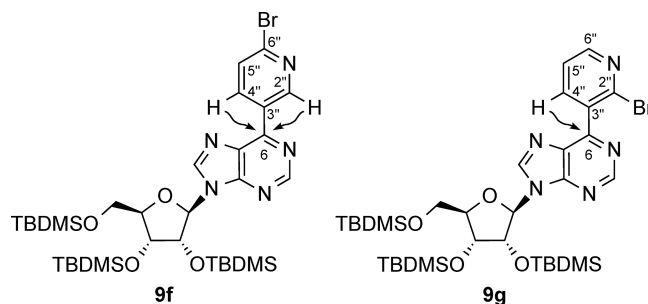


Figure 1. HMBC correlations between 4''-H, 2''-H and C-6 for **9f** and 4''-H and C-6 for **9g**.

In addition, we tested the preparation and reactivity of the Grignard reagent **7h** obtained from 3-bromo-2-chloropyridine (**6h**). The transmetallation of the latter proved to be chemoselective giving the 2-chloro-3-pyridinyl Grignard reagent and then compound **9h**, which was obtained in 65% yield on reaction with **1**. In an attempt to further expand the scope of the process and access new C⁶-heteroaryl nucleosides, we tested the introduction at this position of a quinolyl residue. Purine ribonucleosides bearing a quinoline ring at C-6 are unprecedented. Application of the strategy used for bromopyridines was initially attempted and the required Grignard reagents were prepared in the usual manner by treating 2-bromoquinoline (**6i**) and 3-bromoquinoline (**6j**) with *i*PrMgCl (1 equiv.). However, the subsequent reaction with **1** gave complex reaction mixtures from which the expected C⁶-quinolyl derivative **9i** was obtained in 20% yield after purification, whereas no compound corresponding to **9j** could be recovered. We attributed these unsatisfactory results to the low-yielding formation or the absence of any formation of Grignard reagents **7i** and **7j**, respectively. In fact, it is reported that bromoquinolines preferably undergo nucleophilic attack at C–Br rather than transmetallation due to the low energy of their LUMO levels.^[14] An alternative approach to the use of quinolyl Grignard reagents exploits the reactivity of lithium tri(quinolyl)magnesium complexes, obtained by the transmetallation reaction of lithium tributylmagnesium and 2- or 3-bromoquinolines, a procedure reported to yield C-functionalized quinolones.^[14] Disappointingly, by using this procedure (data not shown), we could not improve on the yield of compound **9i**, and again the formation of compound **9j** was not observed in this case. The structures of all the synthesized compounds were ascertained by spectroscopic investigations (¹H and ¹³C NMR, UV, IR, and MS data).

Conclusions

In this paper we describe the synthesis of a collection of C⁶-pyridylpurine ribonucleosides exploiting the electrophilicity of the C-6 purine position of the sugar-protected nebularine N¹-oxide towards a series of pyridinyl Grignard reagents, prepared by transmetallation reactions between *i*PrMgCl and mono- and dihalopyridines. The bromine/magnesium exchange reactions proved to be regioselective

when using unsymmetrical dihalopyridines, allowing bromo- and chloropyridylpurine nucleosides to be obtained. The presence of a halogen atom on the pyridinyl residue in the latter allows for further synthetic elaborations towards more diverse substituted nucleosides. An attempt to extend the synthetic strategy to the preparation of unprecedented C⁶-quinolylpurine nucleosides was also made by using 2- and 3-bromoquinolines; a C⁶-(2-quinolyl)purine nucleoside was obtained, but in a low yield. This result, although unsatisfactory, is promising and prompts further efforts towards the synthesis of this type of substance. Studies are ongoing in our laboratories both towards this goal and to explore the reactivity of the halogenated pyridine ring in the newly prepared nucleosides.

Experimental Section

General Methods: All the reagents were obtained from commercial sources (Sigma–Aldrich) and were used without further purification. ¹H and ¹³C NMR spectra were acquired with a Varian Mercury Plus 400 MHz spectrometer in CD₃OD or C₆D₆. Chemical shifts (δ) are reported in parts per million (ppm) relative to the residual solvent signals: CD₂HOD 3.31 ppm, C₆D₅H 7.15 ppm for ¹H NMR; CD₃OD 49.0 ppm, C₆D₅H 128.6 ppm for ¹³C NMR. The ¹H NMR chemical shifts were assigned on the basis of 2D NMR experiments. The abbreviations s, d, dd, and m represent singlet, doublet, doublet of doublets, and multiplet, respectively. UV spectra were recorded with a Jasco V-530 UV spectrophotometer. High-resolution MS spectra were recorded with a Bruker APEX II FT-ICR mass spectrometer using the electrospray ionization (ESI) technique in positive mode. IR spectra were recorded with a Jasco FT-IR 430 spectrophotometer. Optical rotations were determined with a Jasco polarimeter using a 1-dm cell at 25 °C; concentrations are given in g/100 mL. Column chromatography was performed on silica gel 60 (70–230 mesh ASTM, Merck) and analytical TLC analyses were performed on F₂₅₄ silica gel plates (0.2 mm thick, Merck) with TLC spots being detected under UV light (254 nm).

General Procedure for the Reaction of 1 with Grignard Reagents 7a–i. Synthesis of 9a–i: In a representative experiment, *i*PrMgCl (0.12 mL, 0.24 mmol) was added to 2-bromopyridine (**6a**; 0.023 mL, 0.24 mmol) in dry THF (0.5 mL) at room temperature under nitrogen. After 2 h, **1** (30 mg, 0.049 mmol) dissolved in dry THF (0.5 mL) was added to the reaction mixture, which was then stirred for a further 2 h (TLC monitoring: hexane/AcOEt, 3:7) at room temperature. The reaction was then quenched by the addition of a 1 M solution of NH₄Cl (1 mL), diluted with AcOEt (10 mL), and washed with brine (10 mL). The organic layer was separated, dried (Na₂SO₄), filtered, and concentrated under rotary evaporation. The crude **8a** was dissolved in a mixture of Ac₂O/pyridine (4:6, 0.5 mL) and the solution kept at 50 °C for 1 h (TLC monitoring: AcOEt/MeOH, 9.5:0.5). The mixture was evaporated in vacuo and purified on a column of silica gel eluted with increasing amounts of MeOH in AcOEt (up to 5%). The fractions containing the product were collected and evaporated to afford pure **9a**.

2',3',5'-Tri-*O*-(*tert*-butyldimethylsilyl)-6-(3-pyridyl)nebularine (9b): TLC monitoring (hexane/AcOEt, 1:1), purification through a column of silica gel eluted with increasing amounts of AcOEt in hexane (up to 30%). Amorphous solid (19 mg, 60%). [*a*]_D = −42.0 (*c* = 1.1, CH₃OH). ¹H NMR (400 MHz, CD₃OD): δ = 9.92–9.88 (m, 1 H, arom.), 9.18–9.13 (m, 1 H, arom.), 9.0 (s, 1 H, 2-H), 8.75 (s,

1 H, 8-H), 8.72–8.69 (m, 1 H, arom.), 7.69–7.63 (m, 1 H, arom.), 6.21 (d, *J* = 5.6 Hz, 1 H, 1'-H), 4.95–4.90 (m, 1 H, 2'-H), 4.49–4.44 (m, 1 H, 3'-H), 4.20–4.15 (m, 1 H, 4'-H), 4.09 (dd, *J* = 11.3, 4.6 Hz, 1 H, 5'-H_a), 3.87 (dd, *J* = 11.3, 3.1 Hz, 1 H, 5'-H_b), 0.98 [s, 9 H, C(CH₃)₃], 0.96 [s, 9 H, C(CH₃)₃], 0.78 [s, 9 H, C(CH₃)₃], 0.18 (s, 3 H, CH₃), 0.17 (s, 3 H, CH₃), 0.16 (s, 6 H, 2 CH₃), −0.016 (s, 3 H, CH₃), −0.28 (s, 3 H, CH₃) ppm. ¹³C NMR (100 MHz, CD₃OD): δ = 153.8, 153.5, 152.9, 151.9, 151.3, 146.4, 138.9, 133.2, 132.9, 125.3, 89.6, 87.4, 77.1, 73.7, 63.8, 26.6, 26.4, 26.2, 19.4, 18.9, 18.7, −4.1, −4.2, −4.3, −4.9, −5.2, −5.3 ppm. IR (neat): *v*_{max} = 2950, 2923, 2857, 1577, 1465, 1320, 1256, 1127, 834, 779 cm^{−1}. UV (CH₃OH): *λ*_{max} = 288 nm. HRMS (ESI): calcd. for C₃₃H₅₈N₅O₄Si₃ [*M* + *H*]⁺ 672.3797; found 672.3794.

2',3',5'-Tri-*O*-(*tert*-butyldimethylsilyl)-6-(4-pyridyl)nebularine (9c): 4-Bromopyridine hydrochloride (47 mg, 0.24 mmol) was suspended in dry THF (1 mL) under nitrogen and the mixture cooled to 0 °C. NaH (5.8 mg, 0.24 mmol) was added in one portion and the mixture stirred for 15 min. After warming to room temp., *i*PrMgCl (0.12 mL, 0.24 mmol) was added as for **6a**. TLC monitoring (hexane/AcOEt, 6:4), purification through a column of silica gel eluted with increasing amounts of AcOEt in hexane (up to 30%). Amorphous solid (18 mg, 55%). [*a*]_D = −34.3 (*c* = 0.5, CH₃OH). ¹H NMR (400 MHz, CD₃OD): δ = 9.06 (s, 1 H, 2-H), 8.81–8.74 (complex signal, 5 H, 4 arom.), 8-H), 6.22 (d, *J* = 5.6 Hz, 1 H, 1'-H), 4.95–4.91 (m, 1 H, 2'-H), 4.49–4.45 (m, 1 H, 3'-H), 4.20–4.17 (m, 1 H, 4'-H), 4.09 (dd, *J* = 11.4, 4.5 Hz, 1 H, 5'-H_a), 3.88 (dd, *J* = 11.3, 2.9 Hz, 1 H, 5'-H_b), 0.99 [s, 9 H, C(CH₃)₃], 0.97 [s, 9 H, C(CH₃)₃], 0.79 [s, 9 H, C(CH₃)₃], 0.19 (s, 3 H, CH₃), 0.17 (s, 3 H, CH₃), 0.16 (s, 6 H, 2 CH₃), −0.009 (s, 3 H, CH₃), −0.28 (s, 3 H, CH₃) ppm. ¹³C NMR (100 MHz, CD₃OD): δ = 154.2, 153.4, 152.6, 150.8, 146.9, 144.9, 133.5, 125.0, 89.7, 87.4, 77.1, 73.7, 63.8, 26.6, 26.4, 26.2, 19.4, 18.9, 18.7, −4.1, −4.3, −4.9, −5.2, −5.3 ppm. IR (neat): *v*_{max} = 2956, 2923, 2851, 1569, 1412, 1254, 1091, 793 cm^{−1}. UV (CH₃OH): *λ*_{max} = 290 nm. HRMS (ESI): calcd. for C₃₃H₅₈N₅O₄Si₃ [*M* + *H*]⁺ 672.3797; found 672.3792.

2',3',5'-Tri-*O*-(*tert*-butyldimethylsilyl)-6-(6-bromo-2-pyridyl)nebularine (9d): TLC monitoring (CH₂Cl₂/AcOEt, 95:5), purification through a column of silica gel eluted with increasing amounts of AcOEt in CH₂Cl₂ (up to 5%). Oil (18 mg, 50%). [*a*]_D = −36.7 (*c* = 1.1, CH₃OH). ¹H NMR (400 MHz, CD₃OD): δ = 9.0 (s, 1 H, 2-H), 8.88–8.84 (m, 1 H, arom.), 8.79 (s, 1 H, 8-H), 7.97–7.90 (m, 1 H, arom.), 7.80–7.75 (m, 1 H, arom.), 6.22 (d, *J* = 5.7 Hz, 1 H, 1'-H), 4.95–4.90 (m, 1 H, 2'-H), 4.48–4.44 (m, 1 H, 3'-H), 4.20–4.15 (m, 1 H, 4'-H), 4.08 (dd, *J* = 11.3, 4.5 Hz, 1 H, 5'-H_a), 3.87 (dd, *J* = 11.3, 2.9 Hz, 1 H, 5'-H_b), 0.98 [s, 9 H, C(CH₃)₃], 0.95 [s, 9 H, C(CH₃)₃], 0.78 [s, 9 H, C(CH₃)₃], 0.17 (s, 3 H, CH₃), 0.16 (s, 3 H, CH₃), 0.15 (s, 6 H, 2 CH₃), −0.021 (s, 3 H, CH₃), −0.29 (s, 3 H, CH₃) ppm. ¹³C NMR (100 MHz, CD₃OD): δ = 154.8, 154.4, 153.4, 147.1, 143.6, 141.0, 133.1, 131.3, 126.8, 89.7, 87.5, 77.1, 73.7, 63.8, 26.6, 26.4, 26.2, 19.4, 19.0, 18.7, −4.1, −4.3, −4.9, −5.2 ppm. HRMS (ESI): calcd. for C₃₃H₅₇BrN₅O₄Si₃ [*M* + *H*]⁺ 750.2902; found 750.2907. IR (neat): *v*_{max} = 2956, 2928, 2857, 1566, 1429, 1256, 1072, 834, 790 cm^{−1}. UV (CH₃OH): *λ*_{max} = 304 nm.

2',3',5'-Tri-*O*-(*tert*-butyldimethylsilyl)-6-(5-bromo-3-pyridyl)nebularine (9e): TLC monitoring (hexane/AcOEt, 8:2), purification through a column of silica gel eluted with increasing amounts of AcOEt in hexane (up to 10%). Oil (22 mg, 60%). [*a*]_D = −41.6 (*c* = 0.7, CH₂Cl₂). ¹H NMR (400 MHz, C₆D₆): δ = 10.48–10.46 (m, 1 H, arom.), 9.49–9.46 (m, 1 H, arom.), 8.96 (s, 1 H, 2-H), 8.71–8.68 (m, 1 H, arom.), 8.37 (s, 1 H, 8-H), 6.22 (d, *J* = 4.4 Hz, 1 H, 1'-H), 4.95–4.90 (m, 1 H, 2'-H), 4.55–4.50 (m, 1 H, 3'-H), 4.29–4.24 (m, 1 H, 4'-H), 4.01 (dd, *J* = 11.4, 4.2 Hz, 1 H, 5'-H_a), 3.72

(dd, $J = 11.4, 2.6$ Hz, 1 H, 5'-H_b), 1.00 [s, 9 H, C(CH₃)₃], 0.96 [s, 9 H, C(CH₃)₃], 0.91 [s, 9 H, C(CH₃)₃], 0.13 (s, 3 H, CH₃), 0.12 (s, 3 H, CH₃), 0.094 (s, 3 H, CH₃), 0.078 (s, 3 H, CH₃), 0.048 (s, 3 H, CH₃), -0.082 (s, 3 H, CH₃) ppm. ¹³C NMR (100 MHz, C₆D₆): $\delta = 153.4, 153.2, 152.9, 151.7, 150.4, 144.9, 139.7, 134.1, 133.1, 121.7, 89.9, 85.9, 76.6, 72.5, 62.9, 26.8, 26.6, 26.5, 19.2, 18.9, 18.7, -3.6, -3.9, -4.0, -4.1, -4.7, -4.8$ ppm. IR (neat): $\nu_{\text{max}} = 2956, 2923, 2857, 1580, 1459, 1325, 1256, 1105, 834, 779$ cm⁻¹. UV (CH₃OH): $\lambda_{\text{max}} = 302$ nm. HRMS (ESI): calcd. for C₃₃H₅₇BrN₅O₄Si₃ [M + H]⁺ 750.2902; found 750.2898.

2',3',5'-Tri-*O*-(*tert*-butyldimethylsilyl)-6-(6-bromo-3-pyridyl)nebularine (9f): TLC monitoring (hexane/AcOEt, 85:15), purification through a column of silica gel eluted with increasing amounts of AcOEt in hexane (up to 10%). Amorphous solid (20 mg, 55%). [α]_D = -41.3 ($c = 0.6$, CH₂Cl₂). ¹H NMR (400 MHz, C₆D₆): $\delta = 10.2$ (d, $J = 2.2$ Hz, 1 H, arom.), 8.92 (s, 1 H, 2-H), 8.86 (dd, $J = 8.4, 2.4$ Hz, 1 H, arom.), 8.35 (s, 1 H, 8-H), 7.03 (d, $J = 8.4$ Hz, 1 H, arom.), 6.20 (d, $J = 4.2$ Hz, 1 H, 1'-H), 4.88–4.83 (m, 1 H, 2'-H), 4.51–4.46 (m, 1 H, 3'-H), 4.25–4.20 (m, 1 H, 4'-H), 3.96 (dd, $J = 11.5, 4.1$ Hz, 1 H, 5'-H_a), 3.68 (dd, $J = 11.4, 2.5$ Hz, 1 H, 5'-H_b), 0.96 [s, 9 H, C(CH₃)₃], 0.93 [s, 9 H, C(CH₃)₃], 0.88 [s, 9 H, C(CH₃)₃], 0.075 (s, 3 H, CH₃), 0.067 (s, 3 H, CH₃), 0.059 (s, 3 H, CH₃), 0.043 (s, 3 H, CH₃), 0.013 (s, 3 H, CH₃), -0.10 (s, 3 H, CH₃) ppm. ¹³C NMR (100 MHz, C₆D₆): $\delta = 153.1, 153.0, 152.8, 152.2, 145.8, 144.7, 139.6, 132.9, 131.7, 128.5, 89.9, 85.8, 76.6, 72.4, 62.8, 26.8, 26.6, 26.5, 19.3, 18.9, 18.7, -3.6, -3.9, -4.0, -4.7, -4.8$ ppm. IR (neat): $\nu_{\text{max}} = 2950, 2923, 2851, 1580, 1459, 1322, 1256, 1072, 834, 773$ cm⁻¹. UV (CH₃OH): $\lambda_{\text{max}} = 299$ nm. HRMS (ESI): calcd. for C₃₃H₅₇BrN₅O₄Si₃ [M + H]⁺ 750.2902; found 750.2910.

2',3',5'-Tri-*O*-(*tert*-butyldimethylsilyl)-6-(2-bromo-3-pyridyl)nebularine (9g): TLC monitoring (hexane/AcOEt, 7:3), purification through a column of silica gel eluted with increasing amounts of AcOEt in hexane (up to 25%). Oil (18 mg, 48%). [α]_D = -32.1 ($c = 0.7$, CH₃OH). ¹H NMR (400 MHz, CD₃OD): $\delta = 9.05$ (s, 1 H, 2-H), 8.76 (s, 1 H, 8-H), 8.54 (dd, $J = 4.8, 1.8$ Hz, 1 H, arom.), 8.00 (dd, $J = 7.6, 1.8$ Hz, 1 H, arom.), 7.63 (dd, $J = 7.6, 4.9$ Hz, 1 H, arom.), 6.23 (d, $J = 5.9$ Hz, 1 H, 1'-H), 4.95–4.90 (m, 1 H, 2'-H), 4.48–4.43 (m, 1 H, 3'-H), 4.22–4.16 (m, 1 H, 4'-H), 4.08 (dd, $J = 11.3, 4.7$ Hz, 1 H, 5'-H_a), 3.88 (dd, $J = 11.3, 3.0$ Hz, 1 H, 5'-H_b), 0.98 [s, 9 H, C(CH₃)₃], 0.95 [s, 9 H, C(CH₃)₃], 0.78 [s, 9 H, C(CH₃)₃], 0.18 (s, 3 H, CH₃), 0.16 (s, 3 H, CH₃), 0.15 (s, 6 H, 2 CH₃), -0.012 (s, 3 H, CH₃), -0.29 (s, 3 H, CH₃) ppm. ¹³C NMR (100 MHz, CD₃OD): $\delta = 156.5, 153.4, 153.2, 152.1, 147.1, 141.9, 141.3, 135.2, 133.6, 124.3, 89.7, 87.8, 77.2, 73.9, 63.9, 26.6, 26.4, 26.2, 19.4, 19.0, 18.8, -4.1, -4.2, -4.3, -4.8, -5.2, -5.3$ ppm. IR (neat): $\nu_{\text{max}} = 2956, 2923, 2857, 1594, 1462, 1391, 1253, 1163, 1108, 834, 774$ cm⁻¹. UV (CH₃OH): $\lambda_{\text{max}} = 272$ nm. HRMS (ESI): calcd. for C₃₃H₅₇BrN₅O₄Si₃ [M + H]⁺ 750.2902; found 750.2911.

2',3',5'-Tri-*O*-(*tert*-butyldimethylsilyl)-6-(2-chloro-3-pyridyl)nebularine (9h): TLC monitoring (hexane/AcOEt, 7:3), purification through a column of silica gel eluted with increasing amounts of AcOEt in hexane (up to 25%). Oil (22 mg, 65%). [α]_D = -28.0 ($c = 0.8$, CH₂Cl₂). ¹H NMR (400 MHz, C₆D₆): $\delta = 9.12$ (s, 1 H, 2-H), 8.34 (s, 1 H, 8-H), 8.04 (dd, $J = 4.8, 1.9$ Hz, 1 H, arom.), 7.76 (dd, $J = 7.6, 1.9$ Hz, 1 H, arom.), 6.51 (dd, $J = 7.5, 4.8$ Hz, 1 H, arom.), 6.24 (d, $J = 4.5$ Hz, 1 H, 1'-H), 4.99–4.94 (m, 1 H, 2'-H), 4.57–4.52 (m, 1 H, 3'-H), 4.30–4.25 (m, 1 H, 4'-H), 4.03 (dd, $J = 11.4, 4.4$ Hz, 1 H, 5'-H_a), 3.74 (dd, $J = 11.4, 2.7$ Hz, 1 H, 5'-H_b), 1.01 [s, 9 H, C(CH₃)₃], 0.94 [s, 9 H, C(CH₃)₃], 0.91 [s, 9 H, C(CH₃)₃], 0.13 (s, 3 H, CH₃), 0.12 (s, 3 H, CH₃), 0.076 (s, 6 H, 2 CH₃), 0.064 (s, 3 H, CH₃), 0.039 (s, 3 H, CH₃), -0.087 (s, 3 H, CH₃) ppm. ¹³C NMR (100 MHz, CD₃OD): $\delta = 155.8, 153.1, 152.8,$

151.2, 150.9, 145.1, 141.1, 134.3, 132.3, 122.4, 89.9, 86.0, 76.6, 72.6, 63.0, 26.8, 26.6, 26.5, 19.2, 18.9, 18.7, -3.6, -3.9, -4.0, -4.2, -4.7, -4.8 ppm. IR (neat): $\nu_{\text{max}} = 2956, 2923, 2857, 1591, 1462, 1399, 1328, 1254, 1064, 834, 774$ cm⁻¹. UV (CH₃OH): $\lambda_{\text{max}} = 273$ nm. HRMS (ESI): calcd. for C₃₃H₅₇ClN₅O₄Si₃ [M + H]⁺ 706.3407; found 706.3412.

2',3',5'-Tri-*O*-(*tert*-butyldimethylsilyl)-6-(2-quinolyl)nebularine (9i): TLC monitoring (hexane/AcOEt, 7:3), purification through a column of silica gel eluted with increasing amounts of AcOEt in hexane (up to 30%). Oil (7.1 mg, 20%). [α]_D = -39.5 ($c = 0.5$, CH₃OH). ¹H NMR (400 MHz, CD₃OD): $\delta = 9.14$ (s, 1 H, 2-H), 8.88–8.81 (complex signal, 2 H, arom., 8-H), 8.59–8.54 (m, 1 H, arom.), 8.39–8.37 (m, 1 H, arom.), 8.05–8.03 (m, 1 H, arom.), 7.87–7.83 (m, 1 H, arom.), 7.72–7.68 (m, 1 H, arom.), 6.27 (d, $J = 5.8$ Hz, 1 H, 1'-H), 5.00–4.95 (m, 1 H, 2'-H), 4.51–4.46 (m, 1 H, 3'-H), 4.22–4.18 (m, 1 H, 4'-H), 4.11 (dd, $J = 11.3, 4.7$ Hz, 1 H, 5'-H_a), 3.90 (dd, $J = 11.3, 3.1$ Hz, 1 H, 5'-H_b), 0.99 [s, 9 H, C(CH₃)₃], 0.97 [s, 9 H, C(CH₃)₃], 0.79 [s, 9 H, C(CH₃)₃], 0.19 (s, 3 H, CH₃), 0.18 (s, 3 H, CH₃), 0.17 (s, 6 H, 2 CH₃), -0.003 (s, 3 H, CH₃), -0.27 (s, 3 H, CH₃) ppm. ¹³C NMR (100 MHz, CD₃OD): $\delta = 154.6, 154.5, 154.4, 153.5, 149.4, 147.1, 138.5, 133.4, 131.4, 130.8, 130.1, 129.2, 128.9, 123.5, 89.7, 87.6, 77.1, 73.9, 63.9, 26.6, 26.4, 26.2, 19.4, 19.0, 18.8, -4.1, -4.3, -4.8, -5.1, -5.2$ ppm. IR (neat): $\nu_{\text{max}} = 2956, 2923, 2857, 1572, 1459, 1377, 1256, 1072, 834, 779$ cm⁻¹. UV (CH₃OH): $\lambda_{\text{sh}} = 243, 257$ nm. HRMS (ESI): calcd. for C₃₇H₆₀N₅O₄Si₃ [M + H]⁺ 722.3953; found 722.3960.

Supporting Information (see footnote on the first page of this article): ¹H and ¹³C NMR spectra of all new compounds.

Acknowledgments

This work was supported by the Compagnia di San Paolo Foundation (Progetto FARO 2011, Finanziamento per l'Avvio di Ricerche Originali). The authors are grateful to Dr. Luisa Cuorvo and Dr. Andrea De Fortis Nadi for their technical assistance and to the Centro di Servizio Interdipartimentale di Analisi Strutturale (CSIAS) for the NMR facilities.

- [1] a) L. P. Jordheim, D. Durantel, F. Zoulim, C. Dumontet, *Nat. Rev. Drug Discovery* **2013**, *12*, 447–464; b) E. De Clercq, *Nat. Rev. Drug Discovery* **2002**, *1*, 13–25; c) D. Komiotis, S. Manta, E. Tsoukala, N. Tzioumaki, *Curr. Med. Chem. Anti-Infect. Agents* **2008**, *7*, 219–244; d) C. M. Galmari, J. R. Mackey, C. Dumontet, *Lancet Oncol.* **2002**, *3*, 415–424.
- [2] a) D. A. Malyshev, K. Dhami, T. Laverne, T. Chen, N. Dai, J. M. Foster, I. R. Corrêa, F. E. Romesberg, *Nature* **2014**, *509*, 385–388; b) D. Dziuba, V. Y. Postupalenko, M. Spadafora, A. S. Klymchenko, V. Guérineau, Y. Mély, R. Benhida, A. Burger, *J. Am. Chem. Soc.* **2012**, *134*, 10209–10213; c) G. Oliviero, S. D'Errico, N. Borbone, J. Amato, V. Piccialli, G. Piccialli, L. Mayol, *Eur. J. Org. Chem.* **2010**, *8*, 1517–1524; d) S. D'Errico, G. Oliviero, N. Borbone, J. Amato, V. Piccialli, M. Varra, L. Mayol, G. Piccialli, *Molecules* **2011**, *16*, 8110–8118; e) S. D'Errico, G. Oliviero, N. Borbone, J. Amato, D. D'Alonzo, V. Piccialli, L. Mayol, G. Piccialli, *Molecules* **2012**, *17*, 13036–13044; f) S. D'Errico, G. Oliviero, N. Borbone, J. Amato, V. Piccialli, M. Varra, L. Mayol, G. Piccialli, *Molecules* **2013**, *18*, 9420–9431; g) L. Zilbershtein, A. Silberman, B. Fischer, *Org. Biomol. Chem.* **2011**, *9*, 7763–7773; h) A. A. Tanpure, M. G. Pawar, S. G. Srivatsan, *Isr. J. Chem.* **2013**, *53*, 366–378; i) A. Dumas, N. W. Luedtke, *Chem. Eur. J.* **2012**, *18*, 245–254; j) G. Mata, N. W. Luedtke, *J. Org. Chem.* **2012**, *77*, 9006–9017.
- [3] a) M. Hocek, P. Nauš, R. Pohl, I. Votruba, P. Furman, P. Tharnish, M. Otto, *J. Med. Chem.* **2005**, *48*, 5869–5873; b)

- A. E. A. Hassan, R. A. I. Abou-Elkhair, J. M. Riordan, P. W. Allan, W. B. Parker, R. Khare, W. R. Waud, J. A. Montgomery, J. A. Secrist III, *Eur. J. Med. Chem.* **2012**, *47*, 167–174; c) Y. Ding, J.-L. Girardet, Z. Hong, V. C. H. Lai, H. An, Y.-H. Koh, S. Z. Shaw, W. Zhong, *Bioorg. Med. Chem. Lett.* **2005**, *15*, 709–713; d) L. L. Gundersen, J. Nissen-Meyer, B. Spilberg, *J. Med. Chem.* **2002**, *45*, 1383–1386.
- [4] a) L. A. Agrofoglio, I. Gillaizeau, Y. Saito, *Chem. Rev.* **2003**, *103*, 1875–1916; b) M. Lakshman, J. Hilmer, J. Martin, J. Kee-ler, Y. Dinh, F. Ngassa, L. Russon, *J. Am. Chem. Soc.* **2001**, *123*, 7779–7787; c) L. Gundersen, A. K. Bakkestuen, A. J. Aasen, *Tetrahedron* **1994**, *50*, 9743–9756; d) M. Hocek, *Eur. J. Org. Chem.* **2003**, 245–254.
- [5] a) E. Véliz, P. Beal, *J. Org. Chem.* **2001**, *66*, 8592–8598; b) H. P. Kokatla, M. K. Lakshman, *Org. Lett.* **2010**, *12*, 4478–4481.
- [6] a) S. D’Errico, V. Piccialli, G. Oliviero, N. Borbone, J. Amato, V. D’Atri, G. Piccialli, *Tetrahedron* **2011**, *67*, 6138–6144; b) S. D’Errico, G. Oliviero, J. Amato, N. Borbone, V. Cerullo, A. Hemminki, V. Piccialli, S. Zaccaria, L. Mayol, G. Piccialli, *Chem. Commun.* **2012**, *48*, 9310–9312; c) S. D’Errico, G. Oliviero, N. Borbone, V. Piccialli, V. D’Atri, L. Mayol, G. Piccialli, *Eur. J. Org. Chem.* **2013**, 6948–6954.
- [7] a) M. Coluccia, A. Boccarelli, C. Cermelli, M. Portolani, G. Natile, *Met.-Based Drugs* **1995**, *2*, 249–256; b) S. D’Errico, G. Oliviero, N. Borbone, V. Piccialli, B. Pinto, F. De Falco, M. C. Maiuri, R. Carnuccio, V. Costantino, F. Nici, G. Piccialli, *Molecules* **2014**, *19*, 9339–9353; c) S. D’Errico, G. Oliviero, V. Piccialli, J. Amato, N. Borbone, V. D’Atri, F. D’Alessio, R. Di Noto, F. Ruffo, F. Salvatore, G. Piccialli, *Bioorg. Med. Chem. Lett.* **2011**, *21*, 5835–5838; d) D. Montesarchio, G. Mangiapia, G. Vitiello, D. Musumeci, C. Irace, R. Santamaria, G. D’Errico, L. Paduano, *Dalton Trans.* **2013**, *42*, 16697–16708.
- [8] a) A. E. Goetz, N. K. Garg, *Nat. Chem.* **2013**, *5*, 54–60; b) M. Baumann, I. R. Baxendale, *Beilstein J. Org. Chem.* **2013**, *9*, 2265–2319.
- [9] M. Hocek, A. Holý, I. Votruba, H. Dvořáková, *Collect. Czech Chem. C* **2001**, *66*, 483–499.
- [10] C. Amiable, J. Paoletti, A. Haouz, A. Padilla, G. Labesse, P. A. Kaminski, S. Pochet, *Eur. J. Med. Chem.* **2014**, *85*, 418–437.
- [11] M. Hocek, P. Nauš, R. Pohl, I. Votruba, P. Furman, P. Tharnish, M. Otto, *J. Med. Chem.* **2005**, *48*, 5869–5873.
- [12] F. Trécourt, G. Breton, V. Bonnet, F. Mongin, F. Marsais, G. Quéguiner, *Tetrahedron* **2000**, *56*, 1349–1360.
- [13] a) F. Marsais, F. Trécourt, P. Bréant, G. Quéguiner, *J. Heterocycl. Chem.* **1988**, *25*, 81–87; b) S. V. Amosova, G. M. Gavrilova, *Russ. J. Org. Chem.* **2004**, *40*, 1657–1661; c) C. Gosmini, C. Bassene-Ernst, M. Durandetti, *Tetrahedron* **2009**, *65*, 6141–6146; d) S. Gamsey, A. Miller, M. M. Olmstead, C. M. Beavers, L. C. Hirayama, S. Pradhan, R. A. Wessling, B. Singaram, *J. Am. Chem. Soc.* **2007**, *129*, 1278–1286; e) S. Zhang, L.-Y. Liao, F. Zhang, X. F. Duan, *J. Org. Chem.* **2013**, *78*, 2720–2725; f) P. S. Fier, J. F. Hartwig, *Science* **2013**, *342*, 956–960; g) G. D. Henry, *Tetrahedron* **2004**, *60*, 6043–6061; h) M. Schlosser, F. Mongin, *Chem. Soc. Rev.* **2007**, *36*, 1161–1172.
- [14] S. Dumouchel, F. Mongin, F. Trécourt, G. Queguiner, *Tetrahedron Lett.* **2003**, *44*, 2033–2035.

Received: December 18, 2014

Published Online: February 19, 2015

Article

Synthesis and Pharmacological Evaluation of Modified Adenosines Joined to Mono-Functional Platinum Moieties

Stefano D’Errico ¹, Giorgia Oliviero ^{1,*}, Nicola Borbone ¹, Vincenzo Piccialli ², Brunella Pinto ¹, Francesca De Falco ¹, Maria Chiara Maiuri ^{1,3}, Rosa Carnuccio ¹, Valeria Costantino ¹, Fabrizia Nici ¹ and Gennaro Piccialli ¹

¹ Dipartimento di Farmacia, Università degli Studi di Napoli “Federico II”, via D. Montesano, 49, 80131 Napoli, Italy; E-Mails: stefano.derrico@unina.it (S.D.); borbone@unina.it (N.B.); brunella.pinto87@gmail.com (B.P.); francesca.defalco@unina.it (F.D.F.); mariachiara.maiuri@unina.it (M.C.M.); rosa.carnuccio@unina.it (R.C.); valeria.costantino@unina.it (V.C.); fabrizia.nici@unina.it (F.N.); picciall@unina.it (G.P.)

² Dipartimento di Scienze Chimiche, Università degli Studi di Napoli “Federico II”, via Cintia, 21, 80126 Napoli, Italy; E-Mail: vinpicci@unina.it

³ INSERM U848, IGR, 39 rue C. Desmoulins, 94805 Villejuif, France

* Author to whom correspondence should be addressed; E-Mail: golivier@unina.it; Tel.: +39-081-679-896.

Received: 26 March 2014; in revised form: 23 June 2014 / Accepted: 25 June 2014 /

Published: 3 July 2014

Abstract: The synthesis of four novel platinum complexes, bearing N^6 -(6-amino-hexyl)adenosine or a 1,6-di(adenosin- N^6 -yl)-hexane respectively, as ligands of mono-functional cisplatin or monochloro(ethylendiamine)platinum(II), is reported. The chemistry exploits the high affinity of the charged platinum centres towards the N7 position of the adenosine base system and a primary amine of an alkyl chain installed on the C6 position of the purine. The cytotoxic behaviour of the synthesized complexes has been studied in A549 adenocarcinomic human alveolar basal epithelial and MCF7 human breast adenocarcinomic cancer cell lines, in order to investigate their effects on cell viability and proliferation.

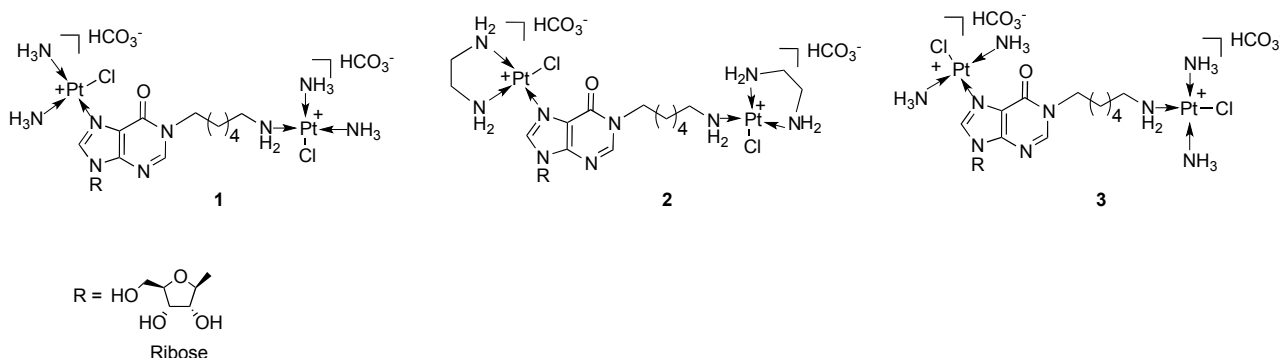
Keywords: platinum complexes; nucleosides; cisplatin; chemotherapy

1. Introduction

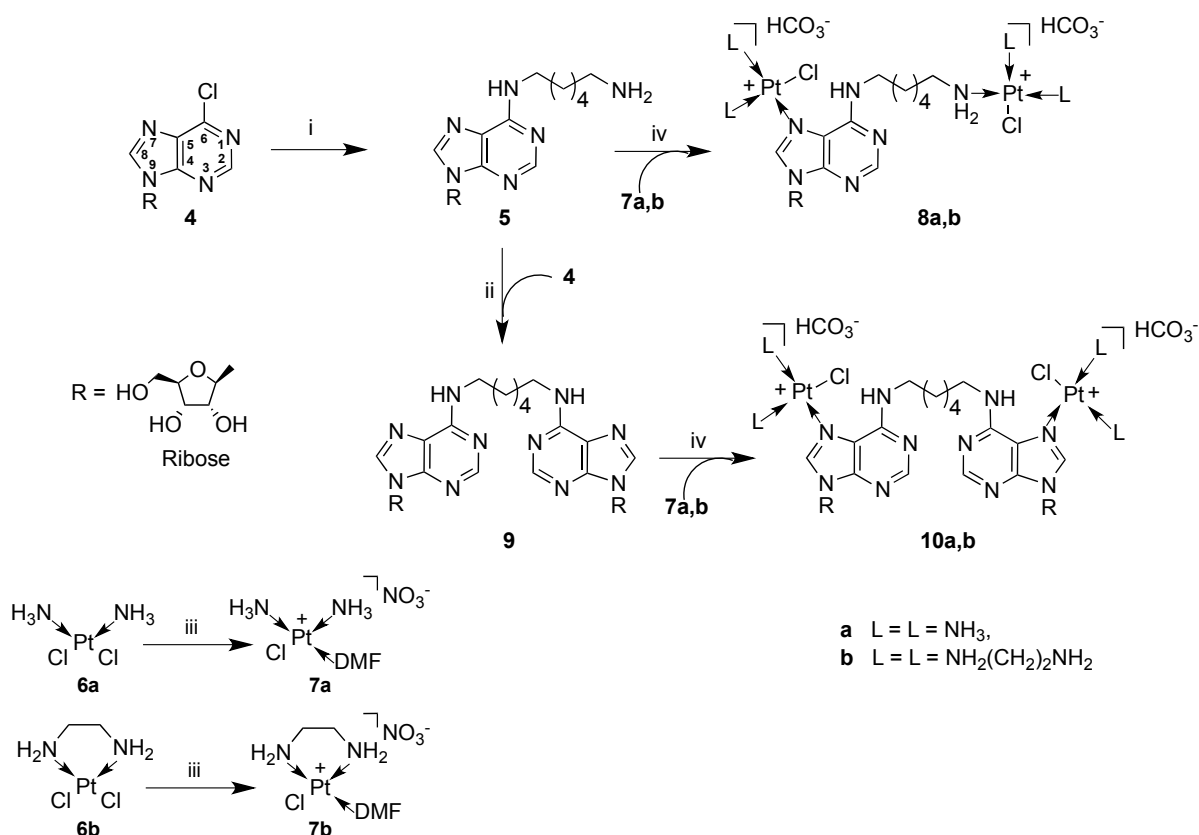
The discovery of the anti-proliferative properties of cisplatin [1] marked the beginning of modern chemotherapy based on the use of metal complexes capable of blocking the replication of cancer cells targeting the nuclear DNA [2,3]. In fact, it is widely accepted that cisplatin, once inside the cell, may form a highly reactive species [4,5] that can react with DNA through the formation of intra-strand linkages [6,7]. Such linkages alter the secondary structure of DNA, resulting in an inhibition of transcription and replication, ultimately leading to cell death [4]. However, the poor solubility in biological fluids [8], the serious side effects [9,10], and, more importantly, the intrinsic and acquired resistance of many types of tumors [5], have limited its use in the clinic. Carboplatin and oxaliplatin, second and third generation anti-neoplastic agents, respectively, are able to enhance the quality of life of patients in terms of dosage and drug administration. However, they can still trigger mechanisms of resistance (intrinsic and/or acquired) during repeated cycles of oncological treatment [5]. It was then discovered that the presence of more charged metal centres separated by unbranched alkylamine chains leads to complexes capable of being uptaken by cells via active import [11] and of overcoming the intrinsic and/or acquired resistance in some tumors [6,12–15]. Based on the understanding that they may exert anti-tumoral activities through inter-strand linkages with DNA that cannot be repaired by enzymes [16], many multinuclear platinum complexes have recently been synthesized, by varying the diamine backbone chain length, or by introducing modified linkers [8,10–12,17,18]. In addition, new Pt-based compounds have been obtained by conjugating biologically important substances or drugs to Pt-containing subunits [19–24] and novel drug-delivery based methodologies have been explored to vehiculate platinum-based anti-cancer complexes directly against tumors [25,26].

Nucleoside and nucleotide anti-metabolites and their base analogues are able to inhibit specific pathways of the cancer cell metabolism by blocking the biosynthesis or the function of nucleic acids. For example, the combination of cisplatin and 5-fluorouracil, a chemotherapeutic agent that inhibits thymidylate synthase, has been extensively used in clinical practice to treat various types of cancer. Acyclovir, a guanosine nucleoside analogue containing an open-chain sugar surrogate, has been used as a ligand for platinum and the corresponding complex exhibits high *in vitro* activity against various herpes viruses [27]. Furthermore, the synthesis and the preliminary pharmacological activity of novel modified adenosines and thymidines, employed as N-donor ligands of platinum(II) dichloride complexes, have been recently reported [28,29].

Recently, we have reported the solid-phase synthesis and the pharmacological activity of the first examples of bis-platinated nucleoside complexes in which the mono-functional metal is linked both to N-7 of the purine nucleus of inosine and to the terminal amino-group of a hexylamine side chain installed on N-1 (compounds **1–3**, Figure 1) [30]. The amino-alkyl chain was introduced on the purine base system through a chemical strategy recently developed by us [30–36]. These complexes showed very good water solubility thanks to the charged platinum centres and to the ribose hydroxyl groups. They were tested against four different human tumor cell lines and, in particular, the complex bearing two monofunctional cisplatin units was revealed to be more cytotoxic than cisplatin against the MCF7 cancer cell line in a short-term exposure assay [30].

Figure 1. Bis-platinated nucleoside complexes synthesized starting from inosine [30].

In the light of the above results, to investigate the importance of nucleoside scaffolds in the construction of novel platinum complexes we have speculated about the antitumoral activity of cisplatin-adenosine complexes. As a result, in this paper we report on the synthesis of four dinuclear platinum complexes **8a,b** and **10a,b** (Scheme 1) carrying N^6 -(6-aminohexyl)adenosine (compound **5**, Scheme 1) or a 1,6-di-(adenosin- N^6 -yl)-hexane (compound **9**, Scheme 1) respectively, as ligands of mono-functional cisplatin or monochloro(ethylene diamine)platinum(II) (compounds **7a** and **7b**, respectively, Scheme 1).

Scheme 1. Synthesis of complexes **8** and **10**.

Reagents and conditions: (i) NH₂(CH₂)₆NH₂ (7 equiv.), TEA, EtOH, 3 h, reflux; (ii) **4** (1.5 equiv.), TEA, EtOH, 5 h, reflux; (iii) AgNO₃ (0.9 equiv.), DMF, 16 h, r.t.; (iv) **7a,b**, 16 h, r.t..

In the case of complexes **8a,b** the monofunctional platinum centres are linked to the N-7 of the purine base and to the terminal amino group of a hexylamine side chain bonded to N-6, whereas for the complexes **10a,b** they are both linked to N-7.

Platinum complexes, endowed with particular structural strains, have been designed to evaluate alternative interactions with DNA strands [8,12,17,37,38]. The novel prepared complexes **8a,b** and **10a,b** are characterized by a rigid planar purine substructure joined to a flexible hexylamine chain. On this basis, it could be expected that they may alter the binding mode with DNA through, for example, base-stacking or by the formation of multiple hydrogen bonds. Therefore, we have investigated the preliminary effects of these compounds on viability and proliferation in two different human cancer cell lines.

2. Results and Discussion

2.1. Synthesis and Characterization

The synthesis of the novel modified adenosine-based platinum complexes **8a,b** and **10a,b** is depicted in Scheme 1. 6-Chloropurine riboside **4** proved to be a good candidate to obtain the key intermediate **5** from which the construction of complexes **8a,b** and **10a,b** has been accomplished. As reported by Schammells *et al.* [39] seven equivalents of 1,6-diaminohexane have proved sufficient to convert **4** into **5** in a very good yield (86%), avoiding the formation of dimeric species, which would complicate the purification procedure. In fact, the recovery of **5** from the reaction mixture was easily performed thanks to its insolubility in EtOH upon cooling. Compound **9** was prepared by reacting **4** with a slight excess of **5**. During the reaction, this substance precipitated from the reaction mixture as a white solid which was then collected in 93% yield by filtration. This represents a very good improvement on the reported yield for **9** (12%) [40].

Next, the platinum-containing moieties were installed. In particular, treatment of **5** and **9** with a seven-fold excess of the suitable platinating complex **7a,b**, activated by overnight reaction with AgNO₃ (0.9 equiv.) in DMF, furnished the bisplatinated compounds **8a,b** and **10a,b**. Purification of these substances could be accomplished by reverse-phase HPLC only using a gradient of CH₃CN in 0.1 M triethylammonium bicarbonate buffer (TEAB) as the solvent mixture, whereas complex chromatographic patterns were observed in the absence of the TEAB.

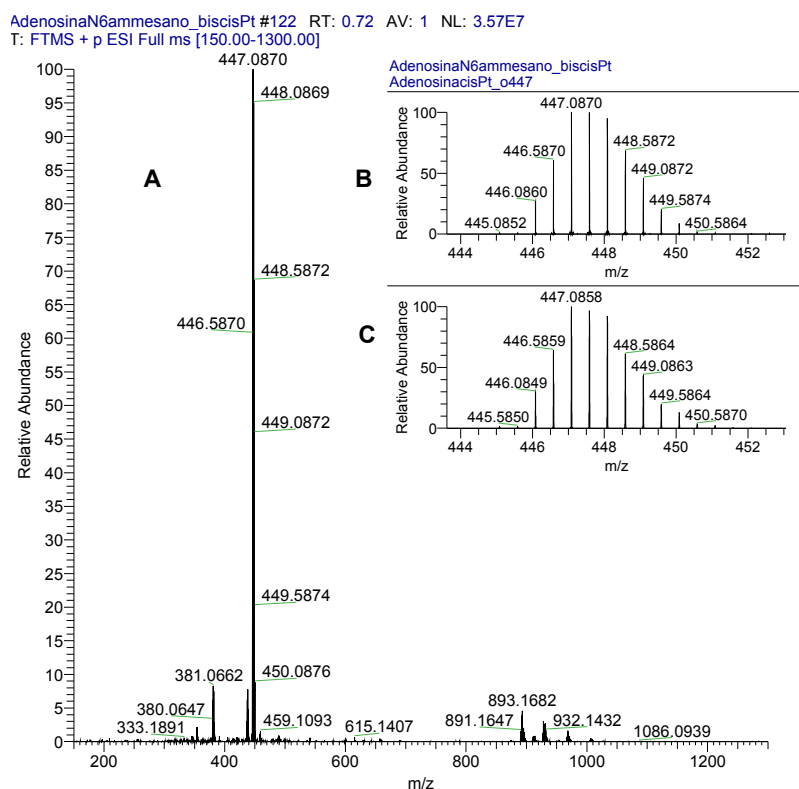
The structures of complexes **8a,b** and **10a,b** (yields 58%–62%) were supported by 2D-NMR and positive mode high resolution mass spectrometry (HRMS) data; whereas their purity was ascertained by CHN analyses.

In Figure 2 (panel A) the representative HRMS spectrum of complex **8a** is reported; in particular, the isotopic pattern of the base peak (expansion, panel B) perfectly fits with that of the calculated one (expansion, panel C), confirming the presence of two Pt and two Cl atoms and a net 2+ charge.

In the ¹H-NMR spectra of **8a,b** and **10a,b** the downfield shift of H-8, compared with the resonance of the same proton in **5** and **7** ($\Delta\delta = 0.6$ and 0.5 , respectively), confirmed the presence of the N(7) → Pt bond in all these substances [41,42]. In Table 1 the differences between the ¹³C-NMR shifts of the Pt-coordinated and not-coordinated purine carbon atoms ($\Delta\delta = \delta_{\text{complex}} - \delta_{\text{ligand}}$, ppm) are listed: in the case of complexes **8a,b** significant coordination shifts were found for the C-5 and C-8 atoms,

whereas for the complexes **10a,b** the C-5 atoms underwent the major shifts. Further evidence of metallation at N-7 come from the increased acidity of the H-8 as indicated by the reduced intensity of the pertinent signal in the ^1H -NMR spectra of **8a,b** and **10a,b**, when these complexes were dissolved in D_2O and the spectra acquired after several hours [43]. ^1H -NMR analyses excluded also the presence of equilibria involving migrations of the platinum moieties from N-7 to N-1 of the nucleobases; such migrations would shift the H-2 resonances of complexes **8a,b** and **10a,b** to higher frequencies in comparison to the same signals of compounds **5** and **9**, respectively [44]. The resonances of the methylene protons belonging to the $\text{CH}_2\text{-NH}_2\text{-Pt}$ moieties were seen as broad partly overlapped triplets in the range 2.3–2.7 ppm, in the proton spectra of **8b** and **10b**, likewise the protons of the methylene group geminal to platinum in **8a** resonated as a triplet at δ 2.6. In ^{13}C -NMR spectra of **8a** and **8b** the 5 ppm downfield shift of the ω -methylene carbon could be a consequence of the NH_2 platination.

Figure 2. HRMS spectrum of complex **8a** (panel A). Expansion of the isotopic pattern of the base peak (panel B) and of the corresponding calculated one (panel C).



In the UV spectra of the complexes **8a,b** and **10a,b** the maxima of absorption appeared red-shifted ($\Delta\lambda = 10\text{--}13$ nm) in respect to those of the free ligands, in accordance with literature data [45]. Comparison of the IR spectra of the ligands and complexes did not provide evidence about the bonding mode of the ligands in the complexes; in fact in the $4000\text{--}2700\text{ cm}^{-1}$ region very little information could be obtained about the nature of metal-ligand interaction, because of the presence of broad and intense bands belonging to hydrogen-bonded hydroxyls of the ribose moieties. The $1800\text{--}400\text{ cm}^{-1}$ region, where vibration frequencies of purine and ribose skeletons fall, did not furnish significant differences between platinated and not-platinated nucleosides. Furthermore, in the region $550\text{--}400\text{ cm}^{-1}$, where the resonances of Pt-N could be expected [45,46], no distinctive bands were observed.

Table 1. Differences between the ^{13}C -NMR shifts of the Pt-coordinated and not-coordinated purine carbons ($\Delta\delta = \delta_{\text{complex}} - \delta_{\text{ligand}}$, ppm).

Entry	^{13}C -NMR ($\Delta\delta$, ppm)				
	C-2	C-4	C-5	C-6	C-8
8a [39]	−1.0	−1.4	−2.9	0.9	2.1
8b [39]	−1.0	−1.3	−2.8	0.9	2.1
10a	−1.9	−2.3	−4.2	−0.1	0.9
10b	−2.0	−2.5	−4.2	0.1	1.1

2.2. Cytotoxicity Studies

The synthesized complexes were subjected to preliminary cell viability and proliferation assays. In particular, the cytotoxic behaviour was studied in A549 adenocarcinomic human alveolar basal epithelial and MCF7 human breast adenocarcinomic cancer cell lines by MTT and BrdU assays, to investigate the potential effects of platinum complexes on cell viability and proliferation, respectively. The incubation of A549 cells with **8a,b** and **10a,b** (50, 100 and 200 μM) for 72 h caused a concentration-dependent reduction of cell survival (Figure 3, panel A) as well as an inhibition of cell proliferation at the higher concentrations (Figure 3, panel B) compared to untreated cells. Indeed, comparable results were obtained when the cell number was directly determined by cell counting (data not shown).

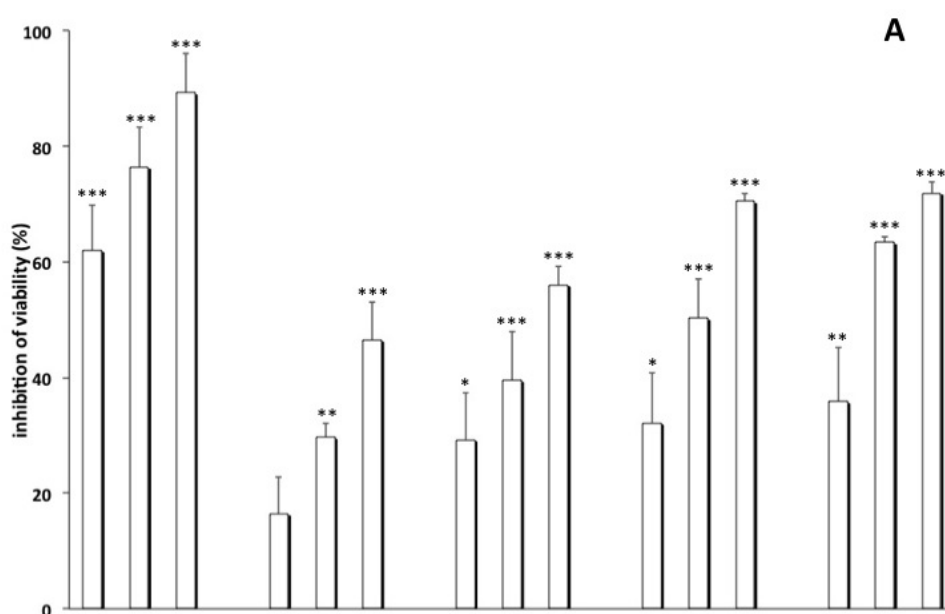
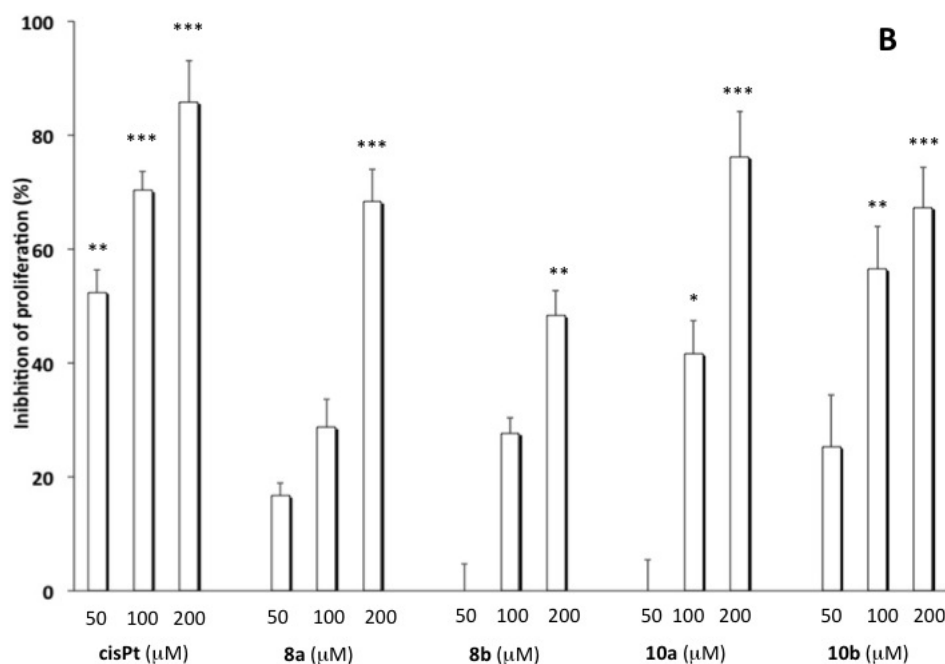
Figure 3. Effect of **8a**, **8b**, **10a** and **10b** on cell viability and proliferation. A549 cells were incubated with cisplatin, **8a**, **8b**, **10a** and **10b** (50, 100 and 200 μM) for 72 h. Thereafter, cell viability (panel A) and proliferation (panel B) were determined, respectively, by MTT and BrdU assay as described in the Experimental Section (** $p < 0.01$, *** $p < 0.001$, * $p < 0.05$ vs. untreated cells).

Figure 3. Cont.



The compounds **8b**, **10a** and **10b** (50, 100 and 200 μM) modified the viability and proliferation of MCF7 cells at higher concentrations, according to the published evidence that these cells have been associated with cisplatin resistance [47]. The compound **8a** proved to reduce the proliferation of the MCF7 cell line with a greater ability than the other compounds. Strikingly, compound **8a** was able to inhibit the cell proliferation slightly better than cisplatin, but only at 50 μM concentration (Figure 4).

Figure 4. Effect of **8a**, **8b**, **10a** and **10b** on cell viability and proliferation. MCF7 cells were incubated with cisplatin, **8a**, **8b**, **10a** and **10b** (50, 100 and 200 μM) for 72 h. Thereafter, cell viability (panel A) and proliferation (panel B) were determined, respectively, by MTT and BrdU assay as described in the Experimental Section (*** $p < 0.001$, ** $p < 0.01$, * $p < 0.05$ vs. untreated cells).

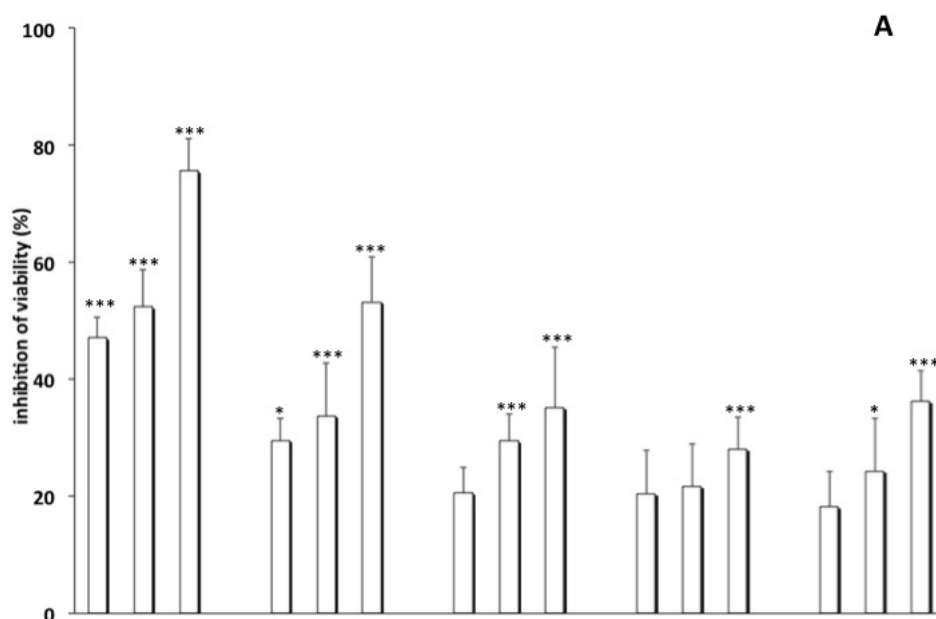
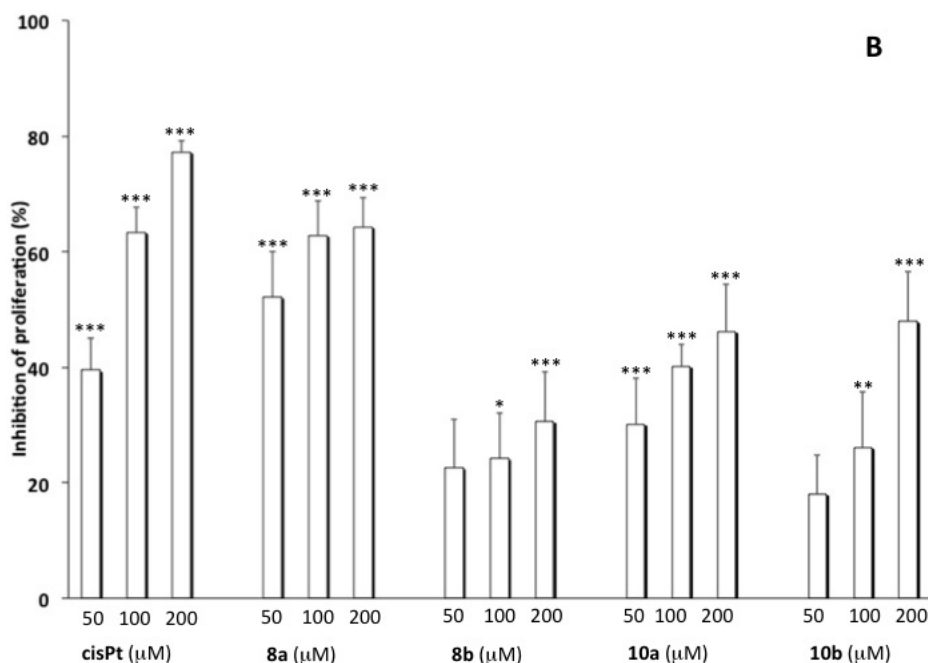


Figure 4. Cont.



3. Experimental Section

3.1. General Methods

All the reagents and solvents were obtained from commercial sources and used without further purification. ^1H - and ^{13}C -NMR spectra were acquired on Varian Mercury Plus 400 MHz instrument using D_2O or $(\text{CD}_3)_2\text{SO}$ as solvents. Chemical shifts were reported in parts per million (δ) relative to the residual solvent signal (^1H : HDO 4.80; ^{13}C : $(\text{CD}_3)(\text{CD}_2\text{H})\text{SO}$ 40.4) and assigned by 2D-NMR experiments. UV spectra were recorded on a Jasco V-530 UV spectrophotometer. IR spectra were recorded on a Jasco FT-IR 430 spectrophotometer. High-resolution MS spectra were recorded on a Thermo Orbitrap XL mass spectrometer using the electrospray ionization (ESI) technique in positive mode. Elemental analyses were performed on a Thermo Finnigan Flash EA 1112 CHN analyzer. RP-HPLC analyses and purifications were carried out on a Jasco UP-2075 Plus pump, equipped with a Jasco UV-2075 Plus UV detector, using a C-18 reverse-phase column (5 μm , 4.8×150 mm), eluted with a linear gradient of CH_3CN in 0.1 M triethylammonium bicarbonate (TEAB) buffer (System A: from 0% to 50% in 90 min, flow 1.3 mL/min, or System B: from 0% to 100% in 90 min, flow 1.3 mL/min). Human alveolar basal carcinoma epithelial cells (A549) and human breast cancer cells (MCF7) were grown in Dulbecco's modified Eagle's medium (DMEM) supplemented with 10% Foetal bovine serum (FBS), 100 U/mL penicillin and 100 U/mL streptomycin at 37 °C under 5% CO_2 . The cell lines were all from the ATCC catalogue. All media and supplements for cell culture were purchased from Gibco-Invitrogen (GE Healthcare).

*N*⁶-(6-Aminohexyl)adenosine (**5**). Compound **5** (326 mg) was obtained by reaction of **4** (297 mg, 0.104 mmol) in accordance to the procedure by Schammells *et al.* [37]. Spectroscopic data and yields were in agreement with those reported by the authors.

1,6-Di-(adenosin-N⁶-yl)-hexane (9). Compound **5** (100 mg, 0.27 mmol), 6-chloropurine riboside (**4**, 116 mg, 0.40 mmol), Et₃N (41 µL, 0.30 mmol) were refluxed in EtOH (1 mL). During the reaction, a colourless solid precipitated from the reaction. After 5 h it was filtered, washed with boiling EtOH and dried, giving **9** as a colourless powder (164 mg, 93%). El. An. Calcd. for C₂₆H₃₆N₁₀O₈: C, 50.64; H, 5.88; N, 22.72. Found: C, 50.68; H, 5.90; N, 22.69. ¹H-NMR and UV data were in agreement with those reported in literature [38]. ¹³C-NMR (100 MHz, (CD₃)₂SO) δ 155.6 (C-2), 153.3 (C-6), 149.1 (C-4), 140.5 (C-8), 120.7 (C-5), 88.9 (C-1'), 86.9 (C-4'), 74.4 (C-2'), 71.6 (C-3'), 62.6 (C-5'), 40.8 (CH₂NH, covered by residual solvent signal), 30.0 (CH₂), 27.1 (CH₂); IR (KBr pellet) 3336, 2935, 2861 1630, 1587, 1537, 1474, 1418, 1369, 1334, 1307, 1221, 1185, 1130, 1097, 1058, 985, 866, 822, 793, 641, 554 cm⁻¹; *m/z* 639.2620 (HRESIMS) ([M + Na]⁺, C₂₆H₃₆N₁₀NaO₈, requires 639.2615).

3.2. General Procedure for the Preparation of Dinuclear Platinum Complexes **8a,b** and **10a,b**

In a representative experiment, cisplatin (57 mg, 0.19 mmol) was activated by treatment with AgNO₃ (29.0 mg, 0.17 mmol) in DMF (2 mL) in the dark (16 h, r.t.). AgCl was removed by filtration and the resulting solution of [Pt(NH₃)₂(Cl)DMF]⁺(NO₃)⁻ in DMF was added to compound **5** (10 mg, 0.027 mmol). The solution was shaken in the dark (16 h, r.t.) and then filtered over a GHP Acrodisc 13 mm syringe filter (0.45 µm GHP membrane). The filter was washed with the minimal amount of DMF and the clarified solution was then subjected to HPLC purification [system A for **8a,b** (t_R: 38.7 min and 38.4 min respectively) and system B for **10a,b** (t_R: 31.0 min and 31.5 min respectively), see General Methods]; the fractions containing the title compound were evaporated under reduced pressure and then lyophilized affording pure **8a**.

Compound 8a. Bis-bicarbonate salt (17 mg, 60%). El. An. Calcd. for C₁₈H₄₀Cl₂N₁₀O₁₀Pt₂: C, 21.24; H, 3.96; N, 13.76. Found: C, 21.21; H, 3.98; N, 13.79. ¹H-NMR (400 MHz, D₂O) δ 8.84 (s, 1H, H-8), 8.33 (s, 1H, H-2), 6.12 (bs, 1H, H-1'), 4.78–4.76 (m, 1H, H-2', partially covered by solvent signal), 4.43–4.36 (m, 1H, H-3'), 4.31–4.25 (m, 1H, H-4'), 3.97–3.76 (m, 2H, H_{a,b}-5'), 3.67–3.55 (m, 2H, CH₂N), 2.62 (t, *J* = 6.4 Hz, 1H, CH₂NH₂Pt), 1.86–1.72 (m, 2H, CH₂), 1.71–1.59 (m, 2H, CH₂), 1.57–1.34 (complex signal, 4H, 2 × CH₂); ¹³C-NMR (100 MHz, D₂O) δ 160.2 (2 × HCO₃⁻), 153.7 (C-2), 153.2 (C-6), 146.8 (C-4), 141.6 (C-8), 116.8 (C-5), 89.1 (C-1'), 85.9 (C-4'), 73.9 (C-2'), 70.1 (C-3'), 61.0 (C-5'), 45.7 (CH₂NH₂), 40.7 (CH₂NH), 29.8 (CH₂), 28.0 (CH₂), 25.4 (CH₂), 25.2 (CH₂). IR (KBr pellet) 3246, 2930, 1626, 1589, 1492, 1339, 1084, 1058, 835, 790, 553 cm⁻¹; UV (H₂O) λ_{max} = 277 nm; HRESI-MS: (*m/z*) 447.0870, calcd. [M]²⁺ 447.0859.

Compound 8b. Bis-bicarbonate salt (17 mg, 58%). El. An. Calcd. for C₂₂H₄₄Cl₂N₁₀O₁₀Pt₂: C, 24.70; H, 4.15; N, 13.09. Found: C, 24.73; H, 4.13; N, 13.06. ¹H-NMR (400 MHz, D₂O) δ 8.85 (s, 1H, H-8), 8.39 (s, 1H, H-2), 6.16 (d, *J* = 5.0 Hz, 1H, H-1'), 4.80 (m, 1H, H-2', covered by solvent signal), 4.48–4.41 (m, 1H, H-3'), 4.37–4.30 (m, 1H, H-4'), 4.00–3.84 (m, 2H, H_{a,b}-5'), 3.78–3.67 (m, 2H, CH₂N), 2.85–2.50 (complex signal, 10H, CH₂NH₂Pt and 4 × CH₂ ethylene diamine moieties), 1.91–1.78 (m, 2H, CH₂), 1.77–1.62 (m, 2H, CH₂), 1.61–1.36 (complex signal, 4H, 2 × CH₂); ¹³C-NMR (100 MHz, D₂O) δ 160.2 (2 × HCO₃⁻), 153.7 (C-2), 153.2 (C-6), 146.9 (C-4), 141.6 (C-8), 116.9 (C-5), 89.1 (C-1'), 85.9 (C-4'), 73.9 (C-2'), 70.1 (C-3'), 61.0 (C-5'), 48.3, 48.0, 47.1 (4 × CH₂ ethylene diamine moieties), 45.9 (CH₂NH₂), 40.7 (CH₂NH), 29.9 (CH₂), 28.1 (CH₂), 25.5 (CH₂), 25.2 (CH₂); IR

(KBr pellet) 3406, 3208, 2931, 1627, 1589, 1470, 1336, 1303, 1232, 1079, 1054, 834, 790, 555, 472 cm^{-1} ; UV (H_2O) $\lambda_{\text{max}} = 278 \text{ nm}$; HRESI-MS: (m/z) 473.1037, calcd. $[\text{M}]^{2+}$ 473.1031.

Compound 10a. Bis-bicarbonate salt (12 mg, 60%). El. An. Calcd. for $\text{C}_{28}\text{H}_{50}\text{Cl}_2\text{N}_{14}\text{O}_{14}\text{Pt}_2$: C, 26.53; H, 3.97; N, 15.47. Found: C, 26.50; H, 3.95; N, 15.45. $^1\text{H-NMR}$ (400 MHz, D_2O) δ 8.85 (s, 2H, $2 \times \text{H-8}$), 8.26 (s, 2H, $2 \times \text{H-2}$), 6.14 (bs, 2H, $2 \times \text{H-1'}$), 4.80 (m, 2H, $2 \times \text{H-2'}$, covered by solvent signal), 4.50–4.40 (m, 2H, $2 \times \text{H-3'}$), 4.38–4.29 (m, 2H, $2 \times \text{H-4'}$), 4.03–3.76 (complex signal, 6H, $2 \times \text{H}_{\text{a,b-5'}}$ and $2 \times \text{CH}_\text{a}\text{N}$), 3.67–3.53 (m, 2H, $2 \times \text{CH}_\text{b}\text{N}$), 1.94–1.75 (m, 4H, $2 \times \text{CH}_2$), 1.73–1.51 (m, 4H, $2 \times \text{CH}_2$); $^{13}\text{C-NMR}$ (100 MHz, D_2O) δ 160.2 (HCO_3^-), 153.7 (C-2), 153.2 (C-6), 146.8 (C-4), 141.4 (C-8), 116.5 (C-5), 89.1 (C-1'), 85.8 (C-4'), 74.0 (C-2'), 70.0 (C-3'), 61.0 (C-5'), 40.5 (CH_2NH), 27.8 (CH_2), 25.2 (CH_2); IR (KBr pellet) 3280, 2933, 1626, 1589, 1492, 1415, 1339, 1306, 1230, 1085, 1059, 985, 864, 790, 552 cm^{-1} ; UV (H_2O) $\lambda_{\text{max}} = 277 \text{ nm}$; HRESI-MS: (m/z) 572.1213, calcd. $[\text{M}]^{2+}$ 572.1226.

Compound 10b. Bis-bicarbonate salt (13 mg, 62%). El. An. Calcd. for $\text{C}_{32}\text{H}_{54}\text{Cl}_2\text{N}_{14}\text{O}_{14}\text{Pt}_2$: C, 29.12; H, 4.12; N, 14.86. Found: C, 29.15; H, 4.10; N, 14.83. $^1\text{H-NMR}$ (400 MHz, D_2O) δ 8.81 (s, 2H, $2 \times \text{H-8}$), 8.24 (s, 2H, $2 \times \text{H-2}$), 6.14 (bs, 2H, $2 \times \text{H-1'}$), 4.80 (m, 2H, $2 \times \text{H-2'}$, covered by solvent signal), 4.49–4.41 (m, 2H, $2 \times \text{H-3'}$), 4.37–4.31 (m, 2H, $2 \times \text{H-4'}$), 4.04–3.83 (m, 4H, $2 \times \text{H}_{\text{a,b-5'}}$), 3.81–3.60 (m, 4H, $2 \times \text{CH}_2\text{N}$), 2.84–2.50 (complex signal, 8H, $4 \times \text{CH}_2$, ethylene diamine moieties), 1.95–1.74 (m, 4H, $2 \times \text{CH}_2$), 1.72–1.52 (m, 4H, $2 \times \text{CH}_2$); $^{13}\text{C-NMR}$ (100 MHz, D_2O) δ 160.1 (HCO_3^-), 153.6 (C-2), 153.2 (C-6), 146.6 (C-4), 141.6 (C-8), 116.5 (C-5), 89.1 (C-1'), 85.7 (C-4'), 74.1 (C-2'), 70.1 (C-3'), 61.2 (C-5'), 48.1, 47.3 ($2 \times \text{CH}_2$ ethylene diamine moieties), 40.5 (CH_2NH), 27.7 (CH_2), 25.1 (CH_2); IR (KBr pellet) 3284, 2930, 1625, 1592, 1490, 1417, 1338, 1310, 1233, 1083, 1061, 980, 860, 791, 554 cm^{-1} ; UV (H_2O) $\lambda_{\text{max}} = 276 \text{ nm}$; HRESI-MS: (m/z) 598.1391, calcd. $[\text{M}]^{2+}$ 598.1382.

3.3. MTT Viability Assay

The cells were plated in 96 culture wells (20×10^4 cells/well) and allowed to adhere overnight. Thereafter, the medium was replaced with fresh medium and the cells were incubated in the absence or presence of cisplatin, **8a**, **8b**, **10a** and **10b** (50, 100 and 200 μM). After 72 h, the cell viability was determined by using 3-(4,5-dimethylthiazol-2-yl)-2,5-diphenyl-2H-tetrazoliumbromide (MTT) conversion assay [48]. Briefly, 10 μL of MTT (5 mg/mL) were added to the cells and incubated for an additional 3 h. After this time point, the cells were lysed and the dark blue crystals solubilized with 150 μL of a solution containing 50% (v:v) DMF, 20% (w:v) SDS with an adjusted pH of 4.5. The optical density (OD) of each well was measured with a microplate spectrophotometer (Multiskan MCCC/340, Titertek, Huntsville, AL, USA) equipped with a 620 nm filter. The experiment was performed twice in triplicate. The vitality inhibition, induced by each compound at the indicated concentrations, was expressed as a percentage *versus* the untreated cells (the control). The viable cells were also counted by the trypan blue exclusion assay and light microscopy.

3.4. BrdU Cell Proliferation Assay

The cells were plated onto 96-well plates (2×10^4 cells/well) overnight. Then, the medium was replaced with fresh medium and the cells were incubated in the absence or presence of cisplatin (50,

100 and 200 μM), **8a**, **8b**, **10a** and **10b** (50, 100 and 200 μM). After 72 h, 5-bromo-2'-deoxyuridine (BrdU; 10 μM) was added and the cells were cultured for a further 12 h. The mitogenic activity was determined according to the manufacturer's instructions (BrdU cell proliferation assay kit, Cell Signaling). The experiment was performed three times in triplicate. The proliferation inhibition, induced by each compound at the indicated concentrations, was expressed as a percentage *versus* the untreated cells (the control).

3.5. Statistical Analysis

The results are expressed as the means \pm SEM of n experiments. The statistical significance was calculated by one-way analysis of variance (ANOVA) and Bonferroni-corrected p -value for multiple comparison testing. The level of statistically significant difference was defined as $p < 0.05$.

4. Conclusions

In summary, in this paper we have reported the synthesis of four novel platinum complexes embodying a N^6 -(6-aminohexyl)adenosine or a 1,6-di-(adenosin- N^6 -yl)-hexane as ligands of monofunctional cisplatin or monochloro(ethylene diamine)platinum(II) moieties, starting from commercially available 6-chloropurine riboside. The designed synthetic route allowed us to obtain the desired platinum complexes without blocking the ribose hydroxyl groups and through easy purification steps.

The effects of these platinum complexes on cell viability and proliferation have been studied in A549 and MCF7 cell lines. Our data demonstrate that these compounds are able to inhibit the survival and proliferation of sensitive cancer cells. Nevertheless, cisplatin remains the most active molecule under our experimental conditions. Further experiments are necessary to understand the mechanism by which **8a** penetrates into the cells and inhibits cell proliferation in the MCF7 cell line.

Acknowledgments

This work was financially supported by “Progetto FARO 2011” (Finanziamento per l’Avvio di Ricerche Originali). We are grateful to Luisa Cuorvo for her technical assistance and to CSIAS (Centro di Servizio Interdipartimentale di Analisi Strutturale) for the NMR facilities.

Author Contributions

Stefano D’Errico, Brunella Pinto and Fabrizia Nici designed and synthesized the compounds shown in Scheme 1, furthermore Stefano D’Errico wrote the initial draft of the paper and edited the final draft. Vincenzo Piccialli wrote an intermediate draft of the paper and helped write and edit the final draft of the manuscript. Nicola Borbone and Valeria Costantino characterized all the novel platinum complexes, analyzed spectroscopic data from the experiments and wrote the pertinent section in Results and Discussion and in the Experimental Section. Francesca De Falco, Maria Chiara Maiuri and Rosa Carnuccio performed the *in vitro* biological assays, analyzed and processed the data obtained from the experiments and wrote the pertinent section in the Results and Discussion and in the Experimental Section. Giorgia Oliviero and Gennaro Piccialli supervised all experiments, reanalyzed

all data for accuracy, and wrote the final draft of the manuscript. All authors reviewed and approved the final version of the manuscript.

Conflicts of Interest

The authors declare no conflict of interest.

References

1. Rosenberg, B.; Vancamp, L.; Krigas, T. Platinum compounds: A new class of potent antitumour agents. *Nature* **1969**, *222*, 385–386.
2. Kelland, L.R.; Farrell, N. *Platinum Based Drugs in Cancer Therapy*; Humana Press: Totowa, NJ, USA, 2000.
3. Allardyce, C.S.; Dorcier, A.; Scolaro, C.; Dyson, P.J. Development of organometallic (organo-transition metal) pharmaceuticals. *Appl. Organometal. Chem.* **2005**, *19*, 1–10.
4. Wexselblatt, E.; Yavin, E.; Gibson, D. Cellular interactions of platinum drugs. *Inorg. Chim. Acta* **2012**, *393*, 75–83.
5. Harper, B.W.; Krause-Heuer, A.M.; Grant, M.P.; Manohar, M.; Garbutcheon-Singh, K.B.; Aldrich-Wright, J.R. Advances in Platinum Chemotherapeutics. *Chem. Eur. J.* **2010**, *16*, 7064–7077.
6. Sigel, A.; Sigel, H. *Metal Ions in Biological Systems: Metal Complexes in Tumor Diagnosis and as Anticancer Agents*; CRC Press: London, UK, 2004.
7. Florea, A.M.; Büsselberg, D. Cisplatin as an Anti-Tumor Drug: Cellular Mechanisms of Activity, Drug Resistance and Induced Side Effects. *Cancers* **2011**, *3*, 1351–1371.
8. Fan, D.; Yang, X.; Wang, X.; Zhang, S.; Mao, J.; Ding, J.; Lin, L.; Guo, Z. A dinuclear monofunctional platinum(II) complex with an aromatic linker shows low reactivity towards glutathione but high DNA binding ability and antitumor activity. *J. Biol. Inorg. Chem.* **2007**, *12*, 655–665.
9. Boulikas, T. Clinical overview on Lipoplatin™: A successful liposomal formulation of cisplatin. *Expert Opin. Investig. Drugs* **2009**, *18*, 1197–1218.
10. Abu-Surrah, A.S.; Kettunen, M. Platinum group antitumor chemistry: Design and development of new anticancer drugs complementary to cisplatin. *Curr. Med. Chem.* **2006**, *13*, 1337–1357.
11. Arnesano, F.; Natile, G. Mechanistic insight into the cellular uptake and processing of cisplatin 30 years after its approval by FDA. *Coord. Chem. Rev.* **2009**, *253*, 2070–2081.
12. Zhang, J.; Wang, L.; Xing, Z.; Liu, D.; Sun, J.; Li, X.; Zhang, Y. Status of Bi- and Multi-Nuclear Platinum Anticancer Drug Development. *Anti Cancer Agents Med. Chem.* **2010**, *10*, 272–282.
13. Wheate, N.; Collins, J.G. Multi-nuclear platinum complexes as anti-cancer drugs. *Coord. Chem. Rev.* **2003**, *241*, 133–145.
14. Roberts, J.D.; Peroutka, J.; Farrell, N. Cellular pharmacology of polynuclear platinum anti-cancer agents. *J. Inorg. Biochem.* **1999**, *77*, 51–57.
15. Pratesi, G.; Perego, P.; Polizzi, D.; Righetti, S.C.; Supino, R.; Caserini, C.; Manzotti, C.; Giuliani, F.C.; Pezzoni, G.; Tognella, S.; *et al.* A novel charged trinuclear platinum complex effective against cisplatin-resistant tumours: Hypersensitivity of p53-mutant human tumour xenografts. *Br. J. Cancer* **1999**, *80*, 1912–1919.

16. Kasparikova, J.; Zehnulova, J.; Farrell, N.; Brabec, V. DNA interstrand cross-links of the novel antitumor trinuclear platinum complex BBR3464. Conformation, recognition by high mobility group domain proteins, and nucleotide excision repair. *J. Biol. Chem.* **2002**, *277*, 48076–48086.
17. Jansen, B.A.J.; Wielaard, P.; Kalayda, G.V.; Ferrari, M.; Molenaar, C.; Tanke, H.J.; Brouwer, J.; Reedijk, J. Dinuclear platinum complexes with N,N'-bis(aminoalkyl)-1,4-diaminoanthraquinones as linking ligands. Part I. Synthesis, cytotoxicity, and cellular studies in A2780 human ovarian carcinoma cells. *J. Biol. Inorg. Chem.* **2004**, *9*, 403–413.
18. Mitova, V.; Bogomilova, A.; Shestakova, P.; Momekov, G.; Momekova, D.; Abbas, R.K.; Koseva, N. Synthesis of a new polynuclear platinum (II) complex and its prodrug forms. Evaluation of their cytotoxic properties. *J. Chem. Technol. Metall.* **2013**, *48*, 17–27.
19. Cincinelli, R.; Musso, L.; Dallavalle, S.; Artali, R.; Tinelli, S.; Colangelo, D.; Zunino, F.; de Cesare, M.; Beretta, G.L.; Zaffaroni, N. Design, modeling, synthesis and biological activity evaluation of camptothecin-linked platinum anticancer agents. *Eur. J. Med. Chem.* **2013**, *63*, 387–400.
20. Robillard, M.S.; Valentijn, A.; Meeuwenoord, N.J.; van der Marel, G.A.; van Boom, J.H.; Reedijk, J. The First Solid-Phase Synthesis of a Peptide-Tethered Platinum (II) Complex. *Angew. Chem. Int. Ed.* **2000**, *112*, 3226–3229.
21. Robillard, M.S.; van Alphen, S.; Meeuwenoord, N.J.; Jansen, B.A.J.; van der Marel, G.A.; van Boom, J.H.; Reedijk, J. Solid-phase synthesis of peptide-platinum complexes using platinum-chelating building blocks derived from amino acids. *New J. Chem.* **2005**, *29*, 220–225.
22. Holmes, R.J.; McKeage, M.J.; Murray, V.; Denny, W.A.; McFadyen, W.D. cis-Dichloroplatinum (II) complexes tethered to 9-aminoacridine-4-carboxamides: Synthesis and action in resistant cell lines *in vitro*. *J. Inorg. Biochem.* **2001**, *85*, 209–217.
23. Cai, L.; Lim, K.; Ren, S.; Cadena, R.S.; Beck, W.T. Synthesis and *in Vitro* Antitumor Activity of Oligonucleotide-Tethered and Related Platinum Complexes. *J. Med. Chem.* **2001**, *44*, 2959–2965.
24. Schmidt, K.S.; Boudvillain, M.; Schwartz, A.; van der Marel, G.A.; van Boom, J.H.; Reedijk, J.; Lippert, B. Monofunctionally trans-Diammine Platinum (II)-Modified Peptide Nucleic Acid Oligomers: A New Generation of Potential Antisense Drugs. *Chem. Eur. J.* **2002**, *8*, 5566–5570.
25. Butler, J.S.; Sadler, P.J. Targeted delivery of platinum-based anticancer complexes. *Curr. Opin. Chem. Biol.* **2013**, *17*, 175–188.
26. Sengupta, P.; Basu, S.; Soni, S.; Pandey, A.; Roy, B.; Oh, M.S.; Chin, K.T.; Paraskar, A.S.; Sarangi, S.; Connor, Y. Cholesterol-tethered platinum II-based supramolecular nanoparticle increases antitumor efficacy and reduces nephrotoxicity. *Proc. Natl. Acad. Sci. USA* **2012**, *109*, 11294–11299.
27. Coluccia, M.; Boccarelli, A.; Cermelli, C.; Portolani, M.; Natile, G. Platinum(II)-Acyclovir Complexes: Synthesis, Antiviral and Antitumour Activity. *Metal-Based Drugs.* **1995**, *2*, 249–256.
28. Nervi, C.; Vigna, M.A.; Cavigliolo, G.; Ravera, M.; Osella, D. Synthesis and characterization of functionalized thymidine as a potential carrier for cisplatin-like drugs. *Inorg. Chim. Acta* **2005**, *358*, 2799–2803.
29. Štarha, P.; Popa, I.; Trávníček, Z.; Vančo, J. N6-Benzyladenosine Derivatives as Novel N-Donor Ligands of Platinum(II) Dichlorido Complexes. *Molecules* **2013**, *18*, 6990–7003.

30. D'Errico, S.; Oliviero, G.; Piccialli, V.; Amato, J.; Borbone, N.; D'Atri, V.; D'Alessio, F.; Di Noto, R.; Ruffo, F.; Salvatore, F.; *et al.* Solid-phase synthesis and pharmacological evaluation of novel nucleoside-tethered dinuclear platinum (II) complexes. *Bioorg. Med. Chem. Lett.* **2011**, *21*, 5835–5838.
31. Oliviero, G.; D'Errico, S.; Borbone, N.; Amato, J.; Piccialli, V.; Piccialli, G.; Mayol, L. Facile Solid-Phase Synthesis of AICAR 5'-Monophosphate (ZMP) and Its 4-N-Alkyl Derivatives. *Eur. J. Org. Chem.* **2010**, *2010*, 1517–1524.
32. Oliviero, G.; Amato, J.; Borbone, N.; D'Errico, S.; Piccialli, G.; Bucci, E.; Piccialli, V.; Mayol, L. Synthesis of 4-N-alkyl and ribose-modified AICAR analogues on solid support. *Tetrahedron* **2008**, *64*, 6475–6481.
33. Oliviero, G.; D'Errico, S.; Borbone, N.; Amato, J.; Piccialli, V.; Varra, M.; Piccialli, G.; Mayol, L. A solid-phase approach to the synthesis of N-1-alkyl analogues of cyclic inosine-diphosphate-ribose (cIDPR). *Tetrahedron* **2010**, *66*, 1931–1936.
34. D'Errico, S.; Oliviero, G.; Borbone, N.; Amato, J.; Piccialli, V.; Varra, M.; Mayol, L.; Piccialli, G. Solid-Phase Synthesis of a New Diphosphate 5-Aminoimidazole-4-carboxamide Riboside (AICAR) Derivative and Studies toward Cyclic AICAR Diphosphate Ribose. *Molecules* **2011**, *16*, 8110–8118.
35. D'Errico, S.; Oliviero, G.; Borbone, N.; Amato, J.; D'Alonzo, D.; Piccialli, V.; Mayol, L.; Piccialli, G. A Facile Synthesis of 5'-Fluoro-5'-deoxyacadesine (5'-F-AICAR): A Novel Non-phosphorylatable AICAR Analogue. *Molecules* **2012**, *17*, 13036–13044.
36. D'Errico, S.; Oliviero, G.; Borbone, N.; Amato, J.; Piccialli, V.; Varra, M.; Mayol, L.; Piccialli, G. Synthesis of New Acadesine (AICA-riboside) Analogues Having Acyclic D-Ribityl or 4-Hydroxybutyl Chains in Place of the Ribose. *Molecules* **2013**, *18*, 9420–9431.
37. Park, G.Y.; Wilson, J.J.; Song, Y.; Lippard, S.J. Phenanthriplatin, a monofunctional DNA-binding platinum anticancer drug candidate with unusual potency and cellular activity profile. *Proc. Natl. Acad. Sci. USA* **2012**, *109*, 11987–11992.
38. Johnstone, T.C.; Alexander, S.M.; Lin, W.; Lippard, S.J. Effects of Monofunctional Platinum Agents on Bacterial Growth: A Retrospective Study. *J. Am. Chem. Soc.* **2014**, *136*, 116–118.
39. Gregg, A.; Bottle, S.E.; Devine, S.M.; Figler, H.; Linden, J.; White, P.; Pouton, C.W.; Urmaliya, V.; Scammells, P.J. Dual acting antioxidant A1 adenosine receptor agonists. *Bioorg. Med. Chem. Lett.* **2007**, *17*, 5437–5441.
40. Agathocleous, D.C.; Page, P.B.C.; Cosstick, R.; Galpin, J.J.; McLennan, A.G.; Prescott, M. Synthesis of bridged nucleosides. *Tetrahedron* **1990**, *46*, 2047–2058.
41. Amo-Ochoa, P.; González, V.M.; Pérez, J.M.; Masaguer, J.R.; Alonso, C.; Navarro-Ranninger, C. Cytotoxicity, DNA binding, and reactivity against nucleosides of platinum (II) and (IV) spermine compounds. *J. Inorg. Biochem.* **1996**, *64*, 287–299.
42. Van Rij, S.; van Zutphen, S.; den Dulk, H.; Brouwer, J.; Reedijk, J. Structure–activity relationship studies for three new asymmetric cis-platinum(II) aminoethanol-based complexes. *Inorg. Chim. Acta* **2006**, *359*, 4125–4129.
43. Girault, J.O.; Chottard, G.; Lallemand, J.Y.; Chottard, J.C. Interaction of cis-[Pt(NH₃)₂(H₂O)₂](NO₃)₂ with ribose and deoxyribose diguanosine phosphates. *Biochemistry* **1982**, *21*, 1352–1356.

44. Arpalahti, J.; Klika, K.D.; Sillanpää, R.; Kivekäs, R. Dynamic processes in platinum(II)-adenosine complexes. Preparation, NMR spectroscopic characterisation and crystal structure of isomeric Pt II (dien)-adenosine complexes. *J. Chem. Soc. Dalton Trans.* **1998**, 1397–1402.
45. Wang, S.; Chu, W.; Wang, Y.; Liu, S.; Zhang, J.; Li, S.; Wei, H.; Zhou, G.; Qin, X. Synthesis, characterization and cytotoxicity of Pt(II), Pd(II), Cu(II) and Zn(II) complexes with 4'-substituted terpyridine. *Appl. Organometal. Chem.* **2013**, *27*, 373–379.
46. Li, L.J.; Wang, C.; Qiao, Y.; Yang, X.Y.; Hua, X.X.; Du, J.L. Platinum(II) complexes of reduced amino acid ester Schiff bases: Synthesis, characterization, and antitumor activity. *Res. Chem. Intermed.* **2014**, *40*, 413–424.
47. Fan, S.; Smith, M.L.; Rivet, D.J.; Duba, D.; Zhan, Q.; Kohn, K.W.; Fornace, A.J.; O'Connor, P.M. Disruption of p53 function sensitizes breast cancer MCF-7 cells to cisplatin and pentoxifylline. *Cancer Res.* **1995**, *55*, 1649–1654.
48. De Stefano, D.; Tommonaro, G.; Malik, S.A.; Iodice, C.; de Rosa, S.; Maiuri, M.C.; Carnuccio, R. Cacospongionolide and Scalaradial, Two Marine Sesterterpenoids as Potent Apoptosis-Inducing Factors in Human Carcinoma Cell Lines. *PLoS One* **2012**, *7*, e33031.

Sample Availability: Samples of the compounds **8a,b** and **10a,b** are available from the authors.

© 2014 by the authors; licensee MDPI, Basel, Switzerland. This article is an open access article distributed under the terms and conditions of the Creative Commons Attribution license (<http://creativecommons.org/licenses/by/3.0/>).